International Journal of Polymer Science

Food Polymers Functionality and Applications

Guest Editors: Xingxun Liu, Fengwei Xie, Xiaoxi Li, Sumei Zhou, and Liyan Chen

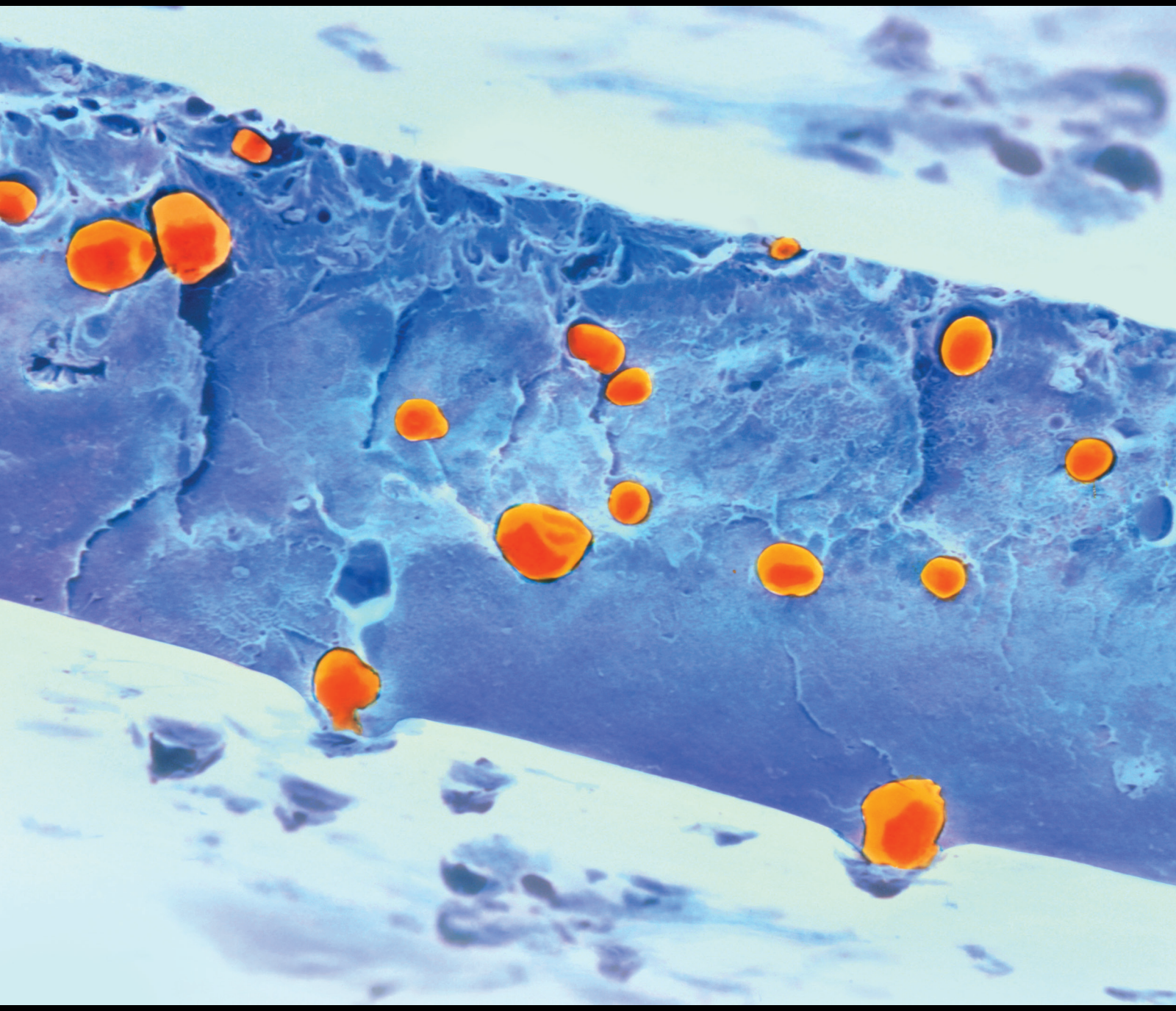

Food Polymers Functionality and Applications

International Journal of Polymer Science

Food Polymers Functionality and Applications

Guest Editors: Xingxun Liu, Fengwei Xie, Xiaoxi Li, Sumei Zhou, and Liyan Chen

Editorial Board

Contents

Hindawi Publishing Corporation
International Journal of Polymer Science
Volume 2015, Article ID 813628, 1 page
http://dx.doi.org/10.1155/2015/813628

Editorial

Food Polymers Functionality and Applications

Xingxun Liu,[1] Fengwei Xie,[2] Xiaoxi Li,[3] Sumei Zhou,[1] and Liyan Chen[4]

[1]*Institute of Food Science and Technology (IFST), Chinese Academy of Agricultural Sciences, Beijing, China*
[2]*Australian Institute for Bioengineering and Nanotechnology, The University of Queensland, Brisbane, QLD 4072, Australia*
[3]*School of Light Industry and Food Science, South China University of Technology, Guangdong, China*
[4]*Bioprocessing Lab, Prairie Aquatech, Brookings, SD 57006, USA*

Correspondence should be addressed to Xingxun Liu; ytboy652@163.com

Received 18 October 2015; Accepted 19 October 2015

Food polymers are polymers from edible plants, animals, and microorganisms that can be used in food systems, including proteins, polysaccharides, and peptides. Generally, food polymers can be classified into three groups based on their sources: (1) plant-based food polymers, such as starch, dietary fiber, and cereal protein; (2) animal-based food polymers, such as meal protein; (3) microorganism-based food polymers, such as fungus polysaccharides. The oils and/or lipid from plant and animals could also be considered as food polymers although their molecular weights are relatively small.

Food polymers represent a dominant area in natural polymers and play an important role in food structure, food functional properties, food processing, and shelf life. The knowledge in this area is commercially important as it will provide a useful practical guideline to food development and industrial production. The new studies of food polymers regarding "molecular design, synthesis/extraction/modification, structure and property, materials preparation, and applications" will give new directions of food science. Therefore, the study of food polymers for food applications could provide a better understanding of food systems, make better use of food macromolecules, and improve food qualities and safety.

In recent years, with the development of fundamental theories and analytical techniques that are related to polymers, specifically food polymers also experience a rapid development with the purpose of improving food systems. This special issue of this journal aims to provide a great opportunity for researchers in the area of food polymer functionality and applications to share their state-of-the-art studies related to food polymers (such as proteins, polysaccharides, and food polymer modifiers). In this special issue, there are original research and review articles that uncover the development of food polymers, including their design, processing, characterization, and microstructures, as well as new technologies related to food polymer processing and characterization. The topics in this special issue specially include the following: (i) new techniques of extracting and modifying food polymers; (ii) recent development in microstructure and nanostructure of food polymers; (iii) the relationship between structures and functionality of food polymers; (iv) novel characterization techniques of food polymers; (v) prospective applications for food polymers.

We hope readers will benefit for their own research from this special issue.

Acknowledgments

We would like to express our appreciation to all the authors for their informative contributions and the reviewers for their support and constructive critiques in making this special issue possible.

Xingxun Liu
Fengwei Xie
Xiaoxi Li
Sumei Zhou
Liyan Chen

Hindawi Publishing Corporation
International Journal of Polymer Science
Volume 2015, Article ID 986324, 10 pages
http://dx.doi.org/10.1155/2015/986324

Research Article

Isolation, Production, and Characterization of Thermotolerant Xylanase from Solvent Tolerant *Bacillus vallismortis* RSPP-15

Rajeeva Gaur, Soni Tiwari, Priyanka Rai, and Versha Srivastava

Department of Microbiology (Centre of Excellence), Dr. Ram Manohar Lohia Avadh University, Faizabad, Uttar Pradesh 224 001, India

Correspondence should be addressed to Rajeeva Gaur; rajeevagaur@rediffmail.com

Received 13 September 2014; Accepted 13 January 2015

Academic Editor: Liyan Chen

Sixty bacterial strains isolated from the soils sample in the presence of organic solvent were screened for xylanase production. Among them, strain RSPP-15 showed the highest xylanase activity which was identified as *Bacillus vallismortis*. The isolate showed maximum xylanase production (3768 U/mL) in the presence of birch wood xylan and beef extract at 55°C pH 7.0 within 48 h of incubation. The enzyme activity and stability were increased 181.5, 153.7, 147.2, 133.6, and 127.9% and 138.2, 119.3, 113.9, 109, and 104.5% in the presence of Co^{2+}, Ca^{2+}, Mg^{+2}, Zn^{+2}, and Fe^{+3} ions (10 mM). Xylanase activity and stability were strongly inhibited in the presence of Hg and Cu ions. The enzyme was also stable in the presence of 30% of *n*-dodecane, isooctane, *n*-decane, xylene, toluene, *n*-hexane, *n*-butanol, and cyclohexane, respectively. The presence of benzene, methanol, and ethanol marginally reduced the xylanase stability, respectively. This isolate may be useful in several industrial applications owing to its thermotolerant and organic solvent resistance characteristics.

1. Introduction

Xylanase (endo-1,4-β-D-xylanohydrolase) is a hydrolytic enzyme that plays an important role in depolymerization of xylan, the main renewable hemicellulosic polysaccharide of plant cell wall. It is produced by many microorganisms like bacteria [1–3], fungi [4, 5], actinomycetes [6], and yeast [7]; though enzyme from fungal and bacterial sources has dominated applications in industrial sectors, bacterial xylanases are preferred as they grow rapidly, need less space, can be easily maintained, and are accessible for genetic manipulations [8]. Bacteria, mainly *Bacillus* sp., are capable of producing alkaline thermostable xylanases. Previous reports stated that *Bacillus* SSP-34, *Bacillus stearothermophilus* strain T6, *Streptomyces, Bacillus* sp. strain NCL 87-6, *Bacillus circulans* AB 16, and *Bacillus pumilus* SV-85S were used efficiently in the production of xylanases [9–12].

Recently, interest in xylanase has evidently increased due its broad variety of biotechnological purposes such as prebleaching of pulp, improving the digestibility of animal feed stocks, alteration of cereal-based stuffs, bioconversion of lignocellulosic material and agrowastes to fermentable products, clarification of fruit juices, and degumming of plant fibers [13, 14]. Cellulase-free xylanases active at high temperature and pH are gaining importance in pulp and paper industry as they reduce the need for toxic chlorinated compounds making the bleaching process environment friendly [15]. Submerged fermentation offers various advantages over solid state fermentation, including fermentation study, greater product yield, and easier scale-up of process. In this study, we isolate an extracellular thermosolvent tolerant xylanase from an alkalophilic strain of *Bacillus vallismortis* RSPP-15 from soil in the presence of organic solvents. After that, we optimized physicochemical and nutritional parameters for better xylanase production for industrial application.

2. Materials and Methods

2.1. Isolation, Screening, and Identification of Thermosolvent Tolerant Xylanase Producing Bacteria. The soil samples were collected aseptically from different sites of pulp and paper industry of Faizabad to isolate xylanase producing bacteria. One-gram soil was suspended in 9.0 mL sterile distilled water, agitated for a minute. Then 0.1 mL suspension was spread

over birch wood xylan agar plates (pH 7.0) containing 1.0% xylan (birchwood); 0.5% ammonium sulphate, and 2% agar. The inoculated plates were overlaid with 7.0 mL of organic solvents (ethanol, propanol, cyclohexane, toluene, butanol, methanol, and isopropanol) and incubated at 55°C, till sufficient growth appeared. After sufficient growth incubated plates were overlaid with Congo-Red solution (0.1%) for 10 min and then washed with 1 N sodium chloride solution for destaining. If a strain was xylanolytic, it started hydrolyzing the xylan present in the surrounding and in the zone degradation there was no red color formation. Selection was done as per colonies with and without clear and transparent zone as xylanase producing and xylanase nonproducing strain, respectively. Bacterial colonies showing clear zones were selected, streaked twice on xylan agar plates for purification, and maintained as pure culture over xylan agar slants (pH 7.0, 4°C). The isolate having maximum clearance zone was selected for further studies. The selected bacterial isolate RSPP-15 was identified by morphological and biochemical characterization as per Bergey's Manual of Systematic Bacteriology [16]. The identity of RSPP-15 was authenticated from Institute of Microbial Technology (IMTECH), Chandigarh, India, based on the phenotypic (16S rDNA) and biochemical tests. The bacterial isolate RSPP-15 was grown on xylan nutrient agar slants at 55°C for 24–48 h. The fully grown slants were stored at 4°C and were subcultured every two weeks.

2.2. Crude Enzyme Preparation and Enzyme Assay. The culture was grown in a 150 mL Erlenmeyer flask that contained 50 mL of basal medium containing 2.0% xylan and 0.5% ammonium sulphate. The pH of the medium was adjusted to 7.0 prior to sterilization. The flask was inoculated and incubated at 55°C for 24 h for sufficient growth. The crude enzyme was filtered and centrifuged at 12000 rpm for 10 min and enzyme assay was carried out. Xylanase was assayed by measuring the reducing sugar released by reaction on birchwood xylan. Xylanase assay was done by Nelson [17] and Somogyi [18] methods using a reaction mixture consisting of 500 μL of substrate solution (1.0% birchwood xylan in 1.0 M phosphate buffer, pH 7.0.), 100 μL of the enzyme solution, and 1 mL of volume maintained by adding 400 μL distilled water. The reaction mixture was incubated for 10 min at 55°C. Reaction was stopped by adding 1 mL of alkaline copper tartrate solution and incubated in boiling water bath for 10 min and cooled; then arsenomolybdate solution was added for color stabilization. Optical density of each sample with reaction mixture was taken at 620 nm in a spectrophotometer (Shimadzu, Japan). One unit of enzyme activity was defined as the amount of enzyme that liberates 1.0 μg of glucose min/mL.

2.3. Biomass Determination. Bacterial cells in broth were harvested by centrifugation (10000 rpm for 10 min at 4°C), washed with distilled water, and dried in an oven at 80°C until reaching a constant weight. The biomass was reported in the form of dry cell mass (g/L).

2.4. Optimization of Physicochemical and Nutritional Parameters for Xylanase Production. The various process parameters influencing xylanase production were optimized individually and independently of the others. The optimized conditions were subsequently used in all the experiments in sequential order. For the optimization, the basal medium was inoculated and incubated at different temperatures, namely, 35, 40, 45, 50, 55, 60, 65, 70, 75, and 80°C under the standard assay conditions. The samples were withdrawn at every 8 h interval up to 72 h to study the effect of incubation period. The influence of pH on the enzyme activity was determined by measuring the enzyme activity at varying pH values ranging from 4.0 to 11.0 at 55°C using different suitable buffers at concentration of 100 mM citrate buffer (pH 4.0–6.0, 1 M), phosphate buffer (7.0-8.0), Tris-HCl buffer (pH 8.0-9.0), and glycine-NaOH (10–11.0) under standard assay conditions. The growth medium was supplemented with different carbon sources, namely, fructose, glucose, lactose, soluble starch, sucrose, birchwood xylan, sugarcane bagasse, wheat bran, rice bran, rice husk, and maize bran (at the level of 2%, w/v). Different organic nitrogen sources (beef extract, gelatin, casein, malt extract, peptone, and yeast extract, 0.5% w/v) and inorganic nitrogen sources (sodium nitrate, ammonium nitrate, ammonium chloride, potassium nitrate, ammonium sulphate, and urea, 0.5% w/v) were also used for enzyme production. Thereafter, optimized carbon and nitrogen sources were further optimized at different concentrations.

2.5. Effect of Metal Ions on Enzyme Activity and Stability. The effect of various metal ions on enzyme activity was investigated by using $FeSO_4$, $CaCl_2$, NaCl, $MgCl_2$, $MnCl_2$, $ZnSO_4$, $CuSO_4$, $CoCl_2$, $HgCl_2$, and $NiCl_2$ at a final concentration of 5 mM and 10 mM. The enzyme was incubated with different metals at 55°C for 1 h to study metal ion stability of the enzyme and assayed under standard assay conditions. The enzyme activity was measured by conducting the reaction at temperature 55°C and pH 7.0. The activity of the enzyme was considered as 100% under standard assay conditions.

2.6. Effect of Organic Solvent on Xylanase Stability. Cell free supernatant having maximum xylanase activity was filtered with nitrocellulose membrane (pore size 0.22 μm) and incubated with 30% (v/v) of different organic solvents, namely, *n*-dodecane, *n*-decane, isooctane, *n*-octane, xylene, *n*-hexane, *n*-butanol, cyclohexane, *n*-heptane, benzene, toluene, ethanol, methanol, and propanol for 7 days in screw crapped tubes at 55°C and 120 rpm. The residual xylanase activity was estimated against the control, in which solvent was not present.

2.7. Characterization of Crude Enzyme

2.7.1. Effect of Temperature on Enzyme Activity and Stability. The influence of temperature on activity of xylanase was studied by incubating the reaction mixture at different temperatures (35–100°C). The enzyme was incubated at different temperatures, 35–100°C, for 1 h to study the stability of the enzyme. The residual xylanase activity was determined by

performing the reaction at temperature 55°C and pH 7.0. The activity of the enzyme was considered as 100% under standard assay conditions.

2.7.2. Effect of pH on Enzyme Activity and Stability. The effect of pH on xylanase activity was measured in the pH range of 4 to 10, using the appropriate buffers at concentration of 100 mM (4.0–6.0, sodium acetate; 6.0–8.0, sodium phosphate; 8.0–10.0, Tris-HCl) under standard assay conditions. To evaluate the stability as a function of pH, 100 μL of the purified enzyme was mixed with 100 μL of the buffer solutions and incubated at 55°C for 1 h; then, aliquots of the mixture were taken to determine the residual xylanase activity (%) under standard assay conditions.

2.8. Statistical Analysis. Each experiment was performed thrice in triplicate, and mean standard deviation for each experimental result was calculated using the Microsoft Excel.

3. Results and Discussion

3.1. Isolation, Screening, and Identification of Thermosolvent Tolerant Xylanase Producing Bacterial Cultures. Sixty (60) bacterial isolates producing variable xylanolytic zones on birchwood xylan agar plates stained with Congo-Red solution followed with sodium chloride solution were studied. The zones of clearance by isolates reflect their extent to xylanolytic activity. Those having clearance zone greater than >1.0 cm were considered as significant isolates. Among 60 bacterial isolates, 35 bacterial isolates exhibited good xylanase activities which were reassessed by loading their culture broth in the wells on birchwood xylan agar plates which stained with Congo-Red solution followed with sodium chloride solution (pH 7.0). The culture broth having good xylanase activity cleared more than >1.0 cm zone within 4-5 h of incubation at 55°C, thereby indicating an extracellular nature of the xylanase. The isolate RSPP-15, showing maximum clearance zone diameter, was selected for further studies.

The efficient strain RSPP-15 was rod-shaped, Gram-positive, motile, aerobe, and facultative in nature. It gave positive results for acetylmethylcarbinol, catalase, and oxidase test. It grew over a wide range of pH (4.0–11), temperatures (10–85°C), and sodium chloride concentrations (0.0–12%) and was able to hydrolyze gelatin, casein, starch, and Tween 20, 40, and 80. It produced acid (acetic and lactic acid) from glucose, xylose, mannitol, and arabinose. It gave positive test for citrate utilization and nitrate reduction. The strain was halotolerant as it grew in the presence of 0.0–12% sodium chloride. On account of morphological and biochemical characteristics, it was identified as *Bacillus* sp. by MTCC MTECH, Chandigarh (India). Analysis of 16S rDNA sequence revealed its 99.3% homology with *Bacillus vallismortis* strains, and it was designated as *Bacillus vallismortis* RSPP-15. The 16S rDNA sequence was submitted to GenBank [JQ: 619483]. The strain RSPP-15 was in the same cluster of phylogenetic tree (Figure 1) with different strains of *Bacillus vallismortis*. However, the 16S rDNA sequence analysis indicates that it is a different and novel strain of *Bacillus vallismortis*.

3.2. Effect of Temperature on Xylanase Production. Influence of temperature on xylanase production in submerged fermentation is one of the important parameters. Figure 2 depicted that the maximum enzyme production (560 U/mL) was obtained at 55°C with 2.3 g/L biomass production while minimum (119.8 U/mL) production was observed at 35°C. It retained its 80% activity at 75°C. Similar results for optimum temperature for xylanase activity of *Bacillus aerophilus* KGJ2 have been reported by Gowdhaman et al. [19]. Xylanase with similar temperature optima had been reported from *Bacillus licheniformis* in the broad range of 40°C to 100°C [20]. Our observations showed that xylanase from *Bacillus vallismortis* RSPP-15 could be useful for industrial applications at the temperature range of 35–70°C. Most of workers have reported that xylanase of *Bacillus* sp. retained its 100% activity at 70–80°C [8, 21]. Thermal stabile xylanase finds potential applications in many industries [22]. Xylanase enzyme produced by *B. vallismortis* RSPP-15 shows interesting characteristics and properties and it appears to be a prospective candidate for application in feed and food industries.

3.3. Effect of Different Incubation Periods on Xylanase Production. Just after optimization of temperature for xylanase production in the liquid medium, incubation period was optimized for enzyme production. The results clearly indicated that *B. vallismortis* RSPP-15 shows maximum 689.2 U/mL enzyme production with 2.3 g/L biomass production within 48 h of incubation (Figure 3). Further increase in the incubation period did not increase the enzyme production but the stability of enzyme is 87% in 72 h. Similarly, Nagar et al. [23] and Kamble and Jadhav [24] reported that the highest enzyme titer from other *Bacillus* spp. was recorded at 48 h and 72 h. In contrast to our results, Kumar et al. [25] reported that xylanase production by *B. pumilus* VLK-1 was maximum (29318 IU/g) in 96 h, after which a gradual decrease was observed. It may be due to denaturation or decomposition of xylanase owing to interaction with other components in the medium, as it is reported elsewhere [24]. Incubation time depends on the characteristics of the culture, growth rate, and enzyme production. Thus our strain produced xylanase within 48 h of incubation and it is thus better than reported by the other workers mentioned above.

3.4. Effect of Initial pH on Xylanase Production. Initial pH of the medium is playing a vital role in enzyme production. To study the effect of initial pH on xylanase production, medium was adjusted using different buffers. It was observed that the maximum xylanase production (756.9 U/mL) with 2.5 g/L biomass production by strain *B. vallismortis* RSPP-15 was achieved at pH 7.0. Xylanase production was also remarkable at pH 6.0–9.0, while the production was less at pH 10.0-11.0 (Figure 4). The enzyme retained its 89% activity at pH 9.0, indicating an alkaliphilic nature of the *B. vallismortis* RSPP-15. Similar pH optimum for xylanase production from *Bacillus* sp. was reported by Guha et al. [26].

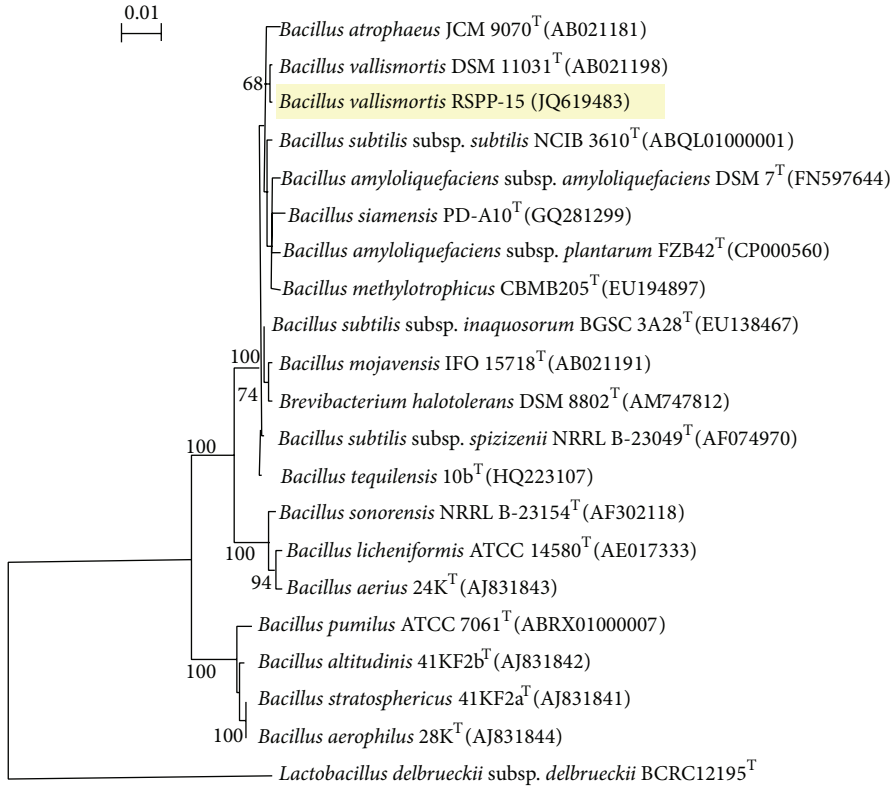

Figure 1: Phylogenetic tree showing relation between strain RSPP-15 and other *Bacillus* strains.

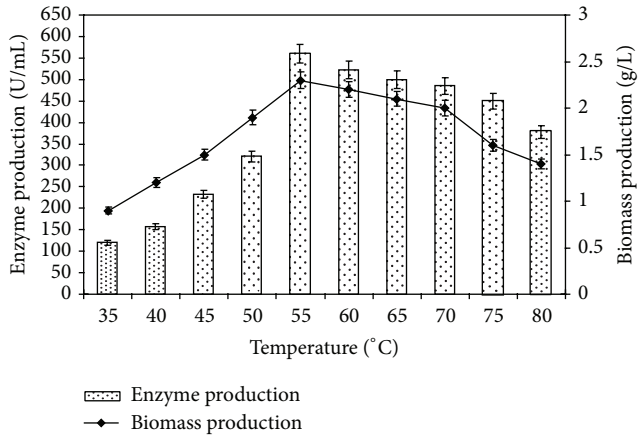

Figure 2: Effect of temperature on xylanase production. The flasks were inoculated with culture in the medium and were incubated at different temperatures (35–80°C) for 48 h at pH 7.0. For enzyme activity reaction mixture was incubated at 55°C for 15 min and reaction was conducted as standard assay method. Error bars presented mean values of ± standard deviation of triplicates of three independent experiments.

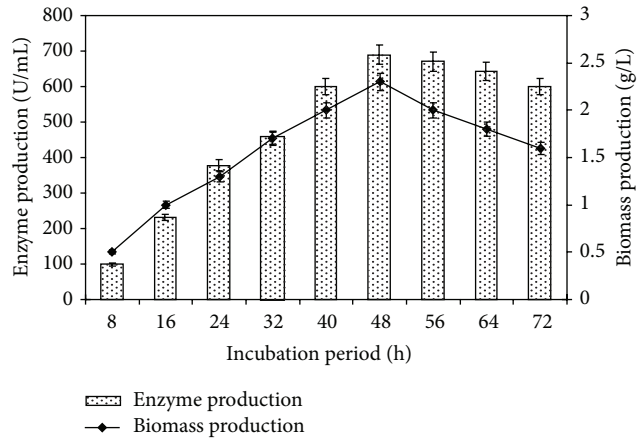

Figure 3: Effect of incubation periods on xylanase production. The flasks were inoculated with culture and were incubated at different incubation periods (8–72 h) at initial pH 7.0, 55°C. For enzyme activity the reaction was assayed at respective incubation periods at 55°C for 15 min. Error bars presented mean values of ± standard deviation of triplicates of three independent experiments.

The enzymes stable in alkaline conditions were characterized by a decreased number of acidic residues and an increased number of arginines [27]. Growth of microorganisms is vastly affected by the medium pH as pH influences the transport of nutrients as well as the enzymatic systems in microorganism [11]. If the pH of the medium is unfavorable, the growth and xylanase production may be restricted due to substrate inaccessibility [19].

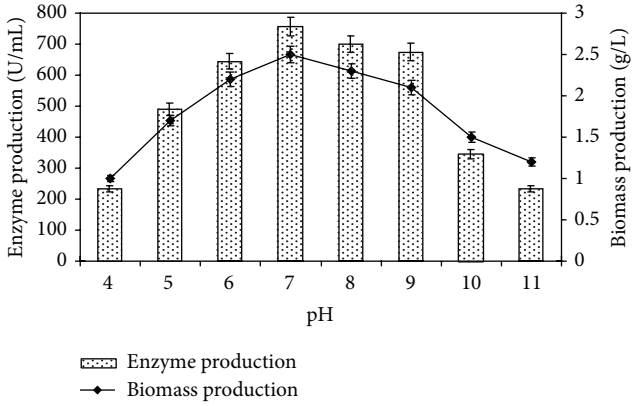

Figure 4: Effect of pH on xylanase production. The flasks were inoculated with culture and were incubated at different pH (4–11) for 48 h at 55°C. For enzyme activity the reaction was assayed at respective pH with buffers (100 mM) at 55°C for 15 min. Error bars presented mean values of ± standard deviation of triplicates of three independent experiments.

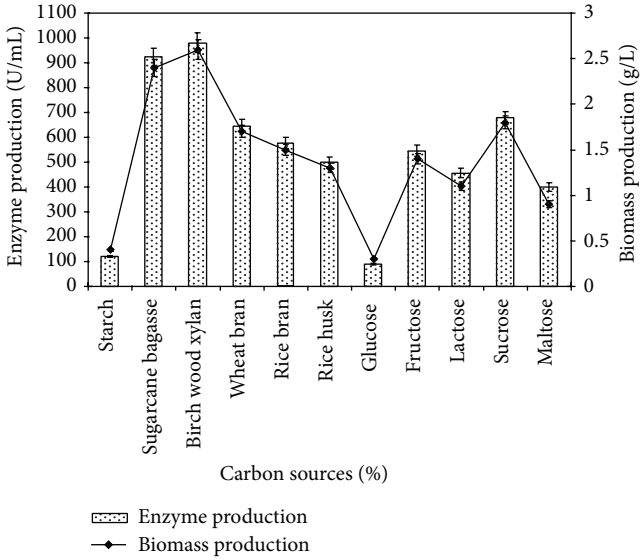

Figure 5: Effect of different carbon sources on xylanase production. Test flasks contained different carbon sources in the medium at a level of 2% (w/v). The flasks were inoculated with culture and incubated at 55°C for 48 h at pH 7.0. Error bars presented mean values of ± standard deviation of triplicates of three independent experiments.

3.5. Effect of Carbon Sources and Their Concentrations on Xylanase Production. Various carbon sources, namely, starch, sugarcane bagasse, birchwood xylan, wheat bran, rice bran, rice husk, glucose, fructose, lactose, maltose, and sucrose, at a concentration of 2.0% (w/v) were individually tested in the basal medium at their optimal temperature, incubation period, and pH to observe the effect on enzyme production by *B. vallismortis* RSPP-15. Out of these carbon sources, birchwood xylan was found the best for xylanase production (980 U/mL) with 2.6 g/L biomass production followed by sugarcane bagasse (923 U/mL) within 48 h (Figure 5). Similarly, Garg et al. [28] and Guha et al. [26] reported that *Bacillus halodurans* MTCC 9512 and *Bacillus* sp. gave the highest enzyme yield with birchwood xylan followed by sugarcane bagasse.

B. vallismortis RSPP-15 showed considerable enzyme production with fructose, lactose, and sucrose (Figure 5). Several workers also reported that most of *Bacillus* spp. showed considerable enzyme production in the presence of sucrose, fructose, and lactose [19, 24]. *B. vallismortis* RSPP-15 also showed considerable enzyme production in the presence of wheat bran, rice bran, and maize bran (Figure 5). Similar result was achieved from *Bacillus* sp. in the presence of wheat bran and rice bran as reported by Guha et al. [26]. *B. vallismortis* RSPP-15 showed minimum enzyme production in the presence of glucose (Figure 5). Garg et al. [28] also observed no xylanase production by *B. halodurans* MTCC 9512 when medium was supplemented with glucose. The production was repressed in the presence of glucose suggesting the possible regulation via catabolite repression. The expression of genes encoding extracellular hydrolytic enzymes such as xylanase is generally activated by specific substrates [29].

In another set of the experiment, different concentrations of birchwood xylan in the medium were tested for xylanase production at the same growth conditions at which carbon sources were evaluated. *B. vallismortis* RSPP-15 showed

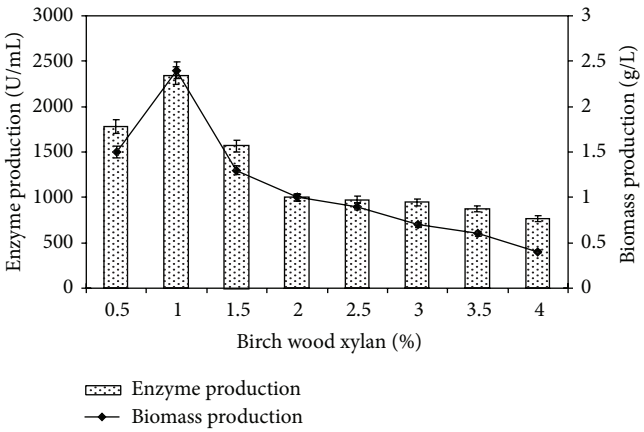

Figure 6: Effect of different concentrations of birch wood xylan on xylanase production. Test flasks contained different concentrations of birch wood xylan (0.5–4.0%, w/v) in the medium. The flasks were inoculated with culture and incubated at 55°C for 48 h at pH 7.0. Error bars presented mean values of ± standard deviation of triplicates of three independent experiments.

2340 U/mL xylanase production with 2.4 g/L biomass production at 1% birchwood xylan; above this concentration enzyme production was slightly decreased (Figure 6). Similarly, Guha et al. [26] reported that the highest xylanase activity was obtained when xylan was used at 1% concentration and enzyme level was decreased with further increase in xylan concentration, yet some other workers reported that 0.5% xylan showed maximum enzyme production [19, 24].

3.6. Effect of Nitrogen Sources on Xylanase Production. Inorganic and organic nitrogen sources, namely, peptone, beef extract, yeast extract, malt extract, gelatin, casein, urea, sodium nitrate, ammonium nitrate, potassium nitrate, ammonium sulphate, and ammonium chloride, at the rate of 0.5% (w/v) were used in the basal medium for xylanase production (Figure 7). The enzyme production by the isolate was maximum in beef extract amended medium (3245 U/mL) followed by peptone, ammonium chloride, and ammonium sulphate. Similar observations were also reported by Swarnalaxmi et al. [20] and Gowdhaman et al. [19]. Haddar et al. [30] also reported that ammonium chloride favored growth and enzyme secretion by bacterial strains followed by yeast extract and soy peptone. Other nitrogen sources like urea showed inhibitory effect on xylanase production of *B. vallismortis* RSPP-15. Gowdhaman et al. [19] have already reported that supplementation of urea at 5 g/L concentration resulted in a decrease in xylanase production.

Different concentrations of beef extract (0.1, 0.2, 0.3, 0.4, 0.5, 0.6, 7.0, 8.0, 9.0, and 1.0%, w/v) in the medium were also tested for xylanase production at the same growth condition at which nitrogen sources were evaluated. *B. vallismortis* RSPP-15 showed higher enzyme production (3768 U/mL) with 2.6 g/L biomass production at 0.3% beef extract concentration; increasing further the concentration, enzyme production was reduced (Figure 8).

3.7. Effect of Metal Ions on Enzyme Activity and Stability. In this experiment, maximum xylanase production was reported in the presence of Co^{2+} (10 mM) followed by Ca^{2+}, Mg^{+2}, Zn^{+2}, and Fe^{+3}. In this experiment, maximum enzyme activity (3768 U/mL) considered 100% xylanase activity. Results suggest that xylanase showed maximum relative activity (181.5, 153.7, 147.2, 133.6, and 127.9%) and stability (138.2, 119.3, 113.9, 109, and 104.5%) in the presence of Co^{2+}, Ca^{2+}, Mg^{+2}, Zn^{+2}, and Fe^{+3} ions, respectively. Some other researchers also reported that Co^{2+}, Ca^{2+}, Mg^{+2}, Zn^{+2}, and Fe^{+3} ions strongly stimulated xylanase activity [31, 32]. The enzyme activities were enhanced in the presence of metal ions, which may be due to the alteration of structural conformation of the enzyme [33]. Xylanase activity was slightly inhibited by Mn^{2+} (Table 1). Xylanase was strongly inhibited in the presence of Cu^{2+} and Hg^{2+}. Similar results were observed in case of *Bacillus subtilis* [34], *Bacillus halodurans* PPKS-2 [35], and *Simplicillium obclavatum* [36]. It has been reported that the xylanase activity was inhibited by Hg^{2+} ion, which might be due to its interaction with sulfhydryl groups of cysteine residue in or close to the active site of the enzyme [37]. The inhibition of xylanase by Cu^{2+} ions could be due to competition between the exogenous cations and the protein-associated cations, resulting in decreased metalloenzyme activity.

3.8. Effect of Organic Solvents on Xylanase Stability. In another approach, the effect of various organic solvents (30%, v/v) on xylanase stability was also investigated for 7 days,

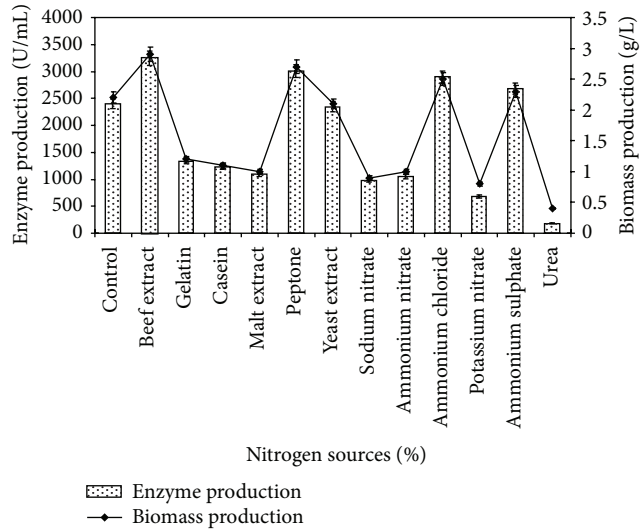

Figure 7: Effect of different nitrogen sources on xylanase production. The control flask does not contain any nitrogen sources. Test flasks contained different nitrogen sources in the medium at a level of 0.5% (w/v). The flasks were inoculated with culture and incubated at 55°C for 48 h at pH 7.0 with 1.0% birch wood xylan. Error bars presented mean values of ± standard deviation of triplicates of three independent experiments.

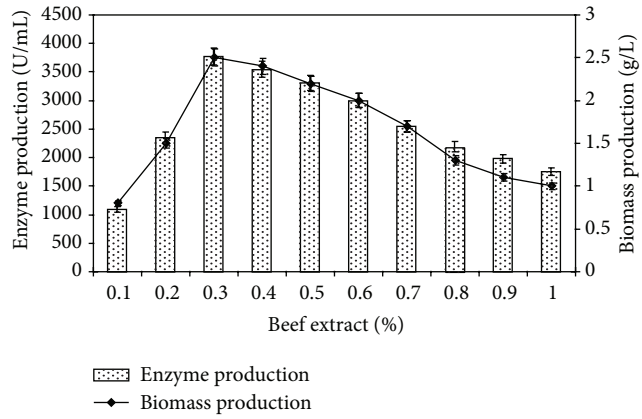

Figure 8: Effect of different concentrations of beef extract on xylanase production. Test flasks contained different concentrations of beef extract (0.1–1.0%, w/v) in the medium. The flasks were inoculated with culture and incubated at 55°C for 48 h at pH 7.0. Error bars presented mean values of ± standard deviation of triplicates of three independent experiments.

and the results are depicted in Table 2. The xylanase of *B. vallismortis* RG-01 is extraordinarily stable in the presence of all organic solvents under study. It was observed that, except benzene, methanol, and ethanol, presence of other solvents enhanced the xylanase activity. After incubation with *n*-dodecane, isooctane, *n*-decane, xylene, toluene, *n*-hexane, *n*-butanol, and cyclohexane, the xylanase activity increased to 230.8, 137.7, 219.8, 107, 190.5, 194.7, 179.3, and 111.6%, respectively. The presence of benzene, methanol, and ethanol marginally reduced the xylanase with residual activities of

Table 1: Effect of metal ions on enzyme activity and stability.

Metal ions	Concentration (mM)	Residual activity (%)	
		Activity	Stability
Control		100.0	100.0
$CaCl_2$	5	104.4	135.2
	10	153.7	119.3
$NiCl_2$	5	101.8	99.1
	10	110.4	100.5
$FeSO_4$	5	112.2	126.3
	10	127.9	104.5
$MgCl_2$	5	110.9	125.6
	10	147.2	113.9
$CuSO_4$	5	62.4	53.5
	10	50.7	42.5
$HgCl_2$	5	41	47.7
	10	21	29
$MnCl_2$	5	90.9	83.9
	10	85.9	80.2
NaCl	5	106.2	101.3
	10	121.9	115.9
$ZnSO_4$	5	102.9	128.4
	10	133.6	109
$CoCl_2$	5	125.4	107.8
	10	181.5	138.2

Enzyme activity was determined at 55°C in the presence of metal ions in the reaction mixture directly and for stability enzyme was preincubated with different metal ions at 55°C for 1 h and assayed as standard assay method. The enzyme activity without incubation with metal ions was taken as 100%. Mean standard deviation for all the values is <±5.0%.

Table 2: Stability of xylanase in the presence of various organic solvents.

Organic solvents (30%)	log *P*	Residual activity (%)							
		1 h	24 h	48 h	72 h	96 h	120 h	144 h	168 h
Methanol	−0.76	100	119.2	131.1	118.5	110.3	101.9	94.5	88.4
Isopropanol	−0.28	89	95.7	100	90.6	87	80	77.9	73.8
Ethanol	−0.24	89	93.6	97.9	90.2	89.2	85.5	80.8	78.3
Benzene	2.13	90	93	100	100	98	94	90	85.8
Cyclohexane	3.3	90	95	100	111.6	101.5	93	92	91.6
Acetone	−0.23	95.3	100.4	100.5	95.4	90	90	83	80
Butanol	−0.80	90.6	179.3	154.7	124.5	112.5	100.8	96.7	90
Toluene	2.5	96.7	190.5	170.6	149.9	100.7	99.0	90.6	90
Isooctane	2.9	97.5	137.7	116.8	102.5	100.6	92.7	90.5	87.9
Xylene	3.1	90	100	107	103	100	96	90	86
Hexane	3.6	98	179	194.7	179.8	147.5	119.9	104	95
n-Decane	5.6	99.8	189.3	219.8	208.4	160.9	137.8	107	90.0
n-Dodecane	6.0	100.8	207.5	230.8	219.5	200.6	160.9	140.0	100.0

Enzyme was preincubated with different organic solvents at a concentration of 30% (v/v) at 55°C for different time periods and assayed as standard assay method. The enzyme activity without incubation with organic solvent was taken as 100%. Mean standard deviation for all the values is <±5.0%.

85.8, 88.4, and 78.3%, respectively. An organic solvent stable alkaline protease has been reported from *P. aeruginosa* PseA by Gupta and Khare [38]. After 10 days of incubation with organic solvent (25%, v/v), the residual protease activities were 112, 75, 98, 92, 97, 94, 75, 90, 96, 102, and 104% in the presence of ethanol, 1-butanol, benzene, toluene, xylene, cyclohexane, hexane, heptane, isooctane, *n*-decane, and *n*-dodecane, respectively. Abusham et al. [39] also reported a protease of *B. subtilis* strain rand with enhanced activity in the presence of organic solvents (25%, v/v) of log *P* value reduced the protease activity by 37–65%. It is therefore evident from our study that xylanase of *Bacillus vallismortis*

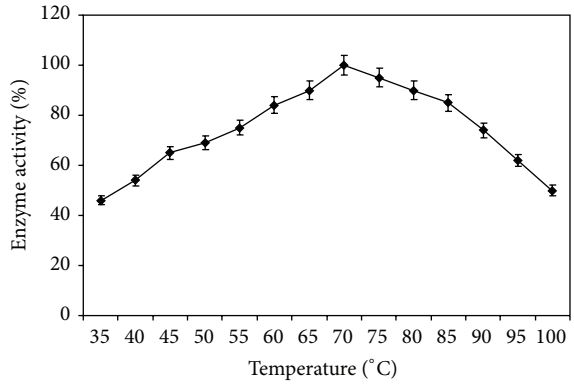

Figure 9: Effect of temperature on enzyme activity. For enzyme activity reaction mixture was incubated at different temperatures (35–105°C) for 1 h and reaction was conducted as standard assay method.

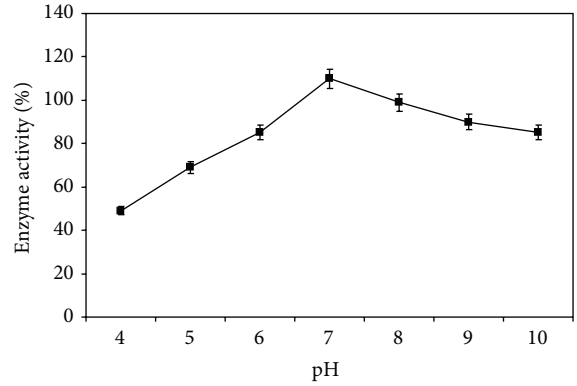

Figure 10: Effect of different pH on enzyme activity. For enzyme activity the reaction was assayed at respective pH and enzyme was preincubated with buffers (100 mM, in ratio 1 : 1) of different pH (4–10) at 55°C for 1 h and assayed by standard assay method.

RG-01 is remarkably stable in the presence of broad range of hydrophilic as well as hydrophobic organic solvents employed in this study. Hence, it is qualified for use in biotechnological applications and bioethanol production, and all its properties make it a useful tool for biobleaching in pulp and paper industry [40].

3.9. Characterization of Crude Enzyme

3.9.1. Effect of Temperature and pH on Enzyme Activity. Influence of temperature on xylanase activity is one of the important parameters. Figure 9 showed that more than 65–90% of the maximum activity was retained between 45°C to 65°C and about 100% activity was retained at 70°C. Xylanase with similar temperature optima had been reported from *Bacillus aerophilus* KGJ2 in the broad range of 30°C to 70°C [19]. Our observations showed that the xylanase from *Bacillus vallismortis* RG-01 could be useful for industrial applications at the temperature range of 45°C–70°C.

The effect of pH on enzyme activity was examined by evaluating the enzyme activity at varying pH values ranging from 4.0 to 10.0 using different suitable buffers. The crude enzyme of *Bacillus vallismortis* RSPP-15 was active at a wide range of pH from 5.0 to 9.0. It is observed that the highest xylanase activity was established at pH 7.0; on the other hand, it was found to be most stable at pH 7.0-8.0 (Figure 10). Similar pattern of pH optimum for enzyme activity was also found in *Bacillus* sp. NTU-06 [41]. Above and below of these pH values, xylanase activity decreased rapidly. Xylanase from *Bacillus vallismortis* RSPP-15 was stable in a range of pH 5.0–9.0 and at pH 10.0 approximately 85% of its activity was retained (Figure 10). The enzymes stable in alkaline conditions were characterized by a decreased number of acidic residues and an increased number of arginines [27].

4. Conclusion

A thermosolvent stable xylanase is produced by a novel isolate *B. vallismortis* RSPP-15. The organism appears to have greater potential for enhanced enzyme production through optimization of nutritional and physical parameters. Tolerance against organic solvent and metal ions facilitates its use for various processes under stressed conditions. Owing to its thermotolerant nature, its xylanase may have potential uses in industries such as detergent, food, pharmaceutical, leather, agriculture, kraft pulp prebleaching process, and molecular biology techniques.

Conflict of Interests

The authors declare that they have no conflict of interests.

Acknowledgment

Financial assistance by Council of Science and Technology, UP, India, is greatly acknowledged by Rajeeva Gaur, Soni Tiwari, Priyanka Rai, and Versha Srivastava.

References

[1] A. Sunna and G. Antranikian, "Xylanolytic enzymes from fungi and bacteria," *Critical Reviews in Biotechnology*, vol. 17, no. 1, pp. 39–67, 1997.

[2] A. Sanghi, N. Garg, J. Sharma, K. Kuhar, R. C. Kuhad, and V. K. Gupta, "Optimization of xylanase production using inexpensive agro-residues by alkalophilic Bacillus subtilis ASH in solid-state fermentation," *World Journal of Microbiology and Biotechnology*, vol. 24, no. 5, pp. 633–640, 2008.

[3] J. Kiddinamoorthy, A. J. Anceno, G. D. Haki, and S. K. Rakshit, "Production, purification and characterization of *Bacillus* sp. GRE7 xylanase and its application in eucalyptus Kraft pulp biobleaching," *World Journal of Microbiology and Biotechnology*, vol. 24, no. 5, pp. 605–612, 2008.

[4] U. A. Okafor, V. I. Okochi, B. M. Onyegeme-okerenta, and S. Nwodo-Chinedu, "Xylanase production by *Aspergillus niger* ANL 301 using agro—wastes," *African Journal of Biotechnology*, vol. 6, no. 14, pp. 1710–1714, 2007.

[5] S. G. Nair, R. Sindhu, and S. Shashidhar, "Purification and biochemical characterization of two xylanases from *Aspergillus*

sydowii SBS 45," *Applied Biochemistry and Biotechnology*, vol. 149, no. 3, pp. 229–243, 2008.

[6] S. Ninawe, M. Kapoor, and R. C. Kuhad, "Purification and characterization of extracellular xylanase from *Streptomyces cyaneus* SN32," *Bioresource Technology*, vol. 99, no. 5, pp. 1252–1258, 2008.

[7] W. Liu, W. Zhu, Y. Lu, J. Kong, and G. Ma, "Production, partial purification and characterization of xylanase from *Trichosporon cutaneum* SL409," *Process Biochemistry*, vol. 33, no. 3, pp. 331–336, 1998.

[8] A. Khasin, I. Alchanati, and Y. Shoham, "Purification and characterization of a thermostable xylanase from *Bacillus stearothermophilus* T-6," *Applied and Environmental Microbiology*, vol. 59, no. 6, pp. 1725–1730, 1993.

[9] M. Ratto, K. Poutanen, and L. Viikari, "Production of xylanolytic enzymes by an alkalitolerant *Bacillus circulans* strain," *Applied Microbiology and Biotechnology*, vol. 37, no. 4, pp. 470–473, 1992.

[10] K. R. Lundgren, L. Bergkvist, S. Hogman et al., "TCF Mill Trial on softwood pulp with Korsnas thermostable and alkaline stable xylanase T6," *FEMS Microbiology Reviews*, vol. 13, no. 2-3, pp. 365–368, 1994.

[11] S. Subramaniyan, P. Prema, and G. S. Sandhia, "Control of xylanase production without protease activity in *Bacillus* sp. by selection of nitrogen source," *Biotechnology Letters*, vol. 23, no. 5, pp. 369–371, 2001.

[12] S. Nagar, A. Mittal, D. Kumar, L. Kumar, R. C. Kuhad, and V. K. Gupta, "Hyper production of alkali stable xylanase in lesser duration by *Bacillus pumilus* SV-85S using wheat bran under solid state fermentation," *New Biotechnology*, vol. 28, no. 6, pp. 581–587, 2011.

[13] M. Kapoor, Q. K. Beg, B. Bhushan, K. Singh, K. S. Dadhich, and G. S. Hoondal, "Application of an alkaline and thermostable polygalacturonase from *Bacillus* sp. MG-cp-2 in degumming of ramie (*Boehmeria nivea*) and sunn hemp (*Crotalaria juncea*) bast fibres," *Process Biochemistry*, vol. 36, no. 8-9, pp. 803–807, 2001.

[14] K. Ratanakhanokchai, K. L. Kyu, and M. Tanticharoen, "Purification and properties of a xylan-binding endoxylanase from alkaliphilic *Bacillus* sp. strain K-1," *Applied and Environmental Microbiology*, vol. 65, no. 2, pp. 694–697, 1999.

[15] M. C. Srinivasan and M. V. Rele, "Microbial xylanases for paper industry," *Current Science*, vol. 77, no. 1, pp. 137–142, 1999.

[16] R. N. Creig and G. J. Holt, *Bergey's Manual of Systematic Bacteriology*, Williams and Willkins, London, UK, 1984.

[17] N. Nelson, "A photometric adaptation of the Somogyi method for the determination of glucose," *The Journal of Biology and Chemistry*, vol. 153, pp. 375–380, 1944.

[18] M. Somogyi, "Notes on sugar determination," *The Journal of Biological Chemistry*, vol. 195, no. 1, pp. 19–23, 1952.

[19] D. Gowdhaman, G. Jeyalakshmi, K. Sugumaran, N. S. Subramanian, R. S. Santhosh, and V. Ponnusami, "Optimization of the xylanase production with the newly isolated *Bacillus aerophilus* KGJ2," *Turkish Journal of Biochemistry*, vol. 39, no. 1, pp. 70–77, 2014.

[20] G. Swarnalaxmi, T. Sathish, R. Subbha, P. Brahmaiah, and N. Hymavathi, "Palm fiber as a novel substrate for enhanced xylanase production by isolated *Aspergillus* sp. RSP-6," *Current Trend in Biotechnology Pharmacy*, vol. 2, no. 3, pp. 447–455, 2008.

[21] F. Uchino and N. Toshihiko, "A thermostable xylanase from a thermophilic acidophilic *Bacillus* sp.," *Agricultural and Biological Chemistry*, vol. 45, no. 5, pp. 1121–1127, 1981.

[22] S. Pathania, N. Sharma, and S. K. Verma, "Optimization of cellulase-free xylanase produced by a potential thermoalkalophilic *Paenibacillus* sp. N_1 isolated from hot springs of Northern Himalayas in India," *Journal of Microbiology, Biotechnology and Food Science*, vol. 2, no. 1, pp. 1–24, 2012.

[23] S. Nagar, V. K. Gupta, D. Kumar, L. Kumar, and R. C. Kuhad, "Production and optimization of cellulase-free, alkali-stable xylanase by *Bacillus pumilus* SV-85S in submerged fermentation," *Journal of Industrial Microbiology and Biotechnology*, vol. 37, no. 1, pp. 71–83, 2010.

[24] R. D. Kamble and A. R. Jadhav, "Optimization and scale up of cellulase-free xylanase production in solid state fermentation on wheat bran by *Cellulosimicrobium* sp. MTCC 10645," *Jordan Journal of Biological Sciences*, vol. 5, no. 4, pp. 289–294, 2012.

[25] V. Kumar, P. Syal, and T. Satyanarayana, "Highly thermo-halo-alkali-stable β-1,4-endoxylanase from a novel polyextremophilic strain of *Bacillus halodurans*," *Bioprocess and Biosystems Engineering*, vol. 36, no. 5, pp. 555–565, 2013.

[26] S. Guha, S. Bhutty, S. M. P. Khurana, and U. K. Kohli, "Optimization of cultural conditions for production of thermo-alkali tolerant xylanase from *Bacillus* sp.," *International Journal of Research in Pure and Applied Microbiology*, vol. 3, no. 4, pp. 116–120, 2013.

[27] N. Hakulinen, O. Turunen, J. Jänis, M. Leisola, and J. Rouvinen, "Three-dimensional structures of thermophilicβ-1,4-xylanases from *Chaetomium thermophilum* and *Nonomuraea flexuosa*: comparison of twelve xylanases in relation to their thermal stability," *European Journal of Biochemistry*, vol. 270, no. 7, pp. 1399–1412, 2003.

[28] S. Garg, R. Ali, and A. Kumar, "Production of alkaline xylanase by an alkalo-thermophilic bacteria, *Bacillus halodurans*, MTCC 9512 isolated from dung," *Current Trends in Biotechnology and Pharmacy*, vol. 3, no. 1, pp. 90–96, 2009.

[29] S. Rodríguez, I. R. Santamaría, J. M. Fernández-Ábalos, and M. Díaz, "Identification of the sequences involved in the glucose-repressed transcription of the *Streptomyces halstedii* JM8 xysA promoter," *Gene*, vol. 351, no. 23, pp. 1–9, 2005.

[30] A. Haddar, D. Driss, F. Frikha, S. Ellouz-Chaabouni, and M. Nasri, "Alkaline xylanases from *Bacillus mojavensis* A21: production and generation of xylooligosaccharides," *International Journal of Biological Macromolecules*, vol. 51, no. 4, pp. 647–656, 2012.

[31] G. Mamo, R. Hatti-Kaul, and B. Mattiasson, "A thermostable alkaline active endo-β-1-4-xylanase from *Bacillus halodurans* S7: purification and characterization," *Enzyme and Microbial Technology*, vol. 39, no. 7, pp. 1492–1498, 2006.

[32] Z. Lv, J. Yang, and H. Yuan, "Production, purification and characterization of an alkaliphilic endo-β-1,4-xylanase from a microbial community EMSD5," *Enzyme and Microbial Technology*, vol. 43, no. 4-5, pp. 343–348, 2008.

[33] R. Khandeparkar and N. B. Bhosle, "Purification and characterization of thermoalkalophilic xylanase isolated from the *Enterobacter* sp. MTCC 5112," *Research in Microbiology*, vol. 157, no. 4, pp. 315–325, 2006.

[34] A. Sanghi, N. Garg, V. K. Gupta, A. Mittal, and R. C. Kuhad, "One-step purification and characterization of cellulase-free xylanase produced by alkalophilic *Bacillus subtilis* ASH," *Brazilian Journal of Microbiology*, vol. 41, no. 2, pp. 467–476, 2010.

[35] P. Prakash, S. K. Jayalakshmi, B. Prakash, M. Rubul, and K. Sreeramulu, "Production of alkaliphilic, halotolerent, thermostable cellulase free xylanase by *Bacillus halodurans* PPKS-2 using agro waste: single step purification and characterization," *World Journal of Microbiology and Biotechnology*, vol. 28, no. 1, pp. 183–192, 2012.

[36] S. Roy, T. Dutta, T. S. Sarkar, and S. Ghosh, "Novel xylanases from *Simplicillium obclavatum* MTCC 9604: comparative analysis of production, purification and characterization of enzyme from submerged and solid state fermentation," *SpringerPlus*, vol. 2, article 382, 2013.

[37] K. B. Bastawde, "Xylan structure, microbial xylanases, and their mode of action," *World Journal of Microbiology and Biotechnology*, vol. 8, no. 4, pp. 353–368, 1992.

[38] A. Gupta and S. K. Khare, "Enhanced production and characterization of a solvent stable protease from solvent tolerant *Pseudomonas aeruginosa* PseA," *Enzyme and Microbial Technology*, vol. 42, no. 1, pp. 11–16, 2007.

[39] R. A. Abusham, R. N. Z. R. A. Rahman, A. Salleh, and M. Basri, "Optimization of physical factors affecting the production of thermo-stable organic solvent-tolerant protease from a newly isolated halo tolerant *Bacillus subtilis* strain Rand," *Microbial Cell Factories*, vol. 8, article 20, 2009.

[40] F. Woldesenbet, N. Gupta, and P. Sharma, "Statistical optimization of the production of a cellulase-free, thermoalkali-stable, salt- and solvent-tolerant xylanase from *Bacillus halodurans* by solid state fermentation," *Archives of Applied Science Research*, vol. 4, pp. 524–535, 2012.

[41] C.-Y. Wang, H. Chan, H.-T. Lin, and Y.-T. Shyu, "Production, purification and characterisation of a novel halostable xylanase from *Bacillus* sp. NTU-06," *Annals of Applied Biology*, vol. 156, no. 2, pp. 187–197, 2010.

Hindawi Publishing Corporation
International Journal of Polymer Science
Volume 2015, Article ID 806791, 9 pages
http://dx.doi.org/10.1155/2015/806791

Research Article

Biodegradable Films Based on Gelatin and Montmorillonite Produced by Spreading

Manuel Fernando Coronado Jorge, Elisabete M. C. Alexandre, Christian Humberto Caicedo Flaker, Ana Mônica Quinta Barbosa Bittante, and Paulo José do Amaral Sobral

Department of Food Engineering, FZEA, University of São Paulo, Avenida Duque de Caxias Norte 225, 13635-900 Pirassununga, SP, Brazil

Correspondence should be addressed to Paulo José do Amaral Sobral; pjsobral@usp.br

Received 9 March 2015; Revised 22 May 2015; Accepted 30 May 2015

Academic Editor: Xingxun Liu

The main objective of this research was to study the properties of gelatin-based nanocomposites reinforced with the montmorillonite (MMT). The gelatin-based nanocomposites were prepared with solutions of 5 g of gelatin/100 g of film-forming solution, 0–10 g of montmorillonite/100 g of gelatin, and 30 g of glycerol/100 g of gelatin and were stored for 7 days at 58% relative humidity or in silica gel, depending on the type of assay. The reinforcement of gelatin-based nanocomposites with montmorillonite increased their thickness and decreased the moisture content. Tensile strength and Young's modulus increased revealing more resistant and rigid nanocomposites. The increase in MMT concentration slightly changed the X-ray diffraction spectra indicating some loss of crystallinity and reinforced films presented less homogeneous structures. The montmorillonite concentration had not a clear effect on the thermal properties and FTIR spectra of nanocomposites were very similar to separated compounds.

1. Introduction

The accumulation of plastic packaging in nature is one of the major environmental problems representing a big challenge in terms of waste treatment and recycling. The development of biopolymers-based films that can replace synthetic materials may be a good alternative, particularly for the food packaging industry. Polysaccharides and proteins are the main biopolymers used in the preparation of such edible and/or biodegradable films [1, 2].

Proteins are macromolecules of interest because they have a structure based on 20 different monomers (amino acid residues), allowing a wider range of functional properties (especially a high intermolecular binding potential) [3]. Gelatin has been one of the most well-studied protein based materials because of its excellent film-forming property and its usefulness as an outer film to protect food by acting as a barrier to gases, and it is produced at relatively low cost all over the world [4]. Gelatin is a protein with the ability to form a tridimensional network, with crystalline intermolecular linking zones. The gelatin gel formation involves the change from a disorganized state to a more arranged state, formed by triple-helix structures typical of collagen in its native state. This structure and physical properties of the gels are a result of the degree of formation of microcrystalline junctions [5].

Gelatin-based films usually present good mechanical resistance and high elasticity but are also sensitive to environmental conditions, as relative humidity, and are affected by several factors such as pH, heat treatment, addition of plasticizers, ion concentration, protein concentration, and its molecular conformation [6]. An alternative to enhance the gelatin-based films properties that has attracted the interest of researchers is related to the reinforcement of films with nanoparticles, producing a material often called bionanocomposites or only nanocomposites [7–9]. The nanocomposites films are thin materials formed by a biopolymer matrix reinforced with a dispersed nanoscale filler. The mechanical and barrier properties are improved

mainly due to the reinforcing effect of the particles, thermal stability usually increases (the thermal expansion coefficient is reduced), and the transparency is usually retained if a perfect dispersion of nanometer-sized filler particles into polymer is achieved [10–14]. The atomic and molecular interactions can also have a significant influence on the macroscopic properties, particularly when the domain size of the load is comparable to the size of the molecule [15].

One of the most widely used nanoparticles in studies of biopolymer-based nanocomposites is the montmorillonite (MMT). MMT is a layered silicate characterized by a moderate negative surface charge [16] that displays a perfect crystalline structure, formed by a two-dimensional layer having a central octahedral sheet of aluminum oxide and magnesium oxide linked with two external silica tetrahedrons [17].

The main objective of this research was to study the properties (physical properties, phase transitions, and microstructure) of gelatin-based nanocomposites reinforced with the montmorillonite (MMT) and produced by spreading.

2. Material and Methods

2.1. Material. The biopolymer used was a pigskin gelatin (bloom 242–248; molecular weight $\approx 5.2 \times 10^4$ Da; moisture content = 9.3%) that was kindly provided by Gelita South America (São Paulo, Brazil). Glycerol (Synth) was the plasticizer and MMT nanoparticles (Nanomer clay, Aldrich, reference number 688659-500G) were the filler. Distilled water was used as solvent to prepare film-forming solutions.

2.2. Production of Nanocomposite-Forming Solutions Based on Gelatin and Montmorillonite. The nanocomposite-forming solutions (NFS) were produced from a mixture of gelatin (5 g of gelatin/100 g of NFS), MMT nanoparticles (0, 5, and 10 g of MMT/100 g of gelatin), and glycerol (30 g of glycerol/100 g of gelatin). The concentration of gelatin was fixed in 5 g of gelatin/100 g of NFS because preliminary tests revealed that nanocomposites produced with a gelatin concentration in NFS greater than 8% were not homogeneous due to the formation of agglomerates [8].

The NFS was prepared in two parallel steps. On one hand, the gelatin was hydrated in distilled water for 30 min at room temperature and then dissolved at 70°C for 30 min using a thermostatic bath (Marconi, model MA 179). On the other hand and at the same time, the MMT was hydrated at room temperature in distilled water containing the glycerol, for 40 min under magnetic agitation. Then, this dispersion was submitted to high speed agitation using a high speed homogenizer (Ultraturrax Ika, model T18 basic) at 18.000 rpm for 10 min. In order to eliminate the air bubbles formed, the dispersion was also treated in an ultrasound bath (Unique, model MaxiClean 1400) at 60°C for 10 min. After that, the MMT dispersion and the gelatin solution were homogenized under mechanical agitation (Tecnal, model TE 039) conditions for 2 min at 70°C. A control film without montmorillonite was also prepared. Three replicates of each film were prepared.

2.3. Nanocomposite Production. The nanocomposites were produced by spreading the NFS over acrylic plates (26 × 30 × 0.2 cm) using an automatic film spreader (TKB Erichsen, model Speed II). The spreading knife speed was set at 35 mm/s; the gap between the knife and the plate was 1.5 mm. The acrylic plate was maintained at 25°C [8, 9]. The nanocomposites were oven-dried for 24 h at 30°C (Marconi, MA 035).

2.4. Nanocomposite Characterization. Nanocomposites produced with and without MMT were characterized in terms of thickness, humidity, mechanical properties (tensile and puncture tests), and thermal properties after 7 days conditioning over NaBr (58% of relative humidity at 25°C). For scanning electron microscopy (SEM) analyses, film crystallinity, Fourier transform infrared (FTIR) spectroscopy, and superficial hydrophobicity assays, all samples were conditioned in desiccators containing silica gel.

All measurements were made in air-conditioned rooms at 22°C, 55 to 65% relative humidity, in triplicate.

The thickness of the nanocomposites was measured with a digital micrometer (±0.001 mm; Mitutoyo, Japan) with a 6.4 mm diameter probe, taking the average at ten different positions of each sample [18].

The moisture content of the nanocomposites was determined gravimetrically according to the ASTM standard method D644-99, by drying the samples at 105°C for 24 h (ASTM 1999).

The mechanical properties were determined by the tensile test (tensile strength—TS, elongation at break—EB, and Young's modulus—YM) and puncture tests (puncture force—PF, and puncture deformation—PD) using the TA.XT2i texturometer (TA Instruments, Surrey, UK), according to the methodology previously described by Thomazine et al. [19] and Gontard et al. [20], respectively.

For the tensile tests, samples from each nanocomposite were cut into small rectangles (15 × 100 mm) and fixed in the grips probe. The initial grip separation distance was fixed in 50 mm and the moving rate set was 0.9 mm/s. At least 15 samples from each film were tested. The tensile strength (force at the break/initial cross-sectional area) and elongation at break ($\Delta l/lo$) were calculated with the Exponent Lite Express Software v.4.0.13.0 (2007) directly from the stress-strain curves and the elastic modulus was calculated as the slope of the initial linear portion of this curve.

For the puncture test, circular samples of nanocomposites were fixed in a 52.6 mm diameter cell and perforated by a 3 mm diameter probe moving at 1 mm/s, in triplicate. The puncture force (PF, N) and the displacement of the probe (D, cm) at the perforation point were determined directly from the force-displacement curves, using the same software [18].

Thermal properties of nanocomposites were analyzed by DSC to determine the glass transition temperatures. These analyses were performed using a differential scanning calorimeter (DSC TA2010) controlled by a TA5000 system (TA Instruments, New Castle, DE, USA) and equipped with a cryogenic quench cooling accessory. The samples of nanocomposites (~10 mg) were placed in hermetically sealed aluminum TA pans and heated from −50 to 200°C at a heating rate of 5°C/min, in double run, always after cooling with

liquid nitrogen in an inert atmosphere (45 mL/min of N_2) [21]. An empty pan was used as reference. The sample weight was measured with a high resolution (±0.00001 g) balance (Ohaus, Analytical Plus). The results were analyzed using the Universal Analysis V1.7F (TA Instruments) software. The temperature where a baseline inflexion occurred was taken as the glass transition temperature. The peak temperature of the endothermic event observed in the thermogram was taken as the melting temperature.

Film crystallinity was evaluated qualitatively by measuring the X-ray diffraction (XRD) with an X-ray diffractometer (RU200B, Rigaku Rotaflex) using a Cu source, according to the method described by Angellier et al. [22].

Fourier transform infrared (FTIR) spectra were recorded using a Perkin Elmer spectrometer Spectrum One (Perkin Elmer, USA) equipped with a universal attenuated total reflectance (UATR) accessory, according to Vicentini et al. [23]. Twenty scans were coadded and recorded between 650 and 4000 cm^{-1} with a 2 cm^{-1} spectral resolution. The FTIR Spectrum Software (Perkin Elmer) was used to analyze the data.

Scanning electron microscopy (SEM) was used to analyze the superficial and internal microstructure of nanocomposites. The samples were maintained in a desiccator with silica gel under vacuum for 1 week and then mounted on an aluminum stub using a double-sided copper tape. Further, the nanocomposites were immersed in liquid nitrogen and fractured to analyze the internal microstructure. All analyses were performed using a SEM (Hitachi, Japan, model TM30000) operating at 15 kV according to Lu et al. [24].

Surface hydrophobicity characteristics of the nanocomposites were evaluated by contact angle measurements using a contact angle meter (Optical Tensiometer, Finland). A drop of ultrapure water with an estimated volume of 10 μL was deposited on the film sample surface (3 × 4 cm^2) with a precision syringe (Hamilton Gastight Syringes, USA) and immediately photographed. The Attension Theta Optical Tensiometer lite Software was used to measure the angle between the drop base (film surface in contact with the water drop) and the tangent to the drop of water. Contact angle measurements were obtained for both sides of the film.

2.5. Statistical Analyses. Experimental data were analyzed to determine whether the variances are statistically homogeneous. The results are expressed as means ± SD. Statistical comparisons were made by analysis of variance followed by Tukey's multiple range tests using the "Statistical Analysis Systems" software (version 9.2, SAS, Statistical Analysis Systems, NC, USA). A significance level was set at 0.05.

3. Results and Discussion

3.1. Thickness and Moisture Content. The average thickness and moisture content of nanocomposites obtained with 5 g of gelatin/100 g of NFS and different concentrations of MMT after 7 days of storage under 58% of relative humidity are shown in Table 1. The incorporation of MMT in gelatin-based films increased their thickness. Samples without MMT presented 0.071 ± 0.007 mm which was significantly different from 0.077 ± 0.005 and 0.080 ± 0.010 mm obtained for nanocomposites prepared with 5 and 10 g of MMT/100 g of gelatin, respectively. Jang et al. [25] used a casting technique and observed no significant effect of nanoparticles on the thickness of the films (based on gelatin and agar). However, Sothornvit et al. [26] observed that the films thickness increased with the addition of nanoparticles in whey protein isolate based composite films.

Table 1: Average thickness, moisture content, and contact angle of the films (± standard deviation) prepared with 5 g of gelatin/100 g NFS and different MMT concentrations.

MMT (g of montmorillonite/ 100 g of gelatin)	Thickness (mm)	Moisture content (%)	Angle with upper surface (°)
0	0.071 ± 0.007^a	20.4 ± 1.4^a	90.3 ± 10.7^a
5	0.077 ± 0.005^b	18.3 ± 1.1^b	94.6 ± 2.2^a
10	0.080 ± 0.010^b	17.3 ± 0.9^b	82.9 ± 8.0^a

Values with different characters differ significantly in the same column ($p < 0.05$).

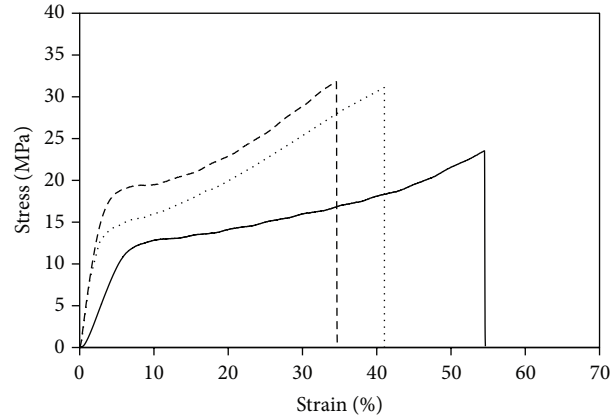

Figure 1: Typical curves for the tensile properties of the nanocomposites prepared with 5 g of gelatin/100 g of NFS and 0 (—), 5 (· · ·), and 10 (- - -) g of MMT/100 g of gelatin.

The charges of MMT decreased significantly the moisture content of the samples. Nanocomposites without MMT presented 20.4 ± 1.4% of moisture while nanocomposites prepared with 5 and 10 g of MMT/100 g of gelatin had 18.3 ± 1.1 and 17.3 ± 0.9% of moisture, respectively. This suggests that MMT decreased the sensitivity of the nanocomposites to the environment humidity. Tunç et al. [16] observed a similar behavior when studying the functional properties of wheat gluten/MMT (1, 2.5, 5, 7.5, and 10 wt%) nanocomposite processed by casting and attributed this behavior to a different structuring of protein network in the presence of MMT.

3.2. Mechanical Properties. Typical curves obtained through the tensile tests are shown in Figure 1. In general, the increase in MMT concentration slightly changed the shape of stress versus strain curves. The tensile strength and Young's modulus increased with the MMT concentration, from 23.5 ± 3.1 to

Table 2: Tensile strength (TS), Young's modulus (YM), elongation at break (EB), puncture force (PF), and puncture deformation (PD) for films prepared with 5 g of gelatin/100 g of NFS and different MMT concentrations and stored under 58% of RH.

MMT (g of montmorillonite/100 g of gelatin)	TS (MPa)	YM (MPa/%)	EB (%)	PF (N)	PD (%)
0	23.5 ± 3.1^{a}	2.1 ± 0.6^{a}	48.7 ± 5.5^{a}	15.5 ± 1.1^{a}	5.3 ± 0.5^{a}
5	31.7 ± 1.8^{b}	5.5 ± 1.0^{b}	40.4 ± 3.4^{b}	15.7 ± 0.8^{a}	7.3 ± 0.6^{b}
10	31.1 ± 1.9^{b}	6.6 ± 0.2^{c}	38.0 ± 3.4^{b}	15.6 ± 0.8^{a}	5.8 ± 1.1^{a}

Values with different characters differ significantly in the same column ($p < 0.05$).

Table 3: Glass transition temperatures, enthalpy, and fusion temperature for nanocomposites prepared with 5 g of gelatin/100 g of NFS and different MMT concentrations and stored under 58% of RH.

MMT (g of montmorillonite/100 g of gelatin)	Glass transition temperature		Enthalpy (J/g)	Fusion temperature (°C)
	T_{g_1} (°C)	T_{g_2} (°C)		
First scan				
0	-74.3 ± 1.2^{a}	43.1 ± 1.0^{a}	20.0 ± 0.6^{a}	66.8 ± 0.6^{a}
5	-73.8 ± 2.2^{a}	45.7 ± 0.5^{ab}	20.6 ± 0.5^{a}	69.1 ± 0.4^{a}
10	-75.3 ± 1.1^{a}	45.8 ± 1.3^{b}	17.7 ± 1.3^{b}	68.9 ± 1.0^{a}
Second scan				
0	-74.2 ± 3.8^{a}	31.5 ± 1.5^{a}		
5	-75.7 ± 2.2^{a}	33.6 ± 1.3^{a}		
10	-74.3 ± 4.0^{a}	32.0 ± 2.3^{a}		

Values with different characters differ significantly in the same column ($p < 0.05$).

31.7 ± 1.8 MPa (for 5% of MMT) and 31.1 ± 1.9 MPa (for 10% of MMT) and from 2.1 ± 0.6 to 5.5 ± 1.0 MPa/% (for 5% of MMT) and 6.6 ± 0.2 MPa/% (for 10% of MMT), respectively (Table 2).

The elongation at break decreased with the introduction of MMT from 48.7 ± 5.5 to 40.4 ± 3.4 and 38.0 ± 3.4% for 5 and 10% of MMT, respectively, indicating that the polymeric matrix was reinforced by the addition of nanoparticles. Cyras et al. [27] and Rao [15] also observed an improvement in mechanical properties of nanocomposites based on starch and gelatin, respectively. Rao [15] verified that a load of 5% of MMT increased by 75% the Young modulus and by 25% the tensile strength. The increase in tensile strength and Young's modulus for nanocomposites reinforced with 10% of MMT was 24% and 68%, respectively.

Bae et al. [28] observed that increasing the amount of MMT increased the tensile strength of the nanocomposites based on fish gelatin. However, Rao [15] and Cyras et al. [27] analyzed the effects of MMT concentration from 0 to 9% and verified that the highest values of tensile strength were achieved for a concentration of 5% of MMT. Similarly, Luecha et al. [29], working with concentrations of 0–10% of MMT in corn zein/montmorillonite nanocomposite, observed that maximum tensile strength for samples with 5% of MMT doubled with respect to films with 0% MMT as well as Tunç and Duman [30] studying a matrix of gluten. Jang et al. [25], working with nanocomposites of gelatin and agar, obtained the maximum tensile strength with 3% MMT. These results show that the technique so-called "casting," and by similarity the spreading technique, required a critical percentage of MMT to obtain intercalated or exfoliated structures.

In relation to results of puncture tests, the puncture force of nanocomposites prepared without MMT (15.5 ± 1.1 N) or reinforced with MMT (15.7±0.8 N for 5% MMT and 15.6± 0.8 N for 10% MMT) was not statistically different (Table 2). Puncture deformation of nanocomposites reinforced with 10 g of MMT/100 g of gelatin (5.8 ± 1.1%) was also statistically similar to control (5.3 ± 0.5%), while 5 g of MMT/100 g of gelatin led to nanocomposites with a higher puncture deformation (7.3 ± 0.6%). Moreover, when the results of mechanical properties were analyzed as a function of thickness, a clear effect of film thickness on the mechanical properties obtained by puncture tests was not observed. Sobral [31] observed that the puncture force in Tilapia myofibrillar protein films increased linearly as a function of the thickness, however without effect on puncture deformation.

3.3. Thermal Properties. In general, the DSC thermograms of all nanocomposites were very similar (Figure 2). In the first scan, the curves were typical of partially crystalline material, while in the second scan, the curves were typical of amorphous material. A phase separation between the fraction rich in glycerol and the fraction rich in gelatin was also observed. Sobral and Habitante [21] obtained similar thermograms using gelatin films, as well as Rao [15], but using gelatin-based nanocomposites.

The MMT concentration had not a clear effect on the thermal properties (Table 3). The melting enthalpy of nanocomposites reinforced with the highest MMT concentration (17.7 ± 1.3 J/g) was significantly lower than that obtained with pure gelatin films (20.0 ± 0.6 J/g) and the glass transition temperature of gelatin-rich fraction determined during first scan increased from 43.1±1.0°C in gelatin films to 45.8±1.3°C for nanocomposites with 10 g MMT/100 g gelatin. On the other hand, the glass transition temperature of the gelatin-rich fraction, determined in the second scan, was not

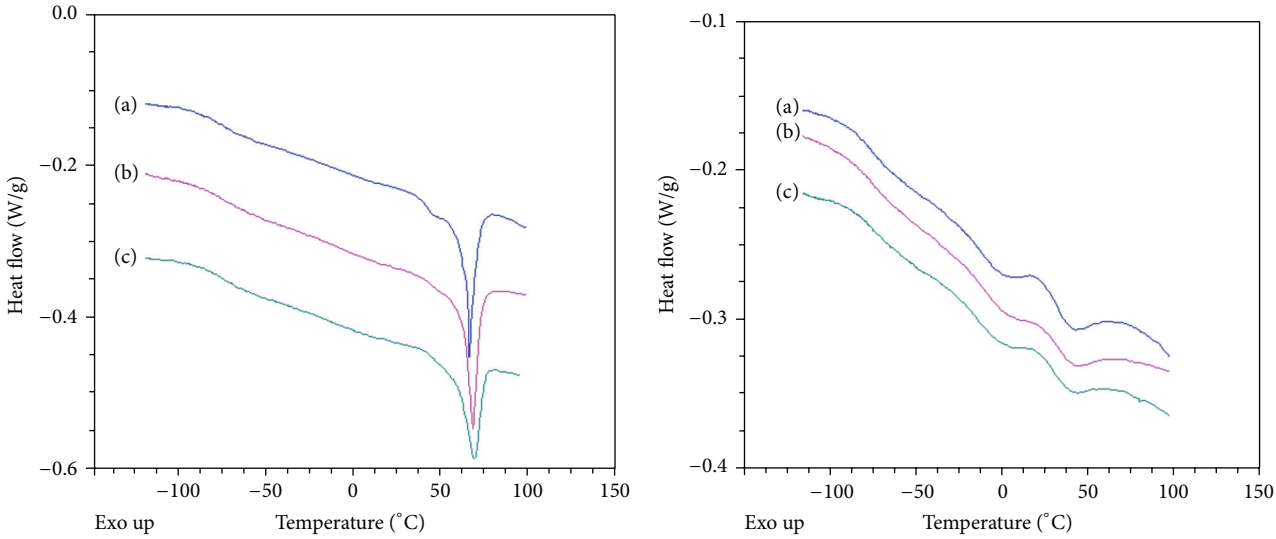

Figure 2: DSC thermograms of the first (left) and second (right) scans for 5% of gelatin nanocomposites with 0% (a), 5% (b), and 10% (c) of MMT and stored at 58% of RH.

significantly different for nanocomposites prepared with or without MMT.

A glass transition temperature of 31.5 ± 1.5°C was obtained for films without MMT and 33.6 ± 1.3 and 32.0 ± 2.3°C for nanocomposites containing 5 and 10 g MMT/100 g gelatin, respectively, while the glass transition temperature of glycerol-rich fraction was affected neither by MMT nor by scanning. Rao [15] also observed that the glass transition temperatures of the nanocomposites with gelatin and MMT were similar to the ones obtained for gelatin-based nanocomposites. Luecha et al. [29] obtained glass transition temperatures of the nanocomposites with zein montmorillonite around 36°C. Rao [15] observed that the melting temperature increased slightly with the addition of montmorillonite in gelatin-based nanocomposites.

3.4. X-Ray Diffraction. The MMT powder presented an X-ray diffraction spectrum with several types of crystals; however the most relevant ones were observed for $2\theta = 7^{\circ}$ and 20° (Figure 3(a)). Similar results were obtained by Faria et al. [32] and Cyras et al. [27] who also analyzed MMT samples and verified that the first peak occurred for 2θ between 7° and 8°. The gelatin spectrum was typical of that protein presenting a predominant peak at $2\theta = 20^{\circ}$ (Figure 3(b)).

Typical X-ray diffraction spectra of 5% gelatin-based nanocomposites with 0, 5, and 10% of MMT are shown in Figures 3(c), 3(d), and 3(e), respectively. In general, the diffraction spectra profile of the nanocomposites prepared with MMT was similar to that obtained with pure gelatin or gelatin-based nanocomposites. The increase in MMT concentration slightly changed the diffraction spectra for $2\theta = 7^{\circ}$, indicating a reduction of samples crystallinity (Figure 3(d)). Gelatin nanocomposites usually exhibit a diffraction peak in $2\theta = 7^{\circ}$, attributed to crystalline triple-helix structures of gelatin [33, 34], and a broad band at $2\theta = 20^{\circ}$, characteristic of an amorphous phase [34].

3.5. Fourier Transform Infrared Spectroscopy. The FTIR spectrum of gelatin and MMT powders (Figures 4(a) and 4(b)) showed quite distinct bands, predominantly in the region of amide III (3283 cm^{-1}), amide II (1523 cm^{-1}), and amide I (1629 cm^{-1}) for gelatin and in the region of carbon and hydroxyl interaction (800–1100 cm^{-1}) for MMT that should be associated with stretch of Si-O [35].

The FTIR spectra of all nanocomposites (control and both concentrations of MMT) were similar (Figures 4(c), 4(d), and 4(e)), although a slight displacement of the bands was observed in relation to the nanocomposites formed without MMT. The concentration of MMT had no impact on the signals of band amide III (3286–3289 cm^{-1}), amide II (1538–1548 cm^{-1}), or amide I (1630–1633 cm^{-1}).

Comparing FTIR spectra of nanocomposites with the FTIR spectrum of MMT powder, it was observed that the peak that appeared quite pronounced at 979 cm^{-1} in the MMT spectrum did not appear in the nanocomposite. However, a peak between 1034 and 1035 cm^{-1} in the spectra of nanocomposites prepared without MMT was observed, which decreased to 1029-1030 cm^{-1} for the nanocomposites with 10 g of montmorillonite/100 g of gelatin. The peaks observed at 921 cm^{-1} may be due to the stretch of COH (plasticizer) or Si–O (the nanoparticle). Similar spectra were observed by Silva et al. [36].

3.6. Scanning Electronic Microscopy. The gelatin nanocomposites without MMT showed a homogeneous, dense, and cohesive internal structure (Figure 5). The incorporation of MMT led to nanocomposites with internal structures less smooth, probably due to the formation of gelatin agglomerates [8]. This effect was more evident for the highest concentrations of MMT.

The incorporation of MMT also had impact on the structure of the film surfaces, the one in contact with the drying air and that in contact with the supporting acrylic

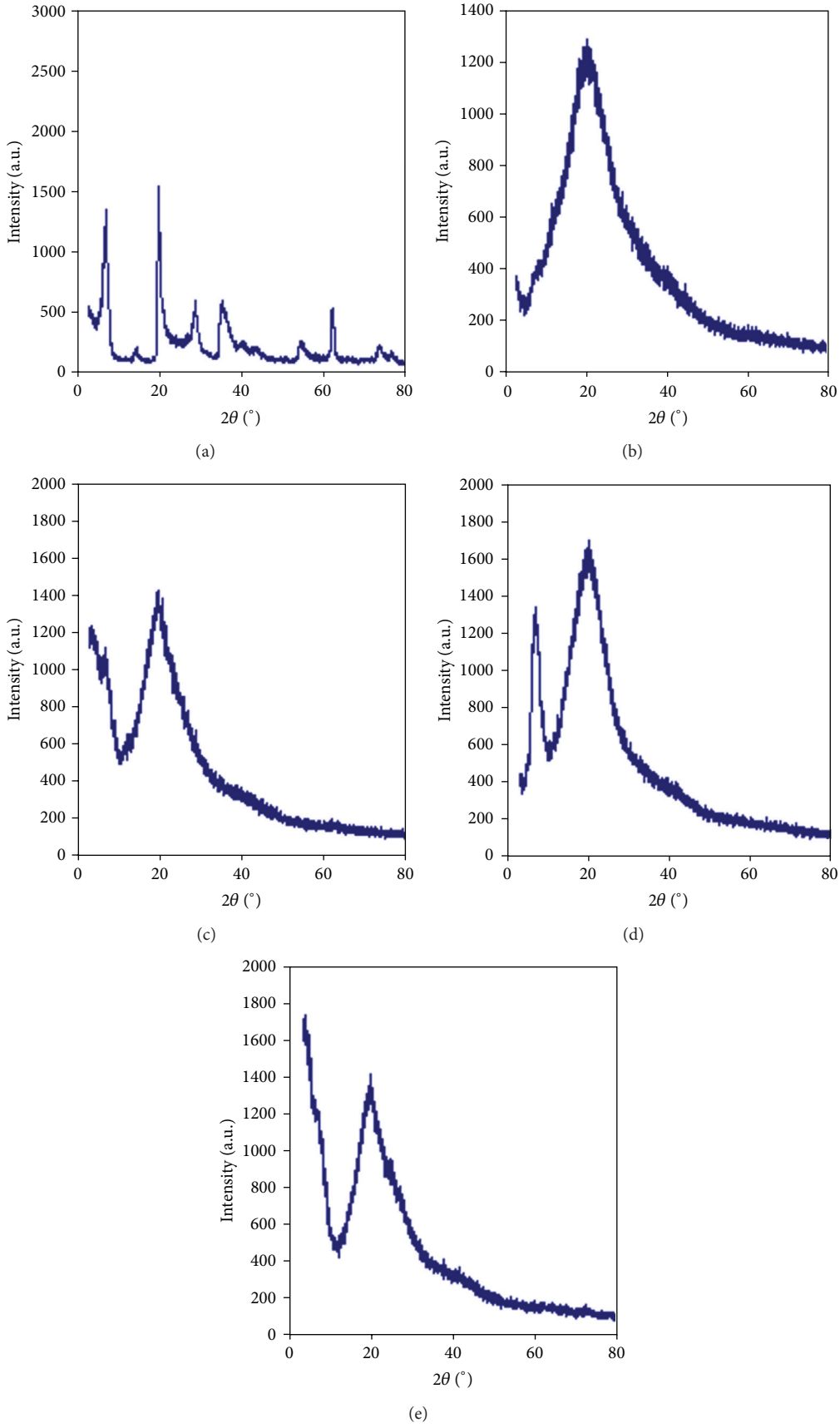

Figure 3: X-ray diffractograms of MMT (a), of gelatin (b), and of 5% gelatin-based nanocomposites with (c) 0%, (d) 5%, and (e) 10% of MMT.

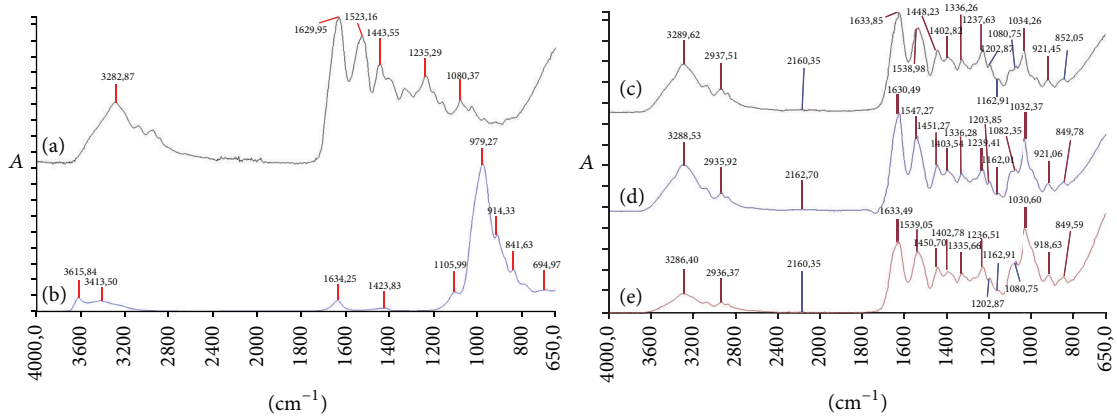

FIGURE 4: FTIR spectra of (a) gelatin and (b) MMT powder and 5% of gelatin-based nanocomposites prepared with (c) 0%, (d) 5%, and (e) 10% of MMT.

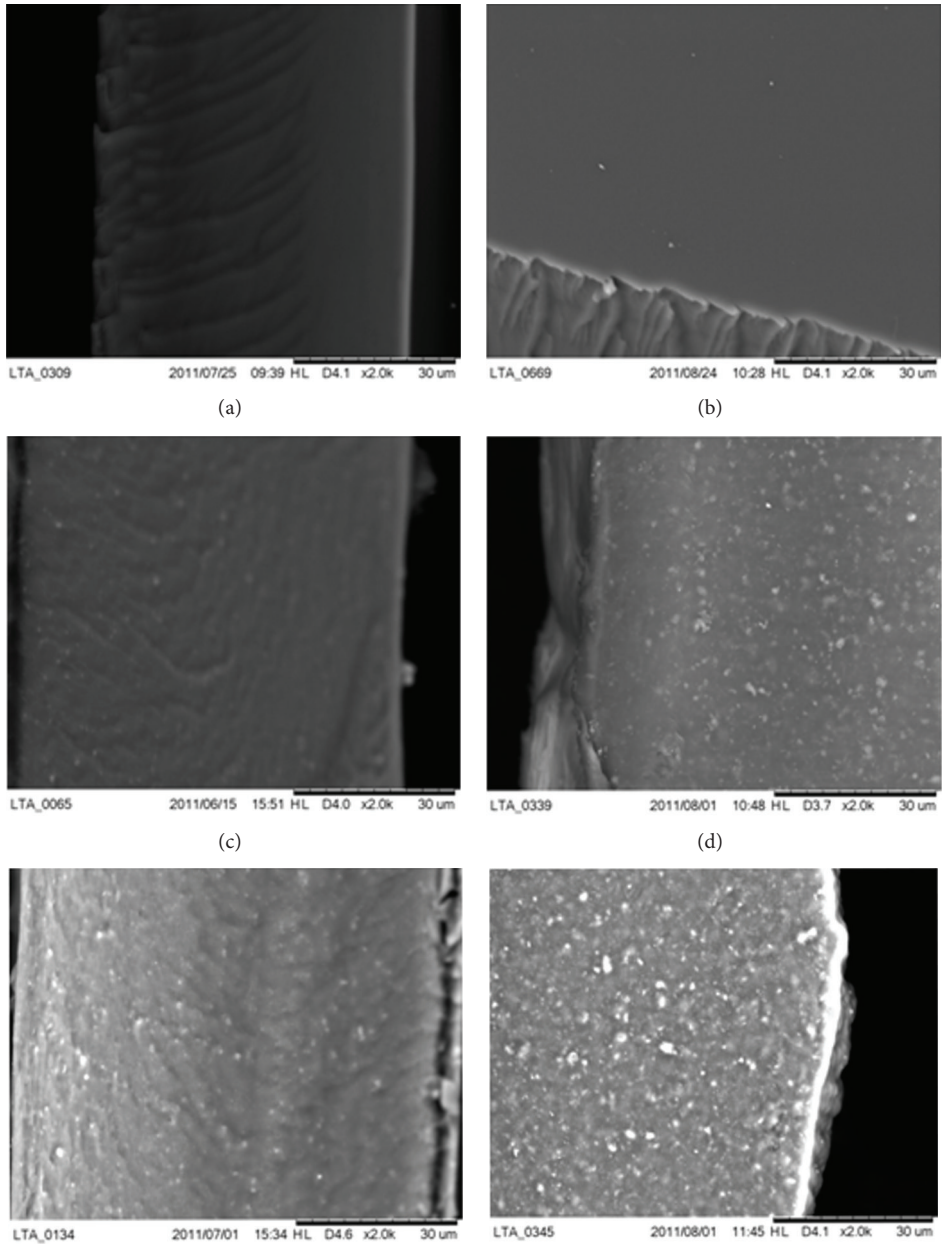

FIGURE 5: Scanning electron microscopy images of cryofractured longitudinal (left) and of the air-dried surface (right) of nanocomposites prepared with 5% of gelatin and 0% (top), 5% (center), and 10% (bottom) of MMT.

plate. The increase of MMT concentration led to an increase of surface roughness, losing the typical smooth surface of films prepared without MMT. A similar behavior was also observed by Rhim [37]. This behavior may be due to the formation of agglomerates, which causes less homogeneous structures or through a possible elutriation of material to the surface during the drying process.

3.7. Surface Hydrophobicity. The water contact angle measurements were carried out to study water absorption properties of the gelatin-based nanocomposites. The contact angle is dependent on the cohesive and adhesive molecular forces within the water and between the water and the film (solid) surface, respectively. Contact angles below 65° are typical of hydrophilic surfaces, while contact angles above 65° are characteristic of hydrophobic surfaces [38]. According to Mohan et al. [39], the hydrophilic behavior of a material can be affected by the roughness of its surface. The incorporation of nanoparticles in the formulations of gelatin-based nanocomposites had not a significant impact on nanocomposites hydrophobicity (Table 1). However, according to Rhim et al. [40], chitosan based films reinforced with MMT presented lower hydrophobicity than films prepared without MMT.

4. Conclusions

In general, the properties of gelatin-based nanocomposites reinforced with MMT were improved. The incorporation of MMT on gelatin-based nanocomposites led to a significant increase of their thickness and a decrease in their moisture content. The mechanical properties were improved by MMT incorporation. Reinforced nanocomposites presented higher tensile strength as well as higher Young's modulus which reveal that nanocomposites become more resistant and rigid. Consequently, the elongation at break decreased. Puncture force and puncture deformation were not affected by MMT concentration. MMT concentration had not a clear effect on the thermal properties. Only the enthalpy and glass transition of gelatin-rich fraction determined in the first scan decrease or increase, respectively, for the highest MMT concentration, but in general the glass transition temperatures were similar for all nanocomposites. The increase in MMT concentration slightly changed the X-ray diffraction spectra indicating some loss of crystallinity. FTIR spectra of the nanocomposites were similar, presenting bands typical of both gelatin and MMT. Hydrophobicity was not affected by the incorporation of MMT, but SEM results showed that reinforced nanocomposites presented structures less homogeneous.

Conflict of Interests

The authors declare that there is no conflict of interests regarding the publication of this paper.

Acknowledgments

The authors are grateful to CAPES for the Ph.D. fellowship of Manuel Fernando Coronado Jorge (PEC-PG) and to FAPESP for the MS fellowship of Christian Humberto Caicedo Flaker (11/15784-1) and Post-Doc fellowship of Elisabete M. C. Alexandre (13/25907-9). Work of the CEPID-FoRC is gratefully acknowledged (13/07914-8).

References

[1] M. O. Nisperos-Carriedo, "Edible coatings and films based on polysaccharides," in *Edible Coatings and Films to Improve Food Quality*, J. M. Krochta, E. A. Baldwin, and M. Nisperos-Carriedo, Eds., pp. 305–336, CRC Press, Boca Raton, Fla, USA, 1994.

[2] A. Nussinovitch, "Biopolymer films and composite coatings," in *Modern Biopolymer Science*, S. Kasapis, I. T. Norton, and J. B. Ubbink, Eds., pp. 295–326, Elsevier, San Diego, Calif, USA, 2009.

[3] M. G. A. Vieira, M. A. da Silva, L. O. dos Santos, and M. M. Beppu, "Natural-based plasticizers and biopolymer films: a review," *European Polymer Journal*, vol. 47, no. 3, pp. 254–263, 2011.

[4] R. Núñez-Flores, B. Giménez, F. Fernández-Martín, M. E. López-Caballero, M. P. Montero, and M. C. Gómez-Guillén, "Physical and functional characterization of active fish gelatin films incorporated with lignin," *Food Hydrocolloids*, vol. 30, no. 1, pp. 163–172, 2013.

[5] D. C. Achet and X. W. He, "Determination of the renaturation level in gelatin films," *Polymer*, vol. 36, no. 4, pp. 787–791, 1995.

[6] I. S. Arvanitoyannis, "Formation and properties of collagen and gelatin films and coatings," in *Protein-Based Films and Coatings*, A. Gennadios, Ed., chapter 11, pp. 275–304, CRC Press, Boca Raton, Fla, USA, 2002.

[7] C. Mu, X. Li, Y. Zhao, H. Zhang, L. Wang, and D. Li, "Freezing/thawing effects on the exfoliation of montmorillonite in gelatin-based bionanocomposite," *Journal of Applied Polymer Science*, vol. 128, no. 5, pp. 3141–3148, 2013.

[8] M. F. C. Jorge, C. H. C. Flaker, S. F. Nassar, I. C. F. Moraes, A. M. Q. B. Bittante, and P. J. D. A. Sobral, "Viscoelastic and rheological properties of nanocomposite-forming solutions based on gelatin and montmorillonite," *Journal of Food Engineering*, vol. 120, pp. 81–87, 2014.

[9] F. M. Vanin, M. H. Hirano, R. A. Carvalho, I. C. F. Moraes, A. M. Q. B. Bittante, and P. J. D. A. Sobral, "Development of active gelatin-based nanocomposite films produced in an automatic spreader," *Food Research International*, vol. 63, pp. 16–24, 2014.

[10] J. M. Lagarón, L. Cabedo, D. Cava, J. L. Feijoo, R. Gavara, and E. Gimenez, "Improving packaged food quality and safety. Part 2: nanocomposites," *Food Additives & Contaminants*, vol. 22, no. 10, pp. 994–998, 2005.

[11] M. S. Hedenqvist, A. Backman, M. Gällstedt, R. H. Boyd, and U. W. Gedde, "Morphology and diffusion properties of whey/montmorillonite nanocomposites," *Composites Science and Technology*, vol. 66, no. 13, pp. 2350–2359, 2006.

[12] J. Weiss, P. Takhistov, and D. J. McClements, "Functional materials in food nanotechnology," *Journal of Food Science*, vol. 71, no. 9, pp. R107–R116, 2006.

[13] J.-W. Rhim, "Physical-mechanical properties of agar/κ-carrageenan blend film and derived clay nanocomposite film," *Journal of Food Science*, vol. 77, no. 12, pp. N66–N73, 2012.

[14] M. Alboofetileh, M. Rezaei, H. Hosseini, and M. Abdollahi, "Effect of montmorillonite clay and biopolymer concentration

on the physical and mechanical properties of alginate nanocomposite films," *Journal of Food Engineering*, vol. 117, no. 1, pp. 26–33, 2013.

[15] Y. Rao, "Gelatin-clay nanocomposites of improved properties," *Polymer*, vol. 48, no. 18, pp. 5369–5375, 2007.

[16] S. Tunç, H. Angellier, Y. Cahyana, P. Chalier, N. Gontard, and E. Gastaldi, "Functional properties of wheat gluten/montmorillonite nanocomposite films processed by casting," *Journal of Membrane Science*, vol. 289, no. 1-2, pp. 159–168, 2007.

[17] M. Alexandre and P. Dubois, "Polymer-layered silicate nanocomposites: preparation, properties and uses of a new class of materials," *Materials Science and Engineering R: Reports*, vol. 28, no. 1, pp. 1–63, 2000.

[18] P. J. A. Sobral, F. C. Menegalli, M. D. Hubinger, and M. A. Roques, "Mechanical, water vapor barrier and thermal properties of gelatin based edible films," *Food Hydrocolloids*, vol. 15, no. 4–6, pp. 423–432, 2001.

[19] M. Thomazine, R. A. Carvalho, and P. J. A. Sobral, "Physical properties of gelatin films plasticized by blends of glycerol and sorbitol," *Journal of Food Science*, vol. 70, no. 3, pp. E172–E176, 2005.

[20] N. Gontard, S. Guilbert, and J.-L. Cuq, "Edible wheat gluten films: influence of the main process variables on film properties using response surface methodology," *Journal of Food Science*, vol. 57, no. 1, pp. 190–195, 1992.

[21] P. J. A. Sobral and A. M. Q. B. Habitante, "Phase transitions of pigskin gelatin," *Food Hydrocolloids*, vol. 15, no. 4–6, pp. 377–382, 2001.

[22] H. Angellier, S. Molina-Boisseau, P. Dole, and A. Dufresne, "Thermoplastic starch—Waxy maize starch nanocrystals nanocomposites," *Biomacromolecules*, vol. 7, no. 2, pp. 531–539, 2006.

[23] N. M. Vicentini, N. Dupuy, M. Leitzelman, M. P. Cereda, and P. J. A. Sobral, "Prediction of cassava starch edible film properties by chemometric analysis of infrared spectra," *Spectroscopy Letters*, vol. 38, no. 6, pp. 749–767, 2005.

[24] Y. Lu, L. Weng, and X. Cao, "Morphological, thermal and mechanical properties of ramie crystallites—reinforced plasticized starch biocomposites," *Carbohydrate Polymers*, vol. 63, no. 2, pp. 198–204, 2006.

[25] S.-A. Jang, G.-O. Lim, and K. B. Song, "Original article: use of nano-clay (Cloisite Na^+) improves tensile strength and vapour permeability in agar rich red algae (*Gelidium corneum*)-gelatin composite films," *International Journal of Food Science and Technology*, vol. 45, no. 9, pp. 1883–1888, 2010.

[26] R. Sothornvit, J.-W. Rhim, and S.-I. Hong, "Effect of nano-clay type on the physical and antimicrobial properties of whey protein isolate/clay composite films," *Journal of Food Engineering*, vol. 91, no. 3, pp. 468–473, 2009.

[27] V. P. Cyras, L. B. Manfredi, M.-T. Ton-That, and A. Vázquez, "Physical and mechanical properties of thermoplastic starch/montmorillonite nanocomposite films," *Carbohydrate Polymers*, vol. 73, no. 1, pp. 55–63, 2008.

[28] H. J. Bae, H. J. Park, S. I. Hong et al., "Effect of clay content, homogenization RPM, pH, and ultrasonication on mechanical and barrier properties of fish gelatin/montmorillonite nanocomposite films," *LWT—Food Science and Technology*, vol. 42, no. 6, pp. 1179–1186, 2009.

[29] J. Luecha, N. Sozer, and J. L. Kokini, "Synthesis and properties of corn zein/montmorillonite nanocomposite films," *Journal of Materials Science*, vol. 45, no. 13, pp. 3529–3537, 2010.

[30] S. Tunç and O. Duman, "Preparation and characterization of biodegradable methyl cellulose/montmorillonite nanocomposite films," *Applied Clay Science*, vol. 48, no. 3, pp. 414–424, 2010.

[31] P. J. A. Sobral, "Influencia da espessura sobre certas propriedades de biofilmes a base de proteinas miofibrilares," *Pesquisa Agropecuária Brasileira*, vol. 35, no. 6, pp. 1251–1259, 2000.

[32] F. C. Faria, A. E. S. Vercelheze, and S. Mali, "Propriedades físicas de filmes biodegradáveis a base de amido de mandioca, álcool polivinílico e montmorilonita," *Química Nova*, vol. 35, no. 3, pp. 487–492, 2012.

[33] I. Yakimets, S. S. Paes, N. Wellner, A. C. Smith, R. H. Wilson, and J. R. Mitchell, "Effect of water content on the structural reorganization and elastic properties of biopolymer films: a comparative study," *Biomacromolecules*, vol. 8, no. 5, pp. 1710–1722, 2007.

[34] M. Pereda, A. G. Ponce, N. E. Marcovich, R. A. Ruseckaite, and J. F. Martucci, "Chitosan-gelatin composites and bi-layer films with potential antimicrobial activity," *Food Hydrocolloids*, vol. 25, no. 5, pp. 1372–1381, 2011.

[35] S. W. Xu, J. P. Zheng, L. Tong, and K. De Yao, "Interaction of functional groups of gelatin and montmorillonite in nanocomposite," *Journal of Applied Polymer Science*, vol. 101, no. 3, pp. 1556–1561, 2006.

[36] G. G. D. Silva, P. J. A. Sobral, R. A. Carvalho, P. V. A. Bergo, O. Mendieta-Taboada, and A. M. Q. B. Habitante, "Biodegradable films based on blends of gelatin and poly (vinyl alcohol): effect of PVA type or concentration on some physical properties of films," *Journal of Polymers and the Environment*, vol. 16, no. 4, pp. 276–285, 2008.

[37] J.-W. Rhim, "Effect of clay contents on mechanical and water vapor barrier properties of agar-based nanocomposite films," *Carbohydrate Polymers*, vol. 86, no. 2, pp. 691–699, 2011.

[38] A. Hambleton, M.-J. Fabra, F. Debeaufort, C. Dury-Brun, and A. Voilley, "Interface and aroma barrier properties of iota-carrageenan emulsion—based films used for encapsulation of active food compounds," *Journal of Food Engineering*, vol. 93, no. 1, pp. 80–88, 2009.

[39] T. Mohan, R. Kargl, A. Doliška et al., "Wettability and surface composition of partly and fully regenerated cellulose thin films from trimethylsilyl cellulose," *Journal of Colloid and Interface Science*, vol. 358, no. 2, pp. 604–610, 2011.

[40] J.-W. Rhim, S.-I. Hong, H.-M. Park, and P. K. W. Ng, "Preparation and characterization of chitosan-based nanocomposite films with antimicrobial activity," *Journal of Agricultural and Food Chemistry*, vol. 54, no. 16, pp. 5814–5822, 2006.

Hindawi Publishing Corporation
International Journal of Polymer Science
Volume 2015, Article ID 714254, 6 pages
http://dx.doi.org/10.1155/2015/714254

Research Article

Effect of the Addition of Essential Oils and Functional Extracts of Clove on Physicochemical Properties of Chitosan-Based Films

Paola Reyes-Chaparro, Nestor Gutierrez-Mendez, Erika Salas-Muñoz, Juan Guillermo Ayala-Soto, David Chavez-Flores, and León Hernández-Ochoa

Facultad de Ciencias Químicas, Universidad Autónoma de Chihuahua, Campus Universitario No. 2, Apartado Postal 669, 31125 Chihuahua, CHIH, Mexico

Correspondence should be addressed to León Hernández-Ochoa; lhernandez@uach.mx

Received 10 February 2015; Revised 6 May 2015; Accepted 18 June 2015

Academic Editor: Xingxun Liu

Mechanical and barrier properties of chitosan films prepared with essential oils of clove and functional extract were studied. The films made with functional extracts (esters E_6 and E_7) presented the significant increment of extensibility compared with the untreated chitosan films. In the case of punction test, the films made with the esters E_6 and E_7 resisted more the applied strength before tearing up compared with the chitosan control film (without any treatment). Thermogravimetric analysis values were determined for the chitosan control film and chitosan film treated with clove essential oil obtaining 112.17°C and 176.73°C, respectively. Atomic force microscopy (AFM) was used to determine their morphology by analyzing their surfaces and phase arrangement; AFM was also used to observe the porosity in chitosan-based antimicrobial films and the chitosan films incorporating functional extracts. The water vapour permeability (WVP) data showed that incorporating the functional extract to the formulation of films has a positive effect on water vapour barrier properties. In general, the incorporation of essential oils and functional extract of clove at 20% in chitosan films caused microstructural changes that were dependent on the different affinity of components.

1. Introduction

Polymers derived from renewable resources are now considered promising alternatives to traditional petropolymers as they mitigate current environmental concern (raw renewable materials/biodegradability) [1]. Chitin is the most important component of the exoskeleton of invertebrates, molluscs, and lower forms of vegetal life (fungus and mold). It is nature's second most abundant polysaccharide after cellulose; their chemical formula is similar, but chitin has an acetamide instead of the hydroxyl group of C_2 [2, 3]. Chitin is not present as a natural chemical entity, but it is considered the product of the separation of several constituents; it is bound to proteins, minerals, and pigments in a complex matrix named chitinase structure. It is a linear polymer with a predominance of residues of 2-acetamido-2-deoxy-D-glucopyranose (N-acetyl-D-glucosamine) and in a lower proportion 2-amine-2-deoxy-β-D-glucopyranose (D-glucosamine) [3]. Once it is isolated, it presents a colorless, crystalline dust (insoluble in water, organic solvents, acids, and alkalis diluted and concentrated). Its low solubility is due to the formation of intermolecular hydrogen bonds between the chains β-(1-4)-glycoside and to its rigid crystalline structure [4, 5]. Chitin's main derivate is chitosan, which is produced by alkaline or enzymatic deacetylation or chitin. This biopolymer contains a higher proportion of D-glucosamine groups than N-acetyl-D-glucosamine. Thereby, chitosan dissolves at low concentrations of aqueous solutions of organic acids, for instance, acetic and formic acids, and inorganic acids, yielding in all cases viscose solutions. This is due to the fact that the amine group is totally protonated at pH 3.0. Complete deacetylation is hardly achieved and normally unnecessary since the solubility in diluted acids is reached starting with 60% degree of deacetylation. Chitosan is a linear polyaminosaccharide of high molecular weight, and its derivates are used in a wide variety of applications, for instance, alternative materials of biodegradable and antimicrobial flexible films, the latter due to its capacity of absorbing nutrients used by bacteria and

the capacity to bond water and inhibit the enzymatic system [6]. These materials' efficiency depends on their molecular weight and their degree of deacetylation [7, 8]. Some authors [7–9] mention that chitosan has antimicrobial activity against certain bacteria, molds, and yeasts (except *Zigomycetes* which have chitosan as main component in its cell wall). On the other hand, the medium conditions such as pH, temperature, and food composition are factors that have influence over the antimicrobial capacity. An important application of chitosan is the elaboration of antimicrobial films that can be used to extend fruit, vegetable, and sea or meat products' shelf life, reducing dehydration, oxidative rancidity, and superficial darkening [1, 9–11]. Chitosan has a potential interest as a base for films because it has oxygen-blocking properties. However, chitosan is a hydrophilic molecule that should be treated with some additives to provoke certain hydrophobicity and to improve its mechanical properties [1, 10, 11]. Nevertheless, pure chitosan films are fragile and need plasticizer to reduce frictional forces between the polymer chains, as hydrogen bonds or ionic forces, thus improving mechanical properties [12].

The replacement of synthetic products with more natural alternatives is safer when the new product is as effective as the product previously used [13]. The essential oils obtained from spices are among these alternatives, as their active components (including terpenes, aldehydes, acids, alcohols, phenols, esters, and ketones) for their antimicrobial activity [14], and have been recently added to food packing materials [8]. The most common method of essential oils extraction is by hydrodistillation, although the use of petroleum-derived solvents is also used to purify plant-derived compounds. However, the latter method can be dangerous because of the use of explosive and toxic solvents [14]. An option would be the use of alternative solvents, also known as green solvents because they are not derived from petroleum products; therefore, they are not as detrimental to the environment. Among those alternative solvents, fatty acid ethyl esters are extracted from plants, are becoming an important option because of their amphipathic property and biodegradability, and are also nontoxic and nonirritable [15]. Thus, the aim of this work is focused on analyzing the effect of the incorporation of essential oil and functional extract of clove on functional properties of chitosan-based films for food packaging applications.

2. Material and Methods

2.1. Materials. Clove (*Eugenia caryophyllata*) was given by Comercial Cordona from Chihuahua, Mexico. Chitosan (low molecular weight, 75–85% deacetylated CAS 9012-76-4), ethyl caproate (99% CAS. 123-60-0), ethyl heptanoate (99%, CAS 106-30-9), ethyl caprylate (99% CAS. 106-32-1), ethyl nonanoate (97% CAS. 123-29-5), acetic acid (99% CAS 64-19-7), and glycerin (99% CAS 56-81-5) were provided by Sigma-Aldrich.

2.1.1. Essential Oil (EO) and Functional Extracts (EX). Plant material (clove) was subjected to distillation process using a Schilcher device. For hydrodistillation process, plant material was immersed in water and for cohydrodistillation process, fatty acid ethyl esters were added as cosolvents of extraction. The ester used was ethyl heptanoate (E_7); operation conditions depended on the vegetal material used, according to Hernández-Ochoa et al. [15]. 200 g of the clove was added to 4 L of water and 20 mL of ethyl ester. The homogeneous mixture composed of oil and ester was called functional extracts (EX).

2.1.2. Chitosan-Based Films Elaboration. The antimicrobial films were prepared according to Ouattar et al. [16]. The films were prepared by dissolving low molecular weight chitosan in acetic acid aqueous solution (1% v/v), to obtain a final concentration of 2% (w/v). Glycerin 2% (w/v) was added as plasticizer; essential oils and functional extract of clove were also added to the film's mixture. An immersion mixer (Bamix) was used to homogenize all components, and 20 mL of the mixture was poured into glass Petri dishes (15 × 90 mm) and placed in a convection oven (Fisher Scientific) (60°C, 4 h) to form the antimicrobial films.

2.1.3. Tensile Properties. A texturometer (TA XT plus) with a 0.049-N load cell was used. In the puncture test, a bradawl P/2N with a 2.38 mm bit was used. The speed during the test was of 2 mm/s and in the pretest was of 10 mm/s, with a route distance of 10 mm/s. The analysis was carried out in films of 9-cm diameter and 0.054 mm thickness. The bradawl penetration was evaluated in five different parts of the films. The maximum strength was determined for each film formulation. For the extensibility test, a heavy duty platform (HDP)/Tortilla Pastry Burst rig device was used. The speed used in the extensibility test was of 2 mm/s. The analysis was carried out in 12-cm diameter films according to Hernández-Ochoa et al. [15]. All determinations were performed in triplicate.

2.2. Thermogravimetric Analysis. Thermogravimetric analysis (TGA) test was carried out in a TGA-Q400 (TA Instruments, USA). Samples weighing around 5–10 mg were heated under dynamic mode. Measurements were performed at $10^{\circ}C\,min^{-1}$ from 30°C to 600°C under nitrogen atmosphere (low rate $50\,mL\,min^{-1}$) in order to prevent any thermoxidative degradation.

2.3. Atomic Force Microscopy. The porosity of the antimicrobial films was evaluated using this technique. Multimode AFM with Nanoscope IV controller (Veeco Instruments, Santa Barbara, CA, USA) was used for both living cell imaging and force curves collection. This AFM was equipped with a Pico Force module. The Pico Force scanner had a maximum XY scan range of 50 μm × 50 μm and Z range of 20 μm. The sample was prepared taking a small section of the film and placing it in a cell, and the sample was set up in the microscope's sample holder. The upper side of the film was used in the test (in direct contact with a glass dish). A 125 μm long cantilever was used at a resonance frequency of 250–300 KHz and 294 KHz, with amplitude of

1.35 V. The sample was analyzed using the contact mode technique that is based on the monitoring of the change of the cantilever's deflection through a photosensor and a laser beam. The cantilever oscillates at a frequency slightly under its resonance frequency 3–10%, with amplitude in the 20 to 100 nm range. The images obtained were analyzed with the program WsXM 4.0 develop 11.4 determining the pore size, according to the technique described by Lavalle et al. [17].

2.4. Water Vapor Permeability Measurements. The water vapor permeability (WVP) of the films was determined at 25°C and 53–100 RH gradients. The WVP was determined by making a modification of the ASTM-E96-95 gravimetric method for flexible films [18]. Three circular samples were cut (3.5 cm in diameter) per formulation, selecting films without visible defects, such as cracks or visible pores. The thickness of each sample was determined in six random positions. Payne permeability cups of 3.5 cm in diameter were filled with 5 mL distilled water (RH = 100%). Saturated solutions of magnesium nitrate were used to generate 53% RH inside the cabinets. The shiny side of the films was exposed to the atmosphere at the lowest RH (53% RH at 25°C). The cups were weighed using an analytical balance (E02140, Ohaus, USA) (±0.00001 g) at intervals of 1.5 hours during 24 hours. The weight loss versus time plot slope was divided by the exposed film area in order to calculate the water vapor transmission rate (WVTR):

$$\text{WVTR} = \frac{\text{slope}}{\text{film area}}. \quad (1)$$

WVP was determined by using (2), where P_1 is the partial pressure (kPa) inside the cup, P_2 the water vapor partial pressure (kPa) at the film outer surface in the system, and L the average film thickness (mm):

$$\text{WVP} = \left(\frac{\text{WVTR}}{P_2 - P_1}\right) L. \quad (2)$$

2.5. Statistical Analysis. The statistical analysis of the data was performed trough an Analysis of Variance (ANOVA). Tukey test was used for analysis of media, using a 0.95% confidence level. Statistical analysis was realized using the computational software Minitab (version 14.0).

3. Results and Discussion

3.1. Elaboration of Chitosan-Based Films. Chitosan-based films were elaborated incorporating clove (*Eugenia caryophyllata*) essential oil and clove functional extract, as reported by Hernández-Ochoa et al. [15]. The results obtained in the elaboration of the films are shown in Figure 1, where it can be observed that the films had the following general characteristics: minimum porosity, being transparent and elastic, and having no fractures.

The films that contained clove extract and functional extract of clove presented an opaque color and a strong clove odor; chitosan films with no addition of essential oil and functional extracts had an acetic acid odor. Interactions between chitosan and different essential oils and esters can involve the nitrogen residues of the primary aliphatic amine present in chitosan, which gives typical reactions of these functional groups, for instance, N-acylation and the Schiff bases formation. On the other hand, chitosan free amino groups also have an association to hydrogen bonds [3]. As expected esters E_6 and E_7 reacted with transesterification reaction involving the ester carbonyl group (C=O), the amines groups (NH2), and hydroxyls (OH) functional groups, getting amides and ester bonds as functionalizing agents. It can be considered that the esters may participate as acceptors in the hydrogen bonds, but they cannot participate as donors in this type of bonds.

Table 1: Maximum chitosan film's punction and extensibility force with essential oils and functional extract (added esters E_6, E_7) of clove.

Short of film	Extensibility[1] (N)	Punction[2] (N)
Chitosan films	23.63 ± 0.43^a	3.14 ± 0.03^a
Chitosan + essential oil	24.38 ± 3.38^a	5.87 ± 0.31^b
Chitosan + functional extract (E_6)	34.71 ± 1.58^b	7.18 ± 0.16^c
Chitosan + functional extract (E_7)	44.05 ± 3.70^c	9.34 ± 0.55^d

Note. [1]An average of 5 measurements in every film, [2]an average of 15 measurements in every film. Tukey testing: the averages with the same letter do not significantly differ and the averages with different letter show significant differences ($p < 0.05$). Fatty acids ethyl esters used in this study were ethyl caproate (E_6) and ethyl heptanoate (E_7).

3.2. Tensile Properties. Considering the observed visual differences, tensile analyses were done (punction and extensibility) to determine the influence of the addition of essential oils and functional extracts into the chitosan films. Based on punction and extensibility ($p < 0.01$) tests results (Table 1) showed significant differences among the films.

The films made with esters E_6, E_7 had highest levels of extensibility. Compared with the control and chitosan-essential oil clove, films made with esters E_6, E_7 had a larger stretching capacity but there was only a few increments of resistance in the punction test by resisting just 5% more than the strength applied for tearing up of the untreated chitosan film. Low values of chitosan films in both tests are in agreement with previous reports since chitosan films are rigid and fragile. Synthetic polymers such as LDPE (low-density polyethylene) and HDPE (high-density polyethylene) show high elongation values but similar traction resistance to that of biopolymer films, such as chitosan [19]. According to Lara-Sagahon et al. [10] the molecular measurement, configuration, and the polar group total in plasticizers and fatty acids as well as their compatibility with the chitosan chains are responsible for the modification of the mechanical properties, as the results obtained in this study. It is also observed that chitosan films had low values for strain stress compared to the polyethylene film; this agrees with the literature, which refers that chitosan films are rigid and brittle, since they present low values for elastic modulus, high strength, and low strain to breaking [20].

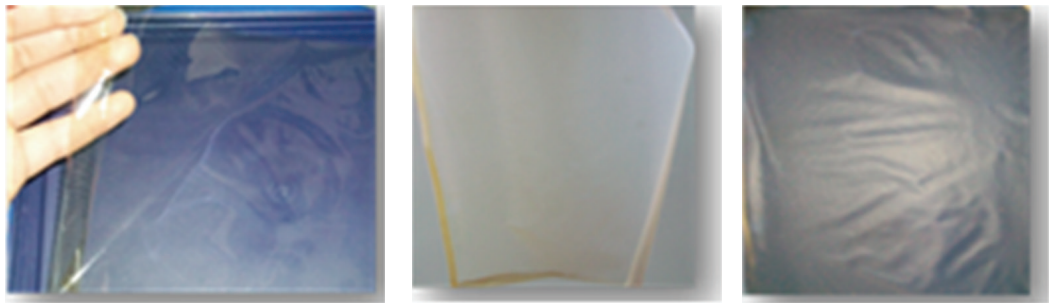

Figure 1: A typical image of a chitosan-based films including spices of essential oils and functional extract of clove.

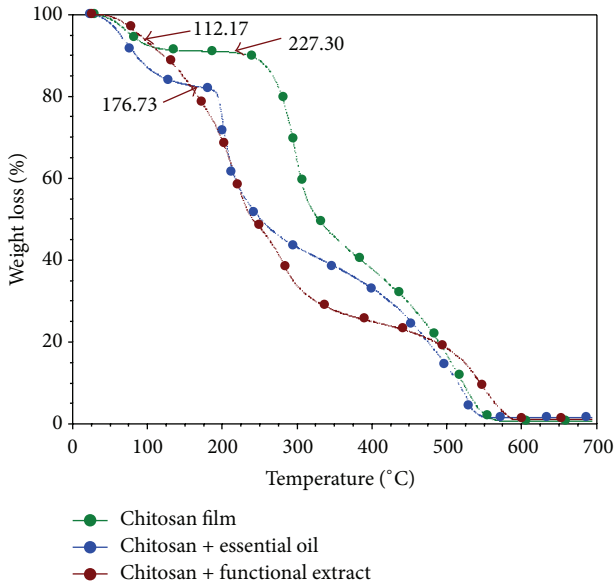

Figure 2: TGA curves for chitosan-based films and chitosan film plus the essential oil of clove. Universal V4.3A TA Instruments.

3.3. Thermogravimetric Analysis. The Tga value for the chitosan and chitosan film plus the clove essential oil and pure chitosan were determined 112.17°C, 176.73°C, and 227.30°C, respectively. For the chitosan film with clove extract, it was not possible to determine (Figure 2). The differences presented in the Tga values are caused by the concentration of the essential oil and the functional extract present in the sample; the lower concentration of these compounds shows a lower Tga value. These Tga values indicate at what temperature the material undergoes degradation and serves to control the film manipulation and elaboration. The changes in Tga might be related to chitosan hydrolysis in the solvents and the formation of a network involving hydrogen bonds with its amine groups. Increasing the chitosan concentration increased the strength of this network as supported in the report from El-Hefian et al. [21]. Also Martins et al. [22] illustrated that weight loss at 200°C related to the chemical absorption of water by hydrogen bonds and elimination of NH_3. Santos et al. [23] observed that the temperature of a maximum speed of decomposition for purified chitosan lowered. It is evinced that there is a relation between the degree of acetylation and thermal stability.

3.4. Surface Morphological Analysis by Atomic Force Microscopy. Through atomic force microscopy, the surface of chitosan-based antimicrobial films and the chitosan films incorporating functional extracts was observed to determine their morphology, phase arrangement, and porosity. Figure 3 shows the images obtained in the Atomic Force Microscope. It can be observed that, in general, the films prepared do not present a transversal porosity. The surface of the film containing essential oil of clove (Figure 3(b)) was covered with small pores and seemed to be sponge-like. It is postulated that the loose structure observed in these films may be caused by the essential oil components disrupting the ordered structure of the chitosan polymers. The same similar results were obtained by Hosseini et al. [24]. The chitosan-based film incorporating functional extract (Figure 3(c)) shows smooth zones, possibly generated by the incorporation of the extract, which may also suppose the penetration of glycerol which is part of the formulation, thus forming more homogeneous zones. Also, bigger pores were observed in the chitosan film with functional extract of clove in comparison with the films made from only chitosan and without incorporating essential oil.

3.5. Water Vapor Permeability (WVP). The resulting WVP data is presented in Figure 4, where it can be observed that incorporating the functional extract to the formulation of the films had a positive effect on water vapor barrier properties. However, the chitosan films incorporating essential oil of clove showed similar value compared to the just chitosan films. These results mean that the incorporation of functional extract (essential oil of clove + ethyl heptanoate) is more effective to improve the barrier properties of chitosan films, even at the low ratio. This increase may be due to destabilization of chitosan matrix by long chain of functional extract molecules, thus widening the interstitial space in the chitosan matrix and thus allowing for an increased diffusion rate of water molecules through the film. This result is supported by

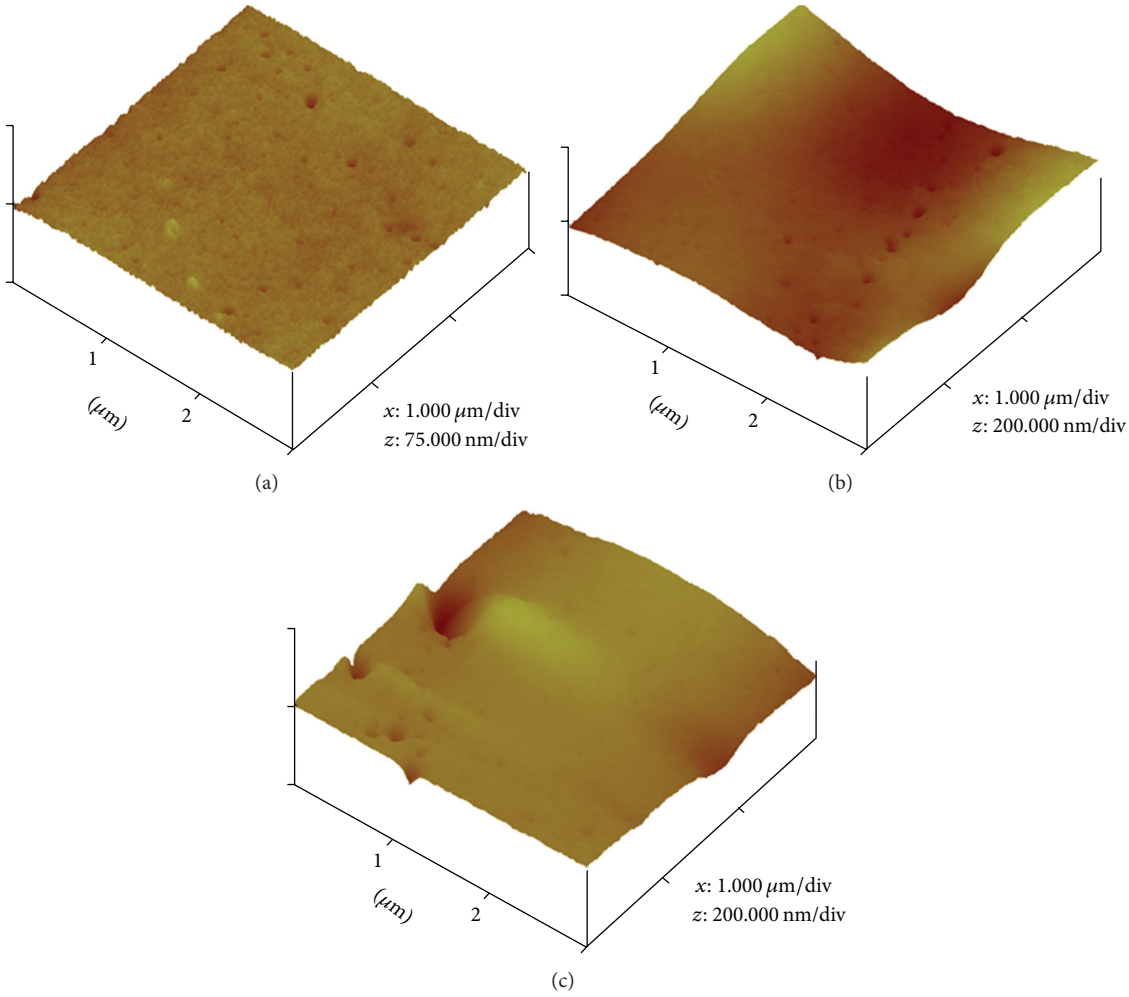

Figure 3: AFM images of the topographic and three-dimensional structures obtained for (a) chitosan films, (b) chitosan film with essential oil of clove, and (c) chitosan film with functional extract of clove.

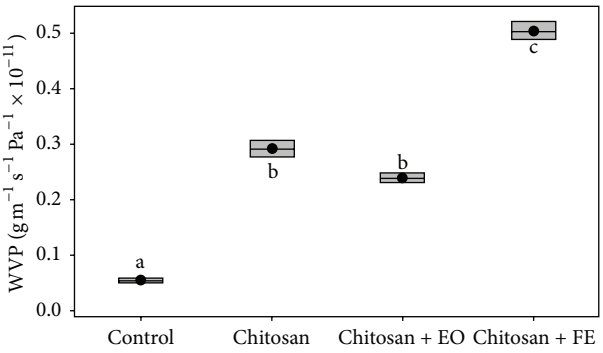

Figure 4: Water vapour permeability of the edible films including essential oils and functional extract of clove. Data are means of three replicates per treatment.

the work of Srinivasa et al. [18], where WVP properties of chitosan lipid blend films were comparable.

4. Conclusions

A complete characterization of chitosan-based films blended with essential oil of clove and the functional extract was carried out. The films that contained clove extract and functional oil presented an opaque color and a strong clove odor; chitosan films with no addition of essential oil and functional extracts were clear and with an acetic acid odor. Tensile analyses showed significant differences among films, based on punction and extensibility ($p < 0.01$) determination. The films made with functional extract (esters E_6 and E_7) presented the highest levels of extensibility as compared to the controls and chitosan-essential oil clove. No significant increment in the results of the punction test for the films treated with the esters, those resisted more strength applied before tearing up than the only chitosan films. The results revealed that the addition of functional extract into in chitosan matrix increased the glass transition temperature of the films. The WVP data showed that incorporating the functional extract to the formulation of films has a positive effect on water vapor barrier properties. In general,

the incorporation of essential oils and functional extract of clove at 20% in chitosan films gave rise to microstructural changes that were dependent on the different affinity of components. The greatest structural change was induced by essential oil that promoted heterogeneity in pore sizes and shape. These results show the feasibility of using essential oils and functional extracts as natural's plasticizers to obtain flexible films. The films could be even a good candidate to be tested as an active packaging system.

Conflict of Interests

The authors declare that there is no conflict of interests regarding the publication of this paper.

Acknowledgments

The authors gratefully acknowledge CIMAV for help in using the Atomic Force Microscope (AFM). Funding for the project was provided by the National Council of Science and Technology of Mexico (CONACYT-Mexico).

References

[1] M. P. Arrieta, J. López, S. Ferrándiz, and M. A. Peltzer, "Characterization of PLA-limonene blends for food packaging applications," *Polymer Testing*, vol. 32, no. 4, pp. 760–768, 2013.

[2] N. E. Suyatma, L. Tighzert, A. Copinet, and V. Coma, "Effects of hydrophilic plasticizers on mechanical, thermal, and surface properties of chitosan films," *Journal of Agricultural and Food Chemistry*, vol. 53, no. 10, pp. 3950–3957, 2005.

[3] A. G. González, A. A. Gardea, and F. C. Navarro, "Nuevas tecnologías de conservación de productos vegetales frescos y cortados," in *Uso del Quitosano en Alimentos*, pp. 381–397, CIAD, 2005.

[4] Q. Cai, Z. Gu, T. Fu, Y. Liu, H. Song, and F. Li, "Kinetic study of chitosan degradation by an electrochemical process," *Polymer Bulletin*, vol. 67, no. 4, pp. 571–582, 2011.

[5] S.-I. Park and Y. Zhao, "Incorporation of a high concentration of mineral or vitamin into chitosan-based films," *Journal of Agricultural and Food Chemistry*, vol. 52, no. 7, pp. 1933–1939, 2004.

[6] K. T. Hwang, S. T. Jung, G. D. Lee, M. S. Chinnan, Y. S. Park, and H. J. Park, "Controlling molecular weight and degree of deacetylation of chitosan by response surface methodology," *Journal of Agricultural and Food Chemistry*, vol. 50, no. 7, pp. 1876–1882, 2002.

[7] L. Hernández-Ochoa, A. Gonzales-Gonzales, N. Gutiérrez-Méndez, G. Vilarem, L. N. Muñoz-Castellanos, and A. Quintero-Ramos, "Estudio de la actividad antimicrobiana de películas elaboradas con quitosano a diferentes pesos moleculares," *Revista Mexicana de Ingeniería Química*, vol. 10, no. 3, pp. 415–424, 2011.

[8] S. Longinos, M. Mendoza, and J. Quezada, "Películas antimicrobianas para carne y productos cárnicos," *Mundo Lácteo y Cárnico*, vol. 5, pp. 12–17, 2005.

[9] N. Bordenave, S. Grelier, and V. Coma, "Hydrophobization and antimicrobial activity of chitosan and paper-based packaging material," *Biomacromolecules*, vol. 11, no. 1, pp. 88–96, 2010.

[10] A. V. Lara-Sagahon, S. P. Miranda, G. Cardenas, and D. Lopez, "Comportamiento de películas de quitosano compuesto en un modelo de almacenamiento de aguacate," *Revista Mexicana de Ingenieria Química*, vol. 47, pp. 331–336, 2003.

[11] K. W. Leong, H.-Q. Mao, V. Chan, and N. Fang, "Interactions of phospholipid bilayer with chitosan: effect of molecular weight and pH," *Biomacromolecules*, vol. 2, no. 4, pp. 1161–1168, 2001.

[12] I. Leceta, P. Guerrero, I. Ibarburu, M. T. Dueñas, and K. De la Caba, "Characterization and antimicrobial analysis of chitosan-based films," *Journal of Food Engineering*, vol. 116, no. 4, pp. 889–899, 2013.

[13] M. S. Rahman, *Handbook of Food Preservation: Packaging As a Preservation Technique*, vol. 10, CRC Press, Boca Raton, Fla, USA, 2007.

[14] M. F. Ortuño, *Manual práctico de aceites esenciales, aromas y perfumes*, Aiyana, Murcia, Spain, 2006.

[15] L. Hernández-Ochoa, C. A. Macías-Castanãeda, G. V. Nevárez-Moorillón, E. Salas-Munãoz, and F. Sandoval-Salas, "Antimicrobial activity of chitosan-based films including spices' essential oils and functional extracts," *CYTA—Journal of Food*, vol. 10, no. 2, pp. 85–91, 2012.

[16] B. Ouattar, R. E. Simard, G. Piett, A. Bégin, and R. A. Holley, "Inhibition of surface spoilage bacteria in processed meats by application of antimicrobial films prepared with chitosan," *International Journal of Food Microbiology*, vol. 62, no. 1-2, pp. 139–148, 2000.

[17] Ph. Lavalle, C. Gergely, F. J. G. Cuisinier et al., "Comparison of the structure of polyelectrolyte multilayer films exhibiting a linear and an exponential growth regime: an in situ atomic force microscopy study," *Macromolecules*, vol. 35, no. 11, pp. 4458–4465, 2002.

[18] P. C. Srinivasa, M. N. Ramesh, and R. N. Tharanathan, "Effect of plasticizers and fatty acids on mechanical and permeability characteristics of chitosan films," *Food Hydrocolloids*, vol. 21, no. 7, pp. 1113–1122, 2007.

[19] P. Sobral, J. Alvarado, N. E. Zaritzky et al., "Films based on biopolymer from conventional and non-conventional sources," in *Food Engineering: Integrated Approaches*, pp. 193–223, Springer, New York, NY, USA, 2008.

[20] F. C. Soares, F. Yamashita, C. M. O. Müller, and A. T. N. Pires, "Thermoplastic starch/poly(lactic acid) sheets coated with cross-linked chitosan," *Polymer Testing*, vol. 32, no. 1, pp. 94–98, 2013.

[21] E. A. El-Hefian, M. M. Nasef, and A. A. Yahaya, "The preparation and characterization of chitosan/poly(vinyl alcohol) blended films," *Journal of Chemistry*, vol. 7, pp. 1212–1219, 2010.

[22] A. F. Martins, A. G. B. Pereira, A. R. Fajardo, A. F. Rubira, and E. C. Muñiz, "Characterization of polyelectrolytes complexes based on N,N,N-trimethyl chitosan/heparin prepared at different pH conditions," *Carbohydrate Polymers*, vol. 86, no. 3, pp. 1266–1272, 2011.

[23] C. Santos, P. Seabra, B. Veleirinho, I. Delgadillo, and J. A. Lópes da Silva, "Acetylation and molecular mass effects on barrier and mechanical properties of shortfin squid chitosan membranes," *European Polymer Journal*, vol. 42, no. 12, pp. 3277–3285, 2006.

[24] M. H. Hosseini, S. H. Razavi, and M. A. Mousavi, "Antimicrobial, physical and mechanical properties of chitosan—based films incorporated with thyme, clove and cinnamon essential oils," *Journal of Food Processing and Preservation*, vol. 33, no. 6, pp. 727–743, 2009.

Hindawi Publishing Corporation
International Journal of Polymer Science
Volume 2015, Article ID 682596, 7 pages
http://dx.doi.org/10.1155/2015/682596

Research Article

The Investigation of Virginiamycin-Added Fungal Fermentation on the Size and Immunoreactivity of Heat-Sensitive Soy Protein

Liyan Chen,[1] Praveen V. Vadlani,[1] Ronald L. Madl,[1] Weiqun Wang,[2] Yongcheng Shi,[1] and William R. Gibbons[3]

[1]*Grain Science and Industry Department, Kansas State University, Manhattan, KS 66506, USA*
[2]*Human Nutrition Department, Kansas State University, Manhattan, KS 66506, USA*
[3]*Biology & Microbiology Department, South Dakota State University, Brookings, SD 57006, USA*

Correspondence should be addressed to Liyan Chen; liyanchen01@gmail.com

Received 21 January 2015; Accepted 15 April 2015

Academic Editor: Long Yu

The usage of soy protein for young monogastric animals is restricted due to potential allergens and high molecular weight. The investigation of fungi fermentation effect on soy protein has been interrupted by substrate sterilization. Virginiamycin at 0.05% was added together with *Aspergillus oryzae* for solid state fermentation (SSF) in unsterilized soy meal (SM). When compared to *A. oryzae* SSF alone, virginiamycin did not cause the interference of fungal fermentation but elucidated the protein degradation. SDS-PAGE results showed that both α and α' subunits of β-conglycinin were degraded significantly. In addition, western blot results showed that the immunoreactive signals of soy protein were considerably reduced in virginiamycin-added fermentation with unsterilized SM. Furthermore, fungal fermentation increased total protein and essential amino acid contents, suggesting the value enhancement of SM products. Taken together, this study demonstrated for the first time that virginiamycin could help investigate fermentation effect on heat-sensitive soy protein. Fermented SM has several potential applications in feed industry.

1. Introduction

Soy meal (SM) is the main protein source for monogastric animals in the United States [1]. But its inclusion in newly weaned pigs is limited because of some antinutritional factors and antigenic soy proteins causing hypersensitivity [2]. To date, 34 soybean proteins have been identified as allergens [3]. All three parts of the β-conglycinin, both acidic and basic subunits of glycinin and P34, have been identified as main allergens for young pigs [3–5]. Some studies indicate that incorporation of antigenic soy proteins such as pure glycinin or β-conglycinin to the diet leads to a reduced weight gain and feed efficiency as well as an increased incidence of diarrhea in pigs [4]. Furthermore, SM contains large molecular size proteins that are difficult for digestion, because many digestion enzymes such as pepsin and trypsin cannot perform their entire function until 3 weeks of age in piglets [4].

Fermentation has been applied to improve soy protein immunity and degrade protein molecular size. Song et al. [6] found that natural fermentation, *Saccharomyces cerevisiae*, and *Bacillus lactis* fermentation of SM reduced in 80%, 77%, and 77% immune response when using 97.5 kUA/l human plasma, respectively. Amnuaycheewa and de Mejia [7] analyzed the profilin in fermented soy products. The reduction in profilin in natto fermented by *Bacillus natto* was 12.8% to 35.4% and for soy paste 12.8% to 46.3%, in comparison to soy flour. But as for the fungal fermentation effect on SM immunity, research is limited. Frias et al. [5] found that *Aspergillus oryzae* or *Rhizopus oryzae* solid state fermentation produced a reduction of immunoreactivity of 68% or 66% of soy meal, respectively. But both fermentations used 121°C 15 min sterilization before and after. Since high heat could denature protein [8] and reduce its immunity [3], it could not elucidate that the deduction of immunity was caused by fermentation. Fungal solid state fermentation of SM has been applied to enhance the nutritional value of SM as monogastric animals' feed [9]. Animal test has already found that feeding fermented SM (FSM) could decrease the immune

response to soy protein in piglets [10]. However, enzymes with different origins have different hydrolytic effect [11]. There is a need to find the proper way to investigate whether and how a specific fungus solid state fermentation affects soy protein immunoreactivity.

Virginiamycin is one of the common antibiotics used in feed industry [12]. Also it has been used in ethanol production to prevent contamination during fermentation [13]. In our research, we applied virginiamycin to inhibit bacteria growth during *A. oryzae* solid state fermentation in unsterilized SMV. In addition, we demonstrated a method to perform fermentation under unsterilized condition and therefore distinctly investigated molecular degradation and immunoreactivity reduction of heat-sensitive soy protein.

2. Materials and Methods

2.1. Microbial Culture. Lyophilized cultures of *A. oryzae* (ATCC 9362) were obtained from the American Type Culture Collection (ATCC, Manassas, VA, USA), revived in potato dextrose broth twice. After revival, culture was inoculated on potato dextrose (PDA) slant, incubated at 30°C for 7 days, and later stored at 4°C for short term preservation. For routine experiments, spore solution was used. Spores were collected from the slants by gently washing with 0.1% Tween 80 to obtain spore suspension of around 10^7 spores/mL. Additionally, spores were suspended in 15% glycerol and stored at −80°C in 1 mL aliquots for long term preservation.

2.2. Substrate Preparation and Fermentation. SM was procured from ADM Alliance Nutrition (Abilene, KS). Solid state fermentation was carried out with three different kinds of substrates, which were original SM with virginiamycin, SM autoclaved at 100°C for 30 min (SM100C), and SM autoclaved at 121°C for 15 min (SM121C). Their corresponding fermented products were characterized as SMV, SM100, and SM121. For SMV, virginiamycin was added at a ratio of 0.05% dry matter base of SM, based on the results of our preliminary experiment. Four milliliters of *A. oryzae* spore solution containing 10^7 spores/mL was inoculated into 20 g substrate. Moisture was adjusted before autoclave. Moisture contributed by inoculation was considered. And final moisture was 50%. The flasks were incubated at 35°C for 36 hr. The fermented samples were then lyophilized and used for analysis.

2.3. Soy Protein Sample Preparation. Lyophilized FSM was milled with mortar and pestle to flour. SM flour was dispersed in distilled water at a ratio of 1 : 10. The mixture pH was adjusted to pH 8.2 by using 2 N NaOH. After 2 hr of shaking at room temperature, the mixture was centrifuged at 5,000 rcf at 4°C to remove insoluble residues. Soy protein in supernatant was precipitated by adjusting the supernatant pH to pH 4.8.

2.4. Differential Scanning Calorimeter (DSC). The denaturation of soy proteins was assessed with a differential scanning calorimeter (DSC) (DSC7, Perkin-Elmer, Norwalk, CT) calibrated with indium and zinc. Wet soy protein samples were hermetically sealed in a large-volume stainless pan. About 10 mg soy protein (dmb) with moisture around 60% was loaded. Samples were scanned from 10 to 150°C at a heating rate of 10°C/min. Denaturation temperatures (T_d) were determined from the peak temperatures. Denaturation enthalpies (ΔH) were calculated from the areas of the denaturation peaks.

2.5. SDS-PAGE. The precipitated wet protein was diluted with distilled water by adjusting pH to pH 8.2 using 2 N NaOH. Protein concentration was determined with Bradford method. SDS-PAGE of soy protein samples was performed on a 4% stacking gel and 12% separating gel. Fifty milligrams of soy protein was inoculated into the gel for each sample. A prestained standard with molecular weight from 8 kDa to 250 kDa was used. Electrophoresis was performed at 120 V for 2 hr. The gel was stained in 0.1% Coomassie brilliant blue R-250 and destained in a solution containing 10% acetic acid and 40% methanol. Densitometry of the gel was analyzed by the Kodak 1D Image Analysis software, version 4.6 (Kodak, Rochester, NY).

2.6. Western Blot Procedures with Human Plasma. Western blot was performed according to the method of Frias et al. [5] with modifications. Human plasma used had soybean-specific IgE 10 kUA/L provided by PlasmaLab International (Everett, WA). After transferring, the membrane was stained with Ponceau S for 5 min to check the transferring effect. Ponceau S was then washed off with distilled water before proceeding to the next step. For the saturation solution, primary and secondary antibodies were prepared in tris-buffered saline (TBS) instead in 0.01% Tween in TBS (TTBS) buffer, to avoid the dark background. The membrane was exposed to Kodak X-ray film.

2.7. Chemical Analyses. The proximate composition was analyzed by the Agricultural Experiment Station Chemical Laboratories, University of Missouri (Columbia, MO) using the following methods: crude protein (AOAC Official Method 990.03, 2006) [14], crude fat (ether extraction, AOAC Official Method 920.39 (A)) [14], crude fiber (AOAC Official Method 978.10, 2006) [14], acid detergent fiber (ADF) (AOAC Official Method 973.18 (A–D), 2006) [14], neutral detergent fiber (NDF) [14], cellulose (AOAC Official Method 973.18 (A–D), 2006) [14], pepsin digestibility (AOAC Official Method 971.09, 2006) [14], amino acid profile (AOAC Official Method 982.30 E (a, b, c), chp.45.3.05, 2006) [14], and available lysine (AOAC Official Method 975.22, chp.45.4.03, 2006) [14].

3. Results

Figure 1 shows the DSC results of soy protein samples pretreated at different temperatures and their corresponding fermentation products. SM and SMV both had two peaks, with the degradation temperatures (T_d) at around 79°C and 96°C. SM100C and SM100 each had one peak at temperature around 97°C. SM121C and SM121 had one indiscernible peak at around 97°C.

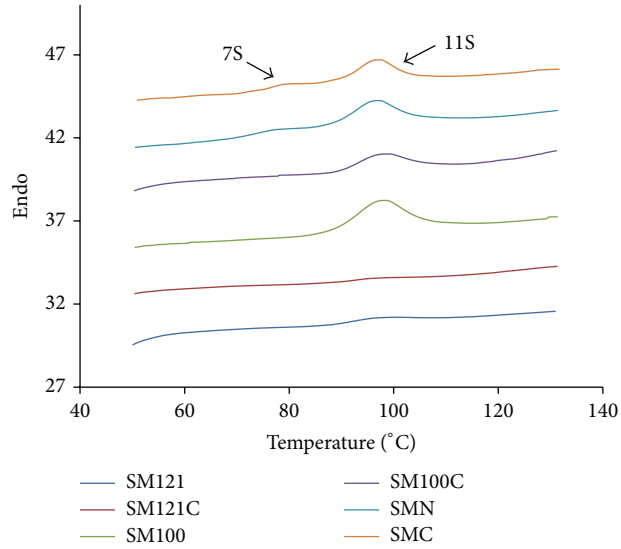

Figure 1: DSC thermogram of soy protein and fermented soy protein pretreated at different conditions.

Figure 2 shows the SDS-PAGE results of soy meal samples with different pretreatment. SM contained 79% bands with molecular weight larger than 60,000 kDa, but SM100C only had 4% bands and SM121C only had 6% bands in that range. For SMV, SM100, and SM121, the three fermented samples, the molecular weight of all peptides was smaller than 60,000 kDa. All the fermented samples had 2% small peptides with molecular weight smaller than 10,000 kDa, which the controlling unfermented samples were not endowed. The α and α' subunits of SM were not shown in SMV, and β-conglycinin was not shown in SM100 and SM121 and their controls.

Figure 3 shows the Ponceau S staining of the membrane after transferring. Comparing with Figure 2, all bands in SDS-PAGE gel had been transferred to the membrane. Figure 4 shows the immunodominant proteins interacting with human plasma 10 kUA/L. SM presented the highest complexity protein profile and plasma immunoreactivity towards α- and α'- (75 kDa) and β- (50 kDa) conglycinin subunits, P34 fraction, and glycinin basic (30 kDa) and acidic (22 kDa) subunits. Its corresponding fermented sample SMV did not have immunoreactive proteins toward α- and α'- (75 kDa) conglycinin subunits. Compared with SM, the immunoreactions signals for β-conglycinin, P34, and acidic (22 kDa) glycinin subunits were weak for SM100C. There was no visible immunoreactivity for β-conglycinin in SM100. SM121 and SM121C had immunoreactive protein towards basic (30 kDa) glycinin only.

The composition changes of SM samples are shown in Table 1. Heat treatment did not significantly influence the content of crude protein, crude fat, crude fiber, total ash, and pepsin digestibility but decreased the content of crude fiber, acid detergent fiber, and cellulose content and increased the neutral detergent fiber. Also, heat treatment decreased the content of available lysine content. The higher the temperature, the lower the available lysine content of heat pretreated soy meal. The content of all components increased after fermentation, except for the fact that pepsin digestibility decreased. Fermented samples with higher heat treatment had higher available lysine.

Table 1: Proximates of soy meal samples.

Samples	SM	SMV	SM100C	SM100	SM121C	SM121
Crude protein	50.46^{b}	58.78^{a}	50.74^{b}	58.82^{a}	50.62^{b}	58.47^{a}
Crude fat	2.93^{a}	3.15^{a}	2.06^{b}	3.07^{a}	2.24^{b}	2.94^{a}
Crude fiber	3.32^{b}	4.14^{c}	3.11^{c}	4.37^{b}	3.02^{c}	5^{a}
Ash	6.68^{d}	8.05^{b}	6.93^{c}	8.24^{a}	6.66^{d}	8.31^{a}
ADF	5.48^{c}	7.7^{a}	4.74^{c}	7.52^{a}	4.67^{c}	7.11^{b}
NDF	8.18^{b}	10.13^{b}	12.38^{b}	11.41^{b}	18.15^{a}	12.3^{b}
Cellulose	5.41^{c}	7.51^{a}	4.75^{d}	7.42^{a}	4.62^{d}	6.99^{b}
Pepsin digestibility	95.33^{a}	93.07^{c}	95.18^{a}	94.1^{b}	94.84^{a}	93.33^{c}
Available lysine	3.06^{b}	3.07^{b}	2.95^{c}	3.08^{b}	2.84^{d}	3.26^{a}

Mean values in a row with different superscript letters are significantly different according to the least-significant difference (LSD) test at the 0.05 level analyzed by SAS software (2009).

Table 2: Amino acids changes of soy protein with different treatment.

Sample	SM	SMV	SM100C	SM100	SM121C	SM121
Hydroxyproline	0^{b}	0.11^{a}	0.1^{a}	0.11^{a}	0^{b}	0.12^{a}
Aspartic acid	5.77^{b}	6.27^{a}	5.62^{c}	6.24^{a}	5.66^{bc}	6.3^{a}
Threonine	1.93^{b}	2.09^{a}	1.92^{b}	2.17^{a}	1.85^{b}	2.15^{a}
Serine	2.14^{a}	2.58^{a}	2.34^{a}	2.57^{a}	2.04^{a}	2.29^{a}
Glutamic acid	8.85^{ab}	8.91^{ab}	8.42^{b}	9.07^{a}	8.66^{ab}	9.02^{a}
Proline	2.53^{bc}	3.04^{a}	2.45^{c}	2.62^{bc}	2.51^{bc}	2.67^{b}
Glycine	2.14^{b}	2.28^{a}	2.05^{b}	2.38^{a}	2.07^{b}	2.39^{a}
Alanine	2.19^{b}	2.41^{a}	2.13^{b}	2.39^{a}	2.13^{b}	2.45^{a}
Cysteine	0.7^{b}	0.8^{a}	0.66^{b}	0.82^{a}	0.67^{b}	0.82^{a}
Valine	2.52^{d}	2.96^{ab}	2.63^{c}	2.89^{b}	2.51^{d}	3.01^{a}
Methionine	0.72^{d}	0.75^{c}	0.68^{f}	0.76^{b}	0.7^{e}	0.78^{a}
Isoleucine	2.39^{dc}	2.52^{b}	2.32^{d}	2.47^{bc}	2.33^{d}	2.63^{a}
Leucine	3.92^{c}	4.43^{a}	3.95^{c}	4.24^{b}	3.84^{d}	4.24^{b}
Tyrosine	1.84^{b}	1.94^{a}	1.78^{b}	1.91^{a}	1.77^{b}	1.93^{a}
Phenylalanine	2.53^{bc}	2.75^{a}	2.48^{c}	2.58^{b}	2.48^{c}	2.59^{b}
Hydroxylysine	0.03^{a}	0.02^{ab}	0.01^{c}	0.02^{ab}	0.02^{ab}	0.02^{ab}
Ornithine	0.03^{b}	0.04^{b}	0.03^{b}	0.05^{b}	0.04^{b}	0.07^{a}
Lysine	3.24^{b}	3.22^{b}	3.12^{c}	3.29^{b}	3.1^{c}	3.51^{a}
Histidine	1.32^{b}	1.38^{a}	1.27^{c}	1.37^{a}	1.27^{c}	1.4^{a}
Arginine	3.64^{a}	3.48^{c}	3.56^{b}	3.48^{c}	3.52^{bc}	3.57^{b}
Tryptophan	0.74^{c}	0.81^{b}	0.79^{b}	0.89^{a}	0.71^{c}	0.92^{a}
Total	49.13^{b}	52.73^{a}	48.28^{b}	52.27^{a}	47.84^{b}	52.83^{a}

Mean values in a row with different superscript letters are significantly different according to the least-significant difference (LSD) test at the 0.05 level analyzed by SAS software (2009).

Amino acid contents of fermented samples are shown in Table 2. Heat treatment did not significantly affect essential amino acids content, except for lysine. Fermentation

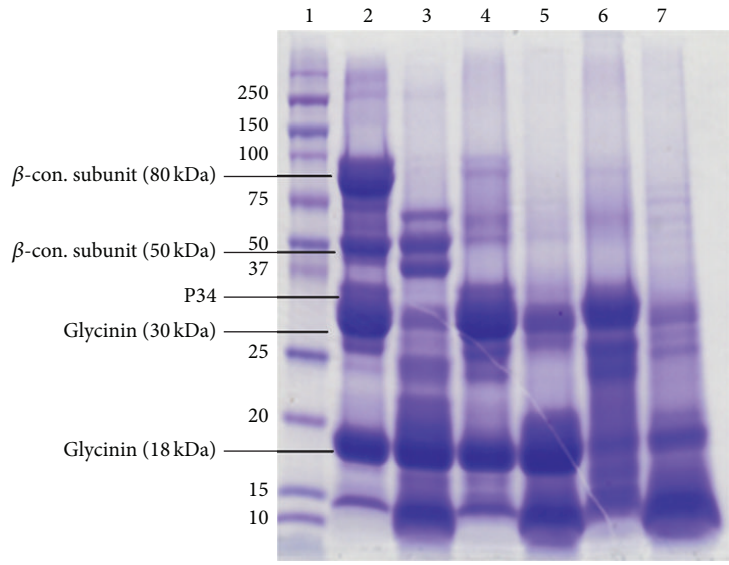

Figure 2: SDS-PAGE for soy protein and fermented soy protein pretreated at different conditions. Lane 1: prestained standard; lane 2: SM; lane 3: SMV; lane 4: SM100C; lane 5: SM100; lane 6: SM121C; lane 7: SM121.

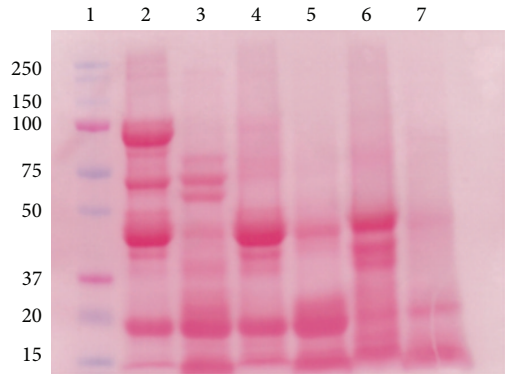

Figure 3: Ponceau S staining of the membrane after transferring. Lane 1: prestained standard; lane 2: SM; lane 3: SMV; lane 4: SM100C; lane 5: SM100; lane 6: SM121C; lane 7: SM121.

increased the total amino acids content of SM, SM100C, and SM121C by 7%, 8%, and 9%, respectively. Fermentation also increased all amino acids contents. The higher the temperature, the higher the amino acid content of fermented samples. Methionine, cysteine, and threonine in SM121 increased by 11.4%, 22.39%, and 16.22% after fermentation, respectively. Lysine and tryptophan in SM121 increased by 13% and 30% compared with SM121C.

4. Discussion

Soy protein denaturation is an endothermic process [15], caused by rupture of inter- and intramolecular bonds. Its denaturation degree could be shown by DSC. Undenatured soy protein has two peaks in the DSC curve, which represent the two main soy storage proteins, conglycinin and glycinin [15]. Glycinin is more heat stable than conglycinin [15]. The T_d for glycinin was in the range of 96.3–97.7°C, while the T_d for conglycinin was in the range of 77.1–79.3°C (Figure 1). Protein denaturation is a nonreversible process [15]. The denatured protein would not show peaks on the DSC diagram. According to Figure 1, protein in SM and SMV was nondenatured; 7S subunits in SM100C and SM100 were denatured; in SM121C and SM121, 7S subunits were totally denatured while 11S subunits were almost totally denatured.

SDS-PAGE is a common method to evaluate protein molecular size. But for heat treated samples, it did not work well, according to our result. The denatured 7S subunit of soy protein was not shown on SM100C and SM121C lanes. This did not mean that SM100C and SM121C had less large molecular weight protein. Protein denaturation was the change of the secondary, tertiary, and quaternary structures. Thermal energy input disrupted the weak bonds stabilizing the native conformation, causing protein to unfold [16]. The denatured protein may form large aggregate [17], which may become insoluble and would not be shown on SDS-PAGE. Wang et al. [16] also showed that 100°C heating for 20 min resulted in the loss of protein bands on SDS gel. The addition of virginiamycin avoided the heat pretreatment of soy meal. *A. oryzae* solid state fermentation could degrade large protein molecules into smaller peptides, as shown by comparing the molecular weight of SM and SMV from Figure 2.

About 34 subunits of soy protein have been recognized as allergens [3]. Our result also showed the strong signal of immunoreactive protein in SM. Heat treatment has been shown to affect allergen conformational epitopes and decrease its immunoreactivity [18]. Western blot has been used to illustrate protein immunoreactivity. Like SDS-PAGE, there was still the problem caused by heat induced protein

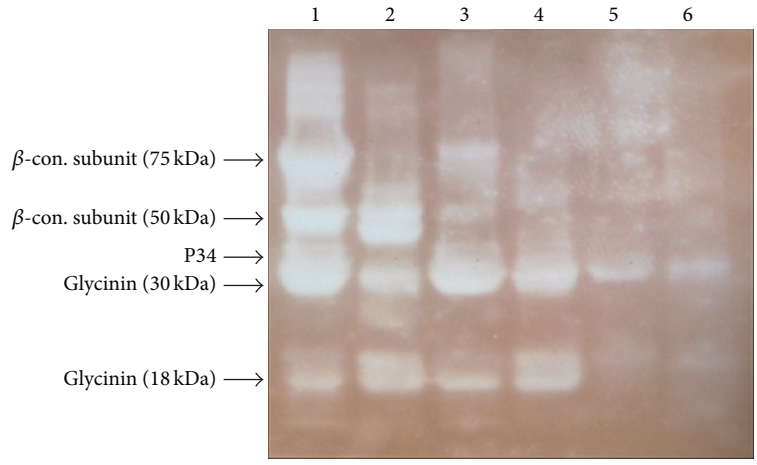

Figure 4: Western blot results of soy protein samples. Lane 1: SM; lane 2: SMV; lane 3: SM100C; lane 4: SM100; lane 5: SM121C; lane 6: SM121.

denature. Subunits of soy protein, like β-conglycinin in SM100C and SM121C and acidic glycinin in SM121C, were not visible on western blot. This did not mean that they did not have immunoreactivity, but they were not present on SDS gel. The virginiamycin addition helped investigate soy protein immunoreactivity change during fermentation process. The weaker immunoreactive signals for SMV, comparing with SM, illustrated that *A. oryzae* solid state fermentation could decrease immunoreactive soy protein.

Natural fermentation has been shown to degrade soy protein molecular size with nonheated samples [5]. In the natural fermentation, various kinds of microorganisms have been involved. Different proteases target different protein subunits [19]. In order to achieve better degradation, it is necessary to investigate the fermentation effect of specific microorganism. Virginiamycin could inhibit bacterial growth while the inoculum of desired fungus could inhibit the growth of other contaminating fungi, according to our results. Virginiamycin addition excluded the necessity of heat treatment, which was beneficial to the protein size and immunoreactivity investigation.

A. oryzae secretes acidic and neutral proteases, which could degrade epitopes [18]. According to our research, *A. oryzae* fermentation provides means to degrade soy protein molecular size while decreasing its immunoreactive protein. Soy protein with low molecular weight and weak or no immunoreactive protein have been added to newly weaned piglets' diet to lower the feeding cost [2]. Fermentation parameters, such as temperature, moisture, and fermentation time, need to be optimized to maximize the protein degradation and to produce hypoallergenic fermented soy products for young pigs.

Acid detergent fiber mainly includes cellulose and lignin. Neutral detergent fiber mainly includes hemicelluloses, cellulose, and lignin. Heat treatment may degrade lignin or catalyze complex structure formation between hemicelluloses and lignin or hemicelluloses with other components, like lysine. Lysine is susceptible to react with other compounds, such as reducing sugars to form Maillard compounds, resulting in the loss of available lysine and reduction of nutritional value. *A. oryzae* secretes various kinds of enzymes, such as α-amylase, carboxymethyl cellulase, pectin lyase, protease, and *endo*-β-xylanase (EC 3.2.1.8) [20] to help utilize soy meal components to meet its growth needs. The enhancement of all components by fermentation was mainly because of the dry matter loss resulting from *A. oryzae* consumption, which concentrated the nutritional compounds. Proper heat could unfold protein structure and make protein easier to digest by proteases. The decrease of the pepsin digestibility may be partially contributed by the increased protein content.

Soy protein is rich in lysine and tryptophan but lacking in methionine and threonine, compared with cereals proteins. SM and maize are main ingredients for monogastric animals' diet and provide complementary amino acid profiles. Amino acids deficiency may decrease feed efficiency and feed intake, cause weight loss, and influence animals' growth performance [21]. *A. oryzae* solid state fermentation enhanced the amino acid contents of all samples, especially for the SM121. One reason for the increase of amino acids is the dry matter loss, which has been illustrated for solid state fermentation [22]. The second reason is the hydrolysis of protein by protease secreted from *A. oryzae* [22]. Also, the increase of *A. oryzae* biomass contributes to the amino acids and protein increase [22]. Heat treatment could expose inside peptide bonds and ease enzymatic hydrolysis. Proper heat treatment might benefit the subsequent fermentation process.

A. oryzae solid state fermentation could degrade large soy protein molecular size and decrease soy protein immunoreactivity. *A. oryzae* protease had priority for α and α' components of β-conglycinin. Virginiamycin facilitated the investigation on fermentation degradation of soy protein, by avoiding the interruption from heating. Fermentation enhanced the nutritional value of soy meal, with higher protein content. Essential amino acids contents were also enhanced by fermentation. Proper heat treatment facilitated the fermentation process. The value added FSM should have a wider market than SM, particularly for newly weaned piglets.

Abbreviations

ATCC:	American Type Culture Collection
DSC:	Differential scanning calorimetry
SDS-PAGE:	Sodium dodecyl sulfate polyacrylamide gel electrophoresis
ADF:	Acid detergent fiber
NDF:	Neutral detergent fiber
AOAC:	Association of Official Analytical Chemists
SM:	Soy meal
FSM:	Fermented soy meal
SMV:	Fermented soy meal with virginiamycin added
SM100C:	Soy meal autoclaved at 100°C for 30 min
SM100:	Fermented soy meal which was autoclaved at 100°C for 30 min
SM121C:	Soy meal autoclaved at 121°C for 15 min
SM121:	Fermented soy meal which was autoclaved at 121°C for 15 min.

Conflict of Interests

The authors declare that there is no conflict of interests regarding the publication of this paper.

Acknowledgments

The authors would like to thank Dr. Timothy Durrett in the Department of Biochemistry, Kansas State University, for helping with the western blot analysis. The authors are grateful to the Department of Grain Science and Industry, Kansas State University, and Kansas Soybean Commission for funding this project. This is Contribution no. 13-155-J from the Kansas Agricultural Experiment Station.

References

[1] L. Chen, Y. Zhang, R. L. Madl, and P. V. Vadlani, "Nutritional enhancement of soybean meal and hull via enzymatic and microbial bioconversion," in *Soybeans: Cultivation, Uses and Nutrition*, J. E. Maxwell, Ed., Nova Science Publishers, New York, NY, USA, 2010.

[2] Y. S. Song, V. G. Pérez, J. E. Pettigrew, C. Martinez-Villaluenga, and E. G. de Mejia, "Fermentation of soybean meal and its inclusion in diets for newly weaned pigs reduced diarrhea and measures of immunoreactivity in the plasma," *Animal Feed Science and Technology*, vol. 159, no. 1-2, pp. 41–49, 2010.

[3] S. Wilson, C. Martinez-Villaluenga, and E. G. de Mejia, "Purification, thermal stability, and antigenicity of the immunodominant soybean allergen P34 in soy cultivars, ingredients, and products," *Journal of Food Science*, vol. 73, no. 6, pp. T106–T114, 2008.

[4] Y. Zhao, G. Qin, Z. Sun et al., "Disappearance of immunoreactive glycinin and β-conglycinin in the digestive tract of piglets," *Archives of Animal Nutrition*, vol. 62, no. 4, pp. 322–330, 2008.

[5] J. Frias, Y. S. Young, C. Martínez-Villaluenga, E. G. De Mejia, and C. Vidal-Valverde, "Immunoreactivity and amino acid content of fermented soybean products," *Journal of Agricultural and Food Chemistry*, vol. 56, no. 1, pp. 99–105, 2008.

[6] Y.-S. Song, J. Frias, C. Martinez-Villaluenga, C. Vidal-Valdeverde, and E. G. de Mejia, "Immunoreactivity reduction of soybean meal by fermentation, effect on amino acid composition and antigenicity of commercial soy products," *Food Chemistry*, vol. 108, no. 2, pp. 571–581, 2008.

[7] P. Amnuaycheewa and E. G. de Mejia, "Purification, characterisation, and quantification of the soy allergen profilin (Gly m 3) in soy products," *Food Chemistry*, vol. 119, no. 4, pp. 1671–1680, 2010.

[8] E. N. C. Mills, J. A. Jenkins, M. J. C. Alcocer, and P. R. Shewry, "Structural, biological, and evolutionary relationships of plant food allergens sensitizing via the gastrointestinal tract," *Critical Reviews in Food Science and Nutrition*, vol. 44, no. 5, pp. 379–407, 2004.

[9] L. Chen, P. V. Vadlani, and R. L. Madl, "High-efficiency removal of phytic acid in soy meal using two-stage temperature-induced *Aspergillus oryzae* solid-state fermentation," *Journal of the Science of Food and Agriculture*, vol. 94, no. 1, pp. 113–118, 2014.

[10] X. Liu, J. Feng, Z. Xu, Y. Lu, and Y. Liu, "The effects of fermented soybean meal on growth performance and immune characteristics in weaned piglets," *Turkish Journal of Veterinary and Animal Sciences*, vol. 31, no. 5, pp. 341–345, 2007.

[11] R. Yamanishi, H. Tsuji, N. Bando et al., "Reduction of the allergenicity of soybean by treatment with proteases," *Journal of Nutritional Science and Vitaminology*, vol. 42, no. 6, pp. 581–587, 1996.

[12] T. J. Dumonceaux, J. E. Hill, S. M. Hemmingsen, and A. G. Van Kessel, "Characterization of intestinal microbiota and response to dietary virginiamycin supplementation in the broiler chicken," *Applied and Environmental Microbiology*, vol. 72, no. 4, pp. 2815–2823, 2006.

[13] S. H. Hynes, D. M. Kjarsgaard, K. C. Thomas, and W. M. Ingledew, "Use of virginiamycin to control the growth of lactic acid bacteria during alcohol fermentation," *Journal of Industrial Microbiology and Biotechnology*, vol. 18, no. 4, pp. 284–291, 1997.

[14] AOAC International, *Official Methods of Analysis of AOAC International*, AOAC International, Gaithersburg, Md, USA, 2006.

[15] R. P. Wool and X. S. Sun, "Thermal and mechanical properties of soy proteins," in *Biobased Polymers and Composites*, R. P. Wool and X. S. Sun, Eds., pp. 292–300, Elsevier Science Publishers, Boston, Mass, USA, 2005.

[16] Y. Wang, X. S. Sun, and D. Wang, "Effects of preheating treatment on thermal property and adhesion performance of soy protein isolates," *Journal of Adhesion Science and Technology*, vol. 21, no. 15, pp. 1469–1481, 2007.

[17] S. Utsumi, S. Damodaran, and J. E. Kinsella, "Heat-induced interactions between soybean proteins: preferential association of 11S basic subunits and β subunits of 7S," *Journal of Agricultural and Food Chemistry*, vol. 32, no. 6, pp. 1406–1412, 1984.

[18] J. Maldonado, A. Gil, E. Narbona, and J. A. Molina, "Special formulas in infant nutrition: a review," *Early Human Development*, vol. 53, pp. S23–S32, 1998.

[19] K. Tsumura, "Improvement of the physicochemical properties of soybean proteins by enzymatic hydrolysis," *Food Science and Technology Research*, vol. 15, no. 4, pp. 381–388, 2009.

[20] L. Chen, R. L. Madl, and P. V. Vadlani, "Value added products from soybean: removal of anti-nutritional factors via bioprocessing," in *Soybean: A Review*, H. El-Shemy, Ed., pp. 161–179, InTech, 2013.

[21] S. Moehn, P. B. Pencharz, and R. O. Ball, "Lessons learned regarding symptoms of tryptophan deficiency and excess from animal requirement studies," *Journal of Nutrition*, vol. 142, no. 12, pp. 2231S–2235S, 2012.

[22] L. Chen, R. L. Madl, and P. V. Vadlani, "Nutritional enhancement of soy meal via *Aspergillus oryzae* solid-state fermentation," *Cereal Chemistry*, vol. 90, no. 6, pp. 529–534, 2013.

Hindawi Publishing Corporation
International Journal of Polymer Science
Volume 2015, Article ID 250146, 8 pages
http://dx.doi.org/10.1155/2015/250146

Research Article

Soy 11S Globulin Acid Subunits as the Novel Food Polymer Carrier

Lei Chen,[1] Dahai Liu,[1] Guohua Wu,[2] and Yuanyuan Ma[1]

[1]*School of Life Sciences, Anhui University, 111 Jiulong Road, Hefei, Anhui 230601, China*
[2]*Laboratory of Quality & Safety Risk Assessment for Sericultural Products and Edible Insects, Ministry of Agriculture, College of Biotechnology and Sericultural Research Institute, Jiangsu University of Science and Technology, Zhenjiang 212018, China*

Correspondence should be addressed to Lei Chen; sunang.32@163.com

Received 3 February 2015; Accepted 13 April 2015

Academic Editor: Liyan Chen

Aflatoxins were conjugated with soy 11S globulins acid subunits and the hapten-specific monoclonal antibodies (McAbs) cross-reactive with four major aflatoxins were achieved using indirect competitive ELISA screening procedure. The two antibodies (clones 1B2 and 2D3) had similar reaction efficiency with aflatoxins B1, B2, and G1 but showed a weak cross-reaction to G2. The clone 4C5 exhibited the highest sensitivity for all four aflatoxins. The concentrations of aflatoxins B1, B2, G1, and G2 at 50% inhibition for 4C5 were 1.1, 1.2, 2.1, and 17.6 pg mL^{-1}. The results indicated that soy 11S globulin acid subunits were suitable novel carriers for aflatoxin antigen in immunization experiments and clone 4C5 could be used for simultaneous analysis of total aflatoxins.

1. Introduction

Aflatoxins are highly toxic and carcinogenic compounds, which are a group of structurally related toxic metabolites produced by *Aspergillus flavus* and *Aspergillus parasiticus* [1]. The kinds of aflatoxins include aflatoxins B1, B2, G1, G2, and M1. Aflatoxins frequently contaminate a wide range of foods and animal feedstuffs. Aflatoxin B1 (AFB1) is the most toxic. These aflatoxins are found consistently contaminating feed and food supplies in many areas [2, 3]. A number of well-established methods have been reported for analyzing aflatoxins in various food systems, such as near infrared spectroscopy [4], high-performance liquid, thin liquid chromatography [5], and immunoaffinity chromatography-performance liquid chromatography [6]. As immunoassay methods, enzyme-linked immunosorbent assay (ELISA) is well suited for the rapid, routine diagnostic application of aflatoxin detection [7]. These methods are advantageous in the simple operation, portability of the equipment, and handholding validation and reliable for the analysis of a large number of samples.

Currently, the conventional immunogenic carriers used in ELISA are bovine serum albumin (BSA), human serum albumin (HSA), and keyhole limpet hemocyanin (KLH). However, when these proteins are used as the immunogen carrier, the affinity of the corresponding antibodies is relatively weak [8]. Additionally, KLH and HSA are also relatively expensive and not easily obtainable. The purpose of this study was to find a suitable protein instead of BSA, KLH, and the like. The ideal carrier should have a comparatively stable structure and strong water-solubility, regardless of being under any organic solvent circumstances. Soy 11S globulin is an inhomogeneous protein whose molecular weight ranges from 340 to 375 kDa [9] which is made up of six acid subunits (A1, A2, A3, A4, A5, and A6) and six alkaline subunits (B1, B2, B3, B4, B5, and B6). In this paper, we report a method in which aflatoxins were conjugated with soy 11S globulins acid subunits initially and the production of generic monoclonal antibodies against major aflatoxins using a two-step screening procedure. Details for the production of desired hybridoma clones are described in this paper.

2. Materials and Methods

2.1. Chemicals and Instruments. Bovine serum albumin (BSA), ovalbumin (OVA), standards of aflatoxins (AFs) B1, B2, G1, G2, and M1, N-hydroxysuccinimide (NHS), 1-(3-dimethylaminopropyl)-3-ethylcarbodiimidehydrochloride

(EDC), tetramethylbenzidine (TMB), goat anti-mouse immunoglobulin horseradish peroxidase (IgG-HRP), and RPMI-1640 medium with l-glutamine and HEPES (free acid, 283.3 g/L) were obtained from HyClone; hypoxanthine, aminopterin, and thymidine (HAT), poly(ethylene glycol) (PEG) 1500, and complete and incomplete Freund's adjuvant were purchased from Sigma Chemical Co. (St. Louis, MO, USA). Mouse monoclonal antibody isotyping kit was obtained from Roche Diagnostics Corporation (Indianapolis, USA). SP2/0 myeloma cells were purchased from China Center for Type Culture Collection (CCTCC). 96-well microtiter plates (Corning-Costar, 3590) and cell culture plates (6, 24, and 96 wells) were from Iwaki, Japan. Polystyrene 96-well microtiter plates were from Costar (Corning, Massachusetts, USA). Female Balb/c mice were purchased from Centers for Disease Control and Prevention of Jilin province.

The absorbance at 450 nm was detected by using a Spectra Max microplate reader (Molecular Devices, USA) ELISA plates were washed with well wash Plus and well absorbances were measured with a microtiter plate reader, which was controlled by a personal computer containing the standard software package Easy Software. They were both from Thermo Electron Co. (MA, USA). Fluorescence measurements were performed on an F-4500 spectrophotometer (HITACHI, Japan) equipped with a 150 W xenon lamp and 5 nm slit width and 1.00 cm quartz cell at a scanning speed of 1200 nm min^{-1}; the temperature was controlled by digital aqueous thermostat.

2.2. Preparation of Soy 11S Globulin and Soy 7S Globulin. Soy 11S globulin and soy 7S globulin were isolated according to a new method [10], which is a modification of the procedure of Deak et al.

2.3. Isolation and Purification of Soy 11S Globulin Acid Subunits. 1.5425 g DTT was added to a solution of 500 mL soy 11S globulin (11 mg/mL, PH 8.0) and shaken for about 1 h; then the protein solution was heated for 30 min and centrifugal separation 3 times (10000 r·min^{-1}, 20 min) at 4°C [11]. The freeze-dried precipitation was basic subunits (BS), and the freeze-dried supernatant was acid subunits (AS). The acid subunits were identified by SDS-PAGE patterns.

2.4. Preparation and Characterization of Aflatoxin B1-AS Conjugates. Aflatoxin B1 was first converted to AFB1-O-carboxymethyloxime (AFB1-oxime) as previously described [12]. Structure characterization of AFB1-oxime was performed by NSI/MS (spray voltage: 2.8 kV, capillary Temp: 270°C, capillary voltage: 36 V, and lens voltages: 115 V). AFB1-AS conjugates were prepared by the EDC-ester method, avoiding unfavorable coupling of activating reagent (DCC) with AS [13]. Briefly, 2 mL of a solution of 4.5 mg soy 11S globulin acid subunits and 50 mg EDC were added to a solution of 2.0 mg AFB1-oxime in 2 mL of dry ethanol and the resulting solution was shaken for 48 h in a closed vial at room temperature. 80 microliters of the AFB1-oxime solution was added to an ice-cold solution of 2.0 mg AS in 230 μL of coupling buffer and shaken for 6 h. The protein conjugates (AFB1-AS) were subsequently purified on a Sephadex G-25 column using PBS as mobile phase [14]. AFB1-AS conjugate was characterized using UV-vis absorption spectrophotometer (UV-2300, Techcomp).

2.5. Preparation of Coating Antigen (AFB1-OVA). AFB1-oxime was conjugated with OVA and the coating antigen (AFB1-OVA) was prepared. Equal volume of glycerol was added to the AFB1-OVA solution and then stored at −30°C after dialyzing.

2.6. Preparation and Characterization of Monoclonal Antibodies

2.6.1. Immunization. Six five-week-old female Balb/c mice were subcutaneously immunized with AFB1-AS conjugates in the initial immunization. The initial dose consisted of 50 μg of AFB1-AS conjugate intraperitoneally injected using Freund's complete adjuvant and the remaining two subsequent injections were given with Freund's incomplete adjuvant at 2-week intervals. After each injection, Antisera were collected from the caudal vein of each mouse and assayed for anti-aflatoxin B1 antibodies [15] by indirect competitive ELISAs (ciELISAs) with aflatoxins B1, B2, G1, and G2 as the competitors. An intraperitoneal booster was given to the mouse whose antiserum exhibited better cross-reactivity (CR) and higher sensitivity with aflatoxins 3 days prior to cell fusion.

2.6.2. Cell Fusion and Screening. At the beginning, SP 2/0 murine myeloma cells were cultured in RPMI-1640 media supplemented with 20% fetal bovine serum. Cell fusion was carried out as described by Devi et al. [16]. The myeloma cells were mixed with mice splenocytes and centrifuged at the ratio of 5–10 : 1. One milliliter of PEG 1500 was dropped into the cell pellet about 1 min at 37°C. After an addition of 30 mL of RPMI-1640 about 5 min, the cells were left aside for 5–10 min. And then the fused cells were mixed with selective semisolid media (RPMI 1640 medium supplemented with 20% (v/v) foetal bovine serum (FBS), 100 μg/mL streptomycin, 100 U/mL penicillin, 1% (w/v) methyl cellulose, 1% (v/v) HEPES, HAT, and 2% (v/v) HFCS) and plated to 6-well plate (1.5 mL/well). The plates were examined for the presence of hybridomas; then culture supernatants were assayed from the wells which contained hybridomas, after 12 days later. Only those hybridomas which maintained absorption values were chosen for further selection, because they had good cross-reactivity with aflatoxins B1, B2, G1, and G2 and had no cross-reactivity with OVA. According to standard methods with some modifications, cells from each interested well were subcloned by limiting dilution to ensure monoclonality [15]. Monoclonal cell strains which secreted desired antibodies were screened out by 2-3 limiting dilutions. According to the freezing protocol, 30 min at 4°C, the resulting hybridoma clones were cryopreserved and propagated in freezing solution, in gas of liquid nitrogen jar overnight, and then stored in liquid nitrogen [17].

2.6.3. Indirect Competitive ELISA Screening. Indirect competitive ELISAs were applied in the two-step screening procedure. To eliminate antibodies and screen positive wells that react with OVA, beside AFB1-OVA (diluted 1 : 250 in coating buffer), OVA alone (twofold concentration of AFB1-OVA) intervals with AFB1-OVA at one row were also coated to plates (100 μL/well). The indirect competitive ELISA was carried out to screen clones that had good cross-reactivity and high sensitivity to four aflatoxins from positive wells [18, 19]. To obtain high affinity antibodies, gradiently decreased concentrations of four aflatoxins (added concentrations were 100, 50, 20, and 10 ng mL^{-1} and the corresponding final concentrations were 50, 25, 10, and 5 ng mL^{-1} resp.) were used for the first screening and the following two or three screenings after subclone.

2.6.4. Titer Assessment and Isotype Determination. Each strain of hybridoma cell was injected into three Balb/c mice. The ascites fluid collected from these three mice was pooled and either used directly in the immunoassays [20] on protein A-sepharose columns by affinity chromatography. The antibody titer was defined as the reciprocal of the highest ascites dilution which gave an absorbance greater than 2.0-fold the background absorbance of the negative serum in the first dilution [21, 22]. The Mabs antibodies isotypes were performed with a commercially available ISO2-1 kit from Sigma in direct ELISAs.

2.6.5. Evaluation of Antibody Cross-Reactivity and Sensitivity. The indirect competitive ELISA format (AFB1-OVA was diluted 1 : 1000 in coating buffer) was used to evaluate the monoclonal antibody sensitivity. Cross-reactivity with aflatoxin M1 was also performed, beside the major aflatoxins. Required as working concentration, the optimum dilution of antibody was defined as the dilution which gave an absorbance most close to 1.0. These data were converted to antibody inhibition, expressed as % $B/B0$, where $B0$ was the absorbance in the absence of analyte and B was the absorbance at each analyte concentration [23]. CR was determined by comparing the IC50 values (concentration resulting in half-maximum inhibition) of analytes for different aflatoxins and calculated as CR (%) = (IC50 AFB1/IC50 analyte) × 100 [24].

3. Results and Discussion

3.1. SDS-PAGE Patterns Identification of Soy 11S Globulin Acid Subunits. They include M. Prestained protein molecular marker 1, soy 11S globulin, marker 2, soy 7S globulin, marker 3, soy 11S globulin acid subunits, and, marker 4, soy 11S globulin basic subunits. Soy 11S globulin basic subunits SDS-PAGE pattern was shown in Figure 1. This result suggests that soy 11S globulin acid subunits were prepared successfully.

3.2. Electrospray Mass Spectrometry Identification of AFB1-Oxime. NSI/MS pattern was shown in Figure 2. The relative molecular mass of AFB1 was 312.3, the peak of m/z 408.06 was quasi-molecular ion peaks of AFB1 carboxymethyl activation-[AFB1-O+Na]+, consistent with the molecular mass of the deserved product C17H12O6. The peak of the m/z 422.06 may be the molecular ion peak of nitrogen conjugate of AFB1 sodium salt-[AFB1-O-N+Na]+; the peak of m/z 312.1 was AFB1 quasi-ion peaks. The result can be preliminarily concluded that the activation product is AFB1 carboxyl activation-AFB1-oxime.

3.3. UV-Vis Absorption Spectrogram Characterization. Ultraviolet absorption spectrogram of AFB1-AS and soy 11S globulin acid subunits was shown in Figure 3. The maximum absorption of AFB1-AS is consistent with AS at 290 nm. This result suggested that AFB1-AS were prepared successfully.

3.4. Resonance Light Scattering Spectra Analysis. Fluorescence spectra analysis of AFB1-AS was shown in Figure 4 at different coupling ratios. The characteristic fluorescence peak of acidic subunits occurs at 350 nm. The conjugation of AFB1 to acidic subunits not only resulted in the decrease of fluorescence intensity of acidic subunits, but also led to the blue shift of maximum emission wavelength from approximately 350 to 320 nm as the coupling ratio increased.

3.5. Monitoring Antiserum Titers and Isotype Determination. AFB1-AS conjugate induced all of the six Balb/c mice to produce hapten-specific antibodies 12 days after the initial immunization. On day 105, 4 of the six mice tested gave high antibody titers more than 8,000 but presented different degrees of reaction capability and sensitivity. Number 1, number 2, and number 4 mice were successively chosen for B-lymphocytes donors and for the subsequent fusion experiments with higher sensitivity and better cross-reactivity. Then we injected three stable hybridoma lines into Balb/c F1 hybrid mice and 8–15 mL ascitic fluid was collected from each mouse. All the last three class-specific McAbs 1B2, 2D3 and 4C5 were IgG class and had no cross-reactivity with BSA and OVA. The results of isotype determination and titration are shown in Table 1.

3.6. Evaluation of Antibody Cross-Reactivity and Sensitivity. The cross-reactivity, sensitivity, and the minimal inhibition values for three monoclonal antibodies are presented in Table 2. As shown in Figure 5, graphs are plotted as percentage inhibition ($B/B0$) against mass of toxin (pg mL^{-1}). In view of different McAbs and different aflatoxins, experiments were performed with different toxins concentration gradient. The antibodies showed good cross-reactivity. The variation coefficients were between 0.2% and 8.8% and the absolute absorbances ($B0$) were between 0.8 and 1.2 units. The two monoclonal antibodies, 1B2 and 2D3, which had similar reaction efficiency with B1, B2, and G1, however, showed a weak cross-reaction with G2. The clone 4C5 had the highest affinity to four aflatoxins and then was grouped in category 3.

The cross-reactivity of three McAbs with aflatoxin M1 was also performed. As shown in Figure 6, graphs plotted as percentage inhibition ($B/B0$) against AFM1 (pg mL^{-1}), experiments were performed with different concentration gradient of aflatoxin M1, aiming at different McAbs. The antibodies

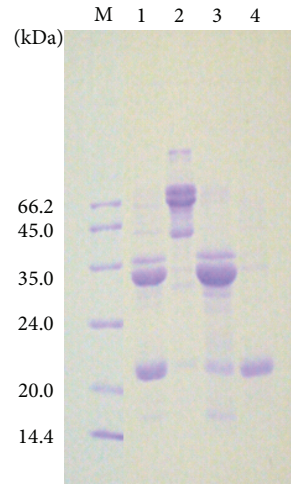

Figure 1: SDS-PAGE patterns of soy 11S globulin acid subunits.

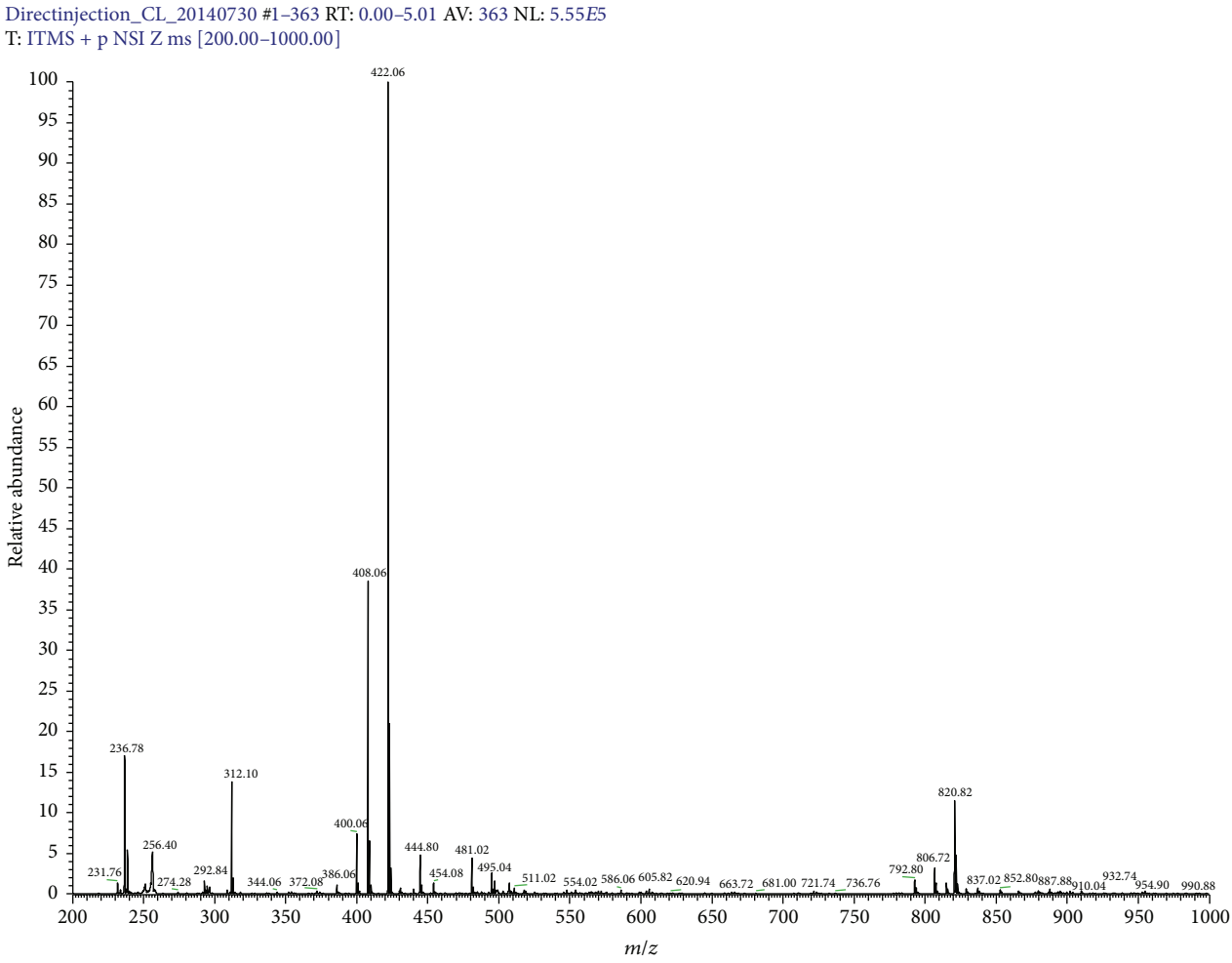

Figure 2: Electrospray mass spectrometry of AFB1-oxime.

Table 1: Results of titers and isotypes of ascites antibodies.

Clones	Isotype	Titer of crude ascites ($\times 10^4$)	OD450 values			
			Negative control serum	Blank control	1% AS	1% OVA
1B2	IgG1	69.0	0.102	0.06	0.07	0.07
2D3	IgG2a	87.5	0.087	0.05	0.06	0.06
4C5	IgG2a	432.0	0.082	0.04	0.05	0.05

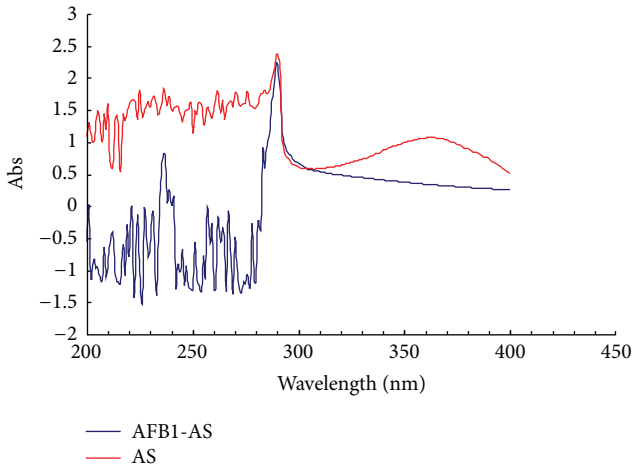

Figure 3: UV-vis absorption spectra of AFB1-AS and AS.

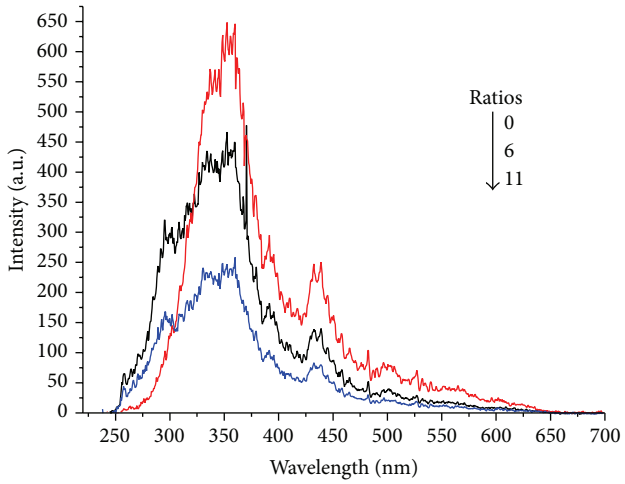

Figure 4: The effect of combination ratios on the resonance light scattering spectra of acidic subunit.

showed good cross-reactivity with aflatoxin M1. The variation coefficients were between 0.5% and 8.6% and the absolute absorbances ($B0$) were between 0.8 and 1.2 units. The cross-reactivity, sensitivity, and the minimal inhibition values for three monoclonal antibodies are presented in Table 3. The clone 4C5 showed the lowest cross-reactivity but exhibited the uppermost sensitivity; next came 1B2 and 2D3. The results of comparison showed that clone 4C5 was the best generic monoclonal antibody against the major aflatoxins.

Table 2: Results of sensitivity (expressed as pg mL^{-1}), cross-reactivity (CR%), and the minimal inhibition values of five monoclonal antibodies with four major aflatoxins.

Aflatoxins	Clones		
	1B2	2D3	4C5
Sensitivity (pg mL^{-1})			
B1	86.0	378.2	1.1
B2	95.5	759.3	1.2
G1	100.5	374.8	2.1
G2	405.6	2237.6	17.6
Cross-reactivity (%)			
B1	100.0	100.0	100.0
B2	92.1	58.5	94.6
G1	83.6	113.7	60.8
G2	18.7	15.9	5.9
Minimal inhibition (pg mL^{-1})			
B1	—*	105.7	—*
B2	0.7	39.8	0.02
G1	0.2	46.6	0.03
G2	1.6	25.9	—*

*Results were out of the measuring range.

Table 3: Results of sensitivity (expressed as pg mL^{-1}) and cross-reactivity (CR%) and the minimal inhibition values of five monoclonal antibodies with aflatoxin M1.

Aflatoxins M	Clones		
	1B2	2D3	4C5
Sensitivity (pg mL^{-1})	201.0	1147.2	13.2
Cross-reactivity (%)	42.8	35.7	9.0
Minimal inhibition (pg mL^{-1})	0.8	26.8	—*

*Refers to that the result was out of the measuring range.

3.7. Discussion. Though procedures have been established for the production of aflatoxins-BSA/OVA conjugates and antibodies to AFB1-BSA/OVA, this study was the first report of aflatoxins being conjugated with other carriers (such as soy 11S globulins acid subunits) and the evaluation of antibody sensitivity and cross-reactivity. The result stated that the AFB1-AS conjugate was prepared successfully. Soy 11S globulin acid subunits have stable structure and strong water-solubility, which are capable of conjugate with aflatoxin under organic solvent circumstances. AFB1-AS conjugate could induce Balb/c mice to produce hapten-specific antibodies, which exhibited the highest sensitivity for all four

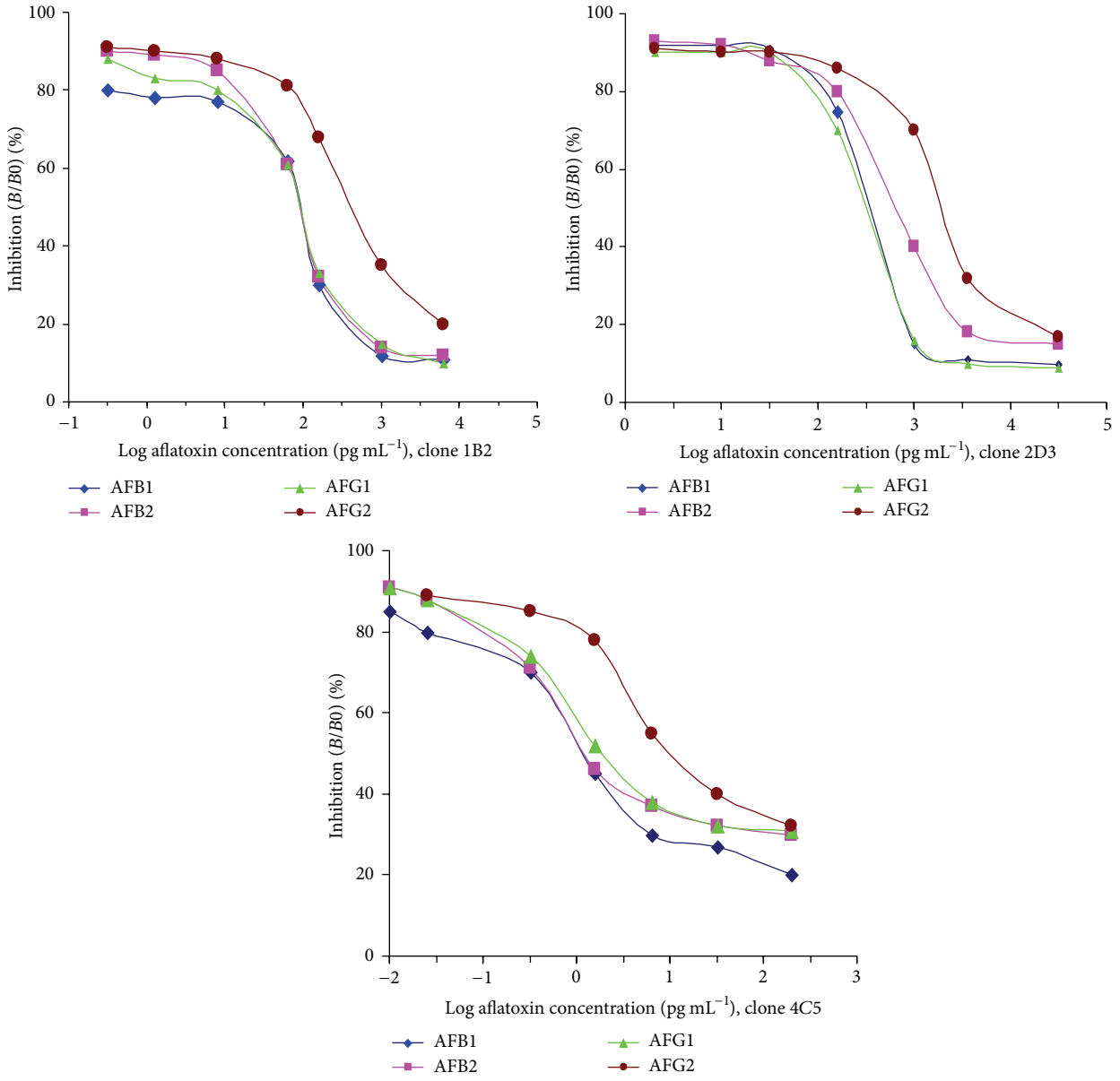

Figure 5: Cross-reactivity of three clones of monoclonal antibodies to four major aflatoxins.

aflatoxins. Nowadays, soybean seeds are cheap in China and soy 11S globulin acid subunits could be isolated from defatted soybean seeds easily. Our research proved that soy 11S globulin acid subunits are a suitable carrier for AFB1-oxime in immunization experiments and could be represented as a cheaper alternative to conventional immunogenic carriers such as BSA or OVA.

4. Conclusions

The novel AFB1-AS conjugates were prepared successfully and the three generic monoclonal antibodies were established by a modified two-step screening procedure for the determination of total aflatoxins. For clone 4C5, which exhibited the highest sensitivity for all four aflatoxins, the concentrations of aflatoxins B1, B2, G1, and G2 at 50% inhibition were 1.1, 1.2, 2.1, and 17.6 pg mL^{-1}, respectively. The results indicated that soy 11S globulin acid subunits are suitable novel carriers for aflatoxin antigen in immunization experiments and the two-step screening procedure (indirect competitive ELISA) was proved to be superior especially for the generation of antihapten McAbs.

Conflict of Interests

The authors declare that there is no conflict of interests regarding the publication of this paper.

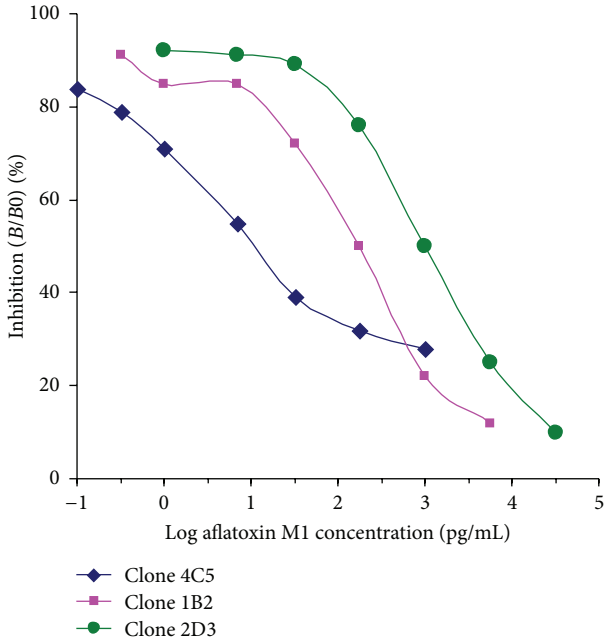

Figure 6: Cross-reactivity of three McAbs to aflatoxin M1.

Acknowledgments

This work was supported by the Education Revitalization Project of Anhui Province, "Stem Cell and Translational Medicine" (Y05201374) and the Natural Science Foundation of Anhui Province of China (Grant no. 1508085MH189); these funds are gratefully acknowledged.

References

[1] E. E. Creppy, "Update of survey, regulation and toxic effects of mycotoxins in Europe," *Toxicology Letters*, vol. 127, no. 1–3, pp. 19–28, 2002.

[2] M. T. Nguyen, M. Tozlovanu, T. L. Tran, and A. Pfohl-Leszkowicz, "Occurrence of aflatoxin B1, citrinin and ochratoxin A in rice in five provinces of the central region of Vietnam," *Food Chemistry*, vol. 105, no. 1, pp. 42–47, 2007.

[3] A. P. Magnoli, L. Tallone, C. A. R. Rosa, A. M. Dalcero, S. M. Chiacchiera, and R. M. T. Sanchez, "Commercial bentonites as detoxifier of broiler feed contaminated with aflatoxin," *Applied Clay Science*, vol. 40, no. 1–4, pp. 63–71, 2008.

[4] J. M. Hernández-Hierro, R. J. García-Villanova, and I. González-Martín, "Potential of near infrared spectroscopy for the analysis of mycotoxins applied to naturally contaminated red paprika found in the Spanish market," *Analytica Chimica Acta*, vol. 622, no. 1-2, pp. 189–194, 2008.

[5] I. Var, B. Kabak, and F. Gök, "Survey of aflatoxin B_1 in helva, a traditional Turkish food, by TLC," *Food Control*, vol. 18, no. 1, pp. 59–62, 2007.

[6] A. C. Manetta, L. Di Giuseppe, M. Giammarco et al., "High-performance liquid chromatography with post-column derivatisation and fluorescence detection for sensitive determination of aflatoxin M_1 in milk and cheese," *Journal of Chromatography A*, vol. 1083, no. 1-2, pp. 219–222, 2005.

[7] E. Calleri, G. Marrubini, G. Brusotti, G. Massolini, and G. Caccialanza, "Development and integration of an immunoaffinity monolithic disk for the on-line solid-phase extraction and HPLC determination with fluorescence detection of aflatoxin B1 in aqueous solutions," *Journal of Pharmaceutical and Biomedical Analysis*, vol. 44, no. 2, pp. 396–403, 2007.

[8] W. Haasnoot, G. Cazemier, J. du Pré, A. Kemmers-Voncken, M. Bienenmann-Ploum, and R. Verheijen, "Sulphonamide antibodies: from specific polyclonals to generic monoclonals," *Food and Agricultural Immunology*, vol. 12, no. 1, pp. 15–30, 2000.

[9] S. Arjunaraja, P. Massari, L. M. Wetzler, A. Lees, J. Colino, and C. M. Snapper, "The nature of an in vivo anti-capsular polysaccharide response is markedly influenced by the composition and/or architecture of the bacterial subcapsular domain," *The Journal of Immunology*, vol. 188, no. 2, pp. 569–577, 2012.

[10] N. A. Deak, P. A. Murphy, and L. A. Johnson, "Characterization of fractionated soy proteins produced by a new simplified procedure," *Journal of the American Oil Chemists' Society*, vol. 84, no. 2, pp. 137–149, 2007.

[11] L. Chen, P. V. Vadlani, and R. L. Madl, "High-efficiency removal of phytic acid in soy meal using two-stage temperature-induced *Aspergillus oryzae* solid-state fermentation," *Journal of the Science of Food and Agriculture*, vol. 94, no. 1, pp. 113–118, 2014.

[12] K. Daigo, S. Sugita, Y. Mochizuki et al., "A simple hybridoma screening method for high-affinity monoclonal antibodies using the signal ratio obtained from time-resolved fluorescence assay," *Analytical Biochemistry*, vol. 351, no. 2, pp. 219–228, 2006.

[13] C. Cervino, D. Knopp, M. G. Weller, and R. Niessner, "Novel aflatoxin derivatives and protein conjugates," *Molecules*, vol. 12, no. 3, pp. 641–653, 2007.

[14] L. Chen, R. L. Madl, and P. V. Vadlani, "Nutritional enhancement of soy meal via *Aspergillus oryzae* solid-state fermentation," *Cereal Chemistry*, vol. 90, no. 6, pp. 529–534, 2013.

[15] H. Aycicek, A. Aksoy, and S. Saygi, "Determination of aflatoxin levels in some dairy and food products which consumed in Ankara, Turkey," *Food Control*, vol. 16, no. 3, pp. 263–266, 2005.

[16] K. T. Devi, M. A. Mayo, K. L. N. Reddy et al., "Production and characterization of monoclonal antibodies for aflatoxin B1," *Letters in Applied Microbiology*, vol. 29, no. 5, pp. 284–288, 1999.

[17] J. K. Gathumbi, E. Usleber, and E. MaErtlbauer, "Production of ultrasensitive antibodies against aflatoxin B1," *Letters in Applied Microbiology*, vol. 32, no. 5, pp. 349–351, 2001.

[18] D. Zhang, P. Li, Q. Zhang et al., "Production of ultrasensitive generic monoclonal antibodies against major aflatoxins using a modified two-step screening procedure," *Analytica Chimica Acta*, vol. 636, no. 1, pp. 63–69, 2009.

[19] A. H. Heussner, I. Moeller, B. W. Day, D. R. Dietrich, and E. O'Brien, "Production and characterization of monoclonal antibodies against ochratoxin B," *Food and Chemical Toxicology*, vol. 45, no. 5, pp. 827–833, 2007.

[20] A. Y. Kolosova, W.-B. Shim, Z.-Y. Yang, S. A. Eremin, and D.-H. Chung, "Direct competitive ELISA based on a monoclonal antibody for detection of aflatoxin B1. Stabilization of ELISA kit components and application to grain samples," *Analytical and Bioanalytical Chemistry*, vol. 384, no. 1, pp. 286–294, 2006.

[21] J. D. Beatty, B. G. Beatty, and W. G. Vlahos, "Measurement of monoclonal antibody affinity by non-competitive enzyme immunoassay," *Journal of Immunological Methods*, vol. 100, no. 1-2, pp. 173–179, 1987.

[22] G. A. Canziani, S. Klakamp, and D. G. Myszka, "Kinetic screening of antibodies from crude hybridoma samples using

Biacore," *Analytical Biochemistry*, vol. 325, no. 2, pp. 301–307, 2004.

[23] J. J. Manclús, A. Abad, M. Y. Lebedev et al., "Development of a monoclonal immunoassay selective for chlorinated cyclodiene insecticides," *Journal of Agricultural and Food Chemistry*, vol. 52, no. 10, pp. 2776–2784, 2004.

[24] K. E. Sapsford, C. R. Taitt, S. Fertig et al., "Indirect competitive immunoassay for detection of aflatoxin B1 in corn and nut products using the array biosensor," *Biosensors and Bioelectronics*, vol. 21, no. 12, pp. 2298–2305, 2006.

Hindawi Publishing Corporation
International Journal of Polymer Science
Volume 2015, Article ID 604759, 10 pages
http://dx.doi.org/10.1155/2015/604759

Research Article

Physicochemical Properties of Edible Chitosan/Hydroxypropyl Methylcellulose/Lysozyme Films Incorporated with Acidic Electrolyzed Water

Ewa Brychcy,[1] Dominika Kulig,[1] Anna Zimoch-Korzycka,[1] Krzysztof Marycz,[2] and Andrzej Jarmoluk[1]

[1]*Department of Animal Products Technology and Quality Management, Wroclaw University of Environmental and Life Sciences, Chelmonskiego 37/41, 51-630 Wroclaw, Poland*
[2]*Electron Microscope Laboratory, Department of Animal Hygiene and Ichthyology, Wroclaw University of Environmental and Life Sciences, Kożuchowska 5B, 51-630 Wroclaw, Poland*

Correspondence should be addressed to Ewa Brychcy; ewa.brychcy@gmail.com

Received 12 March 2015; Revised 8 June 2015; Accepted 24 June 2015

Academic Editor: Xingxun Liu

The treatment with acidic electrolyzed water (AEW) is a promising disinfection method due to its effectiveness in reducing microbial population. The aim of the study was to evaluate physicochemical properties of chitosan/HPMC films incorporated with lysozyme and acidic electrolyzed water. In the composite films, decreasing film solubility and increasing concentration of sodium chloride solution and prolongation of electrolysis time were observed. Electrolysis process with sodium chloride induces spongy network of film structure. The use of AEW has not changed chemical composition of films which was proved by ^{1}H NMR, MALDI-TOF, and FT-IR spectroscopy. The research confirmed that electrolysis significantly improved thermomechanical properties of the examined films. The contact angle values of the films were quite similar and ranged between 56° and 73°. The increase of salt concentration used in the electrolysis process had an impact on increasing flexibility of samples. Application of electrolyzed water in commonly used food processing systems is possible. Fusion of AEW and biopolymers may provide better integration with coated food product and multidirectional protecting effect.

1. Introduction

Packaging is used to maintain appropriate sensory characteristics and nutritional value of food products. It also has protective function against the adverse effect of environment during transportation and storage; additionally, it has an impact on appearance of the final product. In recent years, the application of edible films and coatings based on biopolymers like proteins, polysaccharides, and lipids has raised attention of many researchers [1, 2] mainly because of the fact that biodegradability of protective coatings containing natural polymers reduces the application of synthetic polymers difficult for utilisation [3]. Requirements for the packaging from natural materials depend on the characteristics of food products and their changes during production and storage [4]. Many authors focus on modification of hydrocolloids designed to produce packaging materials with the most preferable properties and multifunctional applications [5, 6].

Chitosan and cellulose derivatives as hydroxypropyl methylcellulose (HPMC) are promising materials for creating edible coatings or films. HPMC is a water soluble cellulose ether hydrocolloid with good film forming characteristics. It is used as a film former, tablet binder, and coating, stabilizing, suspending, and viscosity increasing agent [7, 8]. Cellulose derivative films are poor water vapour barriers, which are the result of the inherent hydrophilic nature of polysaccharides and cellulose derivative films' poor mechanical properties. Improving the moisture barrier would be by incorporation of hydrophobic compounds, such as fatty acids, into the cellulose ether matrix to develop a composite film [9].

Table 1: Experimental design.

Variants	Variability factors		Constant factors				
	NaCl (%)	Electrolysis time (min)	Chitosan (%)	HPMC (%)	Lysozyme (%)	Glycerol (%)	Lactic acid (%)
N0.001E0	0.001	0	1	1	0.2	25 (of dry weight of used polymers)	0.5
N0.01E0	0.01						
N0.1E0	0.1						
N0.001E5	0.001	5					
N0.01E5	0.01						
N0.1E5	0.1						
N0.001E10	0.001	10					
N0.01E10	0.01						
N0.1E10	0.1						

Chitosan is a derivative of chitin, a polysaccharide with linear chain of linked 2-acetamido-2-deoxy-D-glucopyranose units. This material is biodegradable, biocompatible, and nontoxic. Due to its film forming properties and multiple uses in applications of coatings production, drug delivery, nutrients, and controlled release of food ingredients and separation techniques, it is a valuable polymer [10]. It has a high modulus along with low elongation at break owing to the high glass transition temperature (Tg) and crystallinity. Therefore, mixing or copolymerizing chitosan with different polymers can influence its morphology and plasticity [11].

Edible films are not good barriers against water vapour; however, they could be used as a carrier of active compounds, antimicrobial agents, or preservatives, which protect food quality [12]. Such active ingredients of edible films can be lysozyme or acidic electrolyzed water.

Lysozyme is muramidase (N-acetyl-muramyl-hydrolase) which decomposes β-1,4-glycosidic linkage between N-acetylmuramic acid and N-acetylglucosamine in the cell wall of polysaccharides in bacteria. It possesses lytic properties and can be applied as an antiseptic substance [13].

Acidic electrolyzed water is an antimicrobial agent generated by membrane electrolysis of sodium chloride solution. It is characterized by low pH, high oxidation-reduction potential, and free chlorine which is a major germicidal component [14, 15]. The free chlorine in electrolyzed acidic water is associated with a combination of hypochlorous acid and chlorine gas [15]. AEW has the advantages of nonirritating response of mucous membranes and skin tissue [16]. Acidic electrolyzed water can be also used as a component in biomolecular system, such as hydrogels. Polymer hydrogel composites have been synthesised and characterised for their application in electrochemically controlled drug release devices. Polymer hydrogels give the possibility of obtaining various advanced functional polymers. Electrosensitive hydrogels are commonly made of polyelectrolytes and an insoluble, swellable, polymer network with ionic groups [11].

To the best of our knowledge, there is no published study regarding characterization of edible films incorporated with acidic electrolyzed water. Interactions between hydrocolloids and acidic electrolyzed water could affect physicochemical properties of edible films.

Therefore the aim of the present study was to evaluate the physicochemical properties of chitosan/HPMC films incorporated with lysozyme and acidic electrolyzed water. Further investigations will be correlated with antibacterial properties of examined films and their effectiveness in food products.

2. Materials and Methods

2.1. Apparatus. Electrolyzed salt solutions (acidic electrolyzed water, AEW) were generated using a water generator (own design batch type generator, equipped with two titanium electrodes coated with 0.6 μm layer of platinum) by membrane electrolysis of diluted salt solutions (0.001, 0.01, and 0.1%) in various time spans (0, 5, and 10 minutes). The diluted aqueous solutions of sodium chloride (analytical quality, POCH) were added to both the anode and the cathode chambers (2 L in each chamber) of the ionizer.

2.2. Material. A low molecular weight chitosan (CH) obtained from shrimp shells was supplied from Sigma-Aldrich with 20–200 cP viscosity and DD = 75–85%; hydroxypropyl methylcellulose (HPMC) in the METHOCEL SX product was obtained from Dow Chemical Company; lysozyme isolated from hen egg whites with the 2000 U/mg activity was purchased from Ovopol Company (Poland), in addition to lactic acid (PURAC FCC 80), glycerol (analytical quality, POCH), and 80% sodium chloride (analytical quality, POCH).

2.3. Preparation of Polymer Films. The film stock solutions were prepared by dissolving known amount of film material (chitosan, HPMC) in (non)electrolyzed sodium chloride solutions in the amount shown in Table 1 and 0.5% of lactic acid continuously stirred, using mechanic stirrer CAT R-250 (stirring rate 400 rpm), for 16 hours. The lysozyme solution was prepared by dissolving known amount of lysozyme in (non)electrolyzed sodium chloride solutions. Glycerol (as a plasticizer) was added to the homogenous solutions; then all the solutions were mixed together to obtain the final concentration of components presented in Table 1. The final solutions were degassed by centrifugation and poured into a

glass Teflon coated plate of 80 mm × 200 mm and dried for 72 hours. Dehydration was carried out in Binder KBF-LOC 240 chamber at 4°C and relative humidity of 60%. Dried films were taken off and cut out for further tests.

2.4. Film Characterization

2.4.1. Film Solubility in Water. The analysis was performed according to the method described by Pinotti et al. [17]. The percentage of total soluble matter (% solubility) was calculated by the following formula:

$$\% \text{ solubility} = \frac{\text{Initial dry weight} - \text{Final dry weight}}{\text{Initial dry weight}} \times 100. \quad (1)$$

The samples were analysed at least in triplicate.

2.4.2. Scanning Electron Microscopy (SEM). Cross section of the obtained films was performed using EVO LS 15 Zeiss scanning electron microscope. The samples were sputtered with gold for 150 s using Scancoat 6 type (Edwards, London, England) and examined using 20 kV voltage.

2.4.3. Fourier Transform Infrared Spectroscopy (FT-IR). The ATR FT-IR method was used for each sample testing. The spectra were recorded at a resolution of 2 cm^{-1} by 64 scans between 450 and 4000 cm^{-1} in Infinity AR60 spectrometer (ATI Mattson).

2.4.4. ^1H NMR Spectroscopy. The samples were then characterized by nuclear magnetic resonance (NMR) spectroscopy. The nuclear magnetic resonance measurements were performed on a Bruker Avance III. The solid-state CP MAS NMR experiments were performed using the technique of cross-polarization with magic-angle spinning. The spectra for ^{13}C and ^1H nuclei were obtained, respectively, at 100.61 MHz and 400.15 MHz frequency in a MAS BB DVT wide-band probe with 4 mm diameter of zirconium (ZrO_2) rotor. The isotopically labeled *L*-[1-*13*C]-*tyrosine* (Tyr) was applied in order to optimize the parameters for the CP MAS ^{13}C NMR and also to attain the first-order Hartmann-Hahn matching condition. Spectroscopic parameters are as follows: for *^{13}C CP MAS spectrum:* measurement temperature: 298 K, rotation speed: 8 kHz, relaxation time: 3 s, pulse: 90° for ^1H 4 μs, contact time: 2 ms, spectral width SWH: 40 kHz, TD = 3.5 k, and SPINAL decoupling; for *^1H MAS spectrum*: measurement temperature: 298 K, rotation speed: 8 kHz, relaxation time: 2 s, pulse: 90° for ^1H 4 μs, spectral width SWH: 40 kHz, and TD = 16 k.

2.4.5. MALDI-TOF Mass Spectrometry. The samples for the experiment were prepared by mixing 10 μL of examined solution with 10 μL of matrix solution (an aqueous solution of 2,5-dihydroxybenzoic acid (DHB) at a concentration of 10 mg/mL) in Eppendorf tube with a capacity of 0.5 mL. 2 μL of the sample was placed on a measuring plate and left to evaporate the solvent. The plate was then placed in an ion source of the mass spectrometer Voyager-Elite (PerSeptive Biosystems, Framingham, CT, USA). The ionization technique which was applied was matrix assisted laser desorption/ionization (MALDI). The wavelength of the laser radiation and accelerating voltage were at 337 nm and 20 kV, respectively. The positive ions were subjected to registration using ion time of flight (TOF) analyser with the reflection of ions (reflectron). The recorded mass range varied from 300 to 3500 (*m/z*). Mass spectrum is the sum of 200 spectra. The measurements were taken using an external mass calibration based on defined reference mixture spectrum of polyethylene glycols. Processing of spectra was carried out using Data Explorer v. 4 (Applied Biosystems, Foster City, CA, USA).

2.4.6. Dynamic Mechanical Thermal Analysis (DMTA). The tests were performed using Rheometric Scientific DMTA Mk III. The loss modulus, storage modulus, and loss tangent (tan δ) were measured at the temperature range from −80°C to +50°C, with heating rate 2°C/min and frequency of 1 Hz.

2.4.7. Contact Angle Measurements. The measurements were taken with Contact Angle Analyzer (Surface Electro Optics Company) using the sessile drop method. The drop of distilled water (6 μL) was placed on the surface (2 cm^2) of the coating sample.

2.5. Statistical Analysis. The experiments were made in triplicate. The effects of two independent categorical variables such as time of electrolysis and concentration of sodium chloride were evaluated. The obtained data were analyzed using a 2-way factor analysis of variance (ANOVA) using Statistica 10 (StatSoft, Poland). Differences between means were established by Duncan test with 5% significance.

3. Results and Discussion

3.1. Film Solubility in Water. It was found out that the use of the acidic electrolyzed water significantly influences solubility of edible protective films. The films containing 0.1% sodium chloride solution after 10 minutes of electrolysis (N0.1E10) present the lowest solubility of 6% (Figure 1). The highest solubility of 44% was observed in N0.01E0 film. The decreasing film solubility with increasing concentration of sodium chloride solution and prolongation of electrolysis time were observed in composite films (Figure 1). The solubility can be adjusted to enhance the possible applications by controlling the parameters of the solvent used in film formulation [17]. Water solubility is an indicator of the film's water affinity [18]. High solubility may be an advantage for some applications. In some cases, a water-insoluble film is preferred in order to provide water resistance and improve food integrity; in other cases, edible films with high water solubility may be required [1]. The required degree of solubility of the material may be changed depending on intended applications [19].

3.2. Scanning Electron Microscopy (SEM). The scanning electron micrographs of films are shown in Figure 2. The SEM (a), (b), and (c) micrographs showed smooth, compact, and

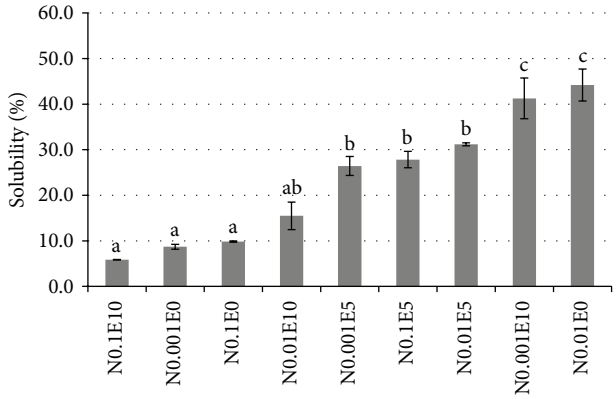

Figure 1: Film solubility in water. Different letters indicate significantly different groups determined by Duncan's test ($P < 0.05$).

homogeneous surface, and no pores or cracks were detected. These results are consistent with those described by Yin et al. [20], Rotta et al. [21], and de Moura et al. [22], where micrographs of cross section confirmed the partial miscibility between chitosan and HPMC. The N0.001E0 and the N0.01E5 films revealed multilayer structures, which could be associated with limited chain mobility [17]. It is related to specificity of used polymers (HPMC, chitosan, and chitooligomers) and causes differences in formation of their chains and functional groups. Electrolysis process with NaCl induces spongy network of film structure, which is shown in Figure 2. Process of electrolysis with NaCl as electrolyte causes lack of creation of crystal structure of components in LCAEW. By subjecting the electrodes to direct current voltage, two kinds of electrolyzed water with different characteristics were produced. In anode chamber of ionizer are present only chloride compounds, such as Cl_2, HOCl, HCl, and chloride ions [15]. Sodium ions are transferred to the cathode as a result of membrane electrolysis and obtained water is not used in this study.

3.3. Fourier Transform Infrared Spectroscopy (FT-IR). The FT-IR spectra of examined films and their ingredients are shown in Figure 3. The spectrum of N0.2E30 sample shows the absorption peak at about 3232 cm^{-1}, which is assigned to stretching vibrations from overlapping O–H and N–H bonds. These findings are in accordance with the results obtained by Leceta et al. [23]. The vibrations indicate inter- and intramolecular hydrogen bonds interaction. The signals observed at 3426 cm^{-1}, 3377 cm^{-1}, 3303 cm^{-1}, and 2878 cm^{-1} were associated with O–H stretching vibration, NH_2 asymmetric stretching, N–H stretching, and C–H stretching, respectively. Similar peak absorption was also reported in the work of Leceta et al. [23]. Characteristic absorption bands of NAG units were observed for C–O stretching of secondary amides at 1656 cm^{-1} and for N–H bending (primary amine) at 1597 cm^{-1}. The absorption bands near 1378 cm^{-1} are associated with the symmetrical skeletal deformation of CH_3 group and those at 1421 cm^{-1} with the O–H (primary alcohol). The absorption bands at 1032 cm^{-1} (stretching vibration of C–O–C ring) are characteristic for the glucopyranose ring. Praxedes et al. [24] indicated that the band peaks at 1409 cm^{-1} and 1316 cm^{-1} correspond to the vibration of –OH and –CH groups in the pyranose ring. Specific bands of (1,4)-glycosidic bridges were observed at 1153 and 897 cm^{-1} [25, 26]. Praxedes et al. [24] observed at the peak of antisymmetric stretching C–O–C glycosidic linkage at 1080 cm^{-1}. Many authors present different wave numbers at which there are adequate absorption bands [27]. The small band with low absorption at 1733 cm^{-1} refers to the acylated group –OH [28]. No significant differences in the positions and intensities of the bands of all the samples were observed. It means that polysaccharides were not degraded by lysozyme or acidity of electrolyzed water. Despite the fact that electrolyzed water has low pH, basically it is a weak acid [15].

3.4. ^1H NMR and ^{13}C NMR Spectroscopy. No significant differences of intensities and widths of ^{13}C individual resonance signals for experimental films were observed (Figure 4). The stability of the fundamental structure of the films was proved by the lack of significant changes in ^{13}C CP MAS NMR spectra. The interactions between large amounts of protons as well as high value of their dipole coupling resulted in broadening of the proton signals in ^1H MAS NMR spectra. Some significant differences of ^1H MAS NMR spectra were noted between N0.001E0, N0.01E0, N0.001E5, N0.01E5, and N0.001E10 and N0.01E10, N0.1E0, N0.1E5, and N0.1E10 samples. The intense signal at about 4.4 ppm was observed in spectra of N0.001E0, N0.01E0, N0.001E5, N0.01E5, and N0.01E10 films. The peak originates predominantly from water protons. Three strong signals at 5, 3.5, and 1.5 ppm were noted. They originate from water protons or glycerol, CH group of chitosan and HPMC (or CH_2 of glycerol), and CH_3 of HPMC. Changes in intensity and width of these signals are probably correlated with different content and cross-linking structures of the films.

3.5. MALDI-TOF Mass Spectrometry. The analysis of the compounds consisting of sugar units conducted by MALDI enables the observation of the oligosaccharides in the molecular weight range from a few to several thousand daltons [29]. Although lysozyme was added to potentially increase antimicrobial activity, it also could cause polysaccharides hydrolysis, which was investigated by others [30]. Park et al. [31] and Zimoch-Korzycka and Jarmoluk [13] noted that lysozyme may cause polysaccharides hydrolysis and their products enhanced inhibition efficacy against many bacteria species. Therefore the research was carried out to identify potential oligomeric products of chitosan and HPMC hydrolysis. The intense peaks of matrix dominate in the mass range from 300 to 500 *m/z*; therefore the mass range over 500 *m/z* was taken into account (Figure 5). No peaks of other *m/z* values, which would create a series of constant mass differences between peaks, indicating the presence of oligomeric products with different composition, were reported. The optimum temperature required for the maximum activity of lysozyme proved to be 37°C [32]. Uncontrolled enzymatic degradation was inhibited by sample storage under cooling condition.

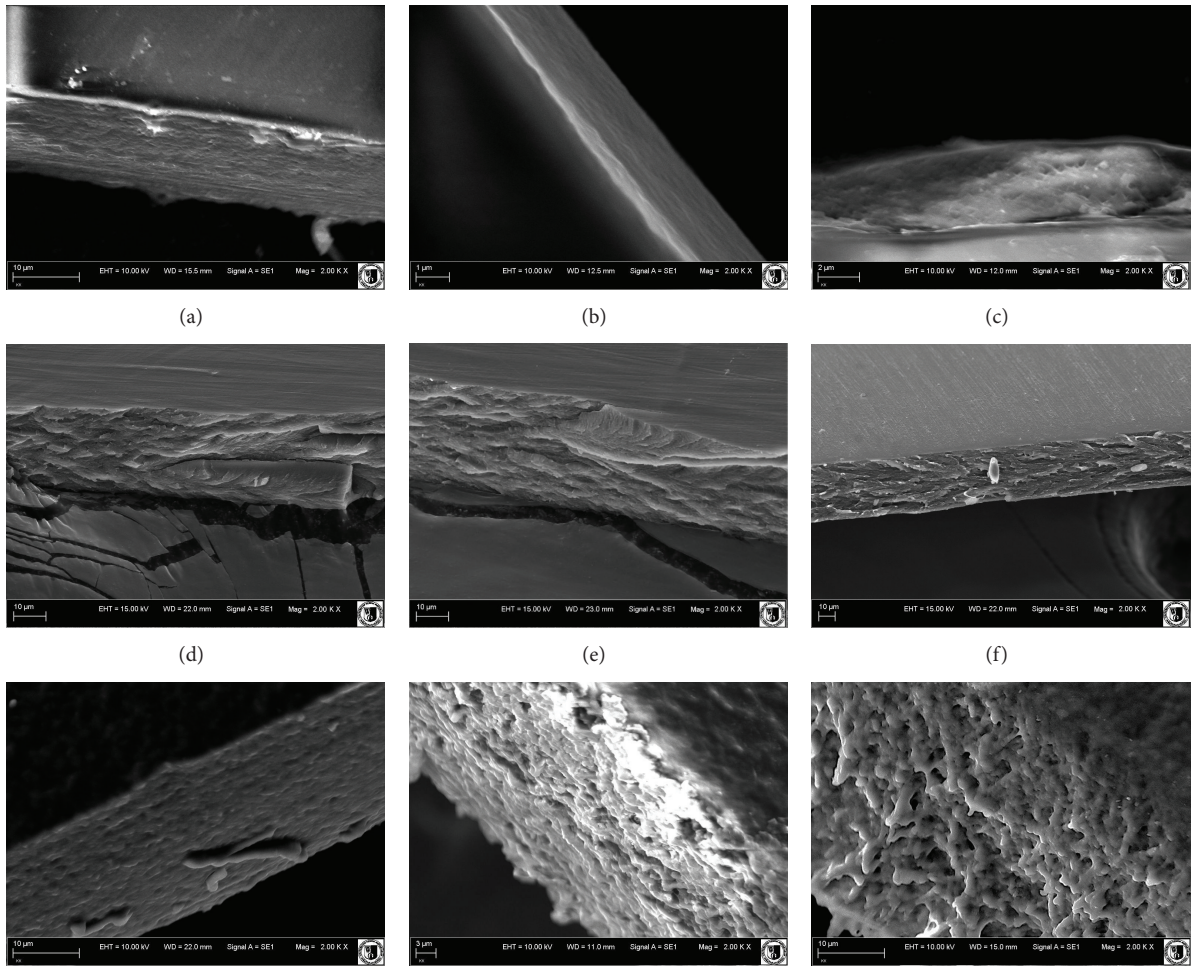

Figure 2: SEM micrographs of the cross section of (a) N0.001E0, (b) N0.001E5, (c) N0.001E10, (d) N0.01E0, (e) N0.01E5, (f) N0.01E10, (g) N0.1E0, (h) N0.1E5, and (i) N0.1E10 films.

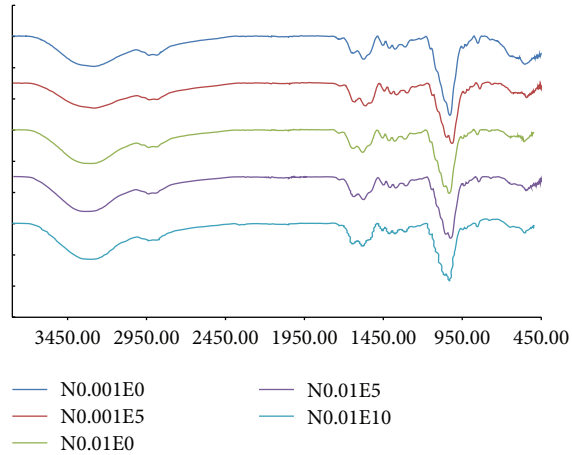

Figure 3: Spectra of Fourier Transform Infrared (FT-IR) for edible films. Reference films: N0.01E0 and N0.001E0; films incorporated with acidic electrolyzed water: N0.01E5 and N0.01E10.

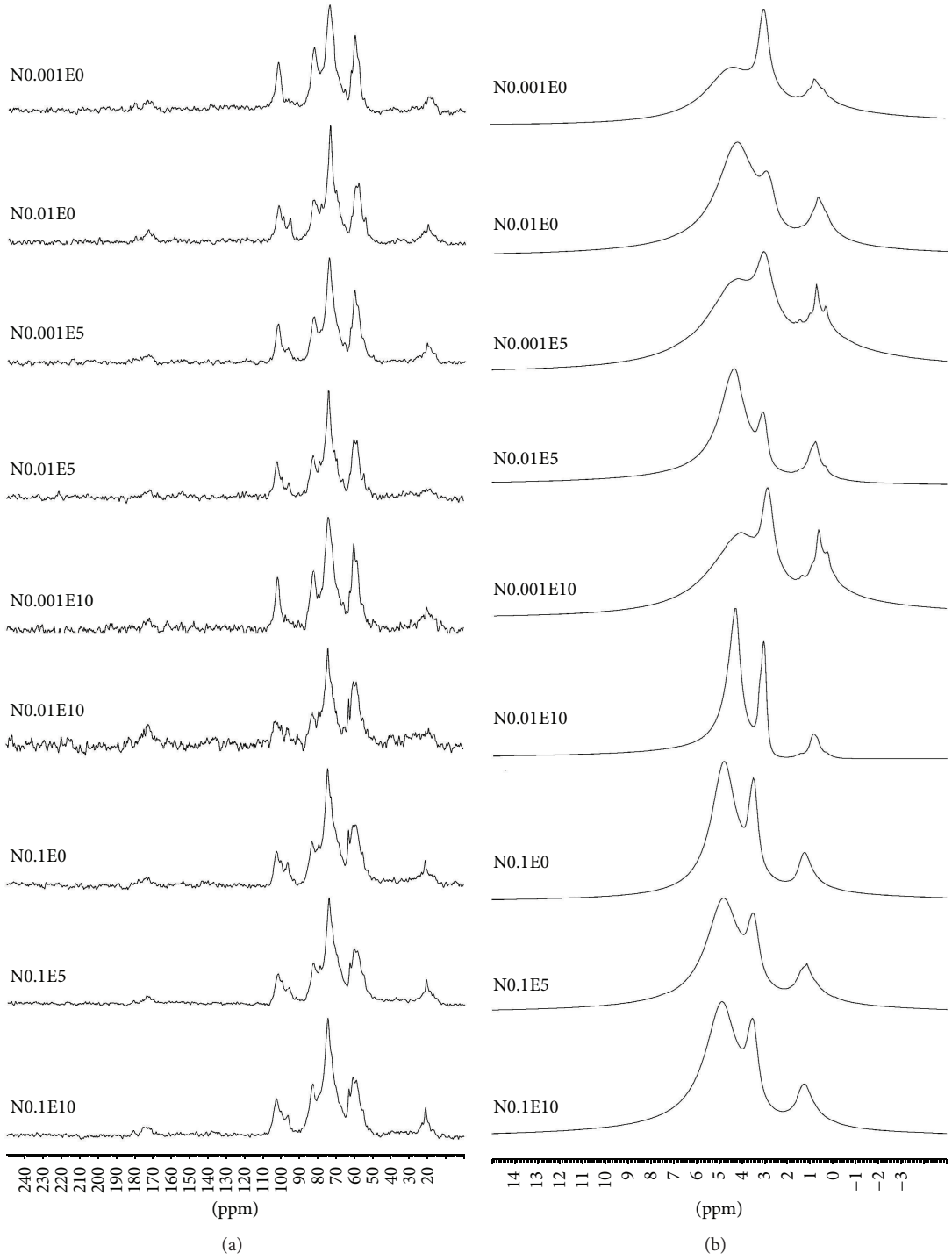

Figure 4: ^{13}C NMR (a) and ^{1}H NMR (b) spectra of examined edible films.

Oligomeric products of chitosan hydrolysis were not found, which was confirmed by MALDI-TOF analysis. Chitosan degradation could lead to reduction of film homogeneity which was not desirable in this study.

3.6. Dynamic Mechanical Thermal Analysis (DMTA). Figure 6 presents the dependence on dynamic mechanical behaviour for selected films (N0.01E0, N0.01E5, N0.01E10, N0.001E0, and N0.1E10) in order to show possible differences caused by AEW. A remarkable signal at 0°C for N0.001E0 and N0.01E0 was noted and probably is associated with the phase transition. The analysis of N0.001E0 and N0.01E5 films showed less intense and more significant peaks at 0°C and −30°C, respectively. Sample N0.01E10 (like N0.1E10 sample) comprises the second loss tangent peak at about 0°C. Rotta et al. [21] and Martínez-Camacho et al. [33] observed a

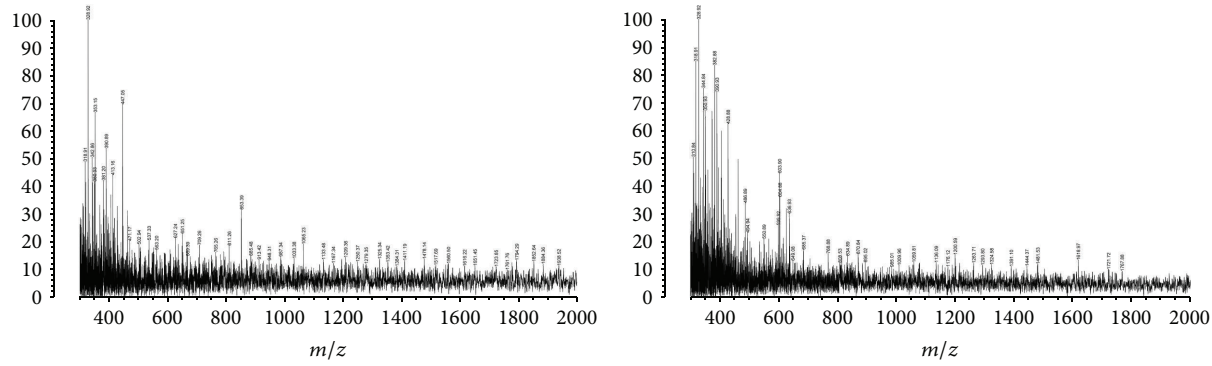

Figure 5: MALDI-TOF mass spectrometry analysis of edible films based on acidic electrolyzed water (N0.1E10) (a) and its reference (N0.1E0) (b).

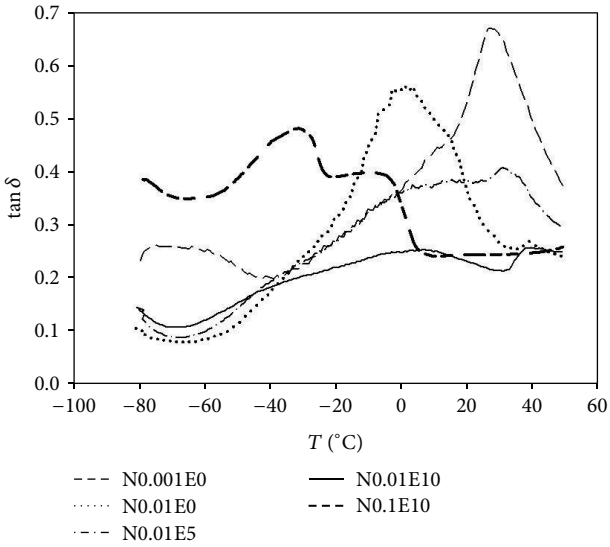

Figure 6: DMTA spectra of tan δ for N0.001E0, N0.01E0, N0.01E5, N0.01E10, and N0.1E10 films.

Tg value of chitosan and hydroxypropyl methylcellulose at 203°C and 164°C, respectively, whereas Kittur et al. [34] and Neto et al. [35] have not found any evidence of Tg. The maximum in the tan δ graph corresponds to transition temperature of the amorphous regions of the polymer (α relaxation) [36]. Tg is strongly dependent on both the film composition and the moisture content and can denote stability of a film. As water content of the amorphous material increases, Tg decreases. Double tangent peak was observed in N0.1E10 film, which suggests the presence of two phase transitions or weak homogeneity of the material. Two separate peaks on the graph of the loss tangent were probably associated with higher NaCl content. Aggregation of fillers would result in the heterogeneous collections of polymer matrix and filler. It was found that with increasing NaCl concentration in examined films α relaxation moves toward higher temperatures and its maximum is lower. The use of AEW caused a shift of the main relaxation to a higher temperature which probably indicates restricted molecular movement [37]. Close to 0° loss tangent values indicate high flexibility of the sample. Process of electrolysis significantly improved thermomechanical properties of polymeric coatings. It was observed that 5-minute electrolysis improved N0.01E5 elasticity by 27.28% and elongation of electrolysis time promotes reduction of tan δ by 54.55% compared to the untreated sample N0.01E0 (0.55°). Electrolysis process created spongy network of films, which was confirmed by SEM analysis. When the porosity of material increases, the elasticity increases also [38].

3.7. Contact Angle Measurements. The photographs of wetting films are shown in Figure 7. The study revealed that there was no significant deformation between films which contained AEW. The destruction of films is caused by dissolution of the sample by its contact with water. This process is accompanied by the formation of stress, which results in deformation of the sample. Among the tested samples N0.01E0 film was subject to insignificant deformation. There are two types of terminal groups in the chemical structure of examined films: hydrophobic methyl group ($-CH_3$) and hydrophilic hydroxyl group (CH_3-OH). During the first phase of the analysis methyl groups were exposed to the outside, which prevented water penetration into the interior of the surface film. The tested surface of the coating was wetted with water, which probably caused its dynamic reorganization. Hydrophilic hydroxyl groups were gradually appearing on the material surface. The water drop was extended, but the penetration was insignificant. Chemical stability of N0.1E0, N0.001E5, N0.1E5, and N0.1E10 films was observed during the time of measurement. It was noted that the contact angle values of the films were quite similar and were in the range 56°–73°. This evidenced insignificant differences in chemical structure surface of the test samples. Contact angles greater than 90° indicate surface hydrophobicity and below 90° correspond to hydrophilicity of the surface [39]. Contact angles below 90 degrees can indicate that examined films are characterized by high wettability. Park et al. [31] observed that the addition of lysozyme causes increased hydrophobic

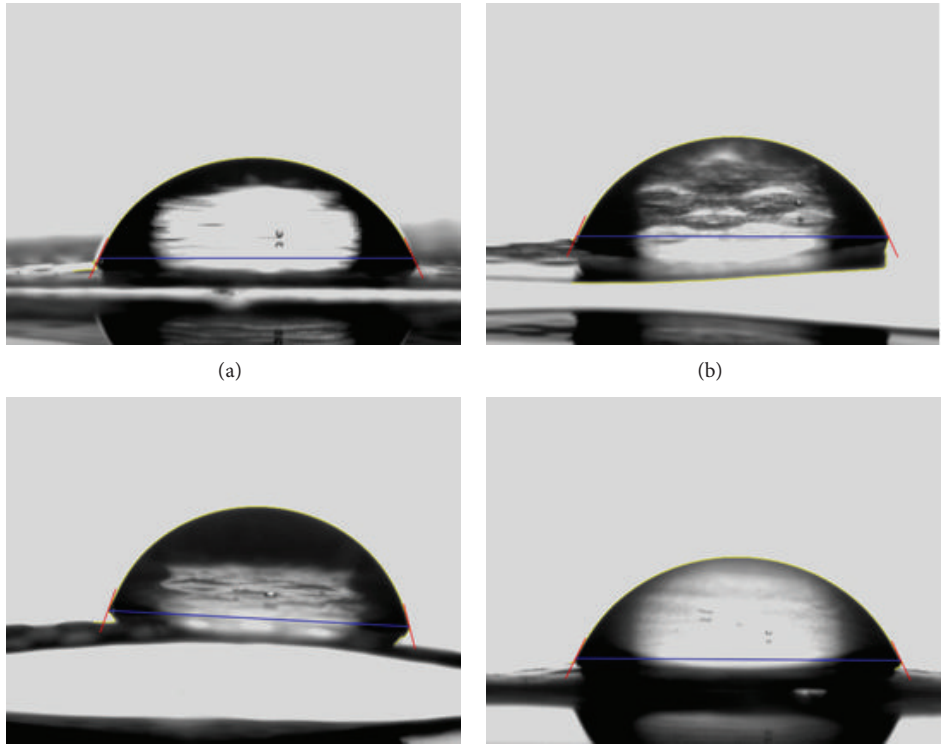

(a) (b) (c) (d)

Figure 7: Images of contact angle for (a) N0.001E0, (b) N0.01E0, (c) N0.01E5, and (d) N0.01E10 films.

side chains in film structure and may be responsible for the decrease in hydrophilicity of lysozyme-chitosan films.

4. Conclusions

Control of AEW production parameters allows modifying properties of edible protective films, including their solubility and wettability, while electrolysis process improves elasticity of the polymeric films. The use of AEW has not caused undesirable changes in chemical composition of films which was proved by ^{1}H NMR, MALDI-TOF, and FT-IR analysis. The use of low salt concentration guarantees obtaining a homogeneous coating surface and desirable cohesion with all components. Application of acidic electrolyzed water generator is possible to be implemented into already existing food processing system. Fusion of AEW with biopolymers and lysozyme is easy to introduce and will provide better integration with coated food product.

Conflict of Interests

The authors declare that there is no conflict of interests regarding the publication of this paper.

Acknowledgments

This research was supported by Wroclaw Centre of Biotechnology, programme The Leading National Research Centre (KNOW) for years 2014–2018. The authors are indebted to researchers from Centre of Molecular and Macromolecular Studies, Polish Academy of Sciences, in Lodz for their support.

References

[1] B. W. S. Souza, M. A. Cerqueira, J. A. Teixeira, and A. A. Vicente, "The use of electric fields for edible coatings and films development and production: a review," *Food Engineering Reviews*, vol. 2, no. 4, pp. 244–255, 2010.

[2] V. Enujiugha, R. Ayodele, and K. Seidu, "Protein-lipid films: applications in food systems," *International Journal of Agriculture and Food Security*, vol. 4, no. 18, pp. 553–570, 2013.

[3] K. Sztuka and I. Kołodziejska, "Jadalne folie oraz powłoki powierzchniowe z polimerów naturalnych stosowane do opakowań żywności," *Polimery*, vol. 9, pp. 625–706, 2008.

[4] S. Guilbert, N. Gontard, and L. G. M. Gorris, "Prolongation of the shelf-life of perishable food products using biodegradable films and coatings," *LWT—Food Science and Technology*, vol. 29, no. 1-2, pp. 10–17, 1996.

[5] M. Ye, H. Neetoo, and H. Chen, "Control of *Listeria monocytogenes* on ham steaks by antimicrobials incorporated into chitosan-coated plastic films," *Food Microbiology*, vol. 25, no. 2, pp. 260–268, 2008.

[6] M. D. R. Moreira, M. Pereda, N. E. Marcovich, and S. I. Roura, "Antimicrobial effectiveness of bioactive packaging materials from edible chitosan and casein polymers: assessment on carrot," *Journal of Food Science*, vol. 76, no. 1, pp. M54–M63, 2011.

[7] F. A. Osorio, P. Molina, S. Matiacevich, J. Enrione, and O. Skurtys, "Characteristics of hydroxy propyl methyl cellulose (HPMC) based edible film developed for blueberry coatings," *Procedia Food Science*, vol. 1, pp. 287–293, 2011.

[8] Siddaramaiah, P. Kumar, K. Divya, B. Mhemavathi, and D. Manjula, "Chitosan/HPMC polymer blends for developing transdermal drug delivery systems," *Journal of Macromolecular Science, Part A: Pure and Applied Chemistry*, vol. 43, no. 3, pp. 601–607, 2006.

[9] O. Skurtys, C. Acevedo, F. Pedreschi, J. Enrione, F. Osorio, and J. Aguilera, "Food hydrocolloid edible films and coatings," *Food Science and Technology*, vol. 3, pp. 6–9, 2010.

[10] F. Al-Sagheer and S. Muslim, "Thermal and mechanical properties of chitosan/SiO_2 hybrid composites," *Journal of Nanomaterials*, vol. 2010, Article ID 490679, 7 pages, 2010.

[11] S. Kaewpirom and S. Boonsang, "Electrical response characterisation of poly(ethylene glycol) macromer (PEGM)/chitosan hydrogels in NaCl solution," *European Polymer Journal*, vol. 42, no. 7, pp. 1609–1616, 2006.

[12] R. Ahmadi, A. Kalbasi-Ashtari, A. Oromiehie, M.-S. Yarmand, and F. Jahandideh, "Development and characterization of a novel biodegradable edible film obtained from psyllium seed (*Plantago ovata* Forsk)," *Journal of Food Engineering*, vol. 109, no. 4, pp. 745–751, 2012.

[13] A. Zimoch-Korzycka and A. Jarmoluk, "The use of chitosan, lysozyme, and the nano-silver as antimicrobial ingredients of edible protective hydrosols applied into the surface of meat," *Journal of Food Science and Technology*, 2014.

[14] Y. Zhao, H. Xin, D. Zhao et al., "Free chlorine loss during spraying of membraneless acidic electrolyzed water and its antimicrobial effect on airborne bacteria from poultry house," *Annals of Agricultural and Environmental Medicine*, vol. 21, no. 2, pp. 249–255, 2014.

[15] S. Hati, S. Mandal, P. S. Minz et al., "Electrolyzed Oxidized Water (EOW): non-thermal approach for decontamination of food borne microorganisms in food industry," *Food and Nutrition Sciences*, vol. 03, no. 06, pp. 760–768, 2012.

[16] C.-Y. Chuang, S. Yang, H.-C. Huang et al., "Applying the membrane-less electrolyzed water spraying for inactivating bioaerosols," *Aerosol and Air Quality Research*, vol. 13, no. 1, pp. 350–359, 2013.

[17] A. Pinotti, M. A. García, M. N. Martino, and N. E. Zaritzky, "Study on microstructure and physical properties of composite films based on chitosan and methylcellulose," *Food Hydrocolloids*, vol. 21, no. 1, pp. 66–72, 2007.

[18] A. I. Bourbon, A. C. Pinheiro, M. A. Cerqueira et al., "Physicochemical characterization of chitosan-based edible films incorporating bioactive compounds of different molecular weight," *Journal of Food Engineering*, vol. 106, no. 2, pp. 111–118, 2011.

[19] J. Rotta, R. Á. Ozório, A. M. Kehrwald, G. M. de Oliveira Barra, R. D. de Melo Castanho Amboni, and P. L. M. Barreto, "Parameters of color, transparency, water solubility, wettability and surface free energy of chitosan/hydroxypropylmethylcellulose (HPMC) films plasticized with sorbitol," *Materials Science & Engineering C*, vol. 29, no. 2, pp. 619–623, 2009.

[20] J. Yin, K. Luo, X. Chen, and V. V. Khutoryanskiy, "Miscibility studies of the blends of chitosan with some cellulose ethers," *Carbohydrate Polymers*, vol. 63, no. 2, pp. 238–244, 2006.

[21] J. Rotta, E. Minatti, and P. L. M. Barreto, "Determination of structural and mechanical properties, diffractometry, and thermal analysis of chitosan and hydroxypropylmethylcellulose (HPMC) films plasticized with sorbitol," *Ciência e Tecnologia de Alimentos*, vol. 31, no. 2, pp. 450–455, 2011.

[22] M. R. de Moura, F. A. Aouada, R. J. Avena-Bustillos, T. H. McHugh, J. M. Krochta, and L. H. C. Mattoso, "Improved barrier and mechanical properties of novel hydroxypropyl methylcellulose edible films with chitosan/tripolyphosphate nanoparticles," *Journal of Food Engineering*, vol. 92, no. 4, pp. 448–453, 2009.

[23] I. Leceta, P. Guerrero, and K. de la Caba, "Functional properties of chitosan-based films," *Carbohydrate Polymers*, vol. 93, no. 1, pp. 339–346, 2013.

[24] A. P. P. Praxedes, A. J. C. da Silva, R. C. da Silva et al., "Effects of UV irradiation on the wettability of chitosan films containing dansyl derivatives," *Journal of Colloid and Interface Science*, vol. 376, no. 1, pp. 255–261, 2012.

[25] P. Gomes, C. A. R. Gomes, M. K. S. Batista, L. F. Pinto, and P. A. P. Silva, "Synthesis, structural characterization and properties of water-soluble N-(γ-propanoyl-amino acid)-chitosans," *Carbohydrate Polymers*, vol. 71, no. 1, pp. 54–65, 2008.

[26] G. Socrates, *Infrared and Raman Characteristic Group Frequencies Tables and Charts*, John Wiley & Sons, New York, NY, USA, 3rd edition, 2001.

[27] C. Le Tien, M. Lacroix, P. Ispas-Szabo, and M.-A. Mateescu, "*N*-acylated chitosan: hydrophobic matrices for controlled drug release," *Journal of Controlled Release*, vol. 93, no. 1, pp. 1–13, 2003.

[28] J. Xu, S. P. McCarthy, R. A. Gross, and D. L. Kaplan, "Chitosan film acylation and effects on biodegradability," *Macromolecules*, vol. 29, no. 10, pp. 3436–3440, 1996.

[29] P. Mischnick, "Mass spectrometric characterization of oligo- and polysaccharides and their derivatives," *Advances in Polymer Science*, vol. 248, pp. 105–174, 2012.

[30] A. Zimoch-Korzycka, C. Gardrat, A. Castellan, V. Coma, and A. Jarmoluk, "The use of lysozyme to prepare biologically active chitooligomers," *Polímeros*, vol. 25, no. 1, pp. 35–41, 2015.

[31] S.-I. Park, M. A. Daeschel, and Y. Zhao, "Functional properties of antimicrobial lysozyme-chitosan composite films," *Journal of Food Science*, vol. 69, no. 8, pp. M215–M221, 2004.

[32] V. Sidhan and S. Gurnani, "Kinetic characterization of rat liver nuclear lysozyme," *Journal of Biosciences*, vol. 4, no. 2, pp. 191–195, 1982.

[33] A. P. Martínez-Camacho, M. O. Cortez-Rocha, J. M. Ezquerra-Brauer et al., "Chitosan composite films: thermal, structural, mechanical and antifungal properties," *Carbohydrate Polymers*, vol. 82, no. 2, pp. 305–315, 2010.

[34] F. S. Kittur, K. V. H. Prashanth, K. U. Sankar, and R. N. Tharanathan, "Characterization of chitin, chitosan and their carboxymethyl derivatives by differential scanning calorimetry," *Carbohydrate Polymers*, vol. 49, no. 2, pp. 185–193, 2002.

[35] C. G. T. Neto, J. A. Giacomettib, A. E. Jobb, F. C. Ferreirab, J. L. C. Fonsecaa, and M. R. Pereiraa, "Thermal analysis of chitosan based networks," *Carbohydrate Polymers*, vol. 62, no. 2, pp. 97–103, 2005.

[36] T. H. Kim, J. Ahn, H. Choi, Y. Choi, and C. Cho, "A novel mucoadhesive polymer film composed of carbopol, poloxamer and hydroxypropylmethylcellulose," *Archives of Pharmacal Research*, vol. 30, no. 3, pp. 381–386, 2007.

[37] K. Piyada, S. Waranyou, and W. Thawien, "Mechanical, thermal and structural properties of rice starch films reinforced with rice starch nanocrystals," *International Food Research Journal*, vol. 20, no. 1, pp. 439–449, 2013.

[38] A. Muscat, U. Prüße, and K.-D. Vorlop, "Stable suport materials for the immobilization of viable cells," in *Immobilized Cells: Basics and Application*, R. H. Wijffels, R. M. Buitelaar, C. Bucke, and J. Tramper, Eds., pp. 55–61, Elsevier Science, Amsterdam, The Netherlands, 1996.

[39] Y. Yuan and T. Lee, "Contact angle and wetting properties," in *Surface Science Techniques*, G. Bracco and B. Holst, Eds., pp. 3–34, Springer, Berlin, Germany, 2013.

Hindawi Publishing Corporation
International Journal of Polymer Science
Volume 2015, Article ID 187961, 15 pages
http://dx.doi.org/10.1155/2015/187961

Research Article

Synthesis and Characterization of Chemically Cross-Linked Acrylic Acid/Gelatin Hydrogels: Effect of pH and Composition on Swelling and Drug Release

Syed Majid Hanif Bukhari,[1] Samiullah Khan,[2] Muhammad Rehanullah,[1] and Nazar Mohammad Ranjha[1]

[1]*Faculty of Pharmacy, Bahauddin Zakariya University, Multan 60800, Pakistan*
[2]*Department of Pharmaceutical Sciences, COMSATS Institute of Information Technology, Abbottabad 22010, Pakistan*

Correspondence should be addressed to Samiullah Khan; sami_pharmacist99@hotmail.com

Received 13 February 2015; Revised 19 April 2015; Accepted 19 May 2015

Academic Editor: Xingxun Liu

This present work was aimed at synthesizing pH-sensitive cross-linked AA/Gelatin hydrogels by free radical polymerization. Ammonium persulfate and ethylene glycol dimethacrylate (EGDMA) were used as initiator and as cross-linking agent, respectively. Different feed ratios of acrylic acid, gelatin, and EGDMA were used to investigate the effect of monomer, polymer, and degree of cross-linking on swelling and release pattern of the model drug. The swelling behavior of the hydrogel samples was studied in 0.05 M USP phosphate buffer solutions of various pH values pH 1.2, pH 5.5, pH 6.5, and pH 7.5. The prepared samples were evaluated for porosity and sol-gel fraction analysis. Pheniramine maleate used for allergy treatment was loaded as model drug in selected samples. The release study of the drug was investigated in 0.05 M USP phosphate buffer of varying pH values (1.2, 5.5, and 7.5) for 12 hrs. The release data was fitted to various kinetic models to study the release mechanism. Hydrogels were characterized by Fourier transformed infrared (FTIR) spectroscopy which confirmed formation of structure. Surface morphology of unloaded and loaded samples was studied by surface electron microscopy (SEM), which confirmed the distribution of model drug in the gel network.

1. Introduction

Stimuli-responsive polymers offer a drug delivery platform that can be utilized to deliver drugs at a controlled rate and in a stable and biologically active form. These polymers respond to small changes in environmental conditions, such as temperature, pH, light, ionic strength, electric or magnetic fields, or the presence of enzymes or specific ligands. Hydrogels are three-dimensional hydrophilic polymer networks that swell in water or biological fluid without dissolving due to chemical or physical cross-links [1]. These three-dimensional networks of a hydrogel are formed by either reversible bonds (physical bonds), which can be made or broken under certain environments, or covalent bonds. If the cross-links are based on physical bonds, such as hydrogen, ionic, or van der Waal's bonds, the responses of the hydrogels to external stimuli are often reversible [2]. In order to keep the spatial structure of hydrogel, the polymer chains are usually physically or chemically cross-linked [3].

Hydrogels have become excellent carriers for release of drugs and bioactive macromolecules either in their swollen equilibrium state or as dynamically swelling systems. The relatively low mechanical strength of the hydrogels can be overcome either by cross-linking, by formation of interpenetrating networks (IPNs) or by crystallization that induces crystallite formation and drastic reinforcement of their structure [4]. The swelling properties of these hydrogels have attracted the attention of researchers and technologists and have found widespread applications in drug delivery devices, separation processes, sensors, contact lens devices, and many other fields [5].

Cross-linking is responsible for the three-dimensional network structures that characterize these materials. The elasticity and swelling properties are attributed to the presence of physical or chemical cross-links within polymer chains. The cross-linking level of the hydrogels is also important because the physical states of the hydrogels alter with the changing of the cross-linking level [6].

Acrylic acid is a pH sensitive, synthetic polymer extensively used in the area of the site-specific drug delivery of the gastrointestinal tract [7]. It is one of the principal superabsorbent polymers and a typical pH-responsive polyelectrolyte. The original pH-dependent release characteristic could be modified by varying the composition of polymers. Therefore pH-responsive polymeric networks have been extensively studied [8]. The interpenetrating networks (IPNs) and copolymers containing acrylic acid have also been reported to exhibit thermoresponsive, electroresponsive, and pH-responsive behavior [9]. Poly(acrylic acid) is well recognized for its polyanionic nature and has been extensively employed in designing pH-responsive macromolecular architectures mainly used in targeted drug delivery [10]. The pKa value of poly(acrylic acid) is between 4.5 and 5.0, and PAA hydrogels swell significantly at the physiological pH of 7.4 due to ionization of the anionic carboxylic acid groups [11].

Gelatin is a protein product produced by partial hydrolysis of collagen extracted from skin, bones, cartilage, and ligaments [12]. Gelatin mainly contains the residues of 3 amino acids, glycine, proline, and 4-hydroxyproline in its structure [13]. Collagen is the major protein component of cartilage, skin, bone, and connective tissue and constitutes the major part of the extracellular matrices in animals; however, collagen has antigenicity due to its animal origin. In contrast, gelatin has relatively low antigenicity because of being denatured [14]. Gelatin is known for its biodegradability, noncarcinogenicity, and hydrophilicity [15]. Among natural polymers, preferred for their low toxicity and biocompatibility, gelatin is a good raw material candidate because of its excellent physical and chemical properties [16]. At a temperature of about 40°C, gelatin aqueous solutions are in the sol state and form physical thermoreversible gels on cooling. During gelling, the chains undergo a conformational disorder-order transition and tend to recover the collagen triple-helix structure [17].

Pheniramine maleate ($C_{16}H_{20}N_2{\cdot}C_4H_4O_4$), chemically known as N,N-dimethyl-3-phenyl-3-(2-pyridyl) propyl amine hydrogen maleate, is an antihistamine H_1 receptor antagonist used as an antihistaminic for the symptomatic relief of a hypersensitivity reaction. It is clinically used for the treatment of acute allergic attacks, all itching skin condition, nausea, vomiting, and vertigo associated with motion sickness [18]. Figure 1 represents the structure of pheniramine maleate.

The purpose of the present study was to prepare AA/Gelatin hydrogels by free radical polymerization method using EGDMA as cross-linking agent and ammonium persulfate as initiator. The prepared hydrogel samples were used to evaluate the effect of pH and composition of IPNs on dynamic and equilibrium swelling and drug release in 0.05 M USP phosphate buffer solutions of varying pH 1.2, pH 5.5, pH 6.5, and pH 7.5. Pheniramine maleate was loaded as model drug in these hydrogel samples. The release pattern of the model drug was studied in USP phosphate buffer solutions of varying pH values. Sol-gel fraction analysis, cross-linked density, porosity, and network parameters were also calculated for these hydrogels. Hydrogels were characterized by Fourier transform infrared spectroscopy (FTIR) to confirm the formation of network and to investigate the presence of specific chemical groups in the hydrogels. The surface morphology of the hydrogels was studied by scanning electron microscopy (SEM).

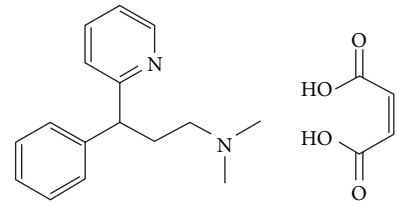

Figure 1: Structure of pheniramine maleate.

2. Experimental Procedures

2.1. Materials. For the preparation of pH sensitive hydrogels, acrylic acid (AA) (Mw ~ 72.06 g mol^{-1}) (Sigma Aldrich) was used as monomer. Gelatin type B from bovine skin (Ge) (Mw ~ 402.47 g mol^{-1}) (Merck, Germany) was used as polymer. Ethylene glycol dimethacrylate (EGDMA) (Aldrich) and ammonium persulfate were used as cross-linking agent and initiator, respectively. Potassium hydrogen phosphate, sodium chloride, sodium hydroxide, and hydrochloric acid (Merck, Germany) were used. For characterization of hydrogels by FTIR, potassium bromide (KBr) was purchased from Fisher Scientific (UK). All chemicals used were of analytical grade.

2.2. Synthesis of Interpenetrating Networks of AA/Gelatin. In the present work, different formulations of hydrogels with different feed composition were prepared by free radical copolymerization technique [7, 19]. A weighed quantity of gelatin (Ge) was added into predetermined amount of distilled water under constant stirring at room temperature. When a clear gelatin solution is formed then ammonium persulfate used at a concentration of 1 wt% of AA was dissolved in this gelatin solution. Varying amounts of ethylene glycol dimethacrylate (EGDMA) as cross-linking agent were added and dissolved in acrylic acid solution. The two solutions were mixed together thoroughly. The final volume of the solution was made up to 100 gm with distilled water. The polymerization of the prepared solution was carried out in glass tubes (Pyrex) having 16 mm internal diameter. These test tubes were deoxygenated with nitrogen gas bubbling for 15–20 minutes and then snugly fitted with lid. The capped tubes were placed in water bath. The temperature was gradually increased to avoid autoacceleration and bubble formation. The temperature scheme for solution polymerization was 45°C for 1 h, 50°C for 2 h, 55°C for 3 h, 60°C for 4 h, and

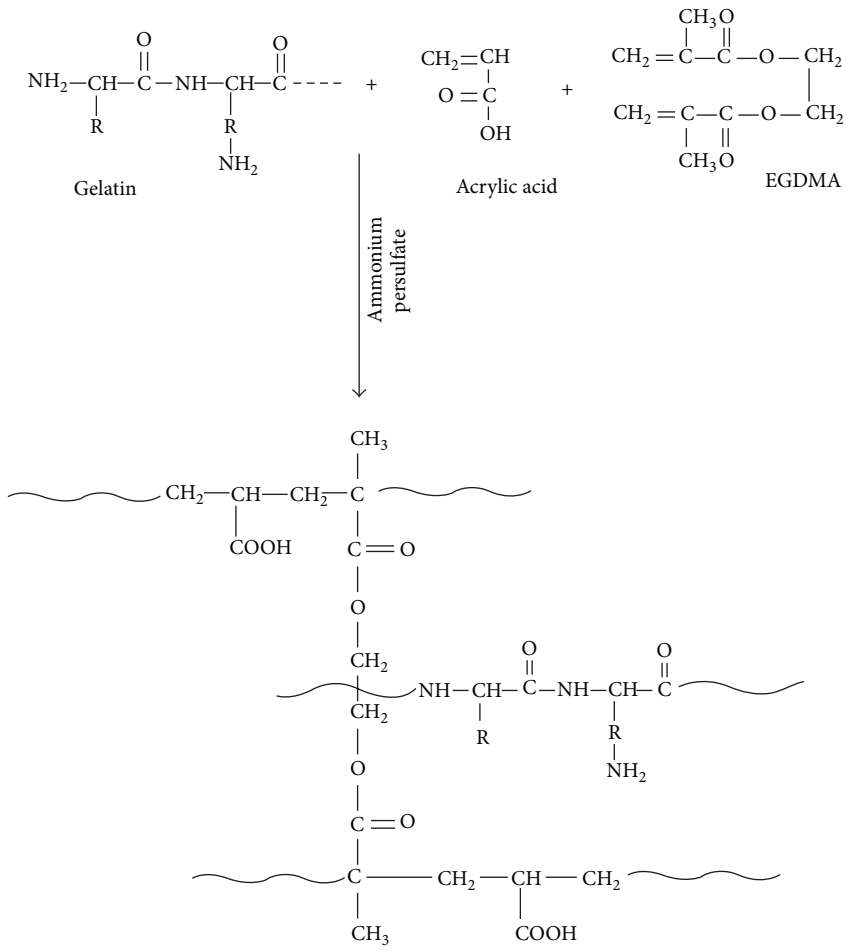

Figure 2: Presumptive structure of EGDMA cross-linked interpenetrating networks of AA/Gelatin hydrogels.

65°C for 24 h. After this period, tubes were cooled to room temperature, and cylinders of obtained gel type product were removed from the tubes and cut into discs of 6 mm size. These cylindrical discs were washed with 50% v/v ethanol water for 1-2 weeks, for complete removal of the unreacted monomers. During this period the solvent was changed daily. These gel discs were thoroughly washed until the pH of the washing was the same as that of ethanol water mixture before washing. Then disks were dried, first at room temperature and then in oven at 40–45°C until the solid reached constant mass. The hydrogels were stored in a desiccator for further use. The presumptive structure of the EGDMA cross-linked interpenetrating networks of AA/Gelatin hydrogels is shown in Figure 2. A list of different composition of AA/Gelatin hydrogels is given in Table 1.

2.3. Swelling Experiments of AA/Gelatin Hydrogels

2.3.1. Dynamic Swelling Experiment. The dynamic swelling experiments were carried out in 100 mL solution at 37°C. Dry discs were weighed and immersed in USP phosphate buffer solutions of varying pH values, that is, 1.2, 5.5, 6.5, and 7.5, with constant ionic strength. Concentration of buffering agent was 0.05 M. Samples were taken out at regular intervals for 8 h and weighed after removing the excess surface water by blotting with filter paper. After weighing, each sample was placed in the same flask. The dynamic swelling ratio of each sample was calculated by [20]

$$q = \frac{W_s}{W_0}, \tag{1}$$

where W_s indicates the weight of hydrated gels after swelling and W_0 shows the initial dry hydrogel disc at time (t).

2.3.2. Equilibrium Swelling Experiments. To carry out the equilibrium swelling experiments, samples remained in the same buffer medium and were used for equilibrium swelling studies. Swelling ratio was equilibrium when hydrogel reached a constant weight. For equilibrium swelling, the swollen gels were weighed regularly to a constant weight which takes 15–21 days.

Equilibrium swelling ratio was calculated by using [21]

$$S_{(\mathrm{Eq})} = \frac{W_h}{W_d}. \tag{2}$$

Table 1: Different composition of AA/Gelatin hydrogels.

Sample codes	AA/100 g solution	GE/100 g solution	AA : GE (wt %)	(EGDM)/100 g solution
U_1	35.00	4.00	89.74/10.26	0.70
U_2	35.00	5.00	87.50/12.50	0.70
U_3	35.00	6.00	85.37/14.63	0.70
U_4	28.00	6.00	82.35/17.65	0.70
U_5	32.00	6.00	84.21/15.79	0.70
U_6	36.00	6.00	85.71/14.29	0.70
U_7	35.00	6.00	85.37/14.63	0.65
U_8	35.00	6.00	85.37/14.63	0.75
U_9	35.00	6.00	85.37/14.63	0.85

2.3.3. Diffusion Coefficient. Release of drug from cross-linked hydrogels generally follows diffusion mechanism. To calculate the diffusion coefficient of hydrated gels, swollen hydrogels were subjected to drying at room temperature and then weighed after 15 minutes till they reached an equilibrium weight. Water diffusion coefficients of hydrogels samples were calculated by [22]

$$D = \pi \left(\frac{h \cdot \theta}{4 \cdot Q_{\text{eq}}} \right)^2, \tag{3}$$

where D represents the diffusion coefficient of the hydrogels, Q_{eq} indicates the equilibrium swelling of the gel, θ is the slope of the linear part of the swelling curves, and h refers to the initial thickness in dry state.

2.4. Interpenetrating Polymeric Networking Parameters of AA/Gelatin Hydrogels

2.4.1. Molecular Weight between Cross-Links (M_c). Flory-Rehner theory was used for calculating average molecular weight (M_c) values between interpenetrating polymeric networking of AA/Gelatin hydrogels, which represents the degree of cross-linking of hydrogel networks between two adjacent cross-links. According to this theory, M_c values increase as the swelling ratio of hydrogels increased. Molecular weight between adjacent cross-links is calculated by using [23]

$$M_c = -\frac{d_p V_s \left(V_{2,s}^{1/3} - V_{2,s}/2 \right)}{\ln\left(1 - V_{2,s}\right) + V_{2,s} + x V_{2,s}^2}. \tag{4}$$

Volume fraction of the polymer $V_{2,s}$ indicates the capacity of hydrogel to allow the diffusion of solvent into the network structure. It is calculated by the following equation:

$$V_{2,s} = \left[1 + \frac{d_p}{d_s} \left(\frac{M_a}{M_b} - 1 \right) \right]^{-1}, \tag{5}$$

where d_p and d_s are densities (g/mL) of the hydrogel and solvent, respectively, M_a and M_b are the masses (g) of the swollen and dry hydrogels, respectively, $V_{2,s}$ (mL/mol) refers to the volume fraction of the swollen hydrogel in the equilibrium state, and χ indicates the Flory-Huggins polymer solvent interaction parameters.

2.4.2. Solvent Interaction Parameters (χ). To investigate the compatibility of monomer and polymer in the AA/Gelatin hydrogels with the molecules of surrounding media, solvent interaction parameters were measured. Flory-Huggins theory was used to calculate solvent interaction parameters (χ). The following equation was used to calculate χ values given in the following [24]:

$$\chi = \frac{\ln\left(1 - V_{2,s}\right) + V_{2,s}}{V_{2,s}^2}, \tag{6}$$

where $V_{2,s}$ (mL/mol) indicates the volume fraction of the hydrated gel in the equilibrium state and χ is the Flory-Huggins polymer solvent interaction parameters.

2.4.3. Cross-Linked Density (q). Cross-linked hydrogels are characterized by cross-linked density. The following equation is used for cross-linked density [25]:

$$q = \frac{M_c}{M_r}, \tag{7}$$

where M_r is molar mass of the repeat unit and is calculated as per

$$M_r = \frac{m_{\text{AA}} M_{\text{AA}} + m_{\text{Ge}} M_{\text{Ge}} + m_{\text{EGDMA}} M_{\text{EGDMA}}}{m_{\text{AA}} + m_{\text{Ge}} + m_{\text{EGDMA}}}, \tag{8}$$

where m_{AA}, m_{Ge}, and m_{EGDMA} are the masses of the monomer (AA), polymer (Ge), and EGDMA, respectively, while M_{AA}, M_{Ge}, and M_{EGDMA} are the molar masses of AA, Ge, and EGDMA, respectively.

2.5. Sol-Gel Fraction Analysis. In order to calculate uncross-linked polymer sol-gel fraction is used. Hydrogel samples were cut into pieces with a diameter of 3-4 mm, first dried at room temperature and then in a vacuum oven at 45°C to a constant weight (W_o), and subjected to Soxhlet extraction for 4 h with deionized water as solvent at boiling temperature. Uncross-linked polymer was removed from the gel structure with this extraction. Extracted gels were dried again in a vacuum oven at 45°C to constant weight (W_i). The gel fraction

was calculated by using initial weight of dry gel (W_o) and weight of extracted dry gel (W_i) according to [26]

$$\text{Sol fraction (\%)} = \left[\frac{W_o - W_i}{W_o}\right] \times 100$$
$$\text{Gel fraction (\%)} = 100 - \text{Sol fraction}. \quad (9)$$

2.6. Porosity Measurement. For the measurement of porosity of hydrogels, which represents the fraction of the volume of pores over the total volume between 0 and 100 percent, solvent replacement method was used. Weighed dried hydrogel discs were immersed in absolute ethanol overnight and weighed after excess ethanol on the surface. The porosity (%) was calculated by [27]

$$\text{Porosity} = \frac{(M_2 - M_1)}{\rho V} \times 100, \quad (10)$$

where M_2 and M_1 are the mass of the hydrogel before and after immersion in ethanol, respectively, ρ is density of absolute ethanol, and V is the volume of the hydrogel.

2.7. Loading of Pheniramine Maleate. Selected samples which showed maximum swellings were used for loading and release study of the model drug, that is, pheniramine maleate. The drug loading into disks of weighed dried hydrogel samples was achieved by soaking them in 1% (w/v) drug solution of the pheniramine maleate up to equilibrium swelling. Drug solution of pheniramine maleate was prepared by dissolving water soluble drug in buffer solution of 7.5 pH. After achieving the equilibrium value, swelled hydrogel discs were removed from the drug solution, blotted with filter paper, first dried at room temperature, and then placed in an oven at 45°C to constant weight [20, 26].

2.8. Quantification of Drug Loading. Amount of drug loaded in discs of hydrogels was calculated by three methods. The first method known as weight method used to calculate the amount of drug loaded in hydrogel discs is represented by [22]

$$\text{Amount of drug} = W_D - W_d. \quad (11)$$

For calculating percentage of drug loading, the following equation is used:

$$\text{Drug Loading \%} = \frac{W_D - W_d}{W_d} \times 100, \quad (12)$$

where W_D is the weight of dried discs of hydrogels after immersion in drug solution and W_d is the weight of dried hydrogel discs before immersion in drug solution.

In the second method to calculate the amount of drug loaded in the hydrogels, drug entrapped in the hydrogel samples was calculated by repeatedly extracting weighed drug loaded hydrogel samples using phosphate buffer solution of pH 7.5. Each time 25 mL fresh phosphate buffer solution of pH 7.5 was used until there was no drug in the drug solution. Drug concentration was determined spectrophotometrically. Total amount of drug present in all portions was considered as amount of drug entrapped or loaded. This method is known as extraction method.

In the third method, which is known to be swelling method, weighed hydrogel discs were placed in drug solution up to equilibrium swelling. Loaded hydrogel discs were weighed again after blotting with blotting paper. Difference in weight before and after swelling is the weight of drug solution. Volume of drug solution absorbed by gel discs can be calculated by knowing the density and weight of drug solution. By knowing the volume of drug solution, amount of drug absorbed by the gel discs was also calculated.

2.9. Drug Release Study In Vitro. Drug release from cross-linked AA/Gelatin hydrogels was measured using the dissolution apparatus (Pharmatest; type PT-DT 7, Germany) and UV-Vis spectrophotometer (IRMECO, UV-Vis U2020). The weighed hydrogels disc was immersed in 500 mL dissolution medium at 37°C and dissolution medium was stirred at a rate of 100 rpm for maintaining a uniform drug concentration in the medium. 0.05 M USP phosphate buffer solutions of pH 1.2, pH 5.5, and pH 7.5 were used for dissolution medium. The determination of pheniramine maleate released was carried out at λ_{max} 265.6 with readings up to 12 hrs. With each sampling 5 mL solution was taken for UV analysis and solution was changed with fresh USP phosphate buffer solution [28, 29].

2.9.1. Analysis of Drug Release Pattern. Release of the solute from the cross-linked structure is based on the swelling of polymers and rate of diffusion. To determine the release mechanism, drug release from the cross-linked interpenetrating networks of AA/Gelatin hydrogels has been studied by zero-order, first-order, Higuchi, and Korsmeyer-Peppas models. Equations (13), (14), (15), and (16) used for these models are given in the following.

Zero-order kinetics [30] is as follows:

$$F_t = K_o t, \quad (13)$$

where F indicates the fraction of drug release in time t and K_o is the zero-order release constant.

First-order kinetics [31] is as follows:

$$\ln(1 - F) = -K_1 t, \quad (14)$$

where F shows the fraction of drug release in time t and K_1 is the first-order release constant.

Higuchi model [22] is as follows:

$$F = K_2 t^{1/2}, \quad (15)$$

where F represents the fraction of drug release in time t and K_2 is the Higuchi constant.

Korsmeyer-Peppas model [23] is as follows:

$$\frac{M_t}{M_\infty} = K_3 t^n. \quad (16)$$

Table 2: Equilibrium swelling ratio of AA/Gelatin hydrogels.

Sample codes	Feed composition (AA/Gelatin)	Degree of cross-linking (EGDMA) % W/W	pH of the solution			
			1.2	5.5	6.5	7.5
U_1	35.00/4.00	0.70	5.48	16.43	29.62	34.58
U_2	35.00/5.00	0.70	5.26	14.82	26.81	30.95
U_3	35.00/6.00	0.70	4.76	12.88	24.01	27.94
U_4	28.00/6.00	0.70	4.22	11.51	22.75	26.18
U_5	32.00/6.00	0.70	4.68	14.66	26.66	32.63
U_6	36.00/6.00	0.70	5.66	17.27	33.56	38.28
U_7	36.00/6.00	0.65	5.52	16.83	33.00	37.21
U_8	36.00/6.00	0.75	4.64	12.64	26.43	27.59
U_9	36.00/6.00	0.85	4.014	8.48	22.75	24.61

Here M_t is the mass of water absorbed at any time (t) or penetrant time (t), M_∞ is the amount of water at equilibrium or mass uptake at equilibrium, K_3 is the kinetic constant, and n is the exponent describing the swelling mechanism.

2.10. FTIR Spectroscopy. For FTIR spectroscopy using pestle and mortar, dried discs of hydrogel samples were powdered. Potassium bromide (Merck, IR spectroscopy grade) was mixed with powdered material in 1 : 100 proportions and dried at 40°C. By applying a pressure of 65 KN (pressure gauge, Shimadzu) for 2 minutes, the mixture was compressed to a semitransparent disc of 12 mm diameter. The FTIR spectrum over the wavelength range of 4500–500 cm^{-1} was recorded using FTIR spectrometer (FT-IR 8400 S, Shimadzu) [20, 24].

2.11. Scanning Electron Microscopy (SEM). The surface morphology of AA/Gelatin hydrogels was determined using a scanning electron microscope (Hitachi, S 3000 H, Japan). Hydrogel samples were mounted on an aluminium mount and sputtered with gold palladium. An accelerating voltage of 10 KV, having working distance of 10–25 mm, is used to scan samples [19, 20].

3. Results and Discussion

3.1. Effect of pH on Swelling and on Drug Release of AA/Gelatin Hydrogels. In order to determine the swelling behavior of the hydrogels, the pH of the medium and pKa values of the acidic component of the polymer play an important role. To attain efficient swelling, the pKa of the buffer components should be above the pKa of the gel carboxylic group. At this pKa, the buffer will accept protons and ionizes the gel. The swelling capacity for the synthesized hydrogels was determined by using buffer solutions of 0.05 M USP phosphate buffer solutions of pH 1.2, pH 5.5, pH 6.5, and pH 7.5. The ionization of carboxylic groups varies with pH of the immersion medium that results in great variation in swelling behavior of hydrogel as shown in Table 2. As the pH of the medium increases above the pKa values of the acidic component of the polymer, it starts swelling due to the ionization of the carboxyl groups. These results can be correlated to Ranjha et al. [19]. At higher pH, the hydrogels swell due to the ionic repulsion of protonated carboxylic groups and collapse at low pH because of influence of unprotonated carboxylic group. The ionized COO^- groups become COOH groups as the pH of the buffer solution decreases and the resulting neutralization of ionic groups causes the hydrogels to be precipitated. Similar results were investigated by Byun et al. [32]. Maximum swelling was obtained at pH 7.5. Most of the carboxylate groups are protonated under acidic pH (pH < 3), so the main anion-anion repulsive forces are eliminated and consequently swelling values are reduced. Some of the carboxylate groups are ionized at higher pH (pH > 4) and the electrostatic repulsion between $-COO^-$ groups results in enhancement of the swelling capacity. Table 2 indicates the effect of pH on equilibrium swelling ratio of the AA/Gelatin hydrogels.

The effect of pH on drug release behavior was investigated by immersing the pheniramine maleate loaded samples in solutions of different pH values (1.2, 6.5, and 7.5). It is observed that by increasing the pH of medium the drug release increased as shown in Table 3. At higher pH (7.5) the osmotic pressure inside the gel also causes maximum drug to release as compared to lower pH (1.2). Figure 3 represents the EGDMA cross-linked AA/Gelatin hydrogels.

3.2. Effect of Acrylic Acid Concentration on Swelling and on Drug Release of AA/Gelatin Hydrogels. To investigate the effect of monomeric composition on swelling and drug release, AA/Ge hydrogels of different monomeric concentrations were prepared using EGDMA as cross-linking agent (0.70 wt% of AA). Figure 4 shows the dynamic swelling behavior of different acrylic acid concentration. The pKa value of acrylic acid is 4.28; therefore, at pH less than 4, acrylic acid chains are in the collapsed state, thus reducing the swelling ratio. However, as the pH increases above 6 and 8, acrylic acid forms carboxylate ions, which cause repulsion between the networks, resulting in rapid increase in the swelling ratio. Similar observations were made by Sullad et al. [5]. In Table 2 the samples (U_4 to U_6) show the effect of monomer concentration on equilibrium swelling ratio, keeping polymer and cross-linker concentrations constant. It is investigated that drug release and swelling of gel increased with increase of acrylic acid concentration due to availability of more carboxylic groups of acrylic acid for ionization and

Table 3: Amount of pheniramine maleate loaded and released.

Sample codes	Amount of pheniramine maleate loaded (g/g of dry gel)			Amount of pheniramine maleate released (%) (pH of the solution)		
	By swelling	By weight	By extraction	1.2	5.5	7.5
U_4	0.069	0.066	0.068	25.53	52.67	71.01
U_5	0.073	0.071	0.075	27.81	56.92	76.54
U_6	0.077	0.075	0.079	29.73	62.45	80.55
U_7	0.081	0.079	0.082	30.37	67.76	82.83
U_8	0.078	0.075	0.071	22.28	54.29	74.45
U_9	0.071	0.069	0.066	20.09	50.62	69.59

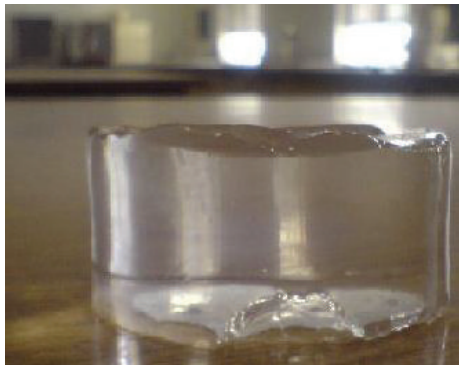

Figure 3: EGDMA cross-linked AA/Gelatin hydrogels.

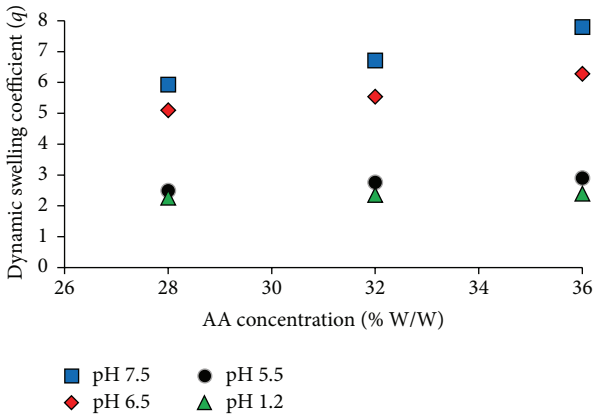

Figure 4: Dynamic swelling coefficient of AA/Gelatin hydrogels with different concentration of acrylic acid (28, 32, and 36 g) using EGDMA as cross-linking agent (0.7%) of acrylic acid in 0.05 M USP phosphate buffer solutions of different pH values at 37°C.

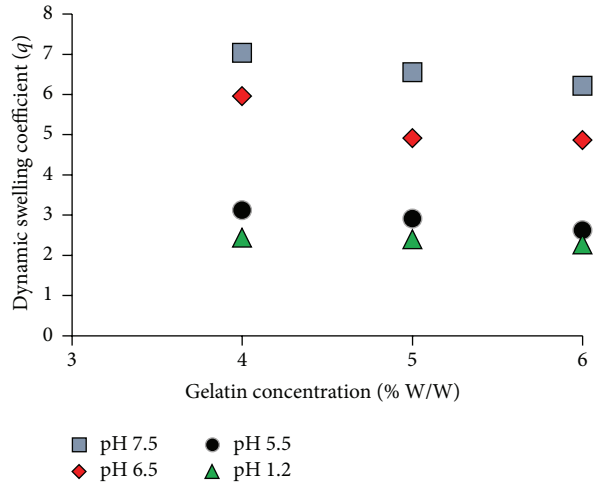

Figure 5: Dynamic swelling coefficient of AA/Gelatin hydrogels with different concentration of gelatin (4.0, 5.0, and 6.0 gm) using EGDMA as cross-linking agent (0.7%) of acrylic acid in 0.05 M USP phosphate buffer solutions of different pH values at 37°C.

electrostatic repulsion along the chain takes place that causes an expansion of the originally coiled molecules.

In order to investigate the effect of acrylic acid concentration on release of the drug, release study was carried out at pH 1.2, pH 5.5, and pH 7.5 for 12 hrs. The effects of acrylic acid concentration on release of drug from hydrogels have been shown in Figure 7. In phosphate buffer at pH 7.5, the amount of drug released from hydrogels was significantly higher than at pH 1.2 and pH 5.5. The swelling of AA/Ge hydrogels increased when the pH of the medium changed from lower to higher. From the results it was observed that increase in the concentration of AA leads to the increased percent drug release. Table 3 indicates the amount of drug loaded and released.

3.3. Effect of Gelatin Concentration on Swelling of AA/Gelatin Hydrogels. Three formulations of AA/Ge hydrogels with varying concentration of gelatin (4.0 g, 5.0 g, and 6.0 g) keeping acrylic acid and EGDMA concentration constant (0.70% of AA) were synthesized and subjected to swelling studies in solutions of different pH values. Figure 5 shows the effect of gelatin concentration on dynamic swelling of these hydrogels. The numerical data showing effect of gelatin (U_1 to U_3) on swelling profile has been demonstrated in Table 2. The concentration of gelatin acts conversely on the swelling behavior as compared to acrylic acid content. The swelling coefficient of prepared hydrogels decreased with the increase in the concentration of gelatin. Below the PI (isoelectric pH) value, the gelatin chains remain protonated. As a result, the chains contain NH_3^+ ions, and the cationic repulsion between them could be responsible for their high swelling.

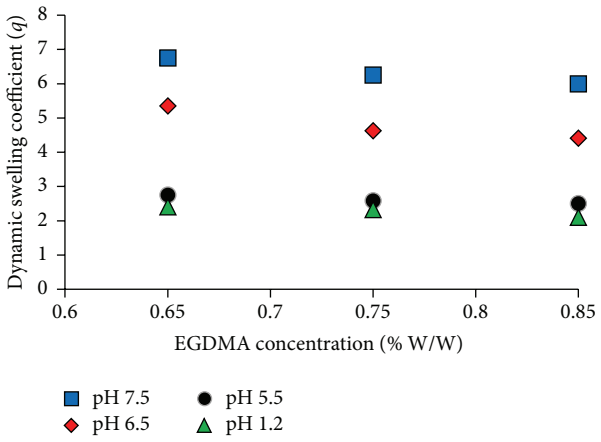

Figure 6: Dynamic swelling coefficient of AA/Gelatin hydrogels with different concentrations of EGDMA as cross-linking agent (0.65%, 0.75%, and 0.85% of acrylic acid) in 0.05 M USP phosphate buffer solutions of different pH values at 37°C.

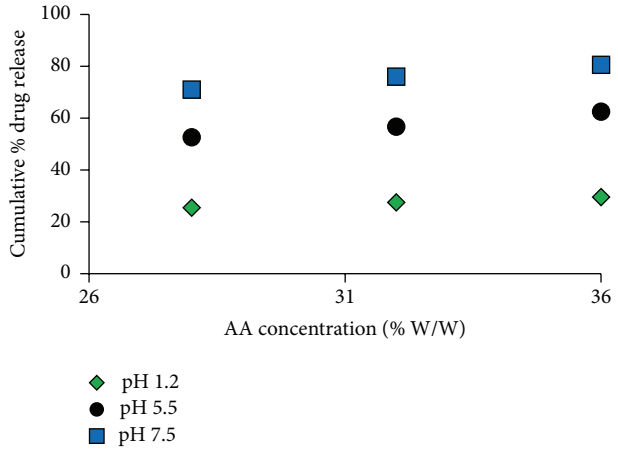

Figure 7: Cumulative % release of pheniramine maleate from AA/Gelatin hydrogels after 12 h using different concentrations of acrylic acid (28.0, 32.0, and 36.0 g) and EGDMA as cross-linking agent (0.7% of AA) at various pH values in 0.05 M USP phosphate buffer solutions.

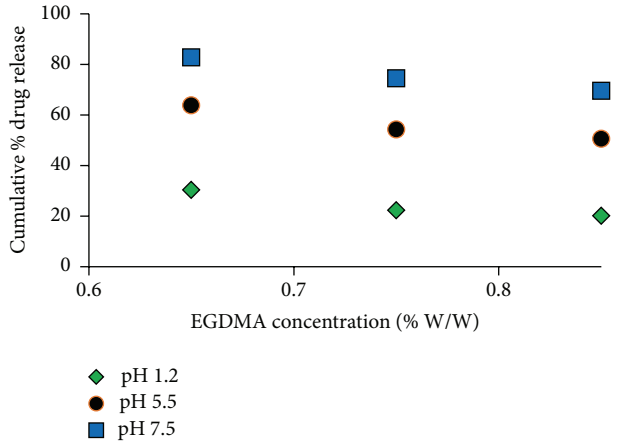

Figure 8: Cumulative % release of pheniramine maleate from AA/Gelatin hydrogels after 12 h using different concentrations of EGDMA as cross-linking agent (0.65%, 0.75%, and 0.85%) at various pH values in 0.05 M USP phosphate buffer solutions.

But the overall increase in gelatin contents has no significant effect on swelling because the percent swelling increased with increasing amounts of acrylic acid at all pH values, whereas increased gelatin content resulted in a decrease in percent swelling. Similar observations were made by Khan and Ranjha [22].

3.4. Effect of Degree of Cross-Linking on Swelling and on Drug Release of AA/Gelatin Hydrogels. The degree of swelling and drug release was also studied to be dependent on the concentration of cross-linking agent (EGDMA). In order to investigate the effect of EGDMA on swelling and release behavior of hydrogels, a series of three AA/Gelatin hydrogels (U_7–U_9) of different cross-linking agent concentration (0.65%, 0.75%, and 0.85% of AA) were prepared as shown in Table 2. In Figure 6 it was observed that swelling of gel decreased with increase of EGDMA concentration due to presence of more physical entanglements between hydrogels. The influence of increasing cross-linking can be described by decrease in mesh size of network. High cross-linked polymers are less acidic because carboxylate groups are concealed and higher cross-linking ratio reduces the process of ionization. It was observed that, at higher concentration of cross-linker, the relaxation of polymer chain decreased which is responsible for the less swelling of hydrogel. Same results were found by Shah et al. [23].

Drug release studies were performed in buffer solutions of different pH values (1.2, 5.5, and 7.5). The results from the study demonstrated that increase in EGDMA concentration will result in decrease in drug release % age due to the tighter hydrogel structure as shown in Table 3. Same observations were reported by Singh et al. [33]. Figure 8 indicates the effect of EGDMA concentration on cumulative % drug release in buffer solutions of various pH values.

3.5. Sol-Gel Analysis. To determine the uncross-linked fraction of the polymer in the hydrogel, sol-gel analysis was performed. It was found that gel fraction of hydrogels increased along with increased concentration of acrylic acid, gelatin, and cross-linker as shown in Table 4. Sol fraction of hydrogels was observed to decrease along the increased concentrations of gelatin, acrylic acid, and EGDMA. Dergunov et al. investigated the similar results [34]. Figures 9, 10, and 11 demonstrate the effect of gelatin concentration, AA concentration, and EGDMA concentration on gel fraction of hydrogel.

3.6. Porosity Measurement. From results in Table 4, it is observed that porosity increases by increasing the concentration of acrylic acid and gelatin due to increasing of viscosity of the hydrogel solution. Viscous solution efficiently prevents the bubbles from escaping from the solution that result in increase of porosity due to formation of interconnected channels. While increasing the EGDMA concentration porosity decreases due to increasing physical entanglement between

Table 4: Sol-gel fraction analysis and porosity measurement of different formulations of AA/Gelatin hydrogels.

Sample codes	Degree of cross-linking (EGDMA) % W/W	Gel fraction (%)	Sol fraction (%)	Porosity (%)
U_1	0.70	84.44	15.56	44.07
U_2	0.70	86.59	13.41	56.81
U_3	0.70	90.22	9.78	62.09
U_4	0.70	87.12	12.88	46.43
U_5	0.70	90.23	9.77	57.47
U_6	0.70	94.54	5.46	63.72
U_7	0.65	85.64	14.36	69.03
U_8	0.75	89.09	10.91	65.32
U_9	0.85	95.23	4.77	62.30

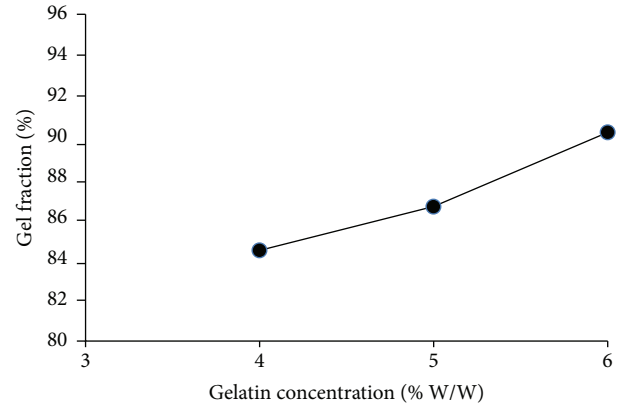

Figure 9: Effect of gelatin concentration on gel fraction of AA/Gelatin hydrogels.

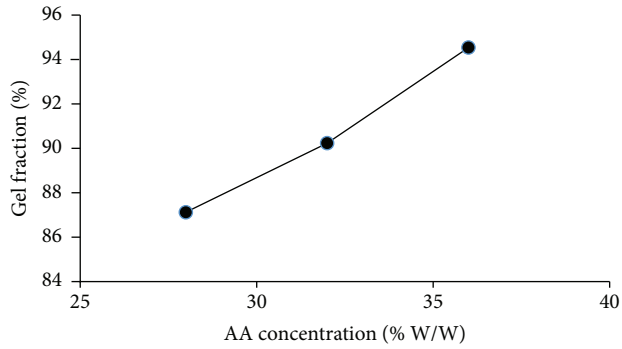

Figure 10: Effect of acrylic acid concentration on gel fraction of AA/Gelatin hydrogels.

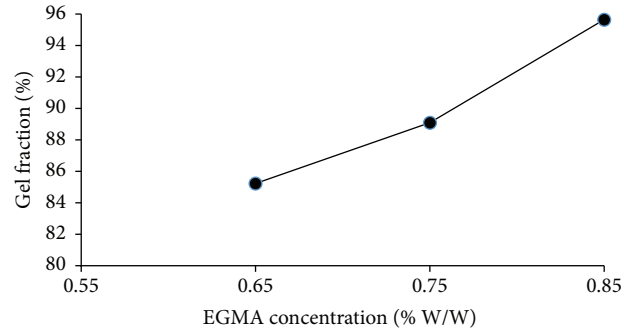

Figure 11: Effect of cross-linking agent concentration (EGDMA) on gel fraction of AA/Gelatin hydrogels.

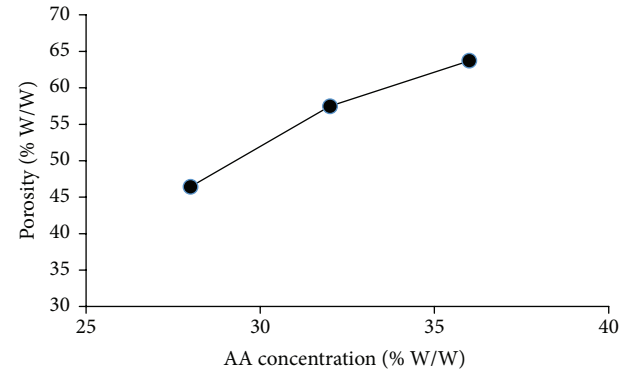

Figure 12: Effect of gelatin concentration on porosity of AA/Gelatin hydrogels.

acrylic acid and gelatin shown in Figures 12, 13, and 14. Increase in cross-linking agent concentration results in increase in entanglement between monomer and polymer which results in decreased porosity. Yin et al. observed the similar results [35].

3.7. Diffusion Coefficient of Polymers (D). During membrane permeation method or sorption and desorption phenomenon Fick's law of diffusion was used. To measure solute diffusion into hydrogel, diffusion coefficient is applied indirectly. Table 5 indicates that diffusion coefficient decreased with the increasing of acrylic acid concentration and gelatin concentration because swelling of polymer increases as the concentration of AA increases. Diffusion coefficient increased with increasing of cross-linking agent concentration.

3.8. Molecular Weight between Cross-Links (M_c) and Solvent Interaction Parameters (χ). It was observed that increase in the concentration of acrylic acid results in increased values of molecular weight between cross-links (M_c). Due to presence

Table 5: Flory-Huggins network parameters of AA/Gelatin hydrogel.

Sample codes	Degree of cross-linking (EGDMA) wt %	$V_{2,s}$	χ	M_c	M_r	Q	$D \times 10^{-5}$ ($cm^2 sec^{-1}$)
U_1	0.70	0.059	−0.520	949.945	106.527	8.917	0.2289
U_2	0.70	0.064	−0.522	856.917	113.876	7.524	0.3038
U_3	0.70	0.065	−0.522	858.763	120.869	7.105	0.3526
U_4	0.70	0.064	−0.527	918.091	130.723	7.023	0.3316
U_5	0.70	0.053	−0.518	1245.87	124.633	9.996	0.1559
U_6	0.70	0.052	−0.515	1291.54	119.702	10.79	0.1487
U_7	0.65	0.049	−0.516	1483.83	120.811	12.28	0.1301
U_8	0.75	0.066	−0.523	1031.95	120.878	8.532	0.2547
U_9	0.85	0.067	−0.523	804.943	120.949	6.659	0.4384

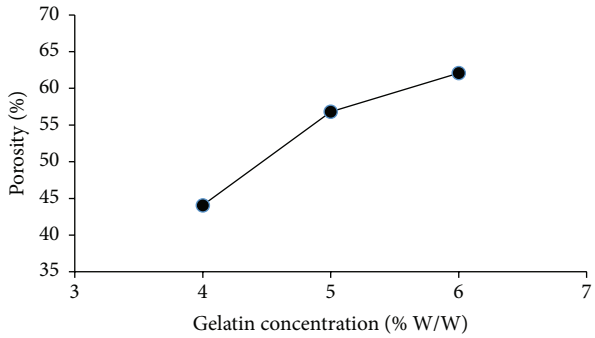

Figure 13: Effect of acrylic acid concentration on porosity of AA/Gelatin hydrogels.

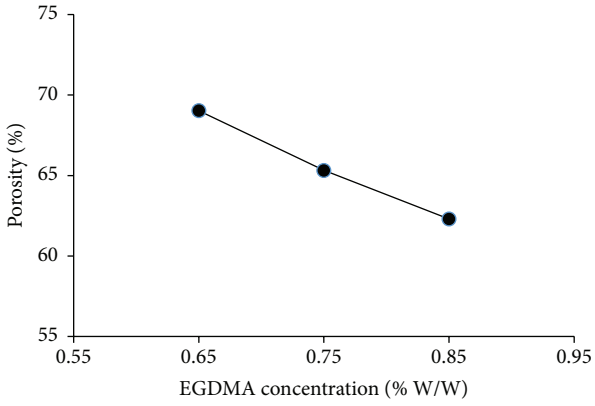

Figure 14: Effect of cross-linking agent (EGDMA) concentration on porosity of AA/Gelatin hydrogels.

of carboxylic groups in polymer chain of acrylic acid, higher swelling of polymer was reported. Cross-linked density (N) is also related to the values of acrylic acid and average molecular weight between cross-links as shown in Table 5. To check the effect of solvent interaction between polymer and solvent, the solvent interaction parameters (χ) were studied. In Table 5 it was reported that greater values of (χ) lead to the weaker interaction between polymer and solvent [36].

3.9. Drug Release Kinetics. Analysis of drug release pattern was studied in phosphate buffer solutions pH 1.2, pH 5.5, and pH 7.5. The data obtained was fitted in zero-order, first-order, Korsmeyer-Peppas, and Higuchi models to evaluate the drug release pattern as given in Tables 6 and 7. The method that best fits the release data was evaluated by the regression coefficient (r). A criterion for selecting the most appropriate model was based on the ideal fit indicated by the values of regression coefficient (r) near to 1. Values of regression coefficient (r) for zero-order and first-order models obtained from drug loaded AA/Ge hydrogels at varying content of acrylic acid and degree of cross-linking are given in Tables 6 and 7. For most of samples, the values of regression coefficient (r) obtained for zero-order release rate constants were found higher than those of first-order release rate constants. It is therefore attributed to the fact that drug release from the samples of varying monomeric compositions and degree of cross-linking are according to zero-order release. In Higuchi model the value of regression coefficient (r) at different monomeric composition and at different degree of cross-linking indicated that the drug release mechanism is diffusion controlled. Figures 15, 16, and 17 indicate the release profile of pheniramine maleate following zero-order release, first-order release, and Higuchi model from AA/Gelatin hydrogels (sample U_7). Effects of monomer concentration and degree of cross-linking on release exponent (n) values are given in Tables 8 and 9, respectively. All samples showed non-Fickian behavior [37].

4. FTIR Spectroscopy

In order to assess the functional groups in monomer and polymer (AA and Ge) and to confirm the formation of cross-linked networks from the hydrogels with EGDMA, samples were analyzed by Fourier transform infrared spectroscopy (FTIR). The FTIR spectra of gelatin, acrylic acid, AA/Gelatin hydrogel, AA/Gelatin drug loaded hydrogel, and pheniramine maleate are shown in Figure 18. In the FTIR spectra of gelatin as shown in Figure 18 (A), the absorption peak at 3321 cm^{-1} is attributed to N–H stretching. Peaks at 3060 and 2948 cm^{-1} are attributed to C–H stretching. The peak at 1664 cm^{-1} refers to the absorption band of amide I and at 1539 cm^{-1} shows the absorption band of amide II [38]. The FTIR spectra of pure AA are shown in Figure 18 (B). The absorption peak of acrylic acid at 3425 cm^{-1} corresponds to O–H stretching, 1691 cm^{-1} is for C=O stretching, 1573 cm^{-1}

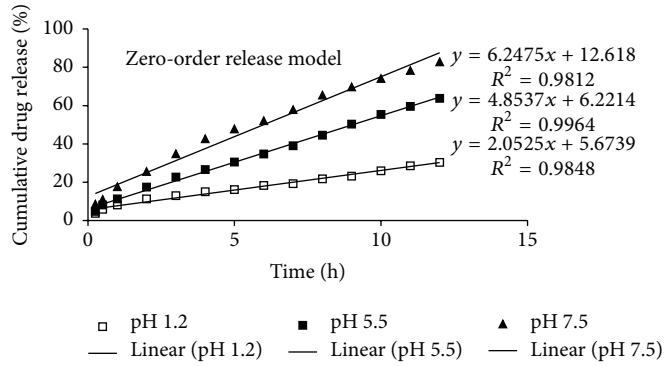

Figure 15: % Cumulative pheniramine maleate release versus time (zero-order release) from EGDMA cross-linked AA/Gelatin hydrogels.

Table 6: Effect of different concentrations of acrylic acid on drug release kinetics of AA/Gelatin hydrogels in solutions of different pH values using EGDMA as cross-linking agent (0.70% w/w).

Sample codes	AA contents (%)	pH	Zero-order kinetics		First-order kinetics		Higuchi model	
			K_o (h^{-1})	r	K_1 (h^{-1})	r	K_2 (h^{-1})	r
U_4	28	1.2	1.75	0.991	0.020	0.991	0.068	0.958
		5.5	3.945	0.997	0.057	0.990	0.157	0.958
		7.5	5.127	0.991	0.092	0.976	0.204	0.959
U_5	32	1.2	2.076	0.992	0.024	0.986	0.081	0.930
		5.5	4.149	0.994	0.063	0.995	0.167	0.979
		7.5	5.177	0.994	0.099	0.951	0.206	0.950
U_6	36	1.2	1.948	0.985	0.023	0.980	0.077	0.942
		5.5	4.401	0.995	0.071	0.986	0.177	0.971
		7.5	5.679	0.985	0.119	0.987	0.232	0.997

Table 7: Effect of degree of cross-linking on drug release kinetics of AA/Gelatin hydrogels in solutions of different pH values.

Sample codes	EGDMA contents (%)	pH	Zero-order kinetics		First-order kinetics		Higuchi model	
			K_o (h^{-1})	r	K_1 (h^{-1})	r	K_2 (h^{-1})	r
U_7	0.65	1.2	2.052	0.984	0.025	0.987	0.0833	0.976
		5.5	4.853	0.996	0.077	0.984	0.195	0.971
		7.5	6.247	0.981	0.134	0.988	0.083	0.976
U_8	0.75	1.2	1.423	0.980	0.016	0.984	0.057	0.973
		5.5	4.176	0.990	0.062	0.995	0.169	0.983
		7.5	5.121	0.989	0.097	0.966	0.211	0.993
U_9	0.85	1.2	1.412	0.977	0.016	0.983	0.058	0.993
		5.5	4.019	0.997	0.056	0.994	0.160	0.963
		7.5	5.251	0.992	0.090	0.989	0.212	0.978

is attributed to C=O bending in –COOH, and 1319 cm^{-1} is for C–C stretching. The FTIR spectrum of AA/Ge hydrogel is different than the spectra of pure Ge and AA as shown in Figure 18 (C). For AA/Ge hydrogel without drug, the vibration absorption peaks at 3060 and 2948 cm^{-1} have weakened or disappeared after chemical cross-linking with EGDMA. This weakening of absorption peak and change in C–C stretching in between 1200 and 1350 confirms the formation of hydrogel. From the FTIR spectra of drug loaded hydrogel shown in Figure 18 (D), it is clear that there is no prominent shift in the major peaks, which shows that there is no chemical interaction between polymers and drug loaded in hydrogel. Figure 18 (E) indicates the FTIR spectra of pure drug.

4.1. Scanning Electron Microscopy (SEM). The morphology of the interpenetrating hydrogels was studied by surface electron microscopy. Figures 19(a) and 19(b) indicate the surface morphology of unloaded and AA/Gelatin hydrogel sample loaded with pheniramine maleate. It was observed

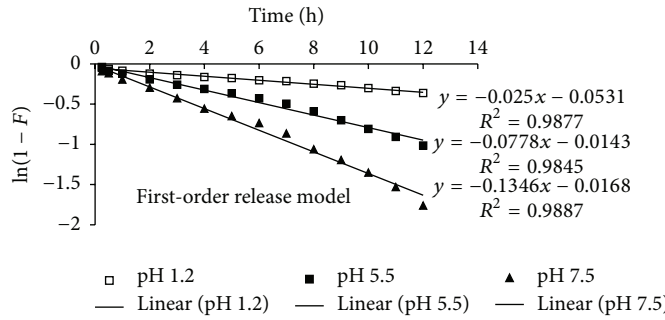

Figure 16: % log cumulative pheniramine maleate release ($1 - F$) versus time (first-order release) from EGDMA cross-linked AA/Gelatin hydrogels.

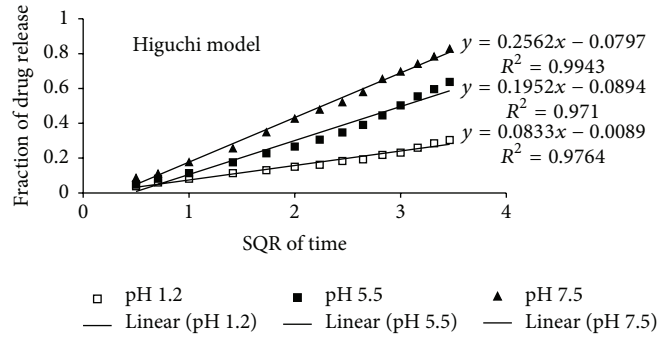

Figure 17: % cumulative pheniramine maleate release versus Sq. Rt. time (Higuchi model) from EGDMA cross-linked AA/Gelatin hydrogels.

Table 8: Effect of different concentration of acrylic acid on drug release mechanism of AA/Gelatin hydrogels in solutions of different pH values using EGDMA as cross-linking agent (0.7% of acrylic acid).

Sample codes	AA contents (%)	pH	Release exponent (n)	r	Order of release
U_4	28	1.2	0.7162	0.995	Non-Fickian
		5.5	0.9463	0.997	Non-Fickian
		7.5	0.9257	0.991	Non-Fickian
U_5	32	1.2	0.7532	0.994	Non-Fickian
		5.5	0.9832	0.994	Non-Fickian
		7.5	0.9573	0.992	Non-Fickian
U_6	36	1.2	0.7261	0.987	Non-Fickian
		5.5	0.8643	0.990	Non-Fickian
		7.5	0.8252	0.985	Non-Fickian

Table 9: Effect of degree of cross-linking on drug release mechanism of AA/Gelatin hydrogels in solutions of different pH values.

Sample codes	EGDMA contents (%)	pH	Release exponent (n)	r	Order of release
U_7	0.65	1.2	0.6242	0.981	Non-Fickian
		5.5	0.8345	0.996	Non-Fickian
		7.5	0.7752	0.984	Non-Fickian
U_8	0.75	1.2	0.7529	0.978	Non-Fickian
		5.5	0.8673	0.990	Non-Fickian
		7.5	0.7868	0.987	Non-Fickian
U_9	0.85	1.2	0.7591	0.992	Non-Fickian
		5.5	0.8765	0.994	Non-Fickian
		7.5	0.7847	0.979	Non-Fickian

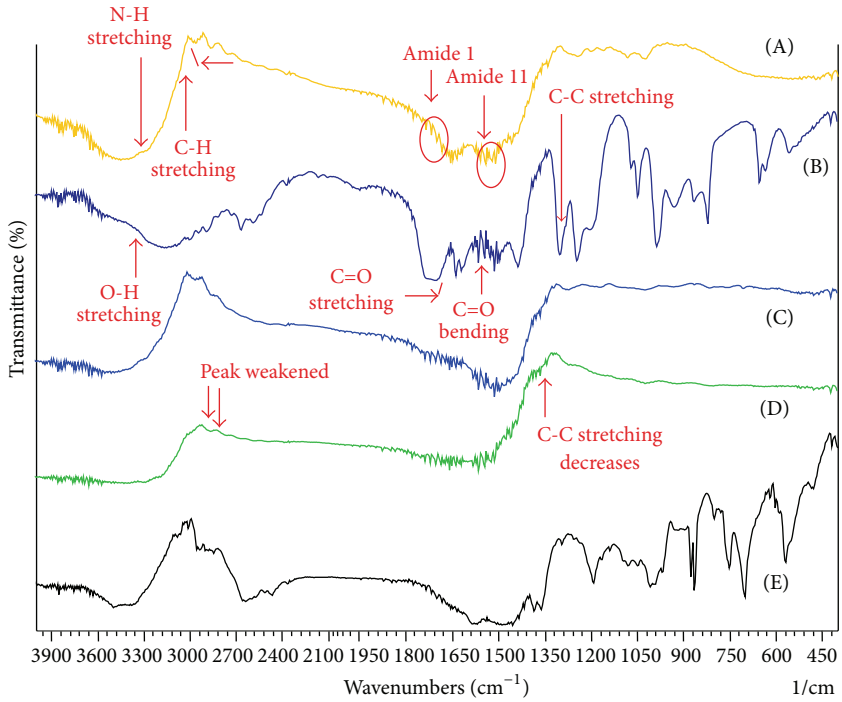

Figure 18: FTIR spectra of (A) pure gelatin, (B) acrylic acid, (C) unloaded AA/Gelatin hydrogel, (D) loaded AA/Gelatin hydrogel, and (E) pheniramine maleate.

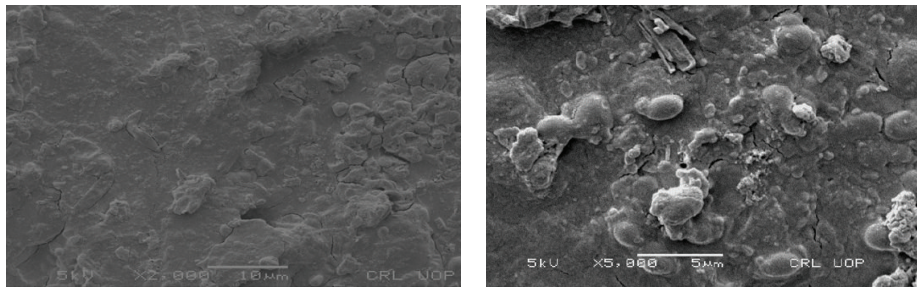

(a) Unloaded (b) Loaded

Figure 19: Surface electron micrographs (SEM) of AA/Gelatin hydrogels of sample U_6: (a) magnification ×2000, (b) magnification ×5000.

that SEM graphs of the hydrogel sample contain pores, which facilitate the adherence of the drug into the interpenetrating network of the hydrogel. Figure 19(b) shows the dispersed white particles at high magnification throughout the hydrogel network which refers to the model drug loaded in these hydrogel samples.

5. Conclusion

In present study, pH sensitive cross-linked AA/Gelatin hydrogels were prepared by free radical polymerization using ethylene glycol dimethacrylate (EGDMA) as cross-linking agent as a carrier for water soluble drugs. To investigate the pH sensitive behavior, hydrogel samples were subjected to swelling experiments in USP phosphate buffer solutions of various pH values. Swelling of polymeric network was found affected by composition and pH of swelling medium. The swelling ratios of these hydrogels showed a regular variation with changing concentrations of the monomer, polymer, and cross-linking agent. The swelling ratios were found to decrease as the polymer and cross-linker concentration increased in the composition of samples. While with the increase of acrylic acid contents in the composition, the dynamic and equilibrium swelling ratio increased due to the electrostatic repulsion between carboxylate ions (COO^-) which leads to chains repulsion and in turn swelling of the network at higher pH values. The swelling and release of the drug decreased with increasing concentration of cross-linking agent due to the tighter hydrogel structure. The drug release from hydrogel is dependent upon the composition as well as the pH of swelling medium. In phosphate buffer of pH 7.5 the rate of drug release was faster as compared to other pH values. Gel fraction of the samples increased with the increasing concentration of monomer, polymer, and cross-linking

agent concentration. Porosity of the hydrogels increased with increasing contents of the acrylic acid and gelatin, while it decreases as the contents of EGDMA increased in the gels. Drug release mechanism was found to be non-Fickian for AA/Gelatin hydrogels. It was concluded that these polymeric networks are pH sensitive and are able to respond to the environmental conditions.

Conflict of Interests

The authors declare that they have no conflict of interests.

Acknowledgments

The authors thank the Faculty of Pharmacy, B. Z. University, for providing laboratory facilities and director of Centralized Resource Laboratory, Department of Physics, University of Peshawar, for providing them with the facility of SEM is acknowledged.

References

[1] N. Devi and A. Narzary, "Release dynamics of brufen from a drug-loaded polymer hydrogel containing polyvinyl alcohol, 2-acrylamide-2-methylpropane sulfonic acid and acrylamide," *International Journal of Polymeric Materials*, vol. 61, no. 11, pp. 821–833, 2012.

[2] T. R. Hoare and D. S. Kohane, "Hydrogels in drug delivery: progress and challenges," *Polymer*, vol. 49, no. 8, pp. 1993–2007, 2008.

[3] W. E. Hennink and C. F. Van Nostrum, "Novel crosslinking methods to design hydrogels," *Advanced Drug Delivery Reviews*, vol. 64, pp. 223–236, 2012.

[4] N. A. Peppas, J. Z. Hilt, A. Khademhosseini, and R. Langer, "Hydrogels in biology and medicine: from molecular principles to bionanotechnology," *Advanced Materials*, vol. 18, no. 11, pp. 1345–1360, 2006.

[5] A. G. Sullad, L. S. Manjeshwar, and T. M. Aminabhavi, "Novel pH-sensitive hydrogels prepared from the blends of poly(vinyl alcohol) with acrylic acid-*graft*-guar gum matrixes for isoniazid delivery," *Industrial and Engineering Chemistry Research*, vol. 49, no. 16, pp. 7323–7329, 2010.

[6] T. Çaykara and E. Turan, "Effect of the amount and type of the crosslinker on the swelling behavior of temperature-sensitive poly(N-tert-butylacrylamide-co-acrylamide) hydrogels," *Colloid and Polymer Science*, vol. 284, no. 9, pp. 1038–1048, 2006.

[7] M. Hanif, N. M. Ranjha, M. H. Shoaib et al., "Preparation, characterization and release of verapmil hydrochloride from polycaprolactone/acrylic acid (PCL/AA) hydrogels," *Pakistan Journal of Pharmaceutical Sciences*, vol. 24, no. 4, pp. 503–511, 2011.

[8] B. S. Kaith, R. Jindal, and G. S. Kapur, "Enzyme-based green approach for the synthesis of gum tragacanth and acrylic acid cross-linked hydrogel: its utilization in controlled fertilizer release and enhancement of water-holding capacity of soil," *Iranian Polymer Journal*, vol. 22, no. 8, pp. 561–570, 2013.

[9] Y. L. Lo, C. Y. Hsu, and H. R. Lin, "PH-and thermo-sensitive pluronic/poly(acrylic acid) *in situ* hydrogels for sustained release of an anticancer drug," *Journal of Drug Targeting*, vol. 21, no. 1, pp. 54–66, 2013.

[10] A. K. Bajpai and S. Kankane, "Evaluation of water sorption property and in vitro blood compatibility of poly(2-hydroxyethyl methacrylate) (PHEMA) based semi interpenetrating polymer networks (IPNs)," *Journal of Materials Science: Materials in Medicine*, vol. 19, no. 5, pp. 1921–1933, 2008.

[11] S. Kheirandish and E. Jabbari, "Effect of surface polarity on wettability and friction coefficient of silicone rubber/poly(acrylic acid) hydrogel composite," *Colloid and Polymer Science*, vol. 284, no. 12, pp. 1411–1417, 2006.

[12] S. J. You, W. S. Ahn, H. S. Jang et al., "Preparation and characterization of gelatin-poly(vinyl alcohol) hydrogels for three-dimensional cell culture," *Journal of Industrial and Engineering Chemistry*, vol. 13, no. 1, pp. 116–120, 2007.

[13] K. Pal, A. K. Banthia, and D. K. Majumdar, "Preparation and characterization of polyvinyl alcohol-gelatin hydrogel membranes for biomedical applications," *AAPS PharmSciTech*, vol. 8, no. 1, article no. 21, pp. E142–E146, 2007.

[14] R. K. Mishra, A. B. Majeed, and A. K. Banthia, "Development and characterization of pectin/gelatinhydrogel membranes for wound dressing," *International Journal of Plastics Technology*, vol. 15, no. 1, pp. 82–95, 2011.

[15] A. K. Bajpai and M. Sharma, "Preparation and characterization of binary grafted polymeric blends of polyvinyl alcohol and gelatin and evaluation of their water uptake potential," *Journal of Macromolecular Science*, vol. 42, no. 5, pp. 663–682, 2005.

[16] Q. Tang, J. Wu, J. Lin, S. Fan, and D. Hu, "A multifunctional poly(acrylic acid)/gelatin hydrogel," *Journal of Materials Research*, vol. 24, no. 5, pp. 1653–1661, 2009.

[17] A. Bigi, G. Cojazzi, S. Panzavolta, K. Rubini, and N. Roveri, "Mechanical and thermal properties of gelatin films at different degrees of glutaraldehyde crosslinking," *Biomaterials*, vol. 22, no. 8, pp. 763–768, 2001.

[18] M. S. Raghu, K. Basavaiah, P. J. Ramesh, S. A. M. Abdulrahman, and K. B. Vinay, "Development and validation of a UV-spectrophotometric method for the determination of pheniramine maleate and its stability studies," *Journal of Applied Spectroscopy*, vol. 79, no. 1, pp. 131–138, 2012.

[19] N. M. Ranjha, G. Ayub, S. Naseem, and M. T. Ansari, "Preparation and characterization of hybrid pH-sensitive hydrogels of chitosan-co-acrylic acid for controlled release of verapamil," *Journal of Materials Science: Materials in Medicine*, vol. 21, no. 10, pp. 2805–2816, 2010.

[20] N. M. Ranjha, J. Mudassir, and Z. Z. Sheikh, "Synthesis and characterization of pH-Sensitive pectin/Acrylic acid hydrogels for verapamil release study," *Iranian Polymer Journal*, vol. 20, no. 2, pp. 147–159, 2011.

[21] N. M. Ranjha, J. Mudassir, and S. Majeed, "Synthesis and characterization of polycaprolactone/acrylic acid (PCL/AA) hydrogel for controlled drug delivery," *Bulletin of Materials Science*, vol. 34, no. 7, pp. 1537–1547, 2011.

[22] S. Khan and N. M. Ranjha, "Effect of degree of cross-linking on swelling and on drug release of low viscous chitosan/poly(vinyl alcohol) hydrogels," *Polymer Bulletin*, vol. 71, no. 8, pp. 2133–2158, 2014.

[23] S. Shah, N. M. Ranjha, and Z. Javaid, "Development and evaluation of pH-dependent interpenetrating network of acrylic acid/polyvinyl alcohol," *Iranian Polymer Journal*, vol. 22, no. 11, pp. 811–820, 2013.

[24] J. Mudassir and N. M. Ranjha, "Dynamic and equilibrium swelling studies: crosslinked pH sensitive methyl methacrylate-co-itaconic acid (MMA-co-IA) hydrogels," *Journal of Polymer Research*, vol. 15, no. 3, pp. 195–203, 2008.

[25] C. S. Fodor, G. Kali, and B. Iván, "Poly(*N*-vinylimidazole)-*l*-poly(tetrahydrofuran) amphiphilic conetworks and gels: synthesis, characterization, thermal and swelling behavior," *Macromolecules*, vol. 44, no. 11, pp. 4496–4502, 2011.

[26] N. M. Ranjha and J. Mudassir, "Swelling and aspirin release study: cross-linked pH-sensitive vinyl acetate-co-acrylic acid (VAC-co-AA) hydrogels," *Drug Development and Industrial Pharmacy*, vol. 34, no. 5, pp. 512–521, 2008.

[27] T. Hussain, N. M. Ranjha, and Y. Shahzad, "Swelling and controlled release of tramadol hydrochloride from a pH-sensitive hydrogel," *Designed Monomers and Polymers*, vol. 14, no. 3, pp. 233–249, 2011.

[28] D. Wang, D. J. T. Hill, F. Rasoul, and A. K. Whittaker, "A study of the swelling and model protein release behaviours of radiation-formed poly(N-vinyl 2-pyrrolidone-*co*-acrylic acid) hydrogels," *Radiation Physics and Chemistry*, vol. 80, no. 2, pp. 207–212, 2011.

[29] P. Basak, B. Adhikari, and A. K. Sen, "Surface cross-linked poly (Vinyl alcohol) hydrogel for colon targeted drug release," *Polymer—Plastics Technology and Engineering*, vol. 50, no. 13, pp. 1357–1361, 2011.

[30] N. Najib and M. S. Suleiman, "The kinetics of drug release from ethylcellulose solid dispersions," *Drug Development and Industrial Pharmacy*, vol. 11, no. 12, pp. 2169–2181, 1985.

[31] H. Hosseinzadeh, "Novel interpenetrating polymer network based on chitosan for the controlled release of cisplatin," *Journal of Basic and Applied Scientific Research*, vol. 2, no. 3, pp. 2200–2203, 2012.

[32] H. Byun, B. Hong, S. Y. Nam et al., "Swelling behavior and drug release of poly(vinyl alcohol) hydrogel cross-linked with poly(acrylic acid)," *Macromolecular Research*, vol. 16, no. 3, pp. 189–193, 2008.

[33] B. Singh, G. S. Chauhan, D. K. Sharma, and N. Chauhan, "The release dynamics of salicylic acid and tetracycline hydrochloride from the psyllium and polyacrylamide based hydrogels (II)," *Carbohydrate Polymers*, vol. 67, no. 4, pp. 559–565, 2007.

[34] S. A. Dergunov, I. K. Nam, G. A. Mun, Z. S. Nurkeeva, and E. M. Shaikhutdinov, "Radiation synthesis and characterization of stimuli-sensitive chitosan-polyvinyl pyrrolidone hydrogels," *Radiation Physics and Chemistry*, vol. 72, no. 5, pp. 619–623, 2005.

[35] L. Yin, L. Fei, F. Cui, C. Tang, and C. Yin, "Superporous hydrogels containing poly(acrylic acid-co-acrylamide)/O-carboxymethyl chitosan interpenetrating polymer networks," *Biomaterials*, vol. 28, no. 6, pp. 1258–1266, 2007.

[36] A. Pourjavadi and S. Barzegar, "Smart pectin-based superabsorbent hydrogel as a matrix for ibuprofen as an oral non-steroidal antiinflammatory drug delivery," *Starch*, vol. 61, no. 3-4, pp. 173–187, 2009.

[37] J. Liu, W. Wang, and A. Wang, "Synthesis, characterization, and swelling behaviors of chitosan-g-poly(acrylic acid)/poly(vinyl alcohol) semi-IPN superabsorbent hydrogels," *Polymers for Advanced Technologies*, vol. 22, no. 5, pp. 627–634, 2011.

[38] Y. Huang, H. Yu, and C. Xiao, "pH-sensitive cationic guar gum/poly (acrylic acid) polyelectrolyte hydrogels: swelling and in vitro drug release," *Carbohydrate Polymers*, vol. 69, no. 4, pp. 774–783, 2007.

Hindawi Publishing Corporation
International Journal of Polymer Science
Volume 2015, Article ID 154262, 10 pages
http://dx.doi.org/10.1155/2015/154262

Research Article

Antioxidant Activity and Functional Properties of Polymerized Whey Products by Glycation Process

Liliana Ortega,[1] Anabel Romero,[1] Claudia Muro,[1] and Francisco Riera[2]

[1]*Departamento de Ingeniería Química e Investigación, Instituto Tecnológico de Toluca, Apartado Postal 890, 52149 Metepec, MEX, Mexico*
[2]*Departamento de Ingeniería Química y Tecnología de Medio Ambiente, Universidad de Oviedo, Oviedo, 33006 Asturias, Spain*

Correspondence should be addressed to Claudia Muro; cmuro@ittoluca.edu.mx

Received 14 March 2015; Revised 8 June 2015; Accepted 23 June 2015

Academic Editor: Xingxun Liu

The antioxidant properties of sweet and acid whey products were incremented by polymerization of their proteins by glycation of whey protein concentrates (WPC) and their hydrolyzates (WPCH) with ribose and glucose in individual experiments under similar concentration. Heating at 50°C during 20 h maximum and pH 7 and pH 9 were used in all tests. The higher activity was found in WPC glycosylates products with ribose at pH 7 and heating during 10–15 h. In comparable form, antioxidant activity in WPCH was incremented by prior hydrolysis to glycation with 25–45% of hydrolysis degree. Further functional properties of whey proteins (solubility, emulsion, and foam) were also improved by the polymerization with ribose. The color of polymerized products due to Maillard reactions was associated with antioxidant activity of each compound; however comparative color in glycosylates products with glucose and ribose did not show this effect.

1. Introduction

Today is known the mediator action of some biopolymers on structure and lipid oxidation of sensitive foods; among them are the functional whey proteins [1–3]. Due to their antioxidative effects (which include chelating of prooxidant transition metals), low molecular weight, easy absorption, high activity, hypoallergenicity, and relatively high stability under different conditions, whey proteins may be utilized in formulations of substitutes of synthetic compounds such as butylated hydroxyanisole (BHA), butylated hydroxytoluene (BHT), and tert-butyl hydroquinone (TBHQ). Mainly proteins as lactoferrin [4], serum albumin [5], and free radical scavenging by amino acid residues such as cysteine and tyrosine [6, 7] are described as retardants of the fast deterioration of foods and to prevent the autoxidation of their components.

However, in order to improve their properties and functionality, currently, various researches have been carried out to get better effects of whey products on foods by treatments aimed at modifying chemical structure. Recent studies show that antioxidant capacity can be incremented by enzymatic hydrolysis [8–11], chemical methods such as acetylation, deamination, succinylation, and reductive alkylation, and creating covalent cross-links (polymerization) between food biopolymers and carbohydrates [12, 13]. In particular, special attention has been provided to the effect exerted by reducing sugars on the structure and protein via Maillard reaction (MR).

Additionally, polymerization or glycation has also a significant impact on protein functionality as gelling, heat stability, emulsifying, and foaming capability. Thus these compounds can exhibit improvement in the antioxidant capacity and functionality when they are added in emulsions [14, 15]. MR products can also increment the properties of the food such as appearance, flavor, and texture during their processing and storage [16–18]. Furthermore, they also may significantly improve the other biological competences as antimicrobial ability and antihypertensive properties [19–21]. However, despite these benefits, the glycation by MR may negatively affect the purpose of modification of whey proteins. Products of MR can act as prooxidants, depending on the states or progress of the reaction. The thermal and pH

conditions, nature, and concentration of proteins and sugars contribute to this drastic and contrary effect.

Sugar fragmentation and degradation of amino acids (Strecker degradation) occurring in advanced stages of the reaction may aggravate antioxidant action. In addition, polymerized compounds which in turn produce irreversible or intermediates reactions and the interaction between them, may also affect the antioxidant activity of the products of glycation. Besides training of melanoidins characterized, many of them with typical aroma and flavor [22] are found as product of MR in advanced stages. Therefore, the manipulation of whey proteins properties is an important topic in food industries and more studies are necessary to determine the potential glycation and their influence on their functionality as food additive. Due to the complexity of MR, it is necessary to deepen the study of parameters to these reactions and type of carbohydrate utilized in the glycation.

The aim of this work was to evaluate the antioxidant activity and functional properties of products obtained by combination of enzymatic hydrolysis and glycation process of proteins concentrates from milk bovine whey. Hydrolyzates were obtained by contact with *Bacillus subtilis*. Nature of the sugar on functionality of products was analyzed by individual experiments with ribose and glucose under controlled conditions of carbohydrate concentration, temperature, and pH.

2. Materials and Methods

2.1. Materials. Samples of 2 L of acid and sweet bovine whey milk were provided by a cheese industry localized in Mexico. The 2,2′azino-bis(3-ethylbenzothiazoline-6-sulfonic acid) (ABTS) and reducing sugars, glucose, ribose, and arabinose were purchased from Sigma Aldrich. Other chemicals agents used were of analytical grade.

2.2. Preparation of Whey Protein Concentrates. Samples of whey of 1 L were filtered to remove fat and casein particles by vacuum filtration using Whatman filter paper number 40.

Then, whey was concentrated by ultrafiltration process (UF) to obtain whey proteins concentrates (WPC). In this case was used cross-flow zirconium-titanium ceramic membrane of 15 kDa cut-off and polymeric membrane (hollow fiber) of 6 kDa cut-off (Pall). Tubular housing of tangential flow of membrane was adapted to a peristaltic pump. The transmembrane pressures were adjusted and controlled to 3.0 and 0.3 bar in ceramic and polymeric membrane, respectively. Whey feeding was performed at 25°C to both concentration processes. In each UF experiment, two streams were obtained: the retentate (WPC) and permeate (lactose and minerals, mainly).

Diafiltration was performed by addition of five volumes of deionized water to the retentate to maintain a constant volume during UF process [23].

UF was stopped after approximately 18 h of filtration. Proteins in whey and WPC were determined by Biuret method. The percent yield (Y) of WPC was calculated using

$$\%Y = \frac{V_2 C_2}{V_1 C_1} (100), \quad (1)$$

where C_2 is protein concentration in the retentate after UF; C_1 is protein concentration in the whey sample; V_1 is initial volume of whey sample; and V_2 is final volume in the retentate after UF.

To perform the next experiments, WPC products were chosen according to the highest proteins concentration.

2.3. Preparation of Hydrolyzed Products from Whey Protein Concentrates. Hydrolyzed products WPCH were obtained by direct contact of substrates WPC with suspended biomass of *Bacillus subtilis* in relation 1 : 1. WPC samples were previously adjusted to pH 7. *B. subtilis* was previously maintained in the laboratory on nutrient broth agar slants (5 g/L beef extract, 10 g/L peptone, 5 g/L sodium chloride, 18 g/L agar, and pH 7–7.4) and stored at 4°C [23].

The hydrolysis was performed in a shaking bath (Shel-Lab) at 100 rpm and 50°C. In this experiment, WPC was used as control group; the sample was treated under the same experimental conditions.

Upon completion of the hydrolysis experiment (24 h), the *B. subtilis* was inactivated at a temperature of 70°C in a water bath for 3 min, then the tubes were centrifuged for 15 minutes at 5000 rpm, and the supernatant was diluted with dilution factor of 100, to determine the protein concentration by Biuret method [23]. Degree of hydrolysis (%DH) of WPC was determined by measuring the proteins concentration every 2 hours during 12 h of uninterrupted hydrolysis and was calculated by [23]

$$\%\mathrm{DH} = \frac{C_o - C_f}{C_f} (100), \quad (2)$$

where C_o is the initial protein concentration in WPC and C_f is the protein concentration in supernatant hydrolyzed product for hydrolysis time.

2.4. Preparation of Polymerized Products from Whey by Glycation Process. Polymerized products from whey by glycation process were obtained by the coupling of the samples WPC and WPCH with a carbohydrate (ribose and glucose), according to a method previously developed [24].

Carbohydrate solution was previously prepared by buffer dissolution pH 7 of sodium citrate and buffer dissolution pH 9 of sodium carbonate, each one with 0.2 g of carbohydrate.

Samples of WPC and WPCH were placed in direct contact with carbohydrate (1 : 4 v/v) at pH 7 and pH 9, in individual experiments. The mixtures were stirred at room temperature for 1 h to form uniform dispersion. Afterwards, the mixtures were then incubated at 50°C during 20 h.

For the period of glycation process, each mixture was sampled in intervals of time of 5 h to 20 h. Products were characterized by color change, antioxidant activity, and functional properties.

Sweet and acid whey were used as control group; the samples were only heated under the same experimental conditions.

Glycated products were identified as W, WPC-R, WPC-G, and WPCH-R, WPCH-G for whey, whey concentrates, and

hydrolyzed product with ribose and glucose in different times of hydrolysis and glycation processes, respectively.

2.5. Determination of the Properties of Whey Products

2.5.1. Antioxidant Activity. The antioxidant activity of whey products was assessed by scavenging of the ABTS radical [25].

ABTS•+ radical was previously prepared as follows: 0.0336 g of ammonium persulfate and 0.0194 g of ABTS were diluted in 30 mL of distilled water. This solution was incubated during 16 h at 25°C in the dark. After this time, 40 mL of ABTS•+ solution was dissolved in 960 mL of absolute ethanol, reaching an absorbance of 0.7 ± 0.2 to 754 nm.

A calibration curve using ascorbic acid 0.002019 M was built as standard substance. Solutions from 0 to 0.8 mM ascorbic acid were prepared in this stage.

Aliquots of 20 μL of these solutions were added to 980 μL of ABTS solution (absorbance of 0.7 ± 0.2 to 754 nm). Each mixture was incubated in the dark for 7 min, and the absorbance at 754 nm was measured for all samples.

The ABTS radical scavenging activity (%AA) was calculated as inhibition percentage according to

$$\%\mathrm{AA} = \frac{A_c - A_s}{A_c}(100), \tag{3}$$

where A_c is the absorbance of the control (ABTS solution without samples) and A_s is the absorbance of the samples of ascorbic acid.

Antioxidant activity of whey products was analyzed in a similar manner. Briefly, 20 μL of each product was mixed with 980 μL of the diluted ABTS, the mixture was incubated in the dark for 7 min, and the absorbance at 734 nm was also measured.

The change in absorbance with the percent inhibition of the radical ABTS•+ was calculated for each sample. The data were reported as antioxidant activity equivalent to ascorbic acid (AAEAA) and %AA [23].

2.5.2. Functional Properties. The functional properties of whey products were analyzed by measuring their solubility at pH 4.5 and 6.8, emulsions, and foaming capacities.

Solubility was calculated as the total protein concentration in the supernatant of products after centrifugation at pH 4.6 as a percentage of the initial concentration at pH 6.8 [26].

Whey products (25 ± 5 mg) were dispersed in 10 mL of deionized water and the pH was adjusted with HCl (1 N) or NaOH (1 N) when necessary. The dispersion was mixed for 30 min and centrifuged continuously (xg × 2056) for 10 min (Hettich Zentrifugen 32 R). The amount of protein in the supernatant was determined by the Biuret method; the solubility was expressed as the percentage of protein in the supernatant, the total in the initial products.

Emulsification capacity of whey products and their stability were analyzed using the method developed by Pearce and Kinsella [27]. In this case, 1.5 mL of corn oil was added to 22.5 mg whey products previously dissolved in 4.5 mL 0.01 M phosphate buffer, pH 7. The mixture was homogenized at 20,000 rpm at room temperature during 1 min.

The stability of products was determined in qualitative form when a breakdown of the emulsion was observed; the volume of added oil was registered and used to calculate the percent %CEM by

$$\%\mathrm{CEM} = \frac{V}{V_1}(100), \tag{4}$$

where V is mL of oil and V_1 is mL of whey products.

Regarding foaming capacity (FC) of products, it was determined at pH 7, adjusting the samples with NaOH (0.1 N) at 20°C.

For the test, 1 mL of sample was mixed with 72 mL of distilled water with stirring for 3 min using a high-speed stirrer of 2000 rpm. FC was determined by volume of sample achieved after this time, using

$$\mathrm{CE} = \frac{V_f - V_i}{V_i}(100), \tag{5}$$

where V_f and V_i are the final and the initial volumes of sample, respectively.

The color change of whey products obtained by MR during glycation was also determined. Spectra of 200 to 700 nm using a Perkin Elmer spectrophotometer Lambda 35 were obtained for each sample. The results were shown as identification of redness and yellowness color in the products. Sample whey was used as standard to obtain the spectra.

2.6. Statistical Analysis. Statistica 7.0 software (Statsoft Inc., Tulsa, OK, USA) was utilized to analyze the data obtained from whey characteristics, antioxidant activity, and functional properties on glycation products in experiments with three replicates. Results were compared using ANOVA and Tukey post hoc test ($P < 0.05$).

3. Results and Discussion

3.1. Products from Whey Proteins Concentrates. The sweet and acid whey samples showed pH of 6.5 and 4.5, respectively, values representing the difference between both whey types, which depends on the technological process used to manufacture the cheese.

The average content (7.89 ± 0.1 and 8.73 ± 0.1 g/L) indicated that both whey types did not have significant difference in protein content and the values obtained were within those reported by Tovar Jiménez et al. [23] (6–13 g/L). Difference in whey features may be attributed to the milk used and the cheese elaboration.

Concerning UF processes of whey, it was found that performing the UF with polymeric membrane was possible to achieve an excellent yield in the protein concentration among 96–98% for sweet and acid whey. The products from UF were identified as WPC-1 (from sweet whey and retentate from polymeric membrane); WPC-2 (from acid whey and retentate from polymeric membrane); WPC-3 (from sweet whey and retentate from ceramic membrane); WPC-4 (from acid whey and retentate from ceramic membrane).

Table 1 shows protein composition of WPC products obtained by UF processes with ceramic membrane of 15 kDa

Table 1: Protein concentration (g/L) in crude whey and WPC products by UF processes.

Membrane		Ceramic	Polymeric
Sample type	Whey	WPC	WPC
Acid	8.73 ± 0.5	5.35 ± 0.4	8.55 ± 0.3
Sweet	7.89 ± 0.3	4.58 ± 0.5	7.41 ± 0.3

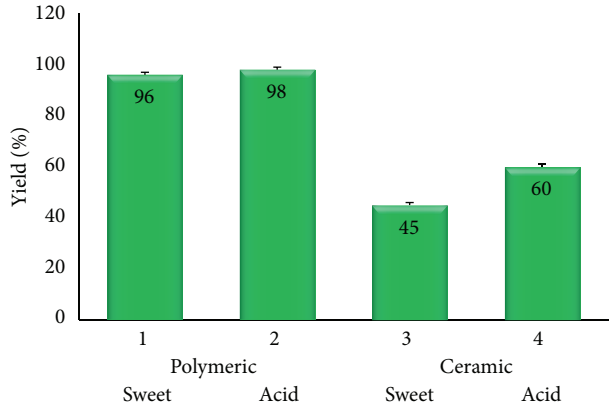

Figure 1: Percentage of yield in WPC by UF processes of sweet and acid whey with polymeric and ceramic membrane.

and polymeric membrane of 3 kDa, while Figure 1 shows the final percent yield (Y) of each WPC. Difference between the yields in the UF is due to cut-off of membranes. Therefore, it is possible that the proteins of great molecular weight as albumin, Immunoglobulins, and lactoferrin are found intact in the WPC from ceramic membrane, but fewer amounts of β-lactoglobulin and α-lactalbumin are present in the retentates from 15 kDa membrane, since another amount of these proteins is found in their permeate streams.

Under yield result in UF process, in this stage were chosen the products WPC-1 and WPC-2 (retentates from polymeric membrane) to continue with their hydrolysis.

3.2. Hydrolyzed Products from Whey Protein Concentrates. Degree of hydrolysis (%DH) achieved during 24 h was 45–60% from WPC-1 and WPC-2, respectively. Data of hydrolysis process are showed in Figure 2. This test indicated that during 12 h the changes were observed as more representative in the two types of whey due to enzymatic action from *B. subtilis*. After this period, the %DH increased very slowly.

Differences of enzymatic action from *B. subtilis* have been reported in other researches; however other substrates and enzymatic extracts or purified enzymes from *B. subtilis* have been used in these experiments. For example, maximum values around 70% of hydrolysis were found on rapeseed meal with enzymatic extract [28] and similar percentage with commercial proteases such as Alcalase on soybean and Subtilisin on whey proteins can be seen in [29, 30]. Particularly, in [30], it was found that 26% DH of whey proteins is obtained after two hours of direct contact with Subtilisin to achieve 70% in 10 h, which could be compared with %DH obtained in this work.

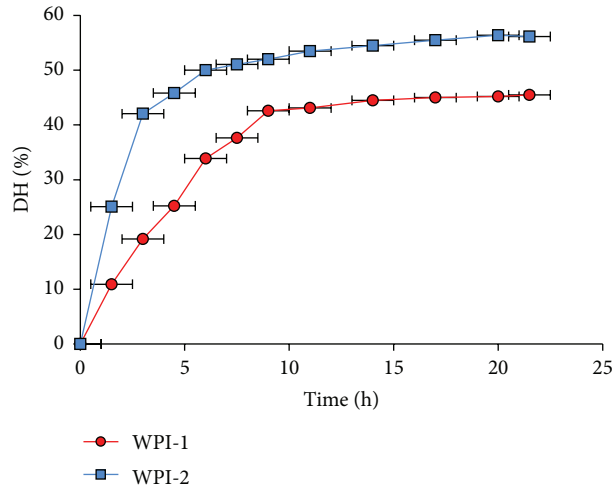

Figure 2: %DH from WPC-1 and WPC-2 with biomass from *B. subtilis*.

3.3. Polymerized Products from Whey Proteins by Glycation Process. Hundred eighty coded polymerized products were obtained during 20 h. Data are reported by conforming sweet or acid whey produced by only heating (W-1 and W-2); glycation of WPC from each whey type and ribose and galactose (WPC-1, WPC-2, WPC-1-R, WPC-1-G, WPC-2-R, and WPC-2-G); and glycation of hydrolyzed products obtained with 25, 35, and 45% DH of WPC of sweet whey hydrolysis and 25, 45, and 60% DH of WPC of acid whey, during 4, 8, and 12 h, respectively (WPCH-1-25-R, WPCH-1-35-R, WPCH-1-45-R, WPCH-2-25-R, WPCH-2-45-R, and WPCH-2-60-R), for pH 7 and pH 9 and of the same form to glucose.

Tables 2 to 6 show a summary of the main results on features of some glycosylated product from sweet and acid whey with ribose and glucose. In particular, products with higher antioxidant activity are shown in Figure 3.

Principally, data of Table 2 correspond to glycosylated products from sweet and acid whey by heating of samples. AAEAA values indicated that a significant enhancement (0.55 to 0.75) was observed in the products by only acid and sweet whey heating for 15–20 h at pH 7. However no enhancement was observed in samples at pH 9.

In relation to WPC products, a higher AAEAA value was obtained in WPC-R conjugates (0.56 to 1.02) at pH 7 with heating time, while the increment of AAEAA in WPC-G conjugates was less (0.56 to 0.78) at pH 7 and pH 9. Data can be observed in Tables 3 and 4.

Information from WPCH conjugate products corresponding to glycosylated WPC with ribose previously hydrolyzed with biomass from *B. subtilis* is shown in Tables 5 and 6. AAEAA values of these products indicate that hydrolyzed WPCH can increment their AAEAA value by polymerization with carbohydrates. In general, WPCH conjugates exhibited adequate potency to react with free radicals. %DH was sufficient to liberate reactive peptides and produce polymerized products with high AAEAAA values in all experiments. Particularly, products with 25% DH from WPC-acid whey-ribose at pH 7 achieved 1.55–1.85 of AAEAA and

Table 2: Features of glycosylated product from sweet and acid whey with heating to 50°C, pH 7 and pH 9.

Sample	Glycosylation time (h)	Product	Antioxidant activity		Functional properties		
			%AA	AAEAA (mM/L)	%Solubility	%Emulsion	%Foam
Sweet whey at pH 7	0	W7-1	25.10 ± 0.2	0.55	80 ± 0.2	20 ± 0.1	1.3 ± 0.2
	5	W7-1-30	29.05 ± 0.2	0.57	78 ± 0.2	22 ± 0.1	1.3 ± 0.2
	10	W7-1-60	32.43 ± 0.1	0.68	78 ± 0.2	21 ± 0.1	1.3 ± 0.1
	15	W7-1-120	34.67 ± 0.2	0.70	75 ± 0.2	22 ± 0.1	1.2 ± 0.2
	20	W7-1-180	35.31 ± 0.2	0.75	75 ± 0.2	20 ± 0.1	1.1 ± 0.1
Sweet whey at pH 9	0	W9-1	19.65 ± 0.5	0.41	75 ± 0.2	20 ± 0.1	1.0 ± 0.1
	5	W9-1-30	20.33 ± 0.2	0.42	71 ± 0.2	19 ± 0.2	1.1 ± 0.1
	10	W9-1-60	20.99 ± 0.3	0.42	74 ± 0.2	20 ± 0.2	1.1 ± 0.1
	15	W9-1-120	21.85 ± 0.3	0.43	75 ± 0.2	19 ± 0.2	1.1 ± 0.2
	20	W9-1-180	22.59 ± 0.3	0.45	75 ± 0.2	19 ± 0.1	1.2 ± 0.1
Acid whey at pH 7	0	W7-2	42.21 ± 0.4	0.62	70 ± 0.1	17 ± 0.1	0.8 ± 0.1
	5	W7-2-30	44.76 ± 0.5	0.65	68 ± 0.2	17 ± 0.1	0.7 ± 0.1
	10	W7-2-60	48.32 ± 0.5	0.73	65 ± 0.1	15 ± 0.1	0.5 ± 0.1
	15	W7-2-120	49.05 ± 0.5	0.75	65 ± 0.1	14 ± 0.2	0.5 ± 0.2
	20	W7-2-180	49.88 ± 0.3	0.76	60 ± 0.1	13 ± 0.1	0.5 ± 0.2
Acid whey at pH 9	0	W9-2	21.22 ± 0.1	0.42	70 ± 0.1	15 ± 0.1	0.8 ± 0.2
	5	W9-2-30	22.54 ± 0.1	0.43	72 ± 0.1	17 ± 0.1	0.8 ± 0.1
	10	W9-2-60	22.78 ± 0.2	0.43	78 ± 0.2	18 ± 0.2	0.8 ± 0.1
	15	W9-2-120	23.94 ± 0.2	0.44	78 ± 0.2	18 ± 0.2	0.9 ± 0.1
	20	W9-2-180	24.05 ± 0.2	0.44	75 ± 0.2	17 ± 0.1	0.8 ± 0.1

Table 3: Features of glycosylated product from WPC of sweet and acid whey with ribose, heating to 50°C, pH 7 and pH 9.

Sample	Glycosylation time (h)	Product	Antioxidant activity		Functional properties		
			%AA	AAEAA (mM/L)	%Solubility	%Emulsion	%Foam
WPC sweet whey with ribose at pH 7	0	WPC7-1-R	51 ± 0.6	0.56	90 ± 0.2	80 ± 0.2	25 ± 0.2
	5	WPC7-1-30-R	53 ± 0.5	0.58	88 ± 0.2	80 ± 0.2	25 ± 0.2
	10	WPC7-1-60-R	55 ± 0.5	0.65	88 ± 0.2	78 ± 0.1	26 ± 0.2
	15	WPC7-1-120-R	60 ± 0.2	0.70	85 ± 0.1	78 ± 0.1	26 ± 0.2
	20	WPC7-1-180-R	77 ± 0.2	0.75	85 ± 0.1	75 ± 0.1	27 ± 0.2
WPC sweet whey with ribose at pH 9	0	WPC9-1-R	40 ± 0.3	0.50	85 ± 0.2	80 ± 0.2	26 ± 0.1
	5	WPC9-1-30-R	41 ± 0.5	0.54	80 ± 0.2	78 ± 0.3	25 ± 0.1
	10	WPC9-1-60-R	45 ± 0.5	0.58	75 ± 0.2	75 ± 0.2	23 ± 0.1
	15	WPC9-1-120-R	54 ± 0.5	0.65	78 ± 0.2	78 ± 0.1	25 ± 0.2
	20	WPC9-1-180-R	60 ± 0.5	0.76	78 ± 0.2	79 ± 0.1	26 ± 0.1
WPC acid whey with ribose at pH 7	0	WPC7-2-R	55 ± 0.5	0.56	89 ± 0.2	82 ± 0.1	30 ± 0.1
	5	WPC7-2-30-R	59 ± 0.5	0.62	88 ± 0.1	80 ± 0.2	30 ± 0.2
	10	WPC7-2-60-R	70 ± 0.3	0.70	85 ± 0.1	78 ± 0.3	27 ± 0.2
	15	WPC7-2-120-R	80 ± 0.5	1.02	85 ± 0.1	80 ± 0.1	25 ± 0.3
	20	WPC7-2-180-R	77 ± 0.5	0.92	83 ± 0.1	78 ± 0.1	23 ± 0.3
WPC acid whey with ribose at pH 9	0	WPC9-2-R	40 ± 0.1	0.50	75 ± 0.1	65 ± 0.1	19 ± 0.2
	5	WPC9-2-30-R	45 ± 0.5	0.53	78 ± 0.1	70 ± 0.3	20 ± 0.3
	10	WPC9-2-60-R	45 ± 0.5	0.55	79 ± 0.1	70 ± 0.1	20 ± 0.2
	15	WPC9-2-120-R	48 ± 0.1	0.55	80 ± 0.2	70 ± 0.1	22 ± 0.3
	20	WPC9-2-180-R	46 ± 0.3	0.50	75 ± 0.2	65 ± 0.1	20 ± 0.3

Table 4: Features of glycosylated product from WPC of sweet whey with glucose and heating to 50°C, pH 7 and pH 9.

Sample	Glycosylation time (h)	Product	Antioxidant activity		Functional properties		
			%AA	AAEAA (mM/L)	%Solubility	%Emulsion	%Foam
WPC sweet whey with glucose at pH 7	0	WPC7-1-G	50 ± 0.5	0.30	70 ± 0.1	62 ± 0.1	25 ± 0.1
	5	WPC7-1-30-G	58 ± 0.6	0.42	75 ± 0.1	66 ± 0.2	28 ± 0.1
	10	WPC7-1-60-G	59 ± 0.5	0.42	75 ± 0.1	65 ± 0.2	30 ± 0.1
	15	WPC7-1-120-G	60 ± 0.7	0.52	77 ± 0.2	65 ± 0.1	30 ± 0.2
	20	WPC7-1-180-G	62 ± 0.5	0.55	75 ± 0.3	61 ± 0.1	25 ± 0.1
WPC sweet whey with glucose at pH 9	0	WPC9-1-G	39 ± 0.5	0.20	71 ± 0.2	60 ± 0.1	20 ± 0.3
	5	WPC9-1-30-G	40 ± 0.3	0.19	70 ± 0.2	62 ± 0.2	22 ± 0.3
	10	WPC9-1-60-G	45 ± 0.5	0.23	70 ± 0.1	65 ± 0.2	22 ± 0.1
	15	WPC9-1-120-G	46 ± 0.5	0.20	75 ± 0.2	66 ± 0.3	25 ± 0.1
	20	WPC9-1-180-G	46 ± 0.5	0.28	78 ± 0.2	67 ± 0.1	25 ± 0.2
WPC acid whey with glucose at pH 7	0	WPC7-2-G	49 ± 0.5	0.30	80 ± 0.1	66 ± 0.1	30 ± 0.2
	5	WPC7-2-30-G	50 ± 0.6	0.30	85 ± 0.1	69 ± 0.1	32 ± 0.2
	10	WPC7-2-60-G	52 ± 0.6	0.30	86 ± 0.1	69 ± 0.1	35 ± 0.1
	15	WPC7-2-120-G	55 ± 0.3	0.35	86 ± 0.1	70 ± 0.1	36 ± 0.1
	20	WPC7-2-180-G	55 ± 0.3	0.33	81 ± 0.2	71 ± 0.1	33 ± 0.1
WPC acid whey with glucose at pH 9	0	WPC9-2-G	55 ± 0.3	0.56	76 ± 0.1	65 ± 0.2	28 ± 0.1
	5	WPC9-2-30-G	58 ± 0.3	0.68	78 ± 0.1	65 ± 0.1	25 ± 0.1
	10	WPC9-2-60-G	69 ± 0.3	0.68	80 ± 0.2	69 ± 0.3	28 ± 0.2
	15	WPC9-2-120-R	78 ± 0.3	0.78	75 ± 0.2	65 ± 0.3	25 ± 0.1
	20	WPC9-2-180-R	75 ± 0.3	0.75	73 ± 0.2	65 ± 0.1	20 ± 0.1

products with 45% DH at pH 9 achieved only 1.1 of AAEAA whereas conjugate products by glycation of hydrolyzed with glucose showed always a lower increase in AAEAA.

In terms of reactants nature, it is understandable that WCPH products were more reactive than WPC; this is due to presence of free amino acids. However, it was found that major contributors to the radical scavenging capacity were primarily composed of WCPH although other authors noted that either the intermediates or the final brown polymer can function as hydrogen donors and that sugar caramelization can also contribute to the antiradical activity [31].

The most reactive peptides are the $-NH_2$ groups of lysine as well as the group $-NH_2$ located at the amino terminus. Therefore, a higher content of residues lysine could lead to a higher degree of protein glycation. The imidazole group of histidine, the indole group of tryptophan, and the guanidino group of arginine residues are also likely to react with reducing sugars, but this possibility is lesser than amino groups [32].

On the other hand, different coloration in conjugates products was also observed during the heating period for each carbohydrate. However, comparative experiments showed that glycosylated products with glucose developed an intense yellow color and characteristic odor, after 15 h of heating, decreasing at pH 9, whereas glycosylated products with ribose acquired a faint brownish yellow in similar period.

Thus, it is possible that ribose present as more reactive than the glucose during the different stages of MR, joining

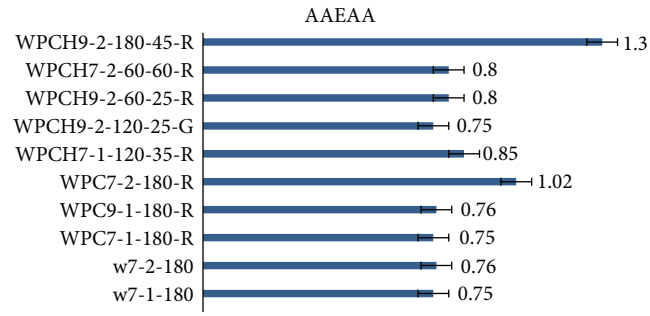

Figure 3: AAEAA of representative glycosylated products from whey milk in individual experiments with ribose and glucose at 50°C and variations of pH 7 and pH 9.

the products substantially to ribose molecules; this reactive property could be associated with antioxidant power of whey products.

Recent researches have shown that the antioxidant properties of the proteins are enhanced by their conjugation particularly with glucose. Conjugate products from ovalbumin-saccharides [33], whey protein isolate (WPI) [34], and specific conjugates α-lactalbumin-glucose [35] showed an increment in their antioxidant activity when the proteins were polymerized with glucose more greatly. These results were highly consistent with the browning intensity of products. Authors found that particularly WPI-conjugates with glucose after 7 days of dry heating at 60°C showed an increase in

Table 5: Features of glycosylated product from hydrolyzates from WPC of sweet whey with ribose heating to 50°C, pH 7 and pH 9.

Sample	Glycosylation time (h)	Product	Antioxidant activity		Functional properties		
			%AA	AAEAA (mM/L)	%Solubility	%Emulsion	%Foam
Hydrolyzate (25% HD) from WPC of sweet whey with ribose at pH 7	0	WPCH7-1-25-R	60 ± 0.7	0.54	90 ± 0.1	80 ± 0.1	10 ± 0.1
	5	WPCH7-1-30-25-R	65 ± 0.5	0.55	90 ± 0.1	78 ± 0.1	15 ± 0.1
	10	WPCH7-1-60-25-R	68 ± 0.7	0.55	90 ± 0.2	75 ± 0.1	15 ± 0.1
	15	WPCH7-1-120-25-R	70 ± 0.8	0.58	89 ± 0.2	75 ± 0.2	15 ± 0.2
	20	WPCH7-1-180-25-R	65 ± 0.6	0.49	85 ± 0.1	70 ± 0.2	10 ± 0.2
Hydrolyzate (35% HD) from WPC of sweet whey with ribose at pH 7	0	WPCH7-1-35-R	75 ± 0.5	0.68	90 ± 0.1	79 ± 0.1	20 ± 0.1
	5	WPCH7-1-30-35-R	75 ± 0.6	0.70	90 ± 0.1	80 ± 0.1	22 ± 0.1
	10	WPCH7-1-60-35-R	89 ± 0.8	1.85	85 ± 0.2	78 ± 0.2	25 ± 0.1
	15	WPCH7-1-120-35-R	85 ± 0.5	0.95	85 ± 0.3	75 ± 0.2	20 ± 0.1
	20	WPCH7-1-180-35-R	75 ± 0.8	0.71	82 ± 0.1	70 ± 0.1	20 ± 0.2
Hydrolyzate (45% HD) from WPC of sweet whey with ribose at pH7	0	WPCH7-1-45-R	64 ± 0.5	0.59	89 ± 0.1	76 ± 0.2	22 ± 0.2
	5	WPCH7-1-30-45-R	65 ± 0.5	0.55	85 ± 0.2	77 ± 0.2	20 ± 0.2
	10	WPCH7-1-60-45-R	63 ± 0.7	0.50	80 ± 0.1	75 ± 0.1	15 ± 0.1
	15	WPCH7-1-120-45-R	50 ± 0.8	0.45	78 ± 0.1	70 ± 0.2	15 ± 0.3
	20	WPCH7-1-180-45-R	40 ± 0.5	0.30	75 ± 0.1	66 ± 0.1	15 ± 0.3
Hydrolyzate (25% HD) from WPC of sweet whey with ribose at pH 9	0	WPCH9-1-25-R	49 ± 0.4	0.28	80 ± 0.1	69 ± 0.1	22 ± 0.1
	5	WPCH9-1-30-25-R	50 ± 0.8	0.30	85 ± 0.1	75 ± 0.1	25 ± 0.1
	10	WPCH9-1-60-25-R	52 ± 0.6	0.35	88 ± 0.2	79 ± 0.2	25 ± 0.3
	15	WPCH9-1-120-25-R	53 ± 0.8	0.35	90 ± 0.2	80 ± 0.2	29 ± 0.1
	20	WPCH9-1-180-25-R	55 ± 0.3	0.4	90 ± 0.2	85 ± 0.1	30 ± 0.1
Hydrolyzate (35% HD) from WPC of sweet whey with ribose at pH 9	0	WPCH9-1-35-R	50 ± 0.5	0.55	90 ± 0.1	88 ± 0.1	33 ± 0.1
	5	WPCH9-1-30-35-R	56 ± 0.5	0.60	87 ± 0.1	89 ± 0.1	30 ± 0.2
	10	WPCH9-1-60-35-R	58 ± 0.8	0.6	88 ± 0.2	78 ± 0.2	29 ± 0.2
	15	WPCH9-1-120-35-R	55 ± 0.7	0.53	85 ± 0.2	75 ± 0.2	25 ± 0.2
	20	WPCH9-1-180-35-R	50 ± 0.5	0.45	88 ± 0.1	80 ± 0.1	28 ± 0.2
Hydrolyzate (45% HD) from WPC of sweet whey with ribose at pH 9	0	WPCH9-1-45-R	50 ± 0.5	0.43	89 ± 0.1	78 ± 0.1	28 ± 0.1
	5	WPCH9-1-30-45-R	48 ± 0.8	0.35	85 ± 0.1	75 ± 0.1	25 ± 0.1
	10	WPCH9-1-60-45-R	45 ± 0.8	0.30	80 ± 0.2	73 ± 0.1	20 ± 0.2
	15	WPCH9-1-120-45-R	44 ± 0.5	0.25	80 ± 0.1	73 ± 0.1	18 ± 0.2
	20	WPCH9-1-180-45-R	40 ± 0.5	0.20	75 ± 0.1	70 ± 0.2	15 ± 0.2

antioxidant activity and an increase in the color. It was seen in UV-vis absorption and fluorescence intensity. Additionally comparative data on WPI alone indicated that the conjugates exhibited a better thermal stability.

Similar results were found in the present research; however here it is shown that conjugates-ribose enhances antioxidant action than glucose. Difference of antioxidant action can also be associated with the presence of complex mix of compounds developed during glycation of whey products. Glucose could play an important role in the reduction of antioxidant activity. Particularly hydroxyl groups could inhibit this power [36, 37].

Carbohydrate type and pH could explain these results. However, reactivity of carbohydrate in glycation process has not been described still in clear form. According to [37], it has been shown that reactivity decreases with the molecular weight of carbohydrate, which would explain that cross-linking and aggregation protein with ribose is incremented in comparison with the glucose and this behavior could be associated with the increment of antioxidant activity of conjugate whey products-ribose. Reactivity of different sugars is also given by the availability of its carbonyl group; for example, glucose presents at least two closed forms (cyclic anomers) in which the carbonyl group has disappeared. Thus a correlation between the reaction rate of glycation and the proportion of the open form of each sugar is also found in these data.

Influence of pH in MR reaction during glycation process may furthermore be observed on antioxidant action of whey products; at basic pH, generally, the polymerization rate increases. However the results cannot be described thus radically.

In an early stage, MR generates Amadori products (glycosylamines N-substituted by sugar-amine condensation) which are present due to reactions between amine groups of proteins and carbonyl groups within the reducing sugar, while intermediate stage and advanced stage are characterized by formation of reactive intermediates such as sugar-derived dicarbonyl compounds as 1-amino-2-deoxy-2-ketoses (e.g., methylglyoxal, 3-deoxyosones, or glyoxal)

Table 6: Features of glycosylated product from hydrolyzates from WPC of acid whey with ribose, heating to 50°C, pH 7 and pH 9.

Sample	Glycosylation time (h)	Product	Antioxidant activity		Functional properties		
			%AA	AAEAA (mM/L)	%Solubility	%Emulsion	%Foam
Hydrolyzate (25% HD) from WPC of acid whey with ribose at pH 7	0	WPCH7-2-25-R	60 ± 0.5	0.60	88 ± 0.3	80 ± 0.1	30 ± 0.2
	5	WPCH7-2-30-25-R	65 ± 0.6	0.58	90 ± 0.2	80 ± 0.2	35 ± 0.2
	10	WPCH7-2-60-25-R	68 ± 0.5	0.60	90 ± 0.1	80 ± 0.2	37 ± 0.2
	15	WPC7-2-120-25-R	67 ± 0.5	0.63	85 ± 0.1	78 ± 0.2	35 ± 0.2
	20	WPC7-2-180-25-R	65 ± 0.5	0.62	85 ± 0.1	79 ± 0.2	32 ± 0.2
Hydrolyzate (45% HD) from WPC of acid whey with ribose at pH 7	0	WPCH7-2-45-R	70 ± 0.5	0.61	90 ± 0.1	77 ± 0.2	30 ± 0.2
	5	WPCH7-2-30-45-R	80 ± 0.4	0.75	85 ± 0.3	75 ± 0.1	28 ± 0.3
	10	WPCH7-2-60-45-R	86 ± 0.6	0.85	85 ± 0.2	77 ± 0.1	30 ± 0.2
	15	WPCH7-2-120-45-R	87 ± 0.5	1.55	84 ± 0.3	75 ± 0.1	25 ± 0.2
	20	WPCH7-2-180-45-R	85 ± 0.6	0.90	87 ± 0.2	73 ± 0.1	25 ± 0.2
Hydrolyzate (60% HD) from WPC of acid whey with ribose at pH 7	0	WPCH7-2-60-R	83 ± 0.5	0.78	90 ± 0.2	75 ± 0.2	30 ± 0.2
	5	WPCH7-2-30-60-R	85 ± 0.6	0.80	90 ± 0.1	77 ± 0.2	30 ± 0.1
	10	WPCH7-2-60-60-R	88 ± 0.5	0.80	90 ± 0.2	80 ± 0.2	30 ± 0.1
	15	WPCH7-2-120-60-R	80 ± 0.4	0.75	85 ± 0.2	78 ± 0.1	25 ± 0.2
	20	WPCH7-2-180-60-R	80 ± 0.7	0.70	80 ± 0.1	75 ± 0.1	20 ± 0.2
Hydrolyzate (25% HD) from WPC of acid whey with ribose at pH 9	0	WPCH9-2-25-R	85 ± 0.7	0.75	90 ± 0.2	79 ± 0.1	30 ± 0.1
	5	WPCH9-2-30-25-R	88 ± 0.5	0.80	90 ± 0.1	80 ± 0.1	30 ± 0.1
	10	WPCH9-2-60-25-R	90 ± 0.5	1.38	86 ± 0.2	78 ± 0.1	28 ± 0.2
	15	WPCH9-2-120-25-R	89 ± 0.5	0.78	85 ± 0.2	75 ± 0.1	25 ± 0.2
	20	WPCH9-2-180-25-R	85 ± 0.6	0.75	82 ± 0.1	73 ± 0.2	25 ± 0.2
Hydrolyzate (45% HD) from WPC of acid whey with ribose at pH 9	0	WPCH9-2-45-R	85 ± 0.5	0.70	90 ± 0.1	75 ± 0.1	30 ± 0.1
	5	WPCH9-2-30-45-R	88 ± 0.5	0.79	85 ± 0.2	80 ± 0.1	30 ± 0.1
	10	WPCH9-2-60-45-R	90 ± 0.4	0.80	83 ± 0.2	80 ± 0.3	30 ± 0.3
	15	WPCH9-2-120-45-R	91 ± 0.5	1.10	80 ± 0.1	80 ± 0.1	30 ± 0.3
	20	WPCH9-2-180-45-R	95 ± 0.3	1.30	78 ± 0.1	80 ± 0.2	25 ± 0.3
Hydrolyzate (60% HD) from WPC of acid whey with ribose at pH 9	0	WPCH9-2-60-R	80 ± 0.5	0.75	80 ± 0.2	75 ± 0.1	20 ± 0.2
	5	WPCH9-2-30-60-R	75 ± 0.5	0.73	75 ± 0.2	70 ± 0.2	20 ± 0.1
	10	WPCH9-2-60-60-R	76 ± 0.3	0.70	72 ± 0.2	70 ± 0.2	19 ± 0.1
	15	WPCH9-2-120-60-R	75 ± 0.4	0.67	70 ± 0.2	65 ± 0.1	17 ± 0.1
	20	WPCH9-2-180-60-R	70 ± 0.5	0.65	70 ± 0.2	65 ± 0.1	15 ± 0.1

which are produced with time, resulting in the formation of polymerized compounds that may be interfering substances affecting the antioxidant activity. In addition, alkaline and/or heat treatment of proteins may be associated with the production of several types of cross-linked amino acids such as dehydroalanine, lysinoalanine, and histidinoalanine, which may affect also antioxidant activity and the nutritional value of the treated whey proteins [37]. Dehydration of sugars occurs by two routes. Under acidic conditions are formed furfurals and at alkaline conditions are formed the reductone. The enolization of the C_2 and C_3 carbons and removal of the amino group in position 1 give rise to the formation of 2,3-dicarbonyl compounds (via 2,3-E), which causes further fragmentation of low molecular weight compounds as ketoaldehydes, reductone, and a-dicarbonyl compounds, while, at acidic pH, enolization of C_1 and C_2 carbon and removal of the amino group in position 1 and the carboxyl group at position 3 are favored, resulting in 1,2-dicarbonyl compounds (via 1,2-E), as glyoxal and methylglyoxal, 1-desoxiglucosulosa, and 3-desoxiglucosulosa, which may undergo further dehydration resulting in furfural, such as 5-(hydroxymethyl) furfural (HMF) [38].

Concerning functional properties of whey glycosylated products, in this work it is shown that conjugates from WPC and WPCH had an excellent solubility; however this value reduced notably in long heating products. Figure 4 shows functional properties of glycosylated products from whey milk in individual experiments with ribose and glucose at 50°C and variations of pH 7 and pH 9.

Emulsion property did not change with respect to value in whey, while foam property was incremented in some cases. In general, a high volume of foam was obtained in WCP and hydrolyzed with heating in 10 h at pH 7.

Under these data, the best products found in these tests were those from WPC-R and WPCH-R at pH 7 with heating for 10–15 h. Therefore, conjugates obtained could be excellent antioxidants and/or functional additives in formulated foods [39].

Current studies have shown that conjugates from sodium caseinate [40] and β-lactoglobulin [41] with galactose have the capacity to form and stabilize food emulsions. The best results were obtained in these experiments with glycated proteins at 50°C and pH 5 during 48 h (corresponding to the latest steps of MR). This behavior can be attributed to the

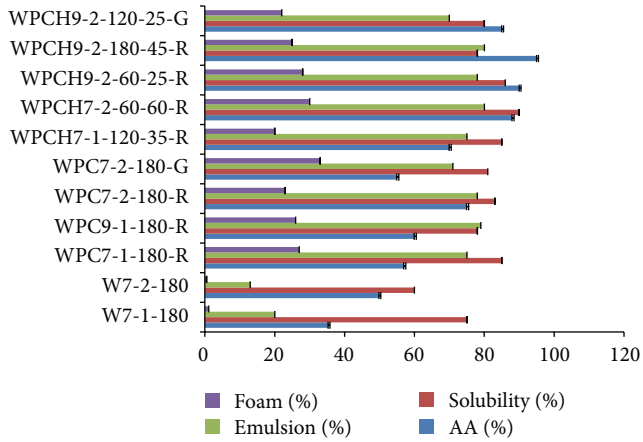

Figure 4: Functional properties of glycosylated products from whey milk in individual experiments with ribose and glucose at 50°C and variations of pH 7 and pH 9.

higher adsorption efficiency and degree of interfacial interaction exhibited by the glycoconjugates with this carbohydrate and the fact that alkaline pH reduces significantly the foam property.

4. Conclusions

The antioxidant activity and functional properties of sweet and acid whey products were incremented by polymerization of their proteins by glycation with heating and addition of glucose and ribose.

Glycation of whey protein concentrates (WPC) and the hydrolyzates (WPCH) with ribose and glucose showed different oxidation values.

The higher activity was found in WPC glycosylates products with ribose at pH 7 and heating at 50°C during 10–15 h. In the same way, antioxidant activity in WPCH was incremented by prior hydrolysis to glycation in products with 25–45% hydrolysis degree at pH 9. In these processes was found an important dependence on pH conditions and carbohydrate reactivity; therefore antioxidant activity was associated with carbohydrate type used in glycation of whey proteins.

Functional properties of these products (solubility, emulsion, and foam) were also maintained or improved by the glycation with ribose.

The color in glycosylates products with glucose was more intense than in products with ribose; however antioxidant activity was not associated with this change. Formation of hydroxyl groups could probably inhibit this action.

Other researchers are required to identify the structure of the compounds in the conjugates that could inhibit the capacities of conjugates with glucose. In addition, practical applications of these products are necessary to test their antioxidant capacity as additive in foods.

Conflict of Interests

The authors declare that there is no conflict of interests regarding the publication of this paper.

References

[1] J. Liu, Q. Ru, and Y. Ding, "Glycation a promising method for food protein modification: physicochemical properties and structure, a review," *Food Research International*, vol. 49, no. 1, pp. 170–183, 2012.

[2] C. Sun and S. Gunasekaran, "Effects of protein concentration and oil-phase volume fraction on the stability and rheology of menhaden oil-in-water emulsions stabilized by whey protein isolate with xanthan gum," *Food Hydrocolloids*, vol. 23, no. 1, pp. 165–174, 2009.

[3] L. M. Tong, S. Sasaki, D. J. McClements, and E. A. Decker, "Mechanisms of the antioxidant activity of a high molecular weight fraction of whey," *Journal of Agricultural and Food Chemistry*, vol. 48, no. 5, pp. 1473–1478, 2000.

[4] J. M. C. Gutteridge, S. K. Paterson, A. W. Segal, and B. Halliwell, "Inhibition of lipid peroxidation by the iron-binding protein lactoferrin," *Biochemical Journal*, vol. 199, no. 1, pp. 259–261, 1981.

[5] E. Meucci, A. Mordente, and G. E. Martorana, "Metal-catalyzed oxidation of human serum albumin: conformational and functional changes. Implications in protein aging," *The Journal of Biological Chemistry*, vol. 266, no. 8, pp. 4692–4699, 1991.

[6] A. Moure, H. Domínguez, and J. C. Parajó, "Antioxidant properties of ultrafiltration-recovered soy protein fractions from industrial effluents and their hydrolysates," *Process Biochemistry*, vol. 41, no. 2, pp. 447–456, 2006.

[7] I. Arcan and A. Yemenicioğlu, "Antioxidant activity of protein extracts from heat-treated or thermally processed chickpeas and white beans," *Food Chemistry*, vol. 103, no. 2, pp. 301–312, 2007.

[8] G.-N. Kim, H.-D. Jang, and C.-I. Kim, "Antioxidant capacity of caseinophosphopeptides prepared from sodium caseinate using Alcalase," *Food Chemistry*, vol. 104, no. 4, pp. 1359–1365, 2007.

[9] T. Bayram, M. Pekmez, N. Arda, and A. S. Yalçin, "Antioxidant activity of whey protein fractions isolated by gel exclusion chromatography and protease treatment," *Talanta*, vol. 75, no. 3, pp. 705–709, 2008.

[10] A. Dryáková, A. Pihlanto, P. Marnila, L. Čurda, and H. J. T. Korhonen, "Antioxidant properties of whey protein hydrolysates as measured by three methods," *European Food Research and Technology*, vol. 230, no. 6, pp. 865–874, 2010.

[11] C. Muro Urista, R. Álvarez Fernández, F. Riera Rodríguez, A. Arana Cuenca, and A. Téllez Jurado, "Review: production and functionality of active peptides from milk," *Food Science and Technology International*, vol. 17, no. 4, pp. 293–317, 2011.

[12] J. A. Gerrard, "Protein-protein crosslinking in food: methods, consequences, applications," *Trends in Food Science and Technology*, vol. 13, no. 12, pp. 391–399, 2002.

[13] N. Liu, T. Zhang, Y. J. Wang, Y. P. Huang, J. H. Ou, and P. Shen, "A heat inducible tyrosinase with distinct properties from *Bacillus thuringiensis*," *Letters in Applied Microbiology*, vol. 39, no. 5, pp. 407–412, 2004.

[14] G. Liu and Q. Zhong, "Thermal aggregation properties of whey protein glycated with various saccharides," *Food Hydrocolloids*, vol. 32, no. 1, pp. 87–96, 2013.

[15] S.-C. Liu, D.-J. Yang, S.-Y. Jin, C.-H. Hsu, and S.-L. Chen, "Kinetics of color development, pH decreasing, and antioxidative activity reduction of Maillard reaction in galactose/glycine model systems," *Food Chemistry*, vol. 108, no. 2, pp. 533–541, 2008.

[16] M. Murakami, H. Tonouchi, R. Takahashi et al., "Structural analysis of a new anti-hypertensive peptide (β-lactosin B) isolated from a commercial whey product," *Journal of Dairy Science*, vol. 87, no. 7, pp. 1967–1974, 2004.

[17] G. P. Rizzi, "Free radicals in the Maillard reaction," *Food Reviews International*, vol. 19, no. 4, pp. 375–395, 2003.

[18] M.-N. Maillard, C. Billaud, Y.-N. Chow, C. Ordonaud, and J. Nicolas, "Free radical scavenging, inhibition of polyphenoloxidase activity and copper chelating properties of model Maillard systems," *LWT—Food Science and Technology*, vol. 40, no. 8, pp. 1434–1444, 2007.

[19] F. J. Morales and M.-B. Babbel, "Antiradical efficiency of Maillard reaction mixtures in a hydrophilic media," *Journal of Agricultural and Food Chemistry*, vol. 50, no. 10, pp. 2788–2792, 2002.

[20] M. S. Rao, S. P. Chawla, R. Chander, and A. Sharma, "Antioxidant potential of Maillard reaction products formed by irradiation of chitosan—glucose solution," *Carbohydrate Polymers*, vol. 83, no. 2, pp. 714–719, 2011.

[21] J. A. Rufián-Henares and F. J. Morales, "Functional properties of melanoidins: in vitro antioxidant, antimicrobial and antihypertensive activities," *Food Research International*, vol. 40, no. 8, pp. 995–1002, 2007.

[22] M. Carabasa-Giribet and A. Ibarz-Ribas, "Kinetics of colour development in aqueous glucose systems at high temperatures," *Journal of Food Engineering*, vol. 44, no. 3, pp. 181–189, 2000.

[23] X. Tovar Jiménez, A. Arana Cuenca, A. Téllez Jurado, A. Abreu Corona, and C. R. Muro Urista, "Traditional methods for whey protein isolation and concentration: effects on nutritional properties and biological activity," *Journal of the Mexican Chemical Society*, vol. 56, no. 4, pp. 369–377, 2012.

[24] A. Fechner, A. Knoth, I. Scherze, and G. Muschiolik, "Stability and release properties of double-emulsions stabilised by caseinate-dextran conjugates," *Food Hydrocolloids*, vol. 21, no. 5-6, pp. 943–952, 2007.

[25] M. Ozgen, R. N. Reese, A. Z. Tulio Jr., J. C. Scheerens, and A. R. Miller, "Modified 2,2-azino-bis-3-ethylbenzothiazoline-6-sulfonic acid (ABTS) method to measure antioxidant capacity of selected small fruits and comparison to ferric reducing antioxidant power (FRAP) and 2,2′-diphenyl-1-picrylhydrazyl (DPPH) methods," *Journal of Agricultural and Food Chemistry*, vol. 54, no. 4, pp. 1151–1157, 2006.

[26] C. V. Morr and E. Y. W. Ha, "Whey protein concentrates and isolates: processing and functional properties," *Critical Reviews in Food Science and Nutrition*, vol. 33, no. 6, pp. 431–476, 1993.

[27] K. N. Pearce and J. E. Kinsella, "Emulsifying properties of proteins: evaluation of a turbidimetric technique," *Journal of Agricultural and Food Chemistry*, vol. 26, no. 3, pp. 716–723, 1978.

[28] R. He, X. Ju, J. Yuan, L. Wang, A. T. Girgih, and R. E. Aluko, "Antioxidant activities of rapeseed peptides produced by solid state fermentation," *Food Research International*, vol. 49, no. 1, pp. 432–438, 2012.

[29] L. Zhang, J. Li, and K. Zhou, "Chelating and radical scavenging activities of soy protein hydrolysates prepared from microbial proteases and their effect on meat lipid peroxidation," *Bioresource Technology*, vol. 101, no. 7, pp. 2084–2089, 2010.

[30] S. B. Kim, H. S. Shin, and J. W. Lim, "Separation of calcium-binding protein derived from enzymatic hydrolysates of cheese whey protein," *Asian Australasian Journal of Animal Sciences*, vol. 17, no. 5, pp. 712–718, 2004.

[31] W.-Q. Wang, Y.-H. Bao, and Y. Chen, "Characteristics and antioxidant activity of water-soluble Maillard reaction products from interactions in a whey protein isolate and sugars system," *Food Chemistry*, vol. 139, no. 1–4, pp. 355–361, 2013.

[32] X. Q. Huang, Z. C. Tu, H. Xiao et al., "Characteristics and antioxidant activities of ovalbumin glycated with different saccharides under heat moisture treatment," *Food Research International*, vol. 48, no. 2, pp. 866–872, 2012.

[33] Q. Liu, B. Kong, J. Han, C. Sun, and P. Li, "Structure and antioxidant activity of whey protein isolate conjugated with glucose via the Maillard reaction under dry-heating conditions," *Food Structure*, vol. 1, no. 2, pp. 145–154, 2014.

[34] M. Daglia, A. Papetti, C. Aceti, B. Sordelli, C. Gregotti, and G. Gazzani, "Isolation of high molecular weight components and contribution to the protective activity of coffee against lipid peroxidation in a rat liver microsome system," *Journal of Agricultural and Food Chemistry*, vol. 56, no. 24, pp. 11653–11660, 2008.

[35] M. S. Rao, S. P. Chawla, R. Chander, and A. Sharma, "Antioxidant potential of Maillard reaction products formed by irradiation of chitosan–glucose solution," *Carbohydrate Polymers*, vol. 83, no. 2, pp. 714–719, 2011.

[36] C. M. Oliver, L. D. Melton, and R. A. Stanley, "Functional properties of caseinate glycoconjugates prepared by controlled heating in the 'dry' state," *Journal of the Science of Food and Agriculture*, vol. 86, no. 5, pp. 732–740, 2006.

[37] J. Buchert, D. E. Cura, H. Ma et al., "Crosslinking food proteins for improved functionality," *The Annual Review of Food Science and Technology*, vol. 1, no. 1, pp. 113–138, 2010.

[38] Y. Sun, S. Hayakawa, M. Chuamanochan, M. Fujimoto, A. Innun, and K. Izumori, "Antioxidant effects of Maillard reaction products obtained from ovalbumin and different D-aldohexoses," *Bioscience, Biotechnology and Biochemistry*, vol. 70, no. 3, pp. 598–605, 2006.

[39] F. Nacka, J.-M. Chobert, T. Burova, J. Léonil, and T. Haertlé, "Induction of new physicochemical and functional properties by the glycosylation of whey proteins," *Journal of Protein Chemistry*, vol. 17, no. 5, pp. 495–503, 1998.

[40] M. Corzo-Martínez, C. Carrera-Sánchez, M. Villamiel, J. M. Rodríguez-Patino, and F. J. Moreno, "Assessment of interfacial and foaming properties of bovine sodium caseinate glycated with galactose," *Journal of Food Engineering*, vol. 113, no. 3, pp. 461–470, 2012.

[41] M. Corzo-Martínez, C. Carrera Sánchez, F. J. Moreno, J. M. Rodríguez Patino, and M. Villamiel, "Interfacial and foaming properties of bovine β-lactoglobulin: galactose Maillard conjugates," *Food Hydrocolloids*, vol. 27, no. 2, pp. 438–447, 2012.

Hindawi Publishing Corporation
International Journal of Polymer Science
Volume 2015, Article ID 168064, 5 pages
http://dx.doi.org/10.1155/2015/168064

Research Article

Rheological Properties of Polysaccharides from Longan (*Dimocarpus longan* Lour.) Fruit

Xingxun Liu,[1] Yongyue Luo,[2] Chunjie Zha,[2] Sumei Zhou,[1] Liya Liu,[1] and Lei Zhao[3]

[1] *Institute of Agro-Products Processing Science and Technology (IAPPST), Chinese Academy of Agricultural Science, Beijing 100193, China*
[2] *Chinese Agricultural Ministry Key Laboratory of Tropical Crop Product Processing, Agricultural Product Processing Research Institute, Chinese Academy of Tropical Agricultural Sciences, Zhanjiang 524001, China*
[3] *College of Food Science, South China Agricultural University, Guangzhou 510642, China*

Correspondence should be addressed to Xingxun Liu; ytboy652@163.com and Yongyue Luo; lyy6226@hotmail.com

Received 26 January 2015; Revised 27 April 2015; Accepted 29 April 2015

Academic Editor: Cornelia Vasile

Longan polysaccharide (LP) was extracted from longan (*Dimocarpus longan* Lour.) pulp. The composition and rheological properties were determined by chemical analysis and dynamic shear rheometer. The flow behavior and viscoelastic behavior of longan polysaccharide (LP) solution were investigated by steady shear and small amplitude oscillatory shear (SAOS) experiments, respectively. The result shows that the solution is a pseudoplastic flow in a range of shear rate (1–100 s^{-1}). The rheological behavior of LP was influenced by cations such as Na^+ and Ca^{2+}. With an increase of apparent viscosity, G' and G'' were accompanied by addition of Na^+ and Ca^{2+}.

1. Introduction

Polysaccharides have attracted much attention due to their broad spectra of therapeutic properties and relatively low toxicity [1–3]. Polysaccharides can be divided into animal polysaccharides, plant polysaccharides, and microbial polysaccharides according to their different sources. Plant polysaccharides are widely distributed and are of higher content among all polysaccharides. Plant polysaccharides also show some bioactivities, such as antioxidation, immunomodulation, antitumor, and hypoglycemic activities, in development of therapeutic drugs and high value healthy food in modern science [4].

Longan (*Dimocarpus longan* Lour.) which belongs to the Sapindaceae family, mainly planted in the south of China [5, 6], was welcomed by consumers due to health benefits [7, 8]. The fresh seed and pericarp of the fruit have been used as traditional Chinese medicines (TCMs) for several decades. Logan pulp and pericarp contain polysaccharides, which have a variety of bioactivities, such as antioxidation [9] and antitumor activities [10] and the activity of antiglycation and antityrosinase [11].

Studying the rheological properties is important to application of polysaccharides functional properties, the gelation processing can be gotten from rheological data, and processing parameters of polysaccharides may affect the jelly preparation [12]. There are many factors that affect the rheological behavior of polysaccharides. The inner factor is microstructure of polysaccharides, such as molecular weight, degree of branches, and functional groups of polysaccharides [13]. Furthermore, temperatures, concentration of polysaccharide, and presence of sugars or salts also have an effect on rheological properties of polysaccharide [14–17]. Previous works on rheological properties of mango polysaccharide [18], psyllium polysaccharide [19], and polysaccharide from boat-fruited sterculia seeds [20], which are affected by factors such as the concentration of polysaccharide, cosolute, and pH conditions, were studied. To the best of our knowledge, there is no paper on rheological properties study on longan polysaccharides.

To the best of our knowledge, there is no paper to report the rheological properties of longan polysaccharide, so the aim of this work is to study the rheological properties of longan polysaccharides for further application. In order to

prepare the polysaccharides, we used ethanol precipitate to prepare water-soluble polysaccharides. The composition and rheological properties were determined by chemical analysis and dynamic shear rheometer.

2. Materials and Methods

2.1. Plant Materials and Sample Preparation. The hot air dried Shixia longan (*Dimocarpus longan* Lour., harvested from Guangdong Province) pulp was soaked into fourfold 80% (v/v) ethanol for 48 hours to remove pigment and then dried before grinding into 200-mesh powder which was subject to further analysis.

2.2. Polysaccharide Extraction. Longan polysaccharide (LP) was extracted by hot water and alcohol precipitation according to Yi's methods [21]. In brief, 10 g of longan fruit pericarp powder was dispersed in 100 mL of distilled water and heated to 90°C for two hours once for three times. The extract was filtered through fourfold gauze and then centrifuged at 3000 rpm for 10 minutes. The supernatant was concentrated to 100 mL using rotatory evaporator (LR4002, Heidolph, Germany) at 65°C under vacuum. Anhydrate ethanol (400 mL) was added to the concentration extract to precipitate polysaccharides overnight at 4°C. The pellet was gathered after centrifugation, successively washed by anhydrate ethanol, absolute ether, and acetone, and then dried at 45°C under vacuum. The content of neutral polysaccharide was determined by the phenol-sulphuric acid method and expressed as glucose equivalents. The content of hexuronic acid was determined by the method of Blumenkrantz and Asboe-Hansen and expressed as glucuronic acid equivalents. The protein content was estimated using Folin-Ciocalteu's reagent and expressed as bovine serum albumin equivalents [8].

2.3. Rheological Measurement

2.3.1. Preparation of Samples. Water-soluble polysaccharide solutions at different concentrations (0.5%, 3.0%, 5.0%, and 10%, w/v) were prepared by dissolving the dried polysaccharide powder in distilled water and samples (5%, w/v) dissolved in different NaCl concentration solutions (0 mM, 50 mM, 150 mM, and 250 mM) and different $CaCl_2$ concentration solutions (0 mM, 50 mM, 150 mM, and 250 mM). All the samples were stirred for 2 h.

2.3.2. Rheological Experiment. Dynamic shear rheological properties such as storage modulus (G'), loss modulus (G''), and complex viscosity (η^*) of the gels were measured under low-amplitude oscillatory shear using plate-and-plate geometry with diameter of 50 mm in an MCR Rheometer (Anton Paar, Austria, DE). The dynamic measurements were performed at a strain value of 0.02 (2%) (within the linear viscoelastic region). Frequency sweep tests of all the solutions were performed using plate/plate geometry (50 mm diameter, 0.5 mm gap) at 25°C and frequency (ω) from 0.1 to 100 s^{-1} to assess the flow behavior of the polysaccharide dispersions.

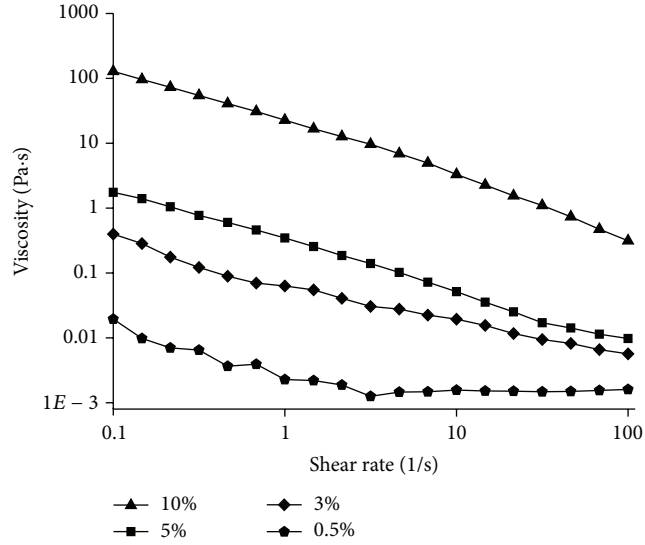

Figure 1: Steady shear flow curves of different concentration of LP.

3. Results and Discussion

The water-soluble polysaccharides were extracted from longan pulp by hot water and alcohol precipitation in this work. The longan polysaccharide (LP) was determined to contain 80.72% of polysaccharides, 5.27% of uronic acids, and 13.10% of proteins, which is similar to previous report [22].

3.1. The Viscosity Change of LP Solution. Studying the viscosity at the low shear rate could permit testing the consistency of the product in the mouth [23] while the viscosity at the high shear rate could provide some information of the product in processing operation, such as mixing and spray drying. In this paper, the effect of concentration on apparent viscosity for 0.5%, 3.0%, 5.0%, and 10.0% (w/v) crude longan polysaccharide solutions is shown in Figure 1. The apparent viscosity of each concentration solution obviously decreased with the increase of shear rate, showing a shear-thinning behavior, which means that this kind of crude longan polysaccharide solution belongs to non-Newtonian fluid (or pseudoplastic flow behavior). From Figure 1, it also could be found that the viscosity increased with increasing LP concentration; however, at lower concentrations (0.5%), the rheological measurements became erratic. The shear-thinning phenomenon could be due to the rate of formation of new entanglements lower than externally imposed disruption rate with increasing in shear rate.

The effect of Na^+ and Ca^{2+} on the flow properties of LP was illustrated in Figures 2 and 3. With progressive addition of Na^+ solution, the viscosity of LP increased little at first (50 mmol/L) and then increased quickly after addition of Na^+ (100 mmol/L). For Ca^{2+}, the viscosity increased rapidly after addition of $CaCl_2$ (50 mmol/L) in Figure 3.

3.2. Cox-Merz Inconformity. The Cox-Merz rule (1) allows us to predict $\eta(\dot{\gamma})$ from oscillatory measurements when $\eta(\dot{\gamma})$ is difficult to measure at high shear rates because of sample

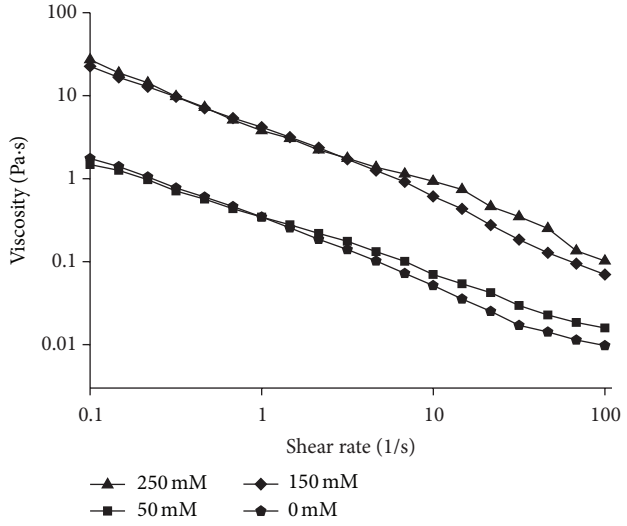

Figure 2: Steady shear flow curves of LP with different concentration of Na^+.

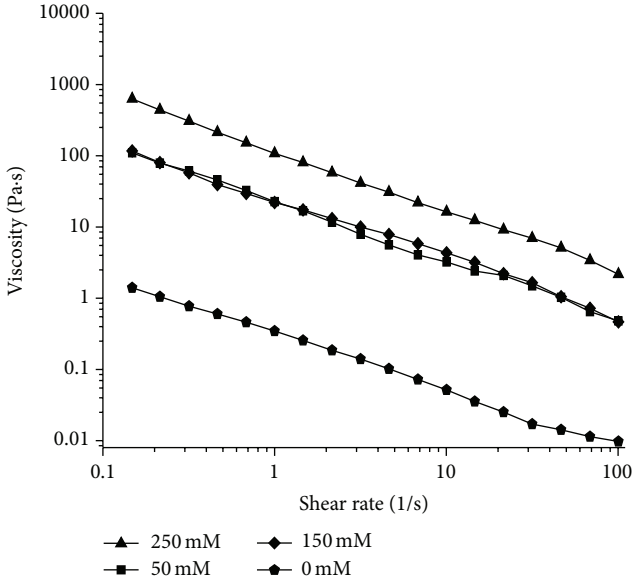

Figure 3: Steady shear flow curves of 5% LP with different concentration of Ca^{2+}.

fracture, secondary flows, and so forth, or we can estimate $\eta^*(\omega)$ from steady state viscosity data when oscillatory mode is not available. Another important application of the Cox-Merz rule is to learn about the microstructure of materials from the degree of conformity with the rule. Therefore, the shear rate dependence of steady shear viscosity and the frequency dependence of complex viscosity were compared to check if LP sample conforms to the Cox-Merz rule. Steady shear viscosity is defined as $\eta = \tau/\dot{\gamma}$ in which τ stands for steady shear stress and $\dot{\gamma}$ for steady shear rate, and complex viscosity is defined as $\eta^* = \sigma/\gamma\omega = G^*/\omega = \sqrt{G'^2 + G''^2}/\omega$, in which σ stands for stress, γ for strain, and ω for frequency. According to the result illustrated in

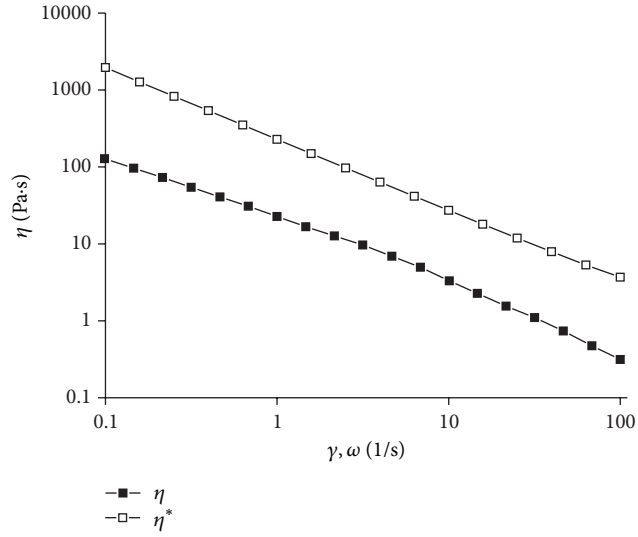

Figure 4: Cox-Merz plot of polysaccharide of 10% solution at 25°C (◆-η; ■-η^*).

Figure 4, the longan polysaccharide solution did not meet Cox-Merz plot as shear viscosity differed in complex dynamic viscosity. This result indicated that it is not appropriate to estimate dynamic viscosity through apparent viscosity for this system, and vice versa. The inconformity of the Cox-Merz rule implies that a network can be broken down during steady shear measurements but remains intact under small amplitude oscillation:

$$\eta(\dot{\gamma}) = \eta^*(\omega)\big|_{\omega=\dot{\gamma}}. \quad (1)$$

3.3. Viscoelastic Properties. The viscoelastic properties of LP were evaluated by SAOS measurements. The frequency dependence of storage modulus (G') and loss modulus (G'') of longan polysaccharide solution with different concentration could be seen in Figure 5. A viscoelastic solid-like behavior with G' higher than G'' over the entire range of ω is clearly seen. Furthermore, both G' and G'' nearly keep a constant during the whole experiment, which means that both G' and G'' exhibit a little dependence of frequency. This phenomenon means that the LP showed typical "weak gel" structure.

The effect of Na^+ and Ca^{2+} on viscoelastic properties of LP was measured and the result could be found in Figures 6 and 7. Immediate sharp increase in G' and G'' (see Figure 4) on progressive addition of NaCl or $CaCl_2$ to 5% LP, with more gradual increase at Na^+ or Ca^{2+} concentrations above ~50 mM, was seen. However, the Ca^{2+} has a more significant effect on G' and G'' than Na^+. Effect of salt on LP is broadly similar to that of gellan, which is anionic and forms double helices [24]. For gellan, monovalent (Group I) metal ions promote gelation by binding to individual double helices, thus suppressing the electrostatic barrier to helix-helix association. Binding occurs only above a minimum critical cation concentration, which for Na^+ is ~65 mM (the concentration at which the moduli and viscosity of LP increase steeply on

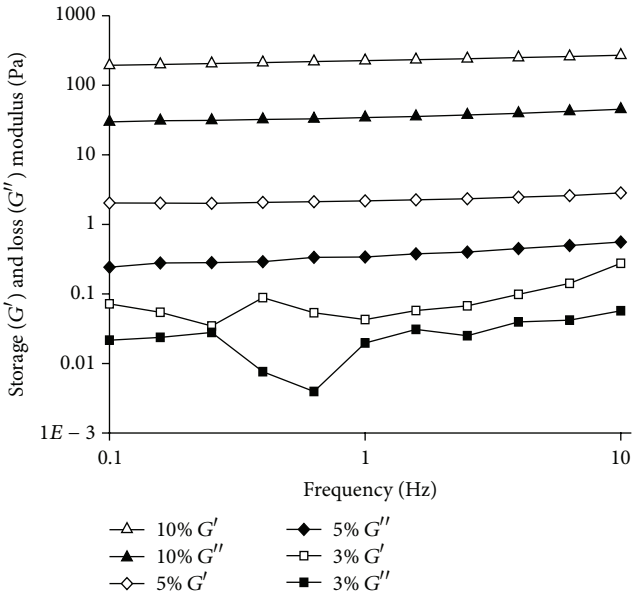

Figure 5: Frequency dependence of storage (G') and loss (G'') modulus of different concentration of LP.

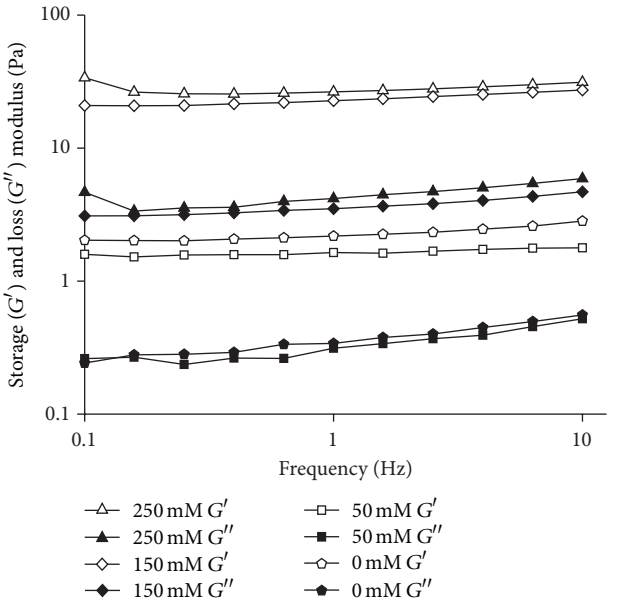

Figure 6: Frequency dependence of storage (G') and loss (G'') modulus of 5% LP with different content of Na^+.

progressive addition of NaCl). Ca^{2+} promotes gelation by binding between helices, and there is an immediate sharp increase in moduli on progressive addition of $CaCl_2$ to gellan solutions (as seems also to occur with LP). These apparent similarities may be coincidental, but the effect of salts on LP in greater detail would be worth exploring, and the details will be studied in the future.

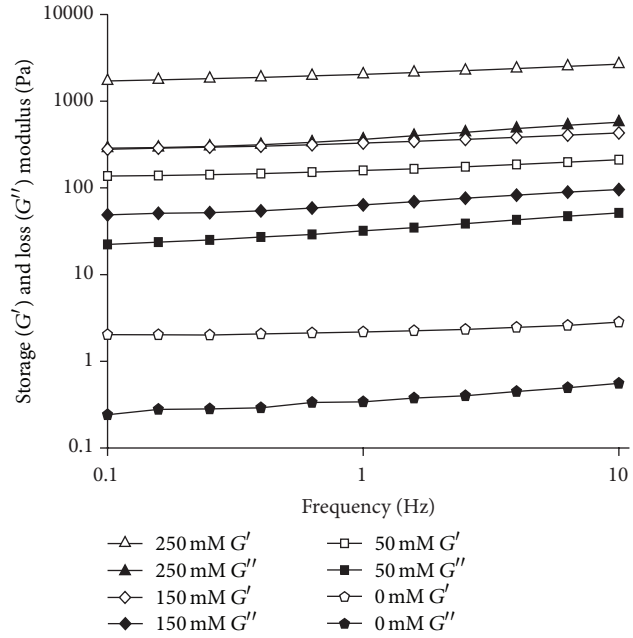

Figure 7: Frequency dependence of storage (G') and loss (G'') modulus of 5% LP with different content of Ca^{2+}.

4. Conclusion

The rheological properties of water-soluble polysaccharides from longan (*Dimocarpus longan* Lour.) fruit were studied in this paper. Steady shear rheological measurements showed a non-Newtonian shear-thinning flow behavior and it disconforms to Cox-Merz empirical correlation. Both fluidlike (G'' dominant) and solid-like (G' dominant) behaviors were observed when a cosolute was added or acidic condition changed. It was found that the addition of Na^+ and Ca^{2+} had influence on viscosity and fluidlike or solid-like behaviors of longan polysaccharide. The current paper provided a preliminary exploration of rheological properties of longan polysaccharide.

Conflict of Interests

The authors declare that there is no conflict of interests regarding the publication of this paper.

Acknowledgments

This work was financially supported by NSFC (31301554) and the national tropical crops engineering development of Reconstruction Project of Chinese National Engineering Research Center (no. 2011FU125Z09).

References

[1] B. Yang, M. Zhao, J. Shi, G. Cheng, N. Ruenroengklin, and Y. Jiang, "Variations in water-soluble saccharides and phenols in longan fruit pericarp after drying," *Journal of Food Process Engineering*, vol. 31, no. 1, pp. 66–77, 2008.

[2] Y.-C. Cheung, X.-X. Liu, W.-Q. Wang, and J.-Y. Wu, "Ultrasonic disruption of fungal mycelia for efficient recovery of polysaccharide-protein complexes from viscous fermentation broth of a medicinal fungus," *Ultrasonics Sonochemistry*, vol. 22, pp. 243–248, 2014.

[3] S. Chen, K.-C. Siu, W.-Q. Wang, X.-X. Liu, and J.-Y. Wu, "Structure and antioxidant activity of a novel poly-N-Acetylhexosamine produced by a medicinal fungus," *Carbohydrate Polymers*, vol. 94, no. 1, pp. 332–338, 2013.

[4] B. Yang, Y. Jiang, R. Wang, M. Zhao, and J. Sun, "Ultra-high pressure treatment effects on polysaccharides and lignins of longan fruit pericarp," *Food Chemistry*, vol. 112, no. 2, pp. 428–431, 2009.

[5] Y. Pan, K. Wang, S. Huang et al., "Antioxidant activity of microwave-assisted extract of longan (*Dimocarpus Longan* Lour.) peel," *Food Chemistry*, vol. 106, no. 3, pp. 1264–1270, 2008.

[6] G. Jiang, L. Wen, F. Chen et al., "Structural characteristics and antioxidant activities of polysaccharides from longan seed," *Carbohydrate Polymers*, vol. 92, no. 1, pp. 758–764, 2013.

[7] B. Yang, M. Zhao, K. N. Prasad, G. Jiang, and Y. Jiang, "Effect of methylation on the structure and radical scavenging activity of polysaccharides from longan (*Dimocarpus longan* Lour.) fruit pericarp," *Food Chemistry*, vol. 118, no. 2, pp. 364–368, 2010.

[8] Y. Yi, S.-T. Liao, M.-W. Zhang et al., "Immunomodulatory activity of polysaccharide-protein complex of longan (dimocarpus longan lour.) pulp," *Molecules*, vol. 16, no. 12, pp. 10324–10336, 2011.

[9] B. Yang, Y. Jiang, M. Zhao et al., "Structural characterisation of polysaccharides purified from longan (*Dimocarpus longan* Lour.) fruit pericarp," *Food Chemistry*, vol. 115, no. 2, pp. 609–614, 2009.

[10] K. Zhong, Q. Wang, Y. He, and X. He, "Evaluation of radicals scavenging, immunity-modulatory and antitumor activities of longan polysaccharides with ultrasonic extraction on in S180 tumor mice models," *International Journal of Biological Macromolecules*, vol. 47, no. 3, pp. 356–360, 2010.

[11] B. Yang, M. Zhao, and Y. Jiang, "Anti-glycated activity of polysaccharides of longan (*Dimocarpus longan* Lour.) fruit pericarp treated by ultrasonic wave," *Food Chemistry*, vol. 114, no. 2, pp. 629–633, 2009.

[12] H. Wang, X. Zhang, Y. Li et al., "Antitumor activity of a polysaccharide from longan seed on lung cancer cell line A549 in vitro and in vivo," *Tumor Biology*, vol. 35, no. 7, pp. 7259–7266, 2014.

[13] Y. Tao and D. Feng, "Dilute solution and rheological properties of hyperbranched polysaccharide from *Pleurotus tuber-regium* sclerotia," *Food Hydrocolloids*, vol. 28, no. 1, pp. 151–158, 2012.

[14] M. T. Nickerson and A. T. Paulson, "Rheological properties of gellan, κ-carrageenan and alginate polysaccharides: effect of potassium and calcium ions on macrostructure assemblages," *Carbohydrate Polymers*, vol. 58, no. 1, pp. 15–24, 2004.

[15] M. T. Nickerson, A. T. Paulson, and F. R. Hallett, "Pre-gel solution properties of gellan polysaccharides: effect of potassium and calcium ions on chain associations," *Food Research International*, vol. 41, no. 5, pp. 462–471, 2008.

[16] M. T. Nickerson, A. T. Paulson, and R. A. Speers, "Rheological properties of gellan solutions: effect of calcium ions and temperature on pre-gel formation," *Food Hydrocolloids*, vol. 17, no. 5, pp. 577–583, 2003.

[17] C. Karakasyan, S. Lack, F. Brunel, P. Maingault, and D. Hourdet, "Synthesis and rheological properties of responsive thickeners based on polysaccharide architectures," *Biomacromolecules*, vol. 9, no. 9, pp. 2419–2429, 2008.

[18] F. Iagher, F. Reicher, and J. L. M. S. Ganter, "Structural and rheological properties of polysaccharides from mango (*Mangifera indica* L.) pulp," *International Journal of Biological Macromolecules*, vol. 31, no. 1–3, pp. 9–17, 2002.

[19] Q. Guo, S. W. Cui, Q. Wang, H. D. Goff, and A. Smith, "Microstructure and rheological properties of psyllium polysaccharide gel," *Food Hydrocolloids*, vol. 23, no. 6, pp. 1542–1547, 2009.

[20] Y. Wu, S. W. Cui, J. Wu, L. Ai, Q. Wang, and J. Tang, "Structure characteristics and rheological properties of acidic polysaccharide from boat-fruited sterculia seeds," *Carbohydrate Polymers*, vol. 88, no. 3, pp. 926–930, 2012.

[21] Y. Yi, S. T. Liao, M. W. Zhang et al., "Physicochemical characteristics and immunomodulatory activities of three polysaccharide-protein complexes of longan pulp," *Molecules*, vol. 16, no. 7, pp. 6148–6164, 2011.

[22] Y. Yi, M.-W. Zhang, S.-T. Liao et al., "Structural features and immunomodulatory activities of polysaccharides of longan pulp," *Carbohydrate Polymers*, vol. 87, no. 1, pp. 636–643, 2012.

[23] E. R. Morris and L. J. Taylor, "Oral perception of fluid viscosity," *Progress in Food and Nutrition Science*, vol. 6, pp. 285–296, 1982.

[24] E. R. Morris, K. Nishinari, and M. Rinaudo, "Gelation of gellan—a review," *Food Hydrocolloids*, vol. 28, no. 2, pp. 373–411, 2012.